toxics

Special Issue Reprint

Occurrence, Accumulation, and Impacts of Environmental Pollutants in Aquatic Systems

Edited by
Fanhao Song, Zhuowei Zhang and Hongbin Lu

mdpi.com/journal/toxics

MDPI

Occurrence, Accumulation, and Impacts of Environmental Pollutants in Aquatic Systems

Occurrence, Accumulation, and Impacts of Environmental Pollutants in Aquatic Systems

Guest Editors

Fanhao Song
Zhuowei Zhang
Hongbin Lu

MDPI

Basel • Beijing • Wuhan • Barcelona • Belgrade • Novi Sad • Cluj • Manchester

Guest Editors

Fanhao Song
State Key Laboratory of Environmental Criteria and Risk Assessment
Chinese Research Academy of Environmental Sciences
Beijing
China

Zhuowei Zhang
School of Energy and Environmental Engineering
Hebei University of Engineering
Handan
China

Hongbin Lu
Institute of Coal Chemistry
Chinese Academy of Sciences
Taiyuan
China

Editorial Office
MDPI AG
Grosspeteranlage 5
4052 Basel, Switzerland

This is a reprint of the Special Issue, published open access by the journal *Toxics* (ISSN 2305-6304), freely accessible at: https://www.mdpi.com/journal/toxics/special_issues/Z4P7XI70Z3.

For citation purposes, cite each article independently as indicated on the article page online and as indicated below:

Lastname, A.A.; Lastname, B.B. Article Title. *Journal Name* **Year**, *Volume Number*, Page Range.

ISBN 978-3-7258-6354-9 (Hbk)
ISBN 978-3-7258-6355-6 (PDF)
https://doi.org/10.3390/books978-3-7258-6355-6

Contents

toxics

MDPI

Editorial

Occurrence, Accumulation, and Impacts of Environmental Pollutants in Aquatic Systems

Hongbin Lu [1], Zhuowei Zhang [2,3,*] and Fanhao Song [4,*]

[1] State Key Laboratory of Coal Conversion, Institute of Coal Chemistry, Chinese Academy of Sciences, Taiyuan 030001, China; luhongbin@sxicc.ac.cn
[2] Hebei Engineering Research Center for Sewage Treatment and Resource Utilization, School of Water Conservancy and Hydroelectric Power, Hebei University of Engineering, Handan 056038, China
[3] Hebei Technology Innovation Center of Water Pollution Control and Water Ecological Remediation, School of Water Conservancy and Hydroelectric Power, Hebei University of Engineering, Handan 056038, China
[4] State Key Laboratory of Environmental Criteria and Risk Assessment, Chinese Research Academy of Environmental Sciences, Beijing 100012, China
* Correspondence: zhangzw9292@163.com (Z.Z.); songfanhao277@163.com (F.S.)

1. Introduction

In response to the growing concerns of environmental pollution and its ecological impacts, this collection of research focuses on the monitoring, behavior, and remediation of various contaminants in aquatic systems. The studies address a range of toxic agents—including heavy metals (e.g., As, Cd, Cr, Cu, Pb) [1], endocrine disruptors like 17β-estradiol [2], and petroleum hydrocarbons [3]—originating from industrial, agricultural, and urban activities. These pollutants enter water bodies, accumulate in aquatic organisms, alter microbial community structures [4], and influence human health and safety. There is an increasing emphasis on developing sensitive, rapid, and eco-friendly monitoring tools, such as electroactive microorganism-based biosensors [5], and on understanding the underlying mechanisms of toxicity and pollutant migration. Concurrently, bioremediation and phytoremediation strategies using native plants [6] and microorganisms [7] are being explored as sustainable solutions to mitigate contamination.

Following a thorough review process, the selected articles collectively highlight innovative approaches in environmental toxicology and remediation. Some studies present novel biosensing techniques using microbial fuel cells for real-time toxicity warning systems [8], while others investigate the use of marine photoautotrophs—such as mangroves, seagrasses, and seaweeds—for effective pollutant removal [9]. Several papers analyze the bioaccumulation of trace metals in marine species and assess ecological risks using bacterial community biomarkers. Additionally, research on the mitigation of lead toxicity in fish using plant-based treatments demonstrates practical bioremediation applications. Together, these contributions represent significant advances in the detection, behavior analysis, and biological remediation of environmental pollutants, offering valuable tools and insights for coastal, aquatic, and wastewater management.

2. An Overview of Published Articles

The review article by Xing et al., "*Research on the Application and Mechanisms of Electroactive Microorganisms in Toxicants Monitoring: A Review*" (contribution 1), presents the principles, applications, and influencing factors of using electroactive microorganisms in

microbial fuel cells (MFCs) for toxicity monitoring. The core principle is that electroactive microorganisms generate electrical signals, which immediately decrease when their activity is inhibited by toxicants. Common MFC configurations include dual-chamber and single-chamber reactors, and their performance can be enhanced through electrode material modification [10]. The voltage inhibition rate is the most commonly used indicator for toxicity assessment [11]. The review identifies that factors such as flow rate, culture time, substrate concentration, and sodium chloride concentration significantly affect the sensitivity and stability of the biosensor. The mechanisms of toxicity involve the inhibition of microbial energy metabolism, key enzymes, and the induction of oxidative stress, which disrupt extracellular electron transfer. Finally, compared to traditional anaerobic toxicity assays (e.g., based on methane production) or luminescent bacteria tests, MFC-based biosensors offer the advantages of rapid response and potential for online monitoring, making them a promising tool for wastewater toxicity early warning systems.

The article by Gao et al., entitled "*Effects of 17β-Estradiol Pollution on Microbial Communities and Methane Emissions in Aerobic Water Bodies*" (contribution 2), investigates the impact of the endocrine-disrupting compound 17β-estradiol (E2) on microbial communities and greenhouse gas emissions in laboratory-simulated aerobic aquatic systems. Experiments were conducted with E2 concentrations of 0 ng/L (control), 100 ng/L (low), and 10,000 ng/L (high). The results showed that E2 contamination stimulated short-term methane (CH_4) emissions, particularly within the first two days. Using 16S rRNA sequencing, the study found that E2 increased the stochasticity of bacterial and archaeal community assembly and weakened microbial interactions. Specifically, E2 pollution significantly decreased the relative abundance of *Proteobacteria* (which includes methanotrophs) [12] and increased the relative abundance of *Planctomycetota* (which may contribute to aerobic methane production) [13]. Functional prediction indicated an increase in the methanogenesis group and a decrease in the methanotrophy group. The study concluded that E2 promotes (CH_4) emissions through three pathways, namely stimulating methanogens like Methanoregula in anoxic microsites, boosting *Planctomycetota* capable of methylphosphonate utilization, and inhibiting methanotrophic bacteria.

The article by Li et al., entitled "*Bioaccumulation of Arsenic, Cadmium, Chromium, Cobalt, Copper, and Zinc in Uroteuthis edulis from the East China Sea*" (contribution 3), analyzes the concentration and distribution of six trace elements (TEs) in different tissues of the squid Uroteuthis edulis. The tissues analyzed were the mantle, digestive gland, gonad, and gill. The study found significant differences in TE concentrations among tissues. The digestive gland accumulated the highest concentrations of Cu, Zn, and Cd, while the gill showed the highest levels of Cr and Co. Arsenic (As) was relatively evenly distributed across all tissues. In terms of the total body burden of TEs, the mantle contributed the highest proportion due to its large mass. Correlation analysis revealed significant positive correlations among Cu, Co, and Cd in certain tissues, possibly related to metallothionein binding. Furthermore, the study compared TE concentrations before and after gonadal maturation. Significant increases in the concentrations of most TEs (except Zn) were observed in the digestive gland of mature individuals, and significant increases in Cr, Cu, and As were found in the gonads, suggesting potential maternal transfer of these elements to offspring.

The article by Roda F. Al-Thani and Bassam T. Yasseen, entitled "*Methods Using Marine Aquatic Photoautotrophs along the Qatari Coastline to Remediate Oil and Gas Industrial Water*" (contribution 4), presents the potential of native marine organisms for remediating pollutants from oil and gas wastewater [14]. The study focused on marine photoautotrophs including the mangrove Avicennia marina, seagrasses (*Halodule uninervis*, *Halophila ovalis*, *Thalassia hemprichii*), and various species of green, brown, and red seaweeds. These organ-

isms and their associated microorganisms were found to remove heavy metals and degrade petroleum hydrocarbons through mechanisms such as phytoextraction, phytostabilization, and phycoremediation [15]. The mangrove A. marina proved efficient in accumulating heavy metals such as Co, Cr, Cu, Fe, Ni, and Zn. Seagrasses were identified as promising candidates for phytoremediation or as bioindicators. Seaweeds demonstrated a high capacity for the biosorption and bioaccumulation of common heavy metals like As, Cd, and Hg [16]. The remediation process was enhanced by the synergistic relationship between plants and their associated microorganisms, where root exudates stimulated microbial activity to degrade organic pollutants.

The article by Li et al., entitled "*Characteristics and Mechanism of Hematite Dissolution and Release on Arsenic Migration in Heterogeneous Materials*" (contribution 5), presents the impact of hematite dissolution on the migration and adsorption of arsenic in a heterogeneous aquifer system. A stratified sand column embedded with a hematite lens at the coarse-to-medium sand interface was designed to simulate groundwater flow. The medium structure significantly influenced arsenic migration, where clay layers directed the lateral migration of arsenic, leading to concentrations in deeper layers up to seven times greater than those on the surface. Solid-phase extraction revealed that arsenic was primarily adsorbed on quartz sand surfaces in a specifically adsorbed state (F2) [17] and bound to amorphous iron–aluminum oxides (F3). Monitoring of aqueous iron (Fe(aq)) showed a rapid increase to a maximum on day 15, followed by a gradual decline, indicating that hematite dissolution was not continuous. The released Fe(aq) subsequently contributed to the formation of fresh iron–aluminum oxides that adsorbed As(V), thereby reducing its concentration and influencing its spatial distribution within the sand column.

The article by Xia et al., entitled "*Using Sediment Bacterial Communities to Predict Trace Metal Pollution Risk in Coastal Environment Management: Feasibility, Reliability, and Practicality*" (contribution 6), presents the distribution and accumulation risk of trace metals (Al, As, Cr, Cu, Fe, Mn, Ni, Sr, Zn) in a tidal gate-controlled coastal river. The study area was divided into the catchment area (CA), estuarine area (EA), and offshore area (OA). The enrichment factor and geoaccumulation index identified As and Cr as the key pollutants, reaching slight-to-moderate pollution levels. The Nemero pollution index was highest in the EA (14.93), indicating a significant pollution risk near the tidal gates. Although Fe and Mn dynamics could partially explain trace metal behavior, they showed no linear relationships with toxic metals. Interestingly, the metabolic abundance of sediment bacterial communities showed strong correlations with various trace metals [18]. These results indicate that bacterial community characteristics can serve as effective biomarkers for assessing trace metal pollution and offer a practical tool for coastal environmental management.

The article by Nimai Chandra Saha et al., entitled "*Toxic Effects of Lead Exposure on Freshwater Climbing Perch, Anabas testudineus, and Bioremediation Using Ocimum sanctum Leaf Powder*" (contribution 7), presents the toxic effects of lead (Pb) on fish and its remediation. The 96 h LC50 value of lead for Anabas testudineus was determined to be 1.08 mg/L using static replacement bioassay. Chronic exposure to sublethal concentrations (10% and 20% of LC50) significantly lowered growth parameters (hepatosomatic index, specific growth rate), hematological biomarkers (RBC, hemoglobin), and increased serum enzyme levels (AST, ALT). Scanning electron microscopy revealed abnormal shapes and surfaces of erythrocytes in exposed fish. The leaf powder of Ocimum sanctum was administered with fish food to mitigate lead toxicity. The results showed that fish treated with the mixture of lead and Ocimum sanctum leaf powder exhibited significant recovery in growth, as well as hematological and biochemical parameters compared to those exposed to lead alone, indicating the remedial role of Ocimum sanctum against lead toxicity.

The article by Porttape Jendanklang et al., entitled "*The Contamination of Microplastic Debris in Blue Swimming Crab Portunus pelagicus from Artisanal Fisheries in the Eastern Gulf of Thailand*" (contribution 8), presents the microplastic (MP) contamination in crabs collected from the coast of Rayong province. The crab samples were collected from four sites in January, April, and August 2024, representing different monsoon seasons. MPs were examined in both external and internal body parts. The overall detection rate of MPs was 72.2% internally and 62.5% externally. The gut was the most contaminated tissue, followed by the gills, while no MPs were found in the hepatopancreas or muscle. MP abundance showed significant seasonal variation, with the highest level in August. Fibers were the dominant shape, blue was the most common color, and the primary polymers identified were polyethylene terephthalate glycol (PETG), nylon, and polypropylene. The study indicates that household laundry fibers and damaged fishing gear are major sources of MP pollution. It is concluded that improving waste management and developing more durable fishing gear are crucial for mitigating this contamination.

Funding: This work was supported by the Regional Cooperation Program of Shanxi Province (No. 202304041101039), the Fundamental Research Program of Shanxi Province (No. 202203021222404), ICC–CAS (No. SCJC-WRW-2023–18), and the National Natural Youth Science Foundation of China (52400088). The editors thank all the authors for their contributions.

Data Availability Statement: No new data were created or analyzed in this study. Data sharing is not applicable to this article.

Conflicts of Interest: The Guest Editor and Guest Co-editors declare that there are no conflicts of interest or agreements with private companies that will prevent us working impartially in the editorial process.

List of Contributions:

1. Xing, F.; Duan, L.; Zhang, H.; Zhang, H.; Li, S. Research on the Application and Mechanisms of Electroactive Microorganisms in Toxicants Monitoring: A Review. *Toxics* **2024**, *12*, 173. https://doi.org/10.3390/toxics12030173.
2. Gao, Z.; Zheng, Y.; Li, Z.; Ruan, A. Effects of 17β-Estradiol Pollution on Microbial Communities and Methane Emissions in Aerobic Water Bodies. *Toxics* **2024**, *12*, 373. https://doi.org/10.3390/toxics12050373.
3. Li, M.; Zhang, B.; Fang, Z. Bioaccumulation of Arsenic, Cadmium, Chromium, Cobalt, Copper, and Zinc in Uroteuthis edulis from the East China Sea. *Toxics* **2024**, *12*, 496. https://doi.org/10.3390/toxics12070496.
4. Al-Thani, R.F.; Yasseen, B.T. Methods Using Marine Aquatic Photoautotrophs along the Qatari Coastline to Remediate Oil and Gas Industrial Water. *Toxics* **2024**, *12*, 625. https://doi.org/10.3390/toxics12090625.
5. Li, Z.; Shan, H.; Rong, W.; Zhao, Z.; Ma, K.; Peng, S.; Wei, S. Characteristics and Mechanism of Hematite Dissolution and Release on Arsenic Migration in Heterogeneous Materials. *Toxics* **2024**, *12*, 687. https://doi.org/10.3390/toxics12090687.
6. Xia, Y.; Liu, J.; Yang, X.; Ling, X.; Fang, Y.; Xu, Z.; Liu, F. Using Sediment Bacterial Communities to Predict Trace Metal Pollution Risk in Coastal Environment Management: Feasibility, Reliability, and Practicability. *Toxics* **2024**, *12*, 839. https://doi.org/10.3390/toxics12120839.
7. Saha, N.C.; Chatterjee, A.; Banerjee, P.; Bhattacharya, R.; Sadhu, A.; Pastorino, P.; Saha, S. Toxic Effects of Lead Exposure on Freshwater Climbing Perch, Anabas testudineus, and Bioremediation Using Ocimum sanctum Leaf Powder. *Toxics* **2024**, *12*, 927. https://doi.org/10.3390/toxics12120927.
8. Jendanklang, P.; Ruengsorn, C.; Meksumpun, S.; Kasamesiri, P. The Contamination of Microplastic Debris in Blue Swimming Crab Portunus pelagicus (Linnaeus, 1758) from Artisanal Fisheries in the Eastern Gulf of Thailand. *Toxics* **2025**, *13*, 813. https://doi.org/10.3390/toxics13100813.

References

1. Ali, M.M.; Awan, F.; Jamil, M.U.; Ijaz, M.; Ullah, A.; Shehzad, W. Genotoxic and oxidative stress assessment of heavy metal contaminated soil and water in human blood and bovine milk samples from the different industrial zones of Punjab, Pakistan. *J. Trace Elem. Med. Biol.* **2025**, *92*, 127790. [CrossRef] [PubMed]
2. Alahadeb, J.I. Effective biodeterioration of a common endocrine disruptor 17β-estradiol using mixed microbial cultures isolated from waste water. *Environ. Res.* **2022**, *206*, 112559. [CrossRef] [PubMed]
3. Wang, M.; Wang, C.; Li, Y. Petroleum hydrocarbons in a water-sediment system from Yellow River estuary and adjacent coastal area, China: Distribution pattern, risk assessment and sources. *Mar. Pollut. Bull.* **2017**, *122*, 139–148. [CrossRef] [PubMed]
4. Hong, Y.; Li, D.; Xie, C.; Zheng, X.; Yin, J.; Li, Z.; Zhang, K.; Jiao, Y.; Wang, B.; Hu, Y.; et al. Combined apatite, biochar, and organic fertilizer application for heavy metal co-contaminated soil remediation reduces heavy metal transport and alters soil microbial community structure. *Sci. Total Environ.* **2022**, *851*, 158033. [CrossRef] [PubMed]
5. Xi, H.; Wang, H.; Li, Y.; Long, X.; Li, X.; Sun, Y.; Wang, W. Advancing Shewanella-based whole-cell biosensors: A comprehensive review on heavy metal detection. *Colloids Surf. B Biointerfaces* **2025**, *256*, 115075. [CrossRef] [PubMed]
6. Liu, N.; Zhao, J.; Du, J.; Hou, C.; Zhou, X.; Chen, J.; Zhang, Y. Non-phytoremediation and phytoremediation technologies of integrated remediation for water and soil heavy metal pollution: A comprehensive review. *Sci. Total Environ.* **2024**, *948*, 174237. [CrossRef] [PubMed]
7. Taharia, M.; Dey, D.; Das, K.; Sukul, U.; Chen, J.-S.; Banerjee, P.; Dey, G.; Sharma, R.K.; Lin, P.-Y.; Chen, C.-Y. Microbial induced carbonate precipitation for remediation of heavy metals, ions and radioactive elements: A comprehensive exploration of prospective applications in water and soil treatment. *Ecotoxicol. Environ. Saf.* **2024**, *271*, 115990. [CrossRef] [PubMed]
8. Safwat, S.M.; Khaled, A.; Elawwad, A.; Matta, M.E. Dual-chamber microbial fuel cells as biosensors for the toxicity detection of benzene, phenol, chromium, and copper in wastewater: Applicability investigation, effect of various catholyte solutions, and life cycle assessment. *Process Saf. Environ. Prot.* **2023**, *170*, 1121–1136. [CrossRef]
9. Talaiekhozani, A.; Rezania, S. Application of photosynthetic bacteria for removal of heavy metals, macro-pollutants and dye from wastewater: A review. *J. Water Process Eng.* **2017**, *19*, 312–321. [CrossRef]
10. Zhang, Q.; Tan, B.; Li, H.; An, F. Nitrogen-doped and catalytically modified electrodes in campus-sourced electrogenic microbe-driven MFCs for enhanced copper ion adsorption. *Bioelectrochemistry* **2026**, *167*, 109077. [CrossRef] [PubMed]
11. Lee, C.; Park, Y.H.; Kang, S.W. Nanoporous Cellulose Acetate-Coated Polypropylene Membranes for Microbial Fuel Cells: Enhanced Long-Term Stability, Fouling Resistance, and Reverse Voltage Suppression. *Biomacromolecules* **2025**, *in press*. [CrossRef] [PubMed]
12. Li, J.; Liu, R.; Liu, X.; Yang, Q.; Zhang, S. Organic matter removal and CH4 production performance recoveries and microbial community changes in upflow anaerobic biofilter after long term starvation. *J. Environ. Sci.* **2025**, *156*, 735–746. [CrossRef] [PubMed]
13. Klimek, D.; Herold, M.; Calusinska, M. Comparative genomic analysis of Planctomycetota potential for polysaccharide degradation identifies biotechnologically relevant microbes. *BMC Genom.* **2024**, *25*, 523. [CrossRef] [PubMed]
14. Kianfar, E. Current situation and future outlook petroleum hydrocarbons in marine systems: A review. *Environ. Technol. Innov.* **2025**, *40*, 104572. [CrossRef]
15. Cozma, P.; Roșca, M.; Minuț, M.; Gavrilescu, M. Phytoremediation: A sustainable and promising bio-based approach to heavy metal pollution management. *Sci. Total Environ.* **2025**, *1001*, 180458. [CrossRef] [PubMed]
16. Greeshma, K.; Kim, H.-S.; Ramanan, R. The emerging potential of natural and synthetic algae-based microbiomes for heavy metal removal and recovery from wastewaters. *Environ. Res.* **2022**, *215*, 114238. [CrossRef] [PubMed]
17. Guo, H.; Stüben, D.; Berner, Z. Arsenic removal from water using natural iron mineral–quartz sand columns. *Sci. Total Environ.* **2007**, *377*, 142–151. [CrossRef] [PubMed]
18. Bo, H.; Li, Z.; Wang, H.; Zhang, H.; Xu, R.; Xue, D.; Li, H.; Wang, W.; Zhang, W.; Zhang, Q.; et al. Long-term exposure to fly ash leachate enhances the bioavailability of potentially toxic metals and decreases bacterial community diversity in sediments. *J. Environ. Manag.* **2025**, *376*, 123428. [CrossRef] [PubMed]

toxics

MDPI

Article

The Contamination of Microplastic Debris in Blue Swimming Crab *Portunus pelagicus* (Linnaeus, 1758) from Artisanal Fisheries in the Eastern Gulf of Thailand

Poratape Jendanklang [1], Chakhrit Ruengsorn [2,*], Shettapong Meksumpun [2] and Pattira Kasamesiri [3]

[1] Department of Fisheries, Rayong Marine Fisheries Research and Development Center, Rayong 21160, Thailand; poratape.j@ku.th
[2] Department of Marine Science, Faculty of Fisheries, Kasetsart University, Bangkok 10900, Thailand; ffisspm@ku.ac.th
[3] Division of Fisheries, Faculty of Technology, Mahasarakham University, Maha Sarakham 44150, Thailand; pattira@msu.ac.th
* Correspondence: ffiscrr@ku.ac.th; Tel.: +66-897718446

Abstract

Microplastics have become a significant concern for human health, primarily because aquatic animals can ingest these particles, which then enter the human food chain. Crabs (*Portunus pelagicus*) were collected along the coastline of Rayong Province in January, April, and August 2024. Crabs were then examined for MP contamination. Our results revealed that MPs were present at all sampling sites, with a detection rate of 62.5% in external body parts and 72.2% in internal body parts. The gut was the most contaminated tissue, followed by the gills, while no MPs were found in the hepatopancreas or muscle tissues. Although overall MP detection and contamination levels were similar across sites, significant differences in abundance were observed between seasons ($p < 0.05$), with August showing the highest contamination levels. Polyethylene terephthalate glycol was the most common polymer detected, followed by nylon, polypropylene, polyethylene, polystyrene, and polyester. Anthropogenic and fishing activities contribute significantly to MP pollution in these crabs. Fibers from household laundry, followed by damaged fishing gear, are major sources of MP pollution. Enhancing the quality and durability of fishing equipment is crucial to reducing the amount of abandoned fishing gear that may be ingested by marine organisms, while the proper collection and management of discarded gear in the ocean should also be emphasized.

Keywords: crab gillnet; fishing gear; microplastic pollution; microplastic migration

1. Introduction

Plastic debris is one of the most serious pollutants contributing to ocean pollution. It is one of the greatest environmental challenges of the 21st century. Recently, Thailand was rated as having the sixth highest rate of plastic flow into oceans in the world [1]. Thailand is also recognized among the nations with challenges in plastic waste management [2]. The presence of plastic debris of varying sizes, ranging from macroplastics to microplastics, poses severe threats to marine ecosystems and biodiversity [3]. Plastic debris such as fishing gear can lead to entanglement and ingestion by organisms [4]. It can cause injury, abnormal mobility, and mortality [5]. Rapid economic and population expansion, lifestyle changes,

ineffective governance practices, and insufficient awareness and knowledge about proper waste disposal can contribute to plastic pollution in our environment [6]. The origins of plastic debris are usually terrestrial and marine. The mismanagement of waste and urban runoff are terrestrial sources of approximately 80% of plastic debris [7,8], while ocean-based sources mostly include damaged and discarded fishing gear, litter from vessels near shore, and offshore industrial activities [9]. Debris can be transported by wind and currents in the ocean, which can lead to it being spread across the world, including remote areas [10].

Microplastics (MPs) are plastic particles less than 5 mm in size that originate from the fragmentation of larger plastics produced for products like cosmetics and synthetic textiles [11–13]. Owing to their small size, these particles can contaminate various ecologies, such as water and sediment in watercourses [14], water and beach sand along shores [15], mangrove sediment [16], and sediment in estuarine systems [17], and they can mix with indoor dust [18] and airborne particulate matter ($PM_{2.5}$) [19]. Moreover, they can accumulate in a wide range of marine organisms, including zooplankton [20], fish larvae [21], bivalves and gastropods [22], pelagic and demersal fishes [23], sea turtles [24], sea birds [25], and cetaceans [26]. When accumulated in organisms, MPs can cause physical harm and blockages, interfere with feeding and respiration, cause malnutrition, and result in exposure to toxic chemicals leached from them [27,28]. They can associate with pollutants and be transferred up through the food chain, potentially leading to adverse health effects [29]. These harmful MP particles not only affect the health of aquatic animals [30], but they can also pose a risk to human health through the consumption of MP-contaminated marine life [31,32].

Blue swimming crab (*Portunus pelagicus*) is a carnivorous bottom-dweller, mainly preying on mollusks, invertebrates, and bony fish [33]. This crab species is found spanning wide-ranging habitats with high commercial importance in various regions, including the Indo-West Pacific region with coastal waters from India, Australia, Africa, and Asia, with particular in Thailand [34]. This crustacean is a commercially important marine species found in various coastal regions in both the Andaman Sea and the Gulf of Thailand, including Rayong Province, which is located in the Eastern Gulf of Thailand. Marine capture by artisanal fisheries in Thailand in 2023 showed the volume of aquatic animals in crab category was 41,442.02 tons, with blue swimming crabs at 34,899.75 tons, accounting for 84.21% of the total catch. In addition, 77.98% of blue swimming crabs were caught by crab gillnets from artisanal fisheries [35]. Crab gillnet is the common fishing gear for catching this economic crab in this region by local fishermen [36]. According to the literature on MPs in crabs in Thailand, recent studies have detected MPs in blue swimming crabs from coastal Chonburi province [37] and Thai vinegar crabs from a mangrove area in Samut Prakan province [38], revealing pervasive plastic pollution. Marine ecosystems in the Rayong province were threatened by MP pollution, as evidenced by the presence of MPs in the environment and organisms around the Rayong province [15,23,39]. This contamination underscores the importance of implementing strategies to mitigate plastic pollution and protect marine and human health in this region.

Due to the characteristics and extent of MPs, the contamination in blue swimming crabs caught from artisanal fisheries remains unclear. Our study aims to study (i) the detection rate of MPs, (ii) the abundance and composition of MPs in tissue, and size and sex of crabs, and (iii) the characteristics of MP contamination in blue swimming crabs along four sampling sites seasonally in the Rayong province, an important fishing ground of blue swimming crabs in the Eastern gulf of Thailand. To reach this purpose, we collected blue swimming crab samples and dissected four parts of the tissue for extracting MPs from internal and external bodies, including interviewing local fishermen by gathering fishing ground data with

a semi-structured interview method to estimate the accumulation of MPs between season and sampling sites to clarify the situation of MP debris in organisms in this area.

2. Materials and Methods

2.1. Study Area and Sampling Sites

Rayong province is located on the eastern coast along the Gulf of Thailand, which is characterized by its industrial, agricultural, and tourism activities. The coastal area of this province spans approximately 100 km [40] and harbors diverse fisheries, including the fishing of blue swimming crab (*P. pelagicus*) by artisanal fisheries, especially crab gillnet. Sample collections were conducted in January, April, and August 2024, which represented the northeast monsoon, transition monsoon, and southwest monsoon, respectively. Crab samples were collected from four sampling sites, including Phayun (PY), Takuan (TK), Suanson (SS), and Wangkaew (WK), along the coast of Rayong province (Figure 1).

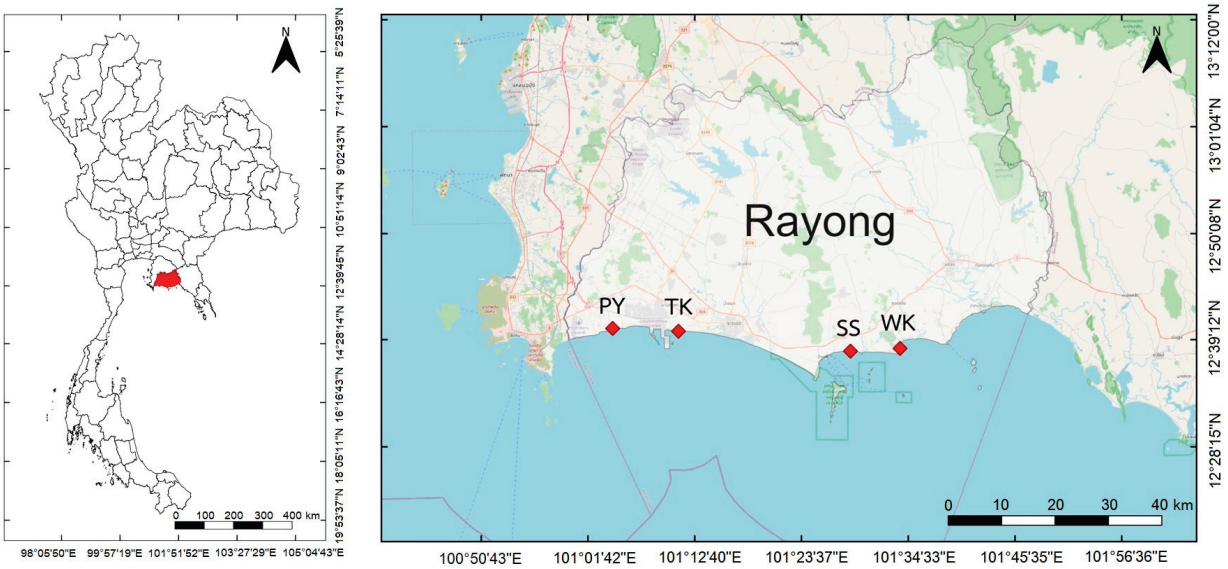

Figure 1. Location of sampling sites along the Rayong province.

2.2. Fisheries Data Gathering

Fisheries data were collected by interviewing local fishermen with a semi-structured interview method using an interview questionnaire form, which is provided in Figure S1. Details of the interview questionnaire form included vessel and fishermen data, characteristics of fishing gear with lifespan and materials, method of fishing operation, fishing ground area, environmental data, species composition, and total catch. This study focused on local fishermen who collected crab samples and were followed up throughout the study to ensure crab samples were caught in their fishing community area. The sample size of interviewed and followed-up fishermen throughout the study was twelve samples (N = 12). However, data on characteristics of fishing gear, materials, lifespan, and fishing grounds of blue swimming crabs by crab gillnet were only used for further discussion.

2.3. Sampling Method

Blue swimming crabs (*P. pelagicus*) were collected from small-scale fisheries in Rayong province from 4 stations, with 12 individuals per station. A total of 48 individuals will be sampled per season, and a total of 144 individuals of *P. pelagicus* will be used throughout the study. The sampling stations include Phayun, Takuan, Suanson, and Wangkaew. Crab samples were categorized into two size groups: small (6 crabs: 3 males, 3 females) and

large (6 crabs: 3 males, 3 females). Sizes of crabs were categorized by sold size. Before analyzed, all samples were measured for outer carapace width and carapace length, and weighed. Crab samples were stored at −20 °C to preserve the samples before dissection and extracting MPs in the laboratory.

2.4. Microplastics Digestion and Separation

The MP separation protocol was adapted from the method developed by the National Oceanic and Atmospheric Administration (NOAA) [41]. Crab samples were individually washed with 100 mL of distilled deionized water for external MP sampling. Washed water from the external body of crab samples individually was defined as external MP contamination, which was digested, separated, and filtered using the same procedure as internal tissues. Procedural and airborne blanks controlled by distilled deionized water were tested in parallel for each group of crabs categorized by sampling site and sampling time using the same procedure as internal tissues. All crabs were dissected to analyze internal contamination, focusing on gut, gill, hepatopancreas, and muscle tissue (excluding muscle tissue of walking and swimming legs) (Figure 2). Each tissue part was weighed separately and subjected to the wet peroxide oxidation (WPO) method. This involved adding 30% hydrogen peroxide (Qrec, Auckland, New Zealand) and 1% potassium hydroxide (Qrec, Auckland, New Zealand) in a 9:1 ratio, increasing the temperature to 75 °C while stirring until organic gas bubbles disappeared, and then allowing 24 h for the removal of organic matter. After completing the WPO method, MPs were separated using a density separation procedure. NaCl solution was added, stirred with a glass rod, and left to settle for 24 h to collect the supernatant, and the settled solution was also collected to prepare filtration, which will recover higher-density polymers. The supernatant and settled solution were filtered separately through a 47 mm diameter glass microfiber filter (Whatman grade GF/C pore size: 1.2 µm) using a vacuum system. The filter paper was dried in an oven at 60 °C and stored in a Petri dish glass with a glass lid for later visualization and identification.

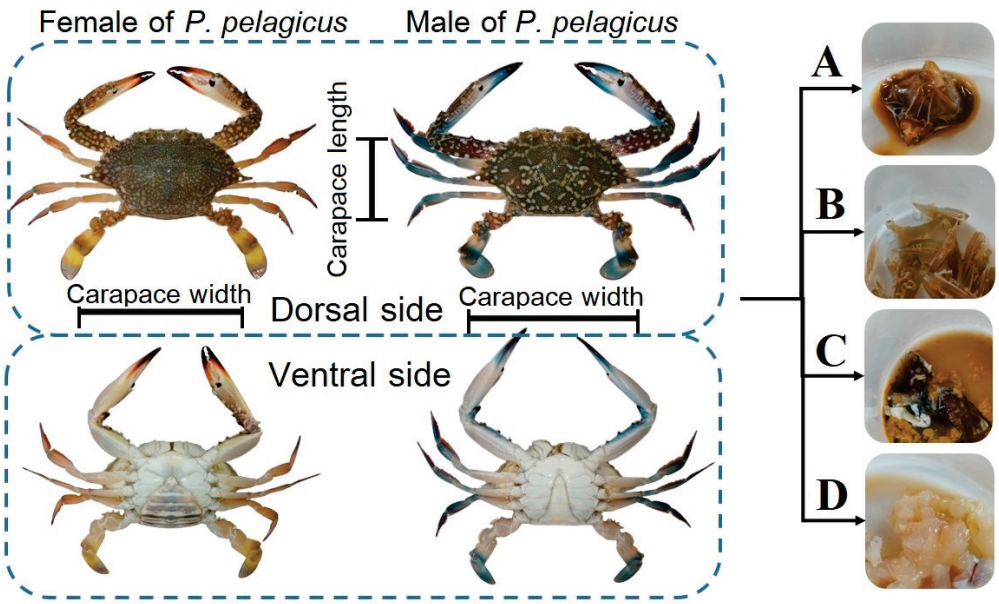

Figure 2. Dissecting by used part: (A) gut, (B) gill, (C) hepatopancreas, and (D) muscle.

2.5. Microplastics Visualization and Identification

MPs on filter paper were analyzed for quantity, size, shape, and color using a stereo microscope with total magnification used as 15× (Olympus SZ51, Hamburg, Germany). A hot

needle test was used to distinguish between plastic and non-plastic materials [42]. Although the hot needle test is a common method for screening plastic and non-plastic materials, it has several limitations that reduce its discriminative power. These limitations can lead to false positives and negatives and could affect results, making them less reliable than advanced methods like FTIR. However, this technique was only used as a preliminary step before identification by FTIR. MP sizes were measured with ImageJ version 1.50i and categorized into three ranges: 15–150 μm, 150–330 μm, and 330–5000 μm. Particle shapes were classified as fiber, fragment, film, and net. The study identified MPs in four colors (black, blue, red, and green); clear items were reported. MP particles were analyzed, 10% from total particles founded in this study. Polymer classifications were confirmed using Fourier-transform infrared spectrophotometry (FTIR Type II; Perkin Elmer, High Wycombe, UK).

2.6. Data Analysis

Average MP abundance was calculated in terms of items/individual and items/g wet weight with standard deviation values. The Shapiro–Wilk test was used to check for normal distribution ($p < 0.05$). Due to the non-normality of the data, nonparametric statistical methods were applied. The Kruskal–Wallis H test and pairwise comparisons were used to analyze the variations in MP abundance across different sampling sites and seasons. The Microplastics Detection Rate (MDR) was also calculated by the quantity of crab samples, which were contaminated in terms of individuals from all samples and categorized by sampling sites, seasonality, size groups of crab, type sex of crab, and part of tissues by Equation (1):

$$\text{MDR (\%)} = C_c/N_c \times 100, \quad (1)$$

where:

MDR = Microplastics Detection Rate (%);
C_c = total contaminated crabs (individuals);
N_c = total crab samples.

2.7. Quality Control

Procedural blank controls were used by distilling deionized water. These processes were tested as three blank parallel controls for each group of crabs categorized by sampling site and sampling time using the same procedure as internal tissues. Procedural blank controls were thirty-six (N = 36). Airborne blank controls were also tested by leaving three Petri dishes with open cover lids in the laboratory throughout the process, then rinsing with 100 mL of distilled deionized water in the Petri dish to test airborne contamination with the same method as the procedural blank controls (N = 36). Results from all procedural and airborne blank controls showed no MP contamination in our laboratory. The blank-corrected counts were equal to raw MPs counts, as no MP contamination was detected in all blanks.

3. Results and Discussion

3.1. Blue Swimming Crab Fishing Ground

Our data showed crab gillnet is the most common fishing gear for blue swimming crab fisheries, especially artisanal fisheries in this study area. Crab gillnets in Rayong province are specifically designed with larger mesh sizes around 3 inches to catch blue swimming crabs, which are made from durable materials like nylon and polyethylene to withstand the coastal environment. Distances from coast to fishing grounds and water depths were collected by a semi-structured interview method from local fishermen for four

locations: PY, TK, SS, and WK. In PY, distances were short (0.5–1 km) with water depths of 2–4 m. TK had distances around 5–7 km with deeper waters (15–18 m). SS showed a greater variability with distances of 10–15 km and water depths of 8–19 m. WK had distances ranging between 3–5 km and water depths of 8–14 m (Figure 3).

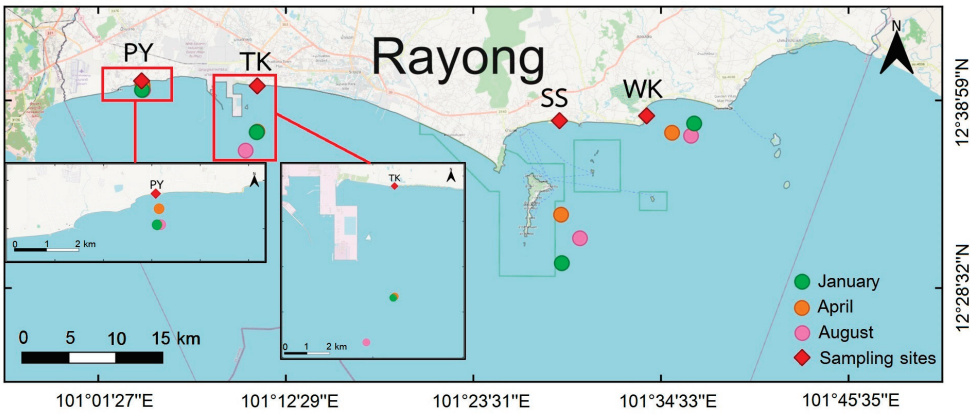

Figure 3. Crab gillnet fishing grounds at four sampling sites in Rayong province. Green, orange, and pink circles indicate January, April, and August, respectively; red diamonds mark the sampling sites.

3.2. Crab Characteristics

A total of 144 individuals of *P. pelagicus* were caught by artisanal fisheries from four sampling sites in Rayong province. The characteristics of the blue swimming crabs in this study were shown in Table 1.

Table 1. Summary of the characteristics of blue swimming crab samples.

SITE	PY	TK	SS	WK
Crab samples (individual)	36	36	36	36
Carapace width (cm)	11.24 ± 0.97	11.02 ± 1.08	11.33 ± 0.98	11.15 ± 0.92
Carapace length (cm)	5.52 ± 0.54	5.38 ± 0.61	5.61 ± 0.60	5.53 ± 0.53
Total weight (g)	103.11 ± 25.28	97.71 ± 33.77	107.15 ± 27.15	98.89 ± 26.18
Gut weight (g)	1.01 ± 0.53	1.02 ± 0.51	1.01 ± 0.48	1.17 ± 0.56
Gill weight (g)	4.33 ± 1.19	4.15 ± 1.66	4.71 ± 1.30	4.54 ± 1.34
Total external detection (individuals)	22	23	23	22
Total internal detection (individuals)	25	29	24	26
Total external MPs (items)	64	100	93	99
Total internal MPs (items)	116	149	132	136
MPs in gut (items)	82	107	100	96
MPs in gill (items)	34	42	32	40

Note: Phayun—PY, Takuan—TK, Suanson—SS, Wangkaew—WK.

3.3. Microplastics Detection Rate

MPs were detected in *P. pelagicus* across all sampling sites and seasons in Rayong province, with an overall detection rate of 72.2% (104 individuals). TK station had the highest detection rates at 83.3%, 75.0%, and 83.3% in January, April, and August 2024, respectively (Figure 4). When compared to other studies, the overall detection rate of MPs in crabs from China (89.3%) showed a higher detection rate than our study [43]. However, a consistent detection rate across seasons and sampling sites indicates contamination is a persistent issue, not limited to specific times and areas in Rayong province. MPs were found in all size groups, with larger crabs having a higher detection rate (80.6%) compared to smaller crabs (63.9%), showing a significant difference (Kruskal–Wallis, $p < 0.05$). When considering specific tissues, guts had a higher detection rate (71.5%) than gills (53.5%), with

a significant difference between them (Kruskal–Wallis, $p < 0.05$). No MPs were detected in the hepatopancreas and muscles of crabs, at least not in detectable amounts. While there was no significant difference in MP detection rates between male and female crabs, males showed a slightly higher detection rate (76.4%) compared to females (68.1%).

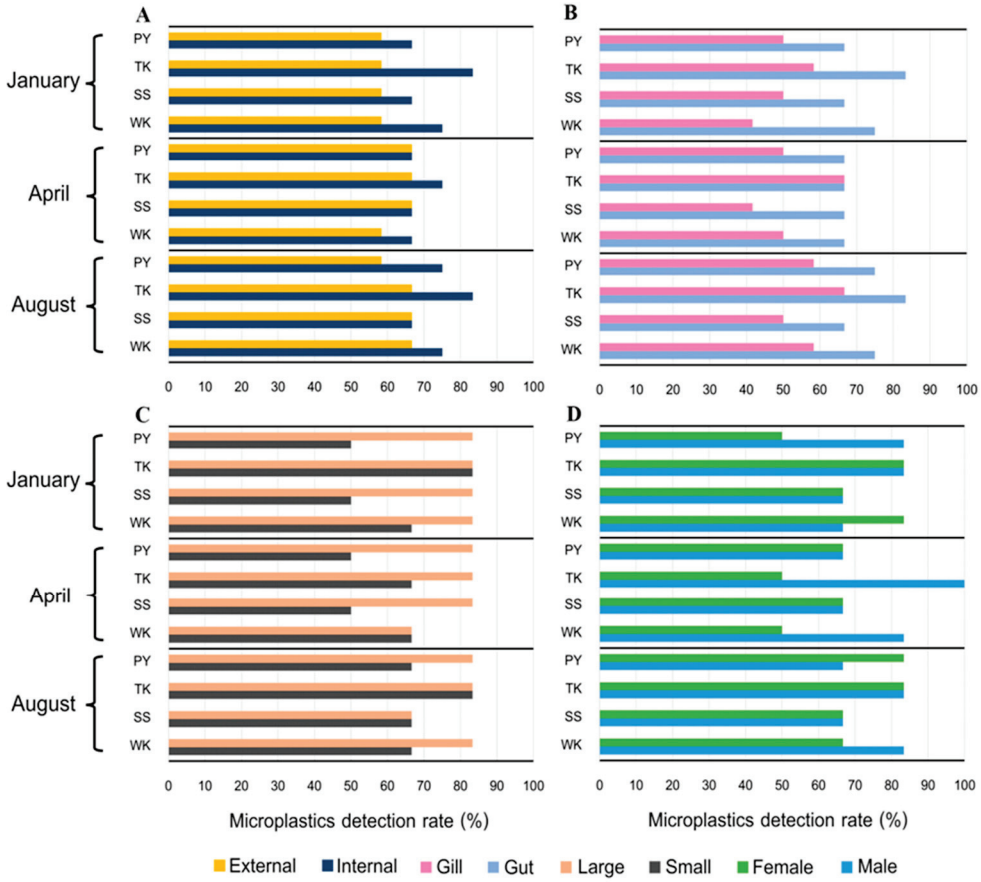

Figure 4. MP detection rate in blue swimming crab (%) in Rayong province categorized by (**A**) internal and external detection rate (%), (**B**) tissue (%), (**C**) size (%), and (**D**) sex in Rayong province: Phayun—PY, Takuan—TK, Suanson—SS, Wangkaew—WK.

3.4. Abundance of MPs

MP contamination in blue swimming crabs varied between internal and external samples, with 533 items found internally and 356 items found externally. The average abundance of MPs within the crabs ranged from 3.38 ± 2.45 to 8.63 ± 2.56 items/individual across all sampling sites and seasonal, and from 0.58 ± 0.41 to 1.70 ± 0.42 items/g wet weight for January, April, and August 2024 (Figure 5). For external contamination, the average abundance ranged from 2.00 ± 1.41 to 5.88 ± 2.70 items/individual over the same periods. The highest internal contamination was recorded at SS in August 2024, with an average of 8.63 ± 2.56 items/individual, while the lowest was found at PY in April 2024, with 3.38 ± 2.45 items/individual. Externally, the highest contamination was observed at WK in August 2024, with 5.88 ± 2.70 items/individual, and the lowest at PY in April 2024, with 2.00 ± 1.41 items/individual. PY is characterized by few beachside seafood restaurants, hotels, and small-scale fishing communities. On the other hand, TK is located near the Nam Hu canal within the industrial zone of Map Ta Phut Industrial Estate, with a densely populated area, and features beachside seafood restaurants, hotels, and small-scale fisheries communities. The SS site is located in a densely populated coastal community, where the mouth of the canal discharges land-based waste into the sea. In addition, this

area is a major tourist destination, with intensive recreational activities, and it also hosts a pier that serves as the main transit point for tourists traveling to Samed Island. These factors likely contribute to the high abundance of microplastic debris observed at this station. Although WK has some tourist activities, including hotels and beachside seafood restaurants similar to other sites, the residential area around WK is less densely populated than SS. These varying environmental conditions, levels of anthropogenic activities, tourist activities from shore [44], and fishing activities around fishing grounds could influence the extent of MP contamination in blue swimming crabs. However, a spatial distribution showed no significant differences in MP contamination between sampling sites. In contrast, the seasonal variation was found to be significant, with the highest contamination in August for both internal and external samples (Kruskal–Wallis, $p < 0.05$). The season also plays a critical role in MP abundance. These differences could be attributed to several factors, including the variations in fishing activity, water currents, and weather patterns in each sampling time that affect the abundance and breakdown of plastic debris and fishing gear. During August 2024, which represents the wet season or southwest monsoon, with a high rainfall and runoff, more MP debris from terrestrial areas might be washed into nearby rivers, increasing MPs concentrations, then flow out into the ocean [14]. When compared to other studies, our study's results were higher than *P. pelagicus* from Chonburi province, Thailand (0.72 items/individual) [37], *Portunus trituberculatus* from Liaohe Estuary, China (1.33 items/individual) [45], *Panopeus herbsti* from the Indian River Lagoon system, USA (4.2 items/individual) [46], *Carcinus aestuarii* from the Northern Adriatic coast, Italy (1.1 ± 0.7 items/individual) [47], and *Emerita analoga* from the Beaches of California, USA (1.39 ± 0.79 items/individual) [48], and, in terms of items/g wet weight, *Portunus sanguinolentus* from Gujarat state, India (0.67 ± 0.62 items/g wet weight) [49].

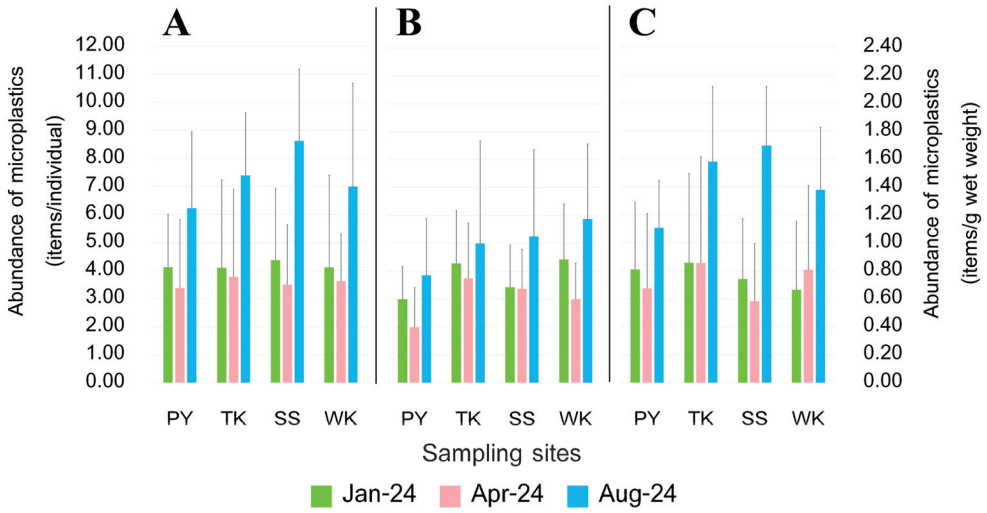

Figure 5. Average abundance of MP contamination of *P. pelagicus*: (**A**) internal contamination in terms of items/individual, (**B**) external contamination in terms of items/individual, and (**C**) internal contamination in terms of items/g wet weight along Rayong province: Phayun—PY, Takuan—TK, Suanson—SS, Wangkaew—WK.

3.4.1. Crab Tissue

MP contamination can expose organisms in four main ways: direct contact, ingestion, inhalation, and entanglement [50]. MPs were found in the gut and gill of crabs, with no contamination detected in the hepatopancreas and muscle tissues (Figure 6A). The gut was the primary site of MP accumulation, accounting for 72.2% of the total contamination, while gill tissue contributed 27.8%. The difference in MP contamination between the gut and gill tissues

was found to be significant (Kruskal–Wallis, $p < 0.05$), which indicates the gut plays a major role in MP ingestion and retention. Similarly to previous studies, MPs in *P. sanguinolentus* [49] and *Carcinus maenas* [51] were recorded to be higher in guts than in gills. The role of the gut in processing food makes it a likely location for the accumulation of ingested MPs. Moreover, crabs use their claws to break fishing nets to free themselves. Many of these severed lines, which are fiber and net, can be ingested by crabs and enter their digestive system [43]. In contrast, the gill showed less accumulation. The primary function of the gill is respiration by water flowed through their body, which might make it less prone to high levels of MP accumulation compared to the gut. The absence of MPs in the hepatopancreas and muscle tissues indicates that these organs are less involved in the direct processing and accumulation, and translocate effectively from the gut to these tissues.

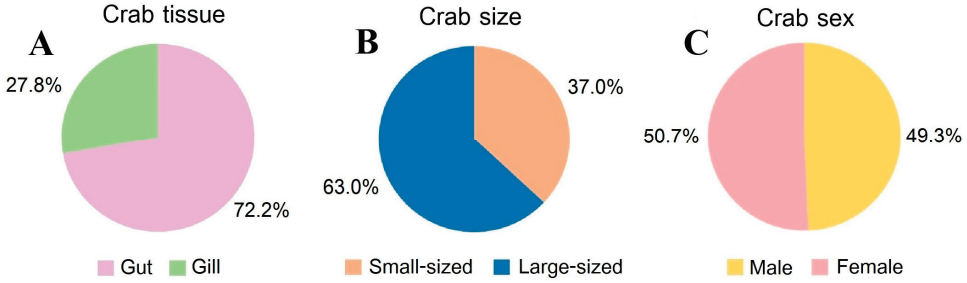

Figure 6. Internal composition of MP contamination in *P. pelagicus* categorized by (**A**) tissue (%), (**B**) size (%), and (**C**) sex (%) in Rayong province.

3.4.2. Crab Size

An analysis of crabs by size revealed a significant disparity in MP contamination between small and large crabs. Small crabs accounted for 37.0% of the contamination, whereas large crabs made up 63.0% (Figure 6B). This difference was significant across all sampling sites and seasons (Kruskal–Wallis, $p < 0.05$), indicating that larger crabs are more likely to have higher levels of MP contamination. According to a previous study, the size of *P. pelagicus* was found to have a small correlation to the abundance of MPs in their digestive tract [52]. However, our result shows a high Spearman's rank correlation between crab size and the abundance of MPs that are contaminated in the internal body (rs = 0.434, $p < 0.01$) and external body (rs = 0.724, $p < 0.01$). This might be due to larger crabs having a greater food intake and feeding activity when compared to smaller crabs. Crabs require food to retain their metabolic demands in their body [53], which, consequently, increases their exposure to MPs in their habitat and environment.

3.4.3. Crab Sex

When comparing male and female crabs, MPs were contaminated in females at a slightly higher rate than males, 49.3% in males and 50.7% in females (Figure 6C), with no significant difference in MP contamination between sexes across any sampling sites or seasons, which indicates that sex does not play a significant role in the differential accumulation of MPs. However, in a previous study in *P. pelagicus*, female crabs were also found to be slightly more contaminated than males [37], in contrast to MPs in *P. sanguinolentus*, which were found to be higher in males than in females [49]. The sex of crab samples and MP contamination with long-term effects in their internal tissue might be studied further in the future. As a result, the size and tissue parts are more critical in determining the levels of contamination rather than sex-specific differences.

3.5. Characteristics of MPs

3.5.1. MP Size

Our study highlights that MPs in *P. pelagicus* are predominantly larger in size, particularly those ranging between 330–5000 μm, which were consistently the most common across all seasons and sampling sites. This size category was notably more prevalent in internal contamination, especially in the gut, reflecting that larger MPs are more frequently ingested by crabs, as larger particles might be less likely to degrade or be filtered out of the digestive tract. Their prevalence in internal contamination indicates these MPs are effectively ingested and retained within the digestive systems of blue swimming crabs. While compared to external contamination, MPs sized 150–330 μm were more frequent, with the exception of SS, where smaller MPs (15–150 μm) were predominant (Figure 7). Seasonal variations in MP size distribution were observed, with larger MPs being more common in April, while MPs sized 150–330 μm were more prevalent in January and August. This variation might be influenced by seasonal changes in MP sources, such as an increased runoff during rainy seasons, and waste management, which could introduce different sizes of MPs into the environment. Site-specific trends showed that larger MPs were dominant in internal contamination across all sites, while external contamination varied, with different sites showing preferences for either smaller or larger MPs. A tissue analysis revealed that the gut primarily accumulated larger MPs (330–5000 μm), while the gills had a higher proportion of MPs sized 150–330 μm (Figure 8). This indicates that different tissues filter and retain MPs differently. The gut has a larger capacity for holding MPs, and its role in digestion could explain the accumulation of larger particles, while gills are involved in filtering water for respiration, and it may capture smaller MPs more effectively. This disparity seems to be linked to the anatomical position of the gill within the crabs and their pathway for gas exchange occurring by seawater flow through their narrow openings. This structure might prevent larger plastic particles from entering their gills [54]. According to a previous study, the size of MPs was found to be higher than *P. pelagicus* from 100–200 μm [55]. Additionally, the size of MPs in the internal body, especially in the range of 330–5000 μm ($r = 0.506$, $p < 0.01$) and 150–330 μm ($r = 0.392$, $p < 0.01$), was found to be related to size of the crabs, with larger crabs accumulating larger MPs and smaller crabs containing a lower composition of large-sized MPs. This could be due to larger crabs having a broader feeding range and being exposed to different environmental conditions compared to smaller crabs. It also underscores how MPs of different sizes may be selectively ingested and retained based on the size of the organism. However, the size composition of MPs between male and female crabs did not show significant differences.

3.5.2. MP Shape

Our study revealed that MPs in *P. pelagicus* were primarily found in four shapes: fibers, fragments, films, and nets (Figure 9). Fibers were the most prevalent type of MPs, observed in both internal and external contamination across all seasons, with a significantly higher abundance (Kruskal–Wallis, $p < 0.05$) compared to other shapes, accounting for 38.5% to 52.1% of internal MPs and 44.5% to 58.1% of external MPs (Figure 10). The net type was found in the second highest abundance, especially from the internal body, at 23.2% to 40.4% across all seasons, highlighting its dominance and indicating that fibers and nets were major components of MP pollution in *P. pelagicus*. The high contamination across sampling times and sampling sites indicates a widespread source of fiber contamination. Fibers are often associated with textiles, fishing gear, and industrial processes. The presence of fibers could be linked to common sources such as marine litter from fishing activities [56] and the breakdown of synthetic textiles from households [57]. Nets were predominantly

found in the internal body, with a significantly higher abundance than the external body. In contrast, fragments were more frequently found externally, significantly higher compared to internal contamination. Films were found at a lower amount, showing similar abundance in both internal and external bodies. A sampling site analysis showed that fibers were the dominant shape at all sampling stations. PY had a high fiber prevalence in both internal and external contamination, while TK exhibited a higher proportion of nets internally and fragments externally. SS showed external contamination was predominantly fragments, while WK also had a high prevalence of fibers.

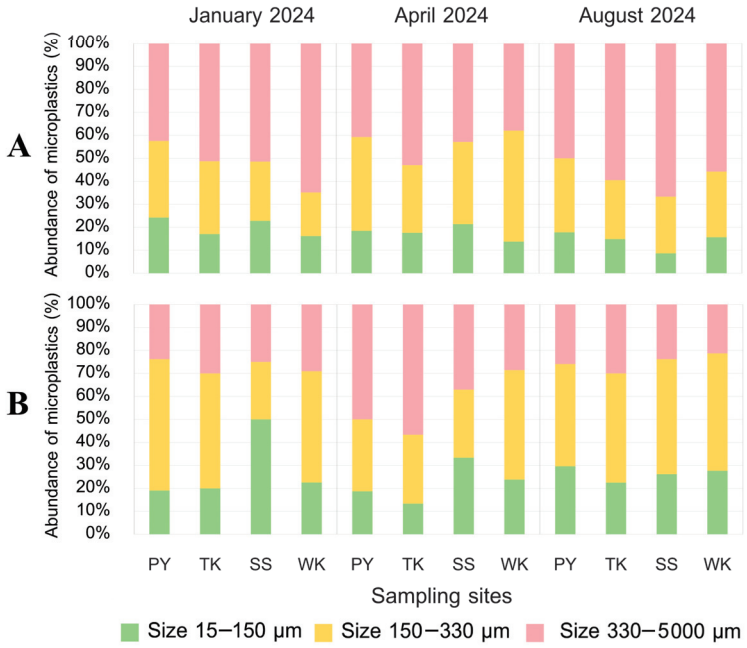

Figure 7. Composition of MP size range (%) (**A**) internally and (**B**) externally along Rayong province: Phayun—PY, Takuan—TK, Suanson—SS, Wangkaew—WK.

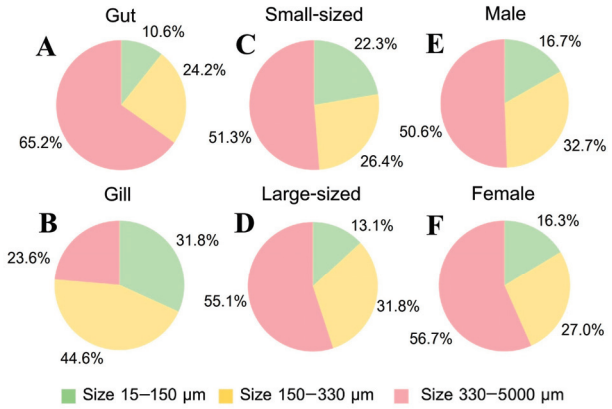

Figure 8. Size composition of MP internal contamination (%) in (**A**) gut and (**B**) gill of *P. pelagicus;* and (**C**) small-sized, (**D**) large-sized, (**E**) male, and (**F**) female *P. pelagicus* in Rayong province.

The shape of MPs did not significantly vary with the size and sex of the crabs, indicating size and sex are not major factors influencing MP shape distribution. However, within tissues, fibers were the most dominant type in gills, while nets were the most dominant type in guts, with significant differences in their proportions compared to other shapes. There was a higher prevalence of nets and fibers in the gut (45.5% and 37.1%) and a high proportion of fiber and fragments in the gills (58.1% and 29.7%) (Figure 11). A variety of MP

shapes show the disintegration of larger plastic debris into smaller particles within marine environments [58]. According to the results, the composition of MPs revealed that fibers were mostly prevalent, followed by net and films. This pattern of dominance by fibers was also observed in the environmental area along the coast of Rayong province [15,39]. Similarly, for *Carcinus aestuarii*, fiber was also found to be the dominant shape in the body [47]. On the other hand, fragments were the most common MP shape found in *P. armatus* [59]. Furthermore, for other marine fauna such as fishes from the Baltic Sea, we found MPs accumulated in the digestive tract and gills, with fiber being the most prevalent among the other forms [60]. This indicates that synthetic microfibers are widely contaminated in aquatic animals across various habitats and feeding strategies which can pose risks to the food chain, and to high-trophic-level organisms [61].

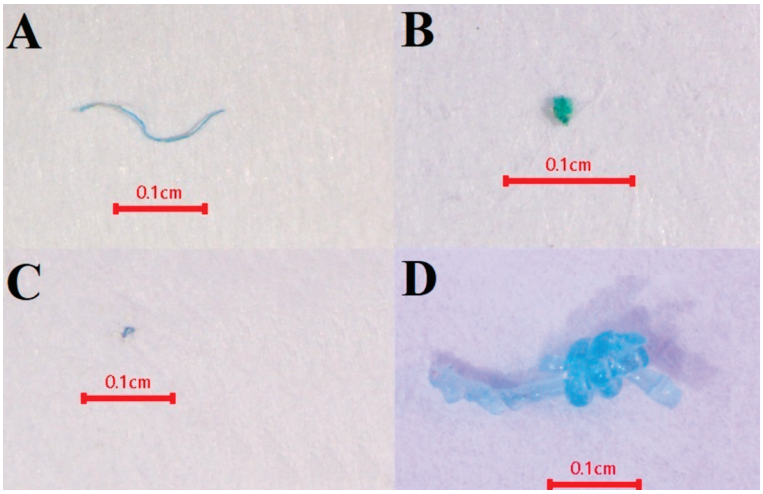

Figure 9. Shape of MPs: (**A**) fiber, (**B**) fragment, (**C**) film, and (**D**) net.

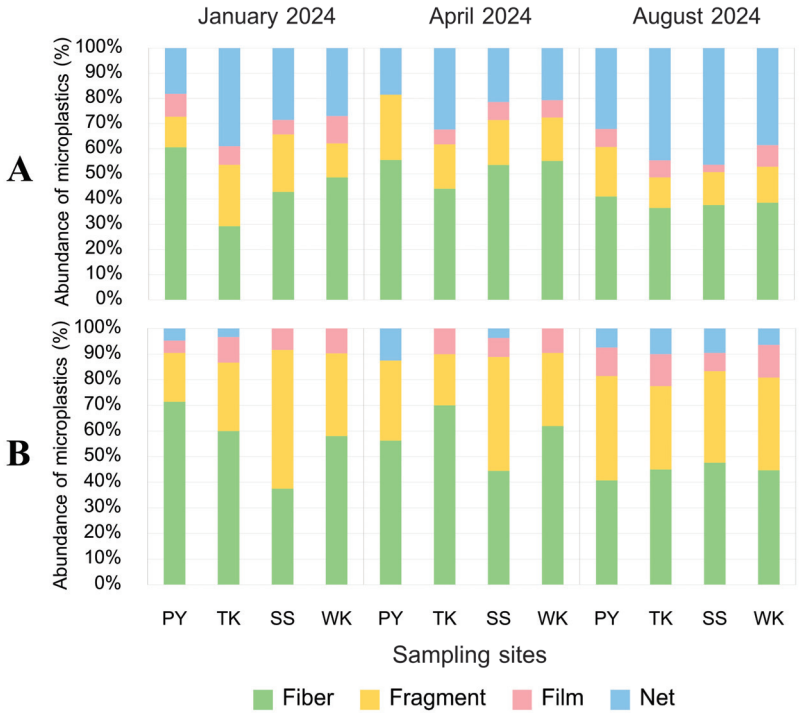

Figure 10. Shape composition of MPs (%) (**A**) internally and (**B**) externally along Rayong province: Phayun—PY, Takuan—TK, Suanson—SS, Wangkaew—WK.

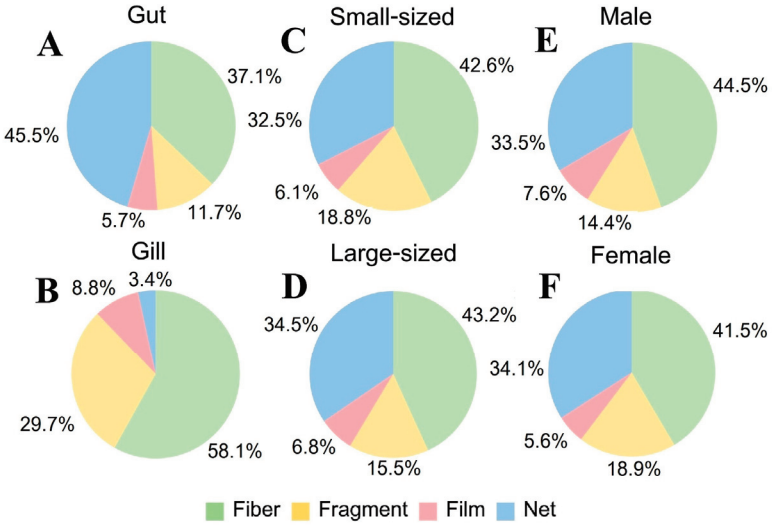

Figure 11. Shape composition of MPs from internal contamination (%) in (**A**) gut and (**B**) gill of *P. pelagicus*, and (**C**) small-sized, (**D**) large-sized, (**E**) male, and (**F**) female *P. pelagicus* in Rayong province.

3.5.3. MP Color

Our study indicates that four colors, black, blue, red, and green, along with clear MPs were detected in the MP samples (Figure 12), with blue MPs being the most prevalent. Blue MPs were consistently found in *P. pelagicus* across all seasons and sampling sites, both internally and externally (Kruskal–Wallis, $p < 0.05$), which related to the shape distribution, with fiber and net shape having significant internal contamination percentages in January, April, and August 2024. Black MPs were found exclusively in fiber shapes, while red and green MPs appeared in both fiber and fragment shapes. Clear MPs were mainly detected as fibers. Analyzing by sampling sites, blue MPs dominated the internal and external contamination at all sites. At Phayun station, blue MPs were the most abundant, followed by black, green, red, and clear internally, while red MPs were the second most common externally, followed by black, green, and clear. Takuan station showed a similar dominance of blue MPs, with black MPs being the second most common both internally and externally (Figure 13). Suanson station also had blue MPs as the most prevalent, followed by black and red internally, while red was the second most common externally. Wangkaew station exhibited blue MPs as the most common internally, followed by black, red, green, and clear, whereas red MPs were the most abundant externally, followed by blue, black, green, and clear. In terms of tissue accumulation, blue MPs were the dominant group in the gut of *P. pelagicus*, followed by black, red, green, and clear. Similarly, in gills, blue MPs were the most common, followed by red, black, green, and clear (Figure 14). Our study did not find a significant relationship between the color of MPs and the size or sex of *P. pelagicus*. The shape of MPs was also linked to their color; blue MPs were mostly found in fiber shapes, while black and clear MPs were predominantly fibers. Red and green MPs appeared only in fibers and fragments. According to a previous study, crabs rely on their vision to identify their food, which might be affected by the size and color of these particles. Due to the characteristics of MPs that seem to be similar in size to sand and resemble the color of their prey, this may cause MPs to appear as prey and sand to crabs. Crabs may mistakenly take these particles, resulting in mistaken consumption [43]. The dominant blue MPs indicate that they might be originating from common marine activities such as fishing, where blue nets and ropes are frequently used, and also from terrestrial waste. Recent studies have demonstrated that blue plastics are a general color of plastic extensively incorporated into synthetic textiles in our daily lives [62]. Moreover, broken fishing nets from fishing

activities, which are usually made from blue fiber MPs, were mostly contaminated in the guts of organisms [56]. The presence of black, red, green, and clear MPs, though less prevalent, also points to various sources, including textile fibers, packaging materials, and other consumer products.

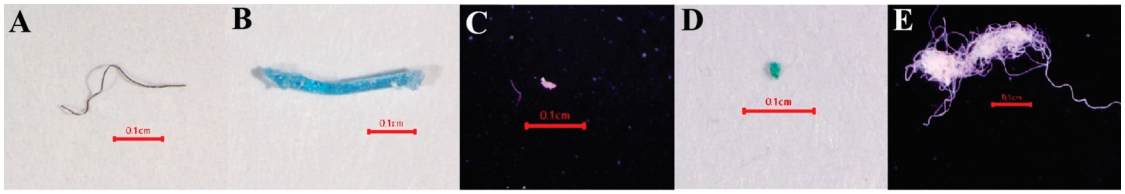

Figure 12. Color of MPs: (**A**) black, (**B**) blue, (**C**) red, (**D**) green, and (**E**) clear.

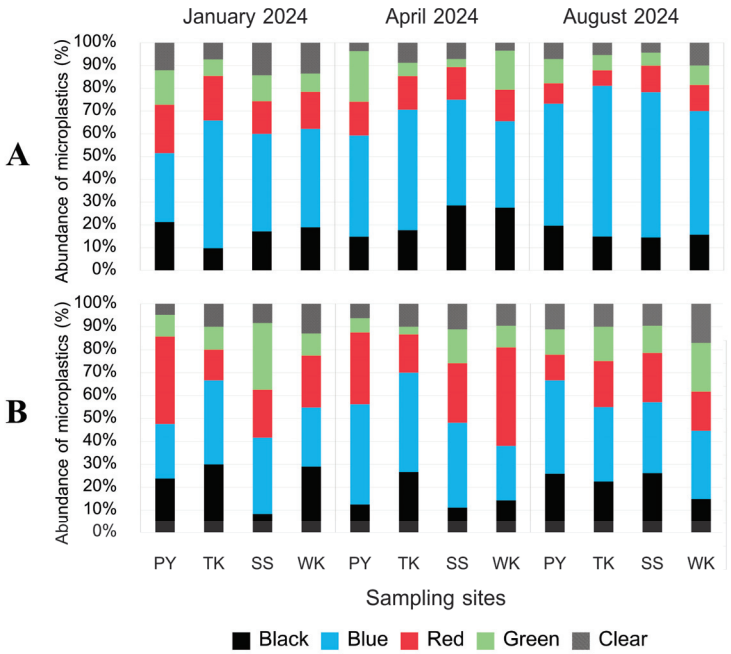

Figure 13. Color composition of MPs (%) (**A**) internally and (**B**) externally along Rayong province: Phayun—PY, Takuan—TK, Suanson—SS, Wangkaew—WK.

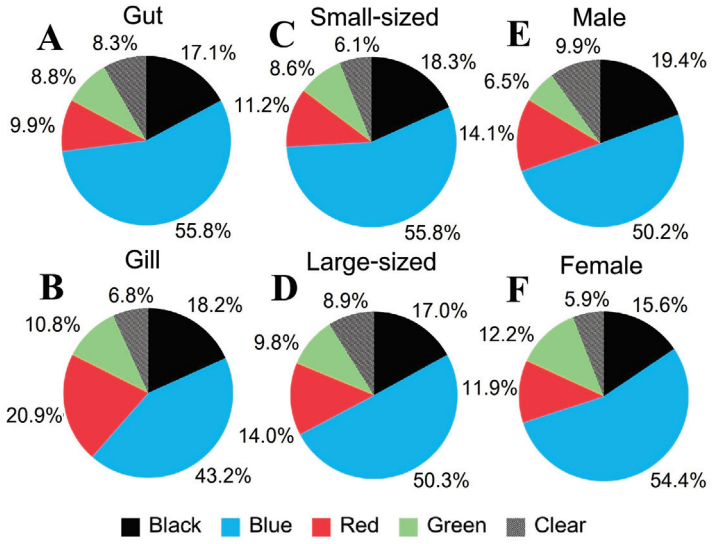

Figure 14. Color composition of MPs from internal contamination (%) in (**A**) gut and (**B**) gill of *P. pelagicus*, and (**C**) small-sized, (**D**) large-sized, (**E**) male, and (**F**) female *P. pelagicus* in Rayong province.

3.5.4. MP Polymer

The FTIR verification results identified seven types of MP polymers (Figure 15), showing a varied distribution across shapes, sampling sites, and tissues. Nylon was mainly found in net shapes, while PETG and PES were primarily found in fiber shapes (Figure 16). PE and PP appeared as fragments and fibers, and PS and AES were found mainly in fragments. These polymers were detected in both internal and external contamination, with distinct patterns at different sampling sites. At the PY site, PETG was the dominant polymer both internally and externally, followed by PES. TK had the highest internal contamination of nylon, while PETG dominated externally. The SS had PETG as the main internal contaminant, while PE was most prevalent externally. WK had PETG as the primary polymer for both internal and external contamination, with different second most abundant polymers for each. Significant differences in the polymer composition were found between the gut and gill tissues of *P. pelagicus*. Nylon was the most common in the gut, while PETG was predominant in the gills (Figure 17). The shape distribution revealed that fibers were mainly PETG and PES, followed by PP and a small proportion of PE, in various colors. Polystyrene and AES were found only in fragment shapes, while films were only PES, and nylon was only in net shapes. Cotton fibers were also detected but were not considered MPs. Nylons are widely used in fishing gear such as webbing nets and ropes for their strength and resistance [63,64], which was predominantly observed in net shapes. This indicates that fishing activities, especially from crab gillnets, are a significant source of nylon contamination in blue swimming crabs. Durable materials like nylon were used as webbing nets for crab gillnets, including the float line and sinker line, with polyethylene and polypropylene rope [40]. They were designed to withstand harsh coastal environments; their degradation over time can contribute to MPs pollution. Although it is a durable material, these monofilament gillnets have a short lifespan, averaging around 1 to 2 months [65].

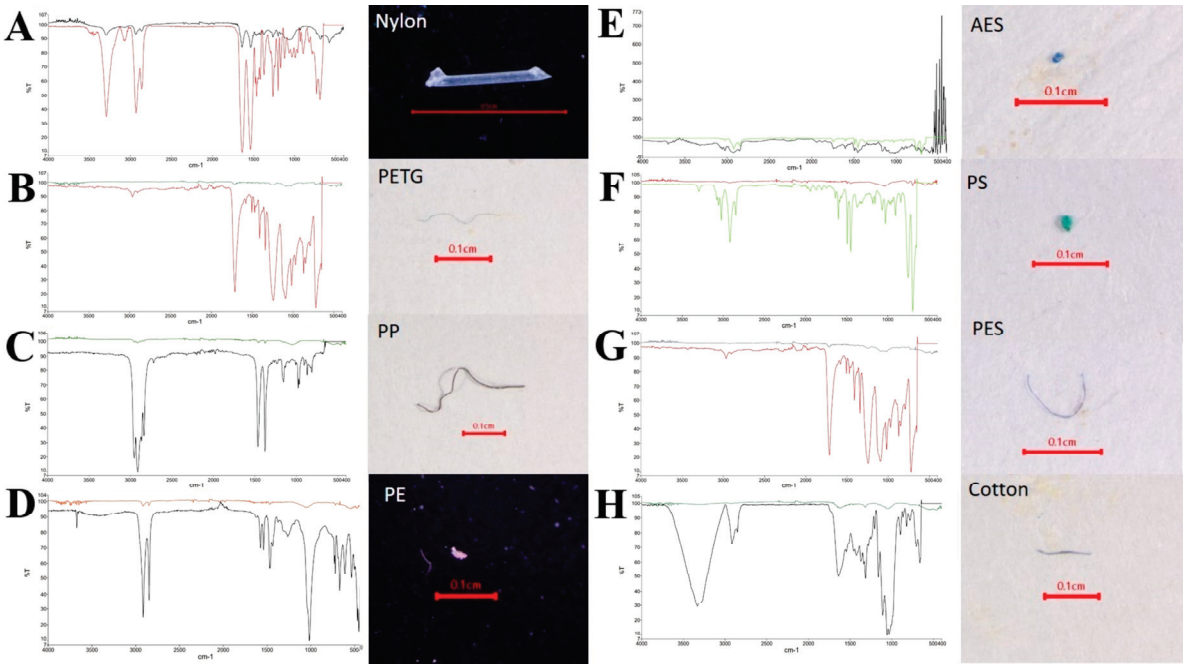

Figure 15. Polymer type of MPs in *P. pelagicus:* (**A**) nylon, (**B**) PETG, (**C**) PP, (**D**) PE, (**E**) AES, (**F**) PS, (**G**) PES, and (**H**) natural fiber—cotton.

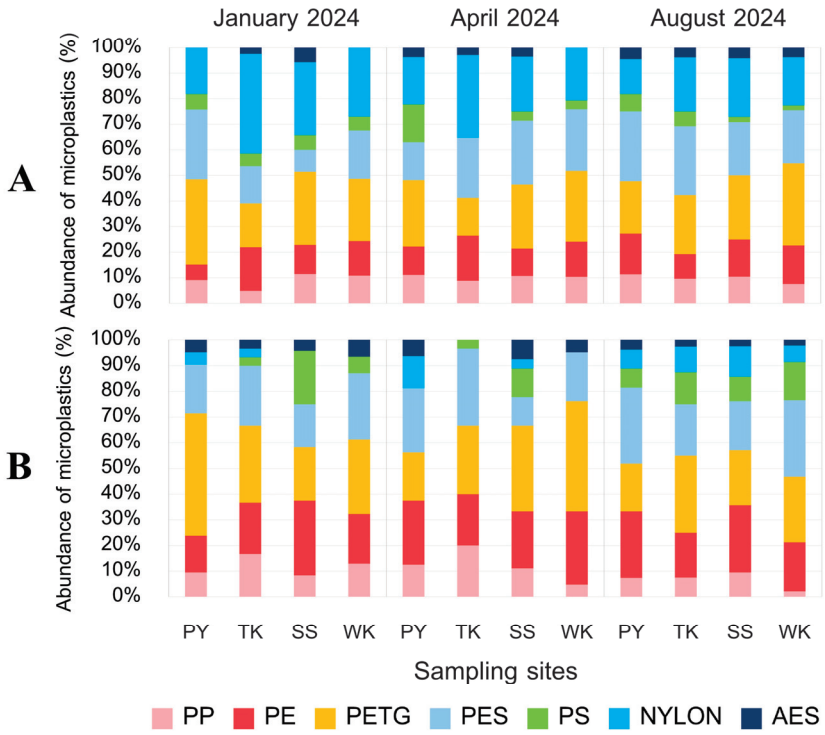

Figure 16. Polymer composition of MPs (%) (**A**) internally and (**B**) externally along Rayong province: Phayun—PY, Takuan—TK, Suanson—SS, Wangkaew—WK.

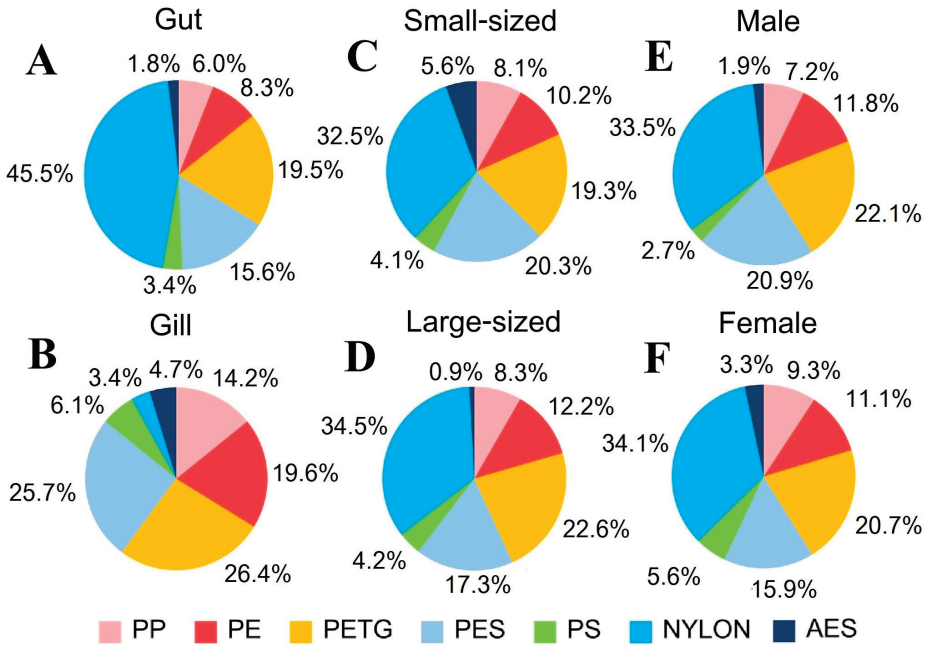

Figure 17. Polymer composition of MPs from internal contamination (%) in (**A**) gut and (**B**) gill of *P. pelagicus*, and (**C**) small-sized, (**D**) large-sized, (**E**) male, and (**F**) female *P. pelagicus* in Rayong province.

It means that they frequently need to be replaced. Broken gillnets and lines in contact with the harsh current during the southwest monsoon can release large amounts of MPs into the environment and these MPs can accumulate in organisms. The input of these MPs from damaged fishing gear will increase the load of MP debris, which exacerbates the contamination problem in the environment. PETG is a thermoplastic formed by polyethylene terephthalate (PET) and ethylene glycol with a high impact resistance and ductility,

which are commonly used in packaging, synthetic textiles, and various industrial applications [66], and also in 3D printing material [67], while polyester was mainly identified as fibers, pointing to sources like deteriorated textiles from household waste [68]. Polypropylene is often found in packaging and household products [69], while polyethylene is widely used in packaging items like shopping bags, plastic bottles, and containers with highly utilized materials in the industry [70,71]. These PE and PP polymers are also commonly used in the production of fishing nets [72], which are observed as both fragments and fibers. Meanwhile, polystyrene is used in domestic plastic products, which are usually used in disposable packaging [73,74], and poly (Acrylonitrile Ethylene Styrene) is used in automotive parts. These PS and AES polymers were primarily detected in the fragment shapes. Their presence indicates origins such as discarded packaging from terrestrial waste. Our study was limited by a lack of environmental samples, such as water and sediment from fishing ground areas, which could provide further insights and potentially clarify the MP situation in Rayong province. However, examining MPs from external biota could define these organisms as confronting the contamination of MPs in their environment. Our study was also limited by the small sample size at each sampling site (N = 12), with subgroup comparisons having only three individuals (N = 3). This low sample size may have reduced the statistical power. Future studies should aim for larger sample sizes to increase the statistical power and validate our findings. Although a hot needle test was performed on all visually identified particles to differentiate them from natural materials, the discriminative power of this method is still limited, and it only separated the plastic and non-plastic categories. Although identifying MP polymer types by FTIR was performed on 10% of total MPs in crab samples, a hot needle test might also assist in verifying MP types within the study. The subsampling uncertainty of all polymer levels was also described. A total of 99 MP particles (approximately 10%) were randomly selected and analyzed using FTIR to determine the polymer composition. To propagate the subsampling uncertainty into the overall dataset, nonparametric bootstrap resampling (5000 iterations) was applied to subsamples. The result indicated 95% confidence intervals (CIs) for polymer proportions were scaled to the total particle count observed microscopically. The extrapolation estimates are indicated in Table S1. Importantly, the reported counts for all polymers fell within the 95% confidence interval derived from the subsample analysis, confirming that the extrapolated estimates are consistent with the uncertainty associated with subsampling.

4. Conclusions

Microplastic contamination in blue swimming crabs (*Portunus pelagicus*) was consistently detected across all sampling stations, indicating that microplastics are widespread in the fishing grounds. Contamination was higher in internal organs than external surfaces, with the gut being the most affected tissue. Seasonal variation was evident, with the highest contamination observed in August 2024. Most of the detected microplastics were fibers, predominantly blue, with polyethylene terephthalate glycol, nylon, and polypropylene being the major polymers. Due to the separation procedure, which only used an NaCl solution, higher-density polymers will settle down to the bottom of the solution and could not be recovered. However, this procedure was adjusted by collecting the settled solution separately and filtering it, which could recover higher-density polymers like polyethylene terephthalate glycol and nylon in samples. These findings highlight that anthropogenic activities, including household wastewater rich in synthetic fibers and the use of nylon crab gillnets, are key contributors to microplastic contamination in this area. To mitigate this issue, efforts should focus on improving waste management practices, reducing fiber release from laundry, and developing more durable and eco-friendly fishing gear. Future

research should investigate the specific sources of microplastics at each site and assess their long-term impacts on marine organisms and ecosystems. Policy interventions and public awareness are also crucial to reducing plastic pollution and safeguarding marine biodiversity and food safety.

Supplementary Materials: The following supporting information can be downloaded at: https://www.mdpi.com/article/10.3390/toxics13100813/s1, Figure S1: Interview questionnaire form; Table S1: Summary of estimated polymer counts and proportions with 95% confidence intervals (CIs) propagated from subsampling uncertainty.

Author Contributions: Conceptualization, S.M.; field sampling, P.J. and C.R.; methodology, P.J.; investigation, P.J.; writing—original draft preparation, P.J. and C.R.; writing—review and editing, C.R. and P.K.; statistics, visualization, and supervision, S.M. All authors have read and agreed to the published version of the manuscript.

Funding: This research received no external funding.

Institutional Review Board Statement: As this is a study carried out with crabs obtained directly from the usual fishing process and no type of procedure has been carried out with them while they were alive, but, rather, they were analyzed directly once they had arrived at port and were already dead, the current regulations do not require permits.

Informed Consent Statement: Not applicable.

Data Availability Statement: The data will be made available upon request.

Acknowledgments: The authors would like to thank all members in the Rayong Fisheries Marine and Development Center, Fisheries Marine and Development Division, Department of Fisheries, Thailand and all members in the Combating Marine Debris Laboratory from the Department of Marine Science, Faculty of Fisheries, Kasetsart University, Thailand for their support during this research and for supporting the FTIR analysis, respectively.

Conflicts of Interest: The authors declare no conflicts of interest.

Abbreviations

The following abbreviations are used in this manuscript:

MPs	Microplastics
PY	The station is called “Payoon”
TK	The station is called “Takuan”
SS	The station is called “Suanson”
WK	The station is called “Wangkaew”
PP	Polypropylene
PE	Polyethylene
PETG	Polyethylene Terephthalate Glycol
PES	Polyester
PS	Polystyrene
AES	poly (Acrylonitrile Ethylene Styrene)

References

1. Jambeck, J.R.; Geyer, R.; Wilcox, C.; Siegler, T.R.; Perryman, M.; Andrady, A.; Law, K.L. Plastic waste inputs from land into the ocean. *Science* **2015**, *347*, 768–772. [CrossRef]
2. Thushari, G.G.N.; Chavanich, S.; Yakupitiyage, A. Coastal debris analysis in beaches of Chonburi Province, eastern of Thailand as implications for coastal conservation. *Mar. Pollut. Bull.* **2017**, *116*, 121–129. [CrossRef]
3. Andrady, A.L. Microplastics in the marine environment. *Mar. Pollut. Bull.* **2011**, *62*, 1596–1605. [CrossRef]

4. Reinert, T.R.; Spellman, A.C.; Bassett, B.L. Entanglement in and ingestion of fishing gear and other marine debris by Florida manatees, 1993 to 2012. *Endanger. Species Res.* **2017**, *32*, 415–427. [CrossRef]
5. Gall, S.C.; Thompson, R.C. The impact of debris on marine life. *Mar. Pollut. Bull.* **2015**, *92*, 170–179. [CrossRef] [PubMed]
6. Jang, Y.C.; Lee, J.; Hong, S.; Mok, J.Y.; Kim, K.S.; Lee, Y.J.; Choi, H.-W.; Kang, H.; Lee, S. Estimation of the annual flow and stock of marine debris in South Korea for management purposes. *Mar. Pollut. Bull.* **2014**, *86*, 505–511. [CrossRef]
7. Lebreton, L.C.M.; van der Zwet, J.; Damsteeg, J.-W.; Slat, B.; Andrady, A.; Reisser, J. River plastic emissions to the world's oceans. *Nat. Commun.* **2017**, *8*, 15611. [CrossRef] [PubMed]
8. Sterl, M.F.; Delandmeter, P.; van Sebille, E. Influence of barotropic tidal currents on transport and accumulation of floating microplastics in the global open ocean. *J. Geophys. Res. Oceans* **2020**, *125*, e2019JC015583. [CrossRef] [PubMed]
9. UNEP. *Marine Litter: A Global Challenge*; United Nations Environment Programme: Washington, DC, USA, 2009; 232p. Available online: https://www.unep.org/resources/report/marine-litter-global-challenge (accessed on 17 December 2024).
10. Eriksen, M.; Lebreton, L.C.M.; Carson, H.S.; Thiel, M.; Moore, C.J.; Borerro, J.C.; Galgani, F.; Ryan, P.G.; Reisser, J. Plastic pollution in the world's oceans: More than 5 trillion plastic pieces weighing over 250,000 tons afloat at sea. *PLoS ONE* **2014**, *9*, e111913. [CrossRef]
11. Moore, C.J. Synthetic polymers in the marine environment: A rapidly increasing, long-term threat. *Environ. Res.* **2008**, *108*, 131–139. [CrossRef]
12. Lusher, A.; Bråte, I.L.N.; Hurley, R.; Iversen, K.; Olsen, M. *Testing of Methodology for Measuring Microplastics in Blue Mussels (Mytilus spp.) and Sediments, and Recommendations for Future Monitoring of Microplastics (R & D-Project)*; Norsk Institutt for Vannforskning: Oslo, Norwegen, 2017; 87p. Available online: https://www.researchgate.net/publication/321724113_Testing_of_methodology_for_measuring_microplasti\relax$\protect\global\let\T1\textellipsis.\kern\fontdimen3\font.\kern\fontdimen3\font.\kern\fontdimen3\font\T1\textellipsis$ (accessed on 8 October 2024).
13. Thompson, R.; Olsen, Y.; Mitchell, R.; Davis, A.; Rowland, S.J.; John, A.W.G.; McGonigle, D.; Russell, A.E. Lost at sea: Where is all the plastic? *Science* **2004**, *304*, 838. [CrossRef]
14. Jendanklang, P.; Meksumpun, S.; Pokavanich, T.; Ruengsorn, C.; Kasamesiri, P. Distribution and flux assessment of microplastic debris in the middle and lower Chao Phraya River, Thailand. *J. Water Health* **2023**, *21*, 771–788. [CrossRef]
15. Prarat, P.; Hongsawat, P. Microplastic pollution in surface seawater and beach sand from the shore of Rayong province, Thailand: Distribution, characterization, and ecological risk assessment. *Mar. Pollut. Bull.* **2022**, *174*, 113200. [CrossRef]
16. Prarat, P.; Hongsawat, P.; Chouychai, B. Microplastic occurrence in surface sediments from coastal mangroves in Eastern Thailand: Abundance, characteristics, and ecological risk implications. *Reg. Stud. Mar. Sci.* **2024**, *71*, 103389. [CrossRef]
17. Chaisanguansuk, P.; Ploenbuppa, S.; Assawincharoenkij, T.; Phantuwongraj, S.; Jiraphinyakul, A. Microplastic contamination in the coastal environment: A case study from the Mae Klong River, Samut Songkhram. *App. Environ. Res.* **2023**, *45*, 2. [CrossRef]
18. Kashfi, F.S.; Ramavandi, B.; Arfaeinia, H.; Mohammadi, A.; Saeedi, R.; De-la-Torre, G.E.; Dobaradaran, S. Occurrence and exposure assessment of microplastics in indoor dusts of buildings with different applications in Bushehr and Shiraz cities, Iran. *Sci. Total Environ.* **2022**, *829*, 154651. [CrossRef] [PubMed]
19. Akhbarizadeh, R.; Dobaradaran, S.; Amouei Torkmahalleh, M.; Saeedi, R.; Aibaghi, R.; Faraji Ghasemi, F. Suspended fine particulate matter (PM2.5), microplastics (MPs), and polycyclic aromatic hydrocarbons (PAHs) in air: Their possible relationships and health implications. *Environ. Res.* **2021**, *192*, 110339. [CrossRef]
20. Yamchomchuen, S.; Meksumpun, S.; Ruengsorn, C.; Phaksopa, J. Contamination of microplastics in zooplankton: A case study in the coastal area Chonburi province. In *Proceedings of 61st Kasetsart University Annual Conference*; Kasetsart University Research and Development Institute: Bangkok, Thailand, 2023; pp. 154–163. Available online: https://annualconference.ku.ac.th/61/eproc/E-ProceedingKUConf61-1.pdf (accessed on 20 November 2024). (In Thai)
21. Steer, M.; Cole, M.; Thompson, R.C.; Lindeque, P.K. Microplastic ingestion in fish larvae in the western English Channel. *Environ. Pollut.* **2017**, *226*, 250–259. [CrossRef] [PubMed]
22. Hongsawat, P.; Thinjong, W.; Chouychai, B.; Punyapalakul, P.; Prarat, P. Microplastics in retail shellfish from a seafood market in eastern Thailand: Occurrence and risks to human food safety. *Mar. Pollut. Bull.* **2024**, *201*, 116228. [CrossRef] [PubMed]
23. Phaksopa, J.; Sukhsangchan, R.; Keawsang, R.; Tanapivattanakul, K.; Thamrongnawasawat, T.; Worachananant, S.; Sreesamran, P. Presence and characterization of microplastics in coastal fish around the Eastern Coast of Thailand. *Sustainability* **2021**, *13*, 13110. [CrossRef]
24. Kimura, R.; Inoguchi, E.; Kitayama, C.; Michishita, M.; Fujinuma, R. Microplastic ingestion by sea turtles around Tokyo Bay: Level of water pollution influences ingestion amounts. *Mar. Pollut. Bull.* **2024**, *206*, 116673. [CrossRef]
25. van Franeker, J.A.; Blaize, C.; Danielsen, J.; Fairclough, K.; Gollan, J.; Guse, N.; Hansen, P.L.; Heubeck, M.; Jensen, J.-K.; Le Guillou, G.; et al. Monitoring plastic ingestion by the northern fulmar *Fulmarus glacialis* in the North Sea. *Environ. Pollut.* **2011**, *159*, 2609–2615. [CrossRef]

26. Moore, R.C.; Loseto, L.; Noel, M.; Etemadifar, A.; Brewster, J.D.; MacPhee, S.; Bendell, L.; Ross, P.S. Microplastics in beluga whales (*Delphinapterus leucas*) from the eastern Beaufort Sea. *Mar. Pollut. Bull.* **2020**, *150*, 110723. [CrossRef]
27. Rochman, C.M.; Hoh, E.; Kurobe, T.; Teh, S.J. Ingested plastic transfers hazardous chemicals to fish and induces hepatic stress. *Sci. Rep.* **2013**, *3*, 3263. [CrossRef]
28. Jeong, E.; Lee, J.; Redwan, M. Animal exposure to microplastics and health effects: A review. *Emerg. Contam.* **2024**, *10*, 100369. [CrossRef]
29. Cverenkárová, K.; Valachovičová, M.; Macku'ak, T.; Žemlička, L.; Bírošová, L. Review microplastics in the food chain. *Life* **2021**, *11*, 1349. [CrossRef]
30. Cox, K.D.; Covernton, G.A.; Davies, H.L.; Dower, J.F.; Juanes, F.; Dudas, S.E. Human consumption of microplastics. *Environ. Sci. Technol.* **2019**, *53*, 7068–7074. [CrossRef] [PubMed]
31. Bhuyan, M.S. Effects of microplastics on fish and in human health. *Front. Environ. Sci.* **2022**, *10*, 827289. [CrossRef]
32. Yuan, Z.; Nag, R.; Cummins, E. Human health concerns regarding microplastics in the aquatic environment—From marine to food systems. *Sci. Total Environ.* **2022**, *823*, 153730. [CrossRef]
33. Kunsook, C.; Gajaseni, N.; Paphavasit, N. The feeding ecology of the blue swimming crab, *Portunus pelagicus* (Linnaeus, 1758), at Kung Krabaen Bay, Chanthaburi Province, Thailand. *Trop. Life Sci. Res.* **2014**, *25*, 13–27. Available online: https://pmc.ncbi.nlm.nih.gov/articles/PMC4156471/pdf/tlsr-25-1-13.pdf (accessed on 17 November 2024). [PubMed]
34. Lai, J.C.Y.; Ng, P.K.L.; Davie, P.J.F. A revision of the *Portunus pelagicus* (Linnaeus, 1758) species complex (Crustacea: Brachyura: Portunidae), with the recognition of four species. *Raffles Bull. Zool.* **2010**, *58*, 199–237. [CrossRef]
35. DOF. *Statistics of Marine Capture of Artisanal Fisheries 2023*; Department of Fisheries, Ministry of Agriculture and Cooperatives: Bangkok, Thailand, 2024; 143p. Available online: https://www4.fisheries.go.th/local/file_document/20240614145556_new.pdf (accessed on 20 October 2024).
36. Chanchiem, T.; Boutson, A.; Kaewnern, M.; Ebata, K.; Arimoto, T. Study on Bycatch and Discards of Bottom Crab Gillnet Targeting Blue Swimming Crab (*Portunus pelagicus*) in Rayong Province, Thailand. SEAFDEC Technical Seminar 2015. Available online: https://repository.seafdec.or.th/bitstream/handle/20.500.12067/1383/4_Thaweesak%28KU%29-Study%20of%20bycatch_crab%20gillnet.pdf?sequence=1&isAllowed=y (accessed on 20 December 2024).
37. Kleawkla, N. Microplastic Fragments in Stomach Content of Blue Swimming Crab, *Portunus pelagicus* from Wonnapha Coastal Wetland, Chonburi Province, Thailand. *Ramkhamhaeng Int. J. Sci. Technol.* **2019**, *2*, 7–16. Available online: https://ph02.tci-thaijo.org/index.php/RIST/article/view/244995 (accessed on 15 December 2024).
38. Jittalerk, R.; Babel, S. Microplastic Contamination in Thai Vinegar Crabs (*Episesarma mederi*), Giant Mudskippers (*Periophthalmodon schlosseri*), and Their Surrounding Environment from the Bang Pu Mangrove Forests, Samut Prakan Province, Thailand. *Mar. Pollut. Bull.* **2024**, *198*, 115849. [CrossRef] [PubMed]
39. Bissen, R.; Chawchai, S. Microplastics on Beaches along the Eastern Gulf of Thailand—A Preliminary Study. *Mar. Pollut. Bull.* **2020**, *157*, 111345. [CrossRef]
40. Boutson, A.; Ebata, K.; Ishikawa, S.; Watanabe, K.; Arimoto, T. *Field Guides on Small-Scale Fisheries in Rayong, Thailand*; Research Institute for Humanity and Nature: Kyoto, Japan, 2016; 73p. Available online: https://www.chikyu.ac.jp/rihn/publicity/detail/184/ (accessed on 16 October 2024).
41. Masura, J.; Baker, J.; Foster, G.; Arthur, C. *Laboratory Methods for the Analysis of Microplastics in the Marine Environment: Recommendations for Quantifying Synthetic Particles in Waters and Sediments*; NOAA Technical Memorandum NOS-OR&R-48; NOAA Institutional Repository: Silver Spring, MD, USA, 2015; 31p. [CrossRef]
42. De Witte, B.; Devriese, L.; Bekaert, K.; Hoffman, S.; Vandermeersch, G.; Cooreman, K.; Robbens, J. Quality Assessment of the Blue Mussel (*Mytilus edulis*): Comparison Between Commercial and Wild Types. *Mar. Pollut. Bull.* **2014**, *85*, 146–155. [CrossRef]
43. Zhang, T.; Sun, Y.; Song, K.; Du, W.; Huang, W.; Gu, Z.; Feng, Z. Microplastics in Different Tissues of Wild Crabs at Three Important Fishing Grounds in China. *Chemosphere* **2021**, *271*, 129479. [CrossRef]
44. Cordova, M.R.; Purwiyanto, A.I.S.; Suteja, Y. Abundance and Characteristics of Microplastics in the Northern Coastal Waters of Surabaya, Indonesia. *Mar. Pollut. Bull.* **2019**, *142*, 183–188. [CrossRef]
45. Wang, F.; Wu, H.; Wu, W.; Wang, L.; Liu, J.; An, L.; Xu, Q. Microplastic Characteristics in Organisms of Different Trophic Levels from Liaohe Estuary, China. *Sci. Total Environ.* **2021**, *789*, 148027. [CrossRef]
46. Waite, H.R.; Donnelly, M.J.; Walters, L.J. Quantity and Types of Microplastics in the Organic Tissues of the Eastern Oyster *Crassostrea virginica* and Atlantic Mud Crab *Panopeus herbstii* from a Florida Estuary. *Mar. Pollut. Bull.* **2018**, *129*, 179–185. [CrossRef]
47. Piarulli, S.; Scapinello, S.; Comandini, P.; Magnusson, K.; Granberg, M.; Wong, J.X.; Sciutto, G.; Prati, S.; Mazzeo, R.; Booth, A.M.; et al. Microplastic in Wild Populations of the Omnivorous Crab *Carcinus aestuarii*: A Review and a Regional-Scale Test of Extraction Methods, Including Microfibres. *Environ. Pollut.* **2019**, *251*, 117–127. [CrossRef]

48. Horn, D.; Miller, M.; Anderson, S.; Steele, C. Microplastics are Ubiquitous on California Beaches and Enter the Coastal Food Web through Consumption by Pacific Mole Crabs. *Mar. Pollut. Bull.* **2019**, *139*, 231–237. [CrossRef]
49. Rabari, V.; Patel, H.; Ali, D.; Yadav, V.K.; Patel, A.; Sahoo, D.K.; Trivedi, J. Ingestion and Polymeric Risk Assessment of Microplastic Contamination in Commercially Important Brachyuran Crab *Portunus sanguinolentus*. *Front. Mar. Sci.* **2023**, *10*, 1286782. [CrossRef]
50. Sucharitakul, P.; Wu, W.M.; Zhang, Y.; Peng, B.Y.; Gao, J.; Wang, L.; Hou, D. Exposure Pathways and Toxicity of Microplastics in Terrestrial Insects. *Environ. Sci. Technol.* **2024**, *58*, 11887–11900. [CrossRef] [PubMed]
51. Watts, A.J.; Lewis, C.; Goodhead, R.M.; Beckett, S.J.; Moger, J.; Tyler, C.R. Uptake and Retention of Microplastics by the Shore Crab *Carcinus maenas*. *Environ. Sci. Technol.* **2014**, *48*, 8823–8830. [CrossRef]
52. Astutik, S.; Abida, I.W. Microplastics in the Gastrointestinal Tract of Blue Crab (*Portunus pelagicus*) Caught by Bandaran, Bangkalan Fishermen at Different Sizes. *Symp. Biol. Educ.* **2023**, *3*, 87–94. [CrossRef]
53. Griffen, B.D. Metabolic Costs of Capital Energy Storage in a Small-Bodied Ectotherm. *Ecol. Evol.* **2017**, *7*, 2423–2431. [CrossRef] [PubMed]
54. Bauer, R.T. Decapod Crustacean Grooming: Functional Morphology, Adaptive Value, and Phylogenetic Significance. In *Functional Morphology of Feeding and Grooming in Crustaceans*; Felgenhaur, B.E., Walting, L., Thistle, A.B., Eds.; A.A. Balkema: Rotterdam, The Netherlands, 1989; pp. 49–58. Available online: https://research.nhm.org/pdfs/31534/31534.pdf (accessed on 12 December 2024).
55. Daniel, D.B.; Ashraf, P.M.; Thomas, S.N. Abundance, Characteristics, and Seasonal Variation of Microplastics in Indian White Shrimps (*Fenneropenaeus indicus*) from Coastal Waters off Cochin, Kerala, India. *Sci. Total Environ.* **2020**, *737*, 139839. [CrossRef]
56. Kasamesiri, P.; Meksumpun, C.; Meksumpun, S.; Ruengsorn, C. Assessment on Microplastics Contamination in Freshwater Fish: A Case Study of the Ubolratana Reservoir, Thailand. *GEOMATE J.* **2021**, *20*, 62–68. [CrossRef]
57. De Falco, F.; Di Pace, E.; Cocca, M. The Contribution of Washing Processes of Synthetic Clothes to Microplastic Pollution. *Sci. Rep.* **2019**, *9*, 6633. [CrossRef]
58. Sathish, N.; Jeyasanta, K.I.; Patterson, J. Abundance, Characteristics and Surface Degradation Features of Microplastics in Beach Sediments of Five Coastal Areas in Tamil Nadu, India. *Mar. Pollut. Bull.* **2019**, *142*, 112–118. [CrossRef]
59. Akhbarizadeh, R.; Moore, F.; Keshavarzi, B. Investigating Microplastics Bioaccumulation and Biomagnification in Seafood from the Persian Gulf: A Threat to Human Health? *Food Addit. Contam.* **2019**, *36*, 1696–1708. [CrossRef]
60. Piskuła, P.; Astel, A.M. Microplastics in Commercial Fishes and By-Catch from Selected FAO Major Fishing Areas of the Southern Baltic Sea. *Animals* **2023**, *13*, 458. [CrossRef]
61. Santonicola, S.; Volgare, M.; Cocca, M.; Dorigato, G.; Giaccone, V.; Colavita, G. Impact of Fibrous Microplastic Pollution on Commercial Seafood and Consumer Health: A Review. *Animals* **2023**, *13*, 1736. [CrossRef]
62. Chinfak, N.; Sompongchaiyakul, P.; Charoenpong, C.; Shi, H.; Yeemin, T.; Zhang, J. Abundance, Composition, and Fate of Microplastics in Water, Sediment, and Shellfish in the Tapi-Phumduang River System and Bandon Bay, Thailand. *Sci. Total Environ.* **2021**, *781*, 146700. [CrossRef] [PubMed]
63. Cerbule, K.; Herrmann, B.; Grimaldo, E.; Brinkhof, J.; Manu, B.S.; Larsen, R.B.; Bak-Jensen, Z. Ghost Fishing Efficiency by Lost, Abandoned or Discarded Pots in Snow Crab (*Chionoecetes opilio*) Fishery. *Mar. Pollut. Bull.* **2023**, *193*, 115249. [CrossRef] [PubMed]
64. Orasutthikul, S.; Unno, D.; Yokota, H. Effectiveness of Recycled Nylon Fiber from Waste Fishing Net with Respect to Fiber Reinforced Mortar. *Constr. Build. Mater.* **2017**, *146*, 594–602. [CrossRef]
65. Masthawee, P.; Chokesanguan, B.; Pornpatimakorn, S. *Study on Monofilament and Multifilament Crab Bottom Gill Net*; Southeast Asian Fisheries Development Center, Training Department: Bangkok, Thailand, 1986, Available online: https://repository.seafdec.or.th/bitstream/handle/20.500.12067/223/TDRES10_Crab_BGN.PDF?sequence=1&isAllowed=y (accessed on 11 November 2024).
66. Sipe, J.M.; Bossa, N.; Berger, W.; von Windheim, N.; Gall, K.; Wiesner, M.R. From Bottle to Microplastics: Can We Estimate How Our Plastic Products Are Breaking Down? *Sci. Total Environ.* **2022**, *814*, 152460. [CrossRef] [PubMed]
67. Guessasma, S.; Belhabib, S.; Nouri, H. Printability and Tensile Performance of 3D Printed Polyethylene Terephthalate Glycol Using Fused Deposition Modelling. *Polymers* **2019**, *11*, 1220. [CrossRef]
68. Yang, T.; Luo, J.; Nowack, B. Characterization of Nanoplastics, Fibrils, and Microplastics Released During Washing and Abrasion of Polyester Textiles. *Environ. Sci. Technol.* **2021**, *55*, 15873–15881. [CrossRef]
69. Alsabri, A.; Tahir, F.; Al-Ghamdi, S.G. Environmental Impacts of Polypropylene (PP) Production and Prospects of Its Recycling in the GCC Region. *Mater. Today Proc.* **2022**, *56*, 2245–2251. [CrossRef]
70. Romani, V.P.; Martins, V.G.; Goddard, J.M. Radical Scavenging Polyethylene Films as Antioxidant Active Packaging Materials. *Food Control* **2020**, *109*, 106946. [CrossRef]
71. Ronca, S. *Polyethylene. Brydson's Plastics Materials*, 8th ed.; Gilbert, M., Ed.; Butterworth-Heinemann: Oxford, UK, 2017; pp. 247–278. [CrossRef]

72. Deshpande, P.C.; Philis, G.; Brattebø, H.; Fet, A.M. Using Material Flow Analysis (MFA) to generate the evidence on plastic waste management from commercial fishing gears in Norway. *Resour. Conserv. Recycl. Adv.* **2020**, *5*, 100024. [CrossRef]
73. Arfin, T.; Mohammad, F.; Yusof, N.A. Applications of polystyrene and its role as a base in industrial chemistry. In *Polystyrene: Synthesis, Characteristics and Applications*; Lynwood, C., Ed.; Nova Science Publishers, Inc.: New York, NY, USA, 2014; pp. 269–280. Available online: http://repo.upertis.ac.id/1928/1/%28Chemistry%20Research%20and%20Applications%29%20Cole%20Lynwood-Polystyrene_%20Synthesis%2C%20Characteristics%20and%20Applications-Nova%20Science%20Pub%20Inc%20%282014%29.pdf (accessed on 22 December 2024).
74. Wang, J.; Lee, J.; Kwon, E.E.; Jeong, S. Quantitative analysis of polystyrene microplastic and styrene monomer released from plastic food containers. *Heliyon* **2023**, *9*, e15787. [CrossRef] [PubMed]

toxics

MDPI

Article

Toxic Effects of Lead Exposure on Freshwater Climbing Perch, *Anabas testudineus*, and Bioremediation Using *Ocimum sanctum* Leaf Powder

Nimai Chandra Saha [1,*], Arnab Chatterjee [2], Priyajit Banerjee [3], Ritwick Bhattacharya [2], Auroshree Sadhu [2], Paolo Pastorino [4,*] and Shubhajit Saha [2]

[1] Department of Zoology, Bidhannagar College, Bidhannagar, Kolkata 700064, West Bengal, India
[2] Ecotoxicology Research Laboratory, Department of Zoology, The University of Burdwan, Burdwan 713104, West Bengal, India; arnab.chat93@gmail.com (A.C.); ritwick111@gmail.com (R.B.); auroshreesadhu7@gmail.com (A.S.); ssaha@zoo.buruniv.ac.in (S.S.)
[3] Department of Biotechnology, Swami Vivekananda University, West Bengal 700121, India; priyajit.research@gmail.com
[4] Istituto Zooprofilattico Sperimentale del Piemonte, Liguria e Valle d'Aosta, 10154 Torino, Italy
* Correspondence: profncsaharesearch@rediffmail.com (N.C.S.); paolo.pastorino@izsto.it (P.P.)

Abstract: The acute and chronic toxicity of lead to *Anabas testudineus* was determined in this study using static replacement bioassay testing. During the chronic toxicity studies, an experiment on the bioremediation of lead toxicity using *Ocimum sanctum* leaf powder was conducted. The 96 h LC_{50} values of lead for *Anabas testudineus* was 1.08 mg/L. Different biomarkers, such as the hepatosomatic index, gonadosomatic index, and fecundity, were significantly lower in fish subjected to 10% and 20% of the 96 h LC_{50} values of lead, compared to controls. The 45-day chronic exposure of fish to lead concentrations of 0.2 mg/L and above significantly lowered the number of total RBC, hemoglobin content, HCT (%), plasma protein, and cholesterol while decreasing the level of total WBC, plasma glucose, creatinine, serum AST and serum ALT. The leaf powder of *Ocimum sanctum* plays a significant role in ameliorating lead toxicity.

Keywords: growth; haematological biomarkers; hepatosomatic index; lead toxicity; oxidative stress enzymes

1. Introduction

Due to the harmful effects on aquatic species and human health, the toxicity of various chemicals in the environment, particularly in water sources, resulting from both natural and human activities, has become a major concern [1–5]. These chemicals adversely affect the survival, growth, well-being, and behaviour of fish [6–10]. Lead (Pb) has been identified as one of the most important and versatile metal ions used in industry, with many applications in metal finishing, storage batteries, paints, and electroplating [11]. Lead, with atomic number 82, is abundant in the environment, ranking 36th in natural abundance [12]. According to WHO guidelines, lead's maximum acceptable limit in drinking water is 0.01 mg/L. Natural sources of lead include volcanic eruptions, marls, gypsum, sea aerosol particles, and biological cycling processes, including the weathering of lead-containing rocks and soils [13].

Furthermore, Pb exposure acts as an immune toxicant in fish, affecting their immune responses [13]. Lead pollution poses a severe environmental health threat due to its non-biodegradability and its long-term detrimental effects through accumulation [13]. Excessive intake of Pb ions can result in damage to the nervous system, brain, kidneys, reproductive system, and even death. Lead contamination has garnered increasing global attention due to its toxic effects on fish, humans, and the environment [14]. Pb toxicity has devastating consequences on fish populations, adversely affecting various metabolic

processes [14]. It also triggers energy-consuming detoxification mechanisms, reducing the energy available for growth [15]. Moreover, lead acts as an endocrine disruptor in fish. Its pro-oxidative properties can induce oxidative stress in fish, leading to oxidative damage to cell membranes [15]. Reports on Pb toxicity in fish and other aquatic organisms highlight the need for further research to better understand lead poisoning in natural water bodies. Consequently, this study aims to estimate the acute and chronic toxicity of Pb to aquatic organisms, assess Pb concentrations in water, and explore bioremediation strategies for safe lead disposal. The objective of this study is to assess the acute and chronic toxicity of lead on fish (*Anabas testudineus*) using static replacement bioassay tests.

Plants absorb a wide range of substances from the soil, some of which have unknown biological function, while others can be harmful even at low concentrations [16]. Since plants form the base of the food chain, there is concern that harmful elements may be transmitted from plants to higher trophic levels [17]. Utilisation of naturally available aromatic and herbs-medicinal plants in feeding the fish is still less on the experimental and commercial level. However, few studies have been conducted to utilize these herbs and plants as feed additives to enhance growth and feed efficiency and also for bioremediation potential during chronic toxicity experiments to mitigate toxicity of different contaminants [18]. Basil (*Ocimum* spp.) meets the criteria as it adapts well to warm environments, does not reproduce aggressively, and does not spread uncontrollably [19]. In this study, the leaf powder of *Ocimum sanctum* was tested for its bioremediation potential during chronic toxicity experiments to mitigate lead toxicity.

2. Material and Methods

2.1. Test Organisms

Adult specimens (n = 256) of the freshwater, air-breathing fish, *Anabas testudineus* [weight 38.24 ± 1.9 g (mean ± SD); length 12.3 ± 2.9 cm (mean ± SD)] used in the study were bought from a fish farm at Burdwan, West Bengal. They were then transferred to the Aquatic Toxicology Laboratory, Department of Zoology, The University of Burdwan, West Bengal.

2.2. Test Chemical

As the test chemical, analytical grade lead oxide (also called lead monoxide), PbO, with 99.99% purity (molecular weight 300.59 g/mol; Sigma Aldrich Inc., Mumbai, India) was used.

2.3. Acute Toxicity Test

2.3.1. Experimental Set Up

Static replacement bioassays were conducted in the laboratory conditions, following the methods described in APHA [20] and Kaviraj et al. [21]. Tube-well water stored beforehand in a tank was used as the diluents medium in the bioassays [22]. The physicochemical water parameters measured prior to treatment were (mean ± SD) as follows: temperature 28.5 ± 1.5 °C, pH 7.11 ± 0.13, CO_2 12.57 ± 1.24 mg/L, dissolved oxygen (DO) 5.85 ± 0.92 mg/L, total alkalinity 175.00 ± 8.07 mg/L as $CaCO_3$, and hardness 106.00 ± 6.70 mg/L as $CaCO_3$. The test organisms were acclimatized to the test condition for 15 days before starting the bioassay. Only healthy specimens were selected at random from a single stock, regardless of sex, before the experiment [23]. Sufficient control was maintained for all bioassay tests [24]. The entire group of test organisms was discarded if mortality in the control group exceeded 5%. LC_{50} values for the test chemicals, along with changes in fish behaviour and respiratory rates, were evaluated during 96 h acute toxicity tests using various nominal concentrations (0.5, 0.7, 0.9, 1.1, 1.3, 1.5, 1.7, 1.9, 2.1, 2.3 and 2.5 mg/L). The exposure concentrations were chosen using the 24 h range finding test [25,26]. Additionally, a 96-h feeding test was conducted with sublethal concentrations of the test chemicals. For the 45-day chronic toxicity tests, sublethal doses were used to assess changes in fish growth rate, haematologicaland biochemical parameters, serum en-

zyme levels, and histopathology, as well as alterations in the physicochemical properties of the test water. The test bioassays were conducted according to the regulations approved by the Institutional Biosafety Committee, The University of Burdwan (BU/IBSC/22/Zo/36).

2.3.2. Respiratory Rate Test

The respiratory rate changes of fish exposed to different lethal concentrations of the toxicants were estimated from the opercula movements of fish/minute, following the methods of Kaviraj, Bhunia, and Saha [21], and Chukwuka et al. [27] during their acute exposure. The total number of opercula movements per minute per fish was evaluated. Six such observations (two from each replicate) were recorded at random for each concentration every 24 h. The respiratory test was conducted for 96 h in 15 L glass aquaria, each holding 10 L of water with four fish. Three replicates of such aquaria were exposed to each concentration of the toxicant and control. Opercula movements were counted at 10.00 A.M. and 4.00 P.M. daily. The opercular movements per minute were recorded at random intervals from two individuals in each aquarium during each observation. To facilitate accurate counting, the aquaria were well-illuminated, with a light source positioned behind each aquarium.

2.3.3. Test for Changes in Behaviour

Behavioral changes in fish exposed to various lethal concentrations of Pb were observed visually during the 96-h acute exposure, following standard protocols [26–29]. Behavioural tests for *Anabas testudineus* were performed in 15 L glass aquaria, each containing 10 L of water. Three replicates of aquaria were used for each toxicant concentration.

2.3.4. Feeding Test

The feeding studies were conducted in 15 L glass aquaria holding 10 L of water, with three adult fish per tank, over a 96-h period using static renewal bioassays. Each test chemical was evaluated at three sublethal concentrations: 10%, 20%, and a combination of 20% of the 96 h LC_{50} value with *Ocimum sanctum* leaf powder, along with a control. The leaf powder comprised one-quarter of the fish's daily meal. The basil powder was mixed with white fish meal, wheat flour, shrimp meal, dried yeast, and soybean meal. The sublethal concentrations were determined based on the 96 h LC_{50} values of the toxicants. Three aquaria were assigned to each sublethal concentration and the control, following a randomized block design. The fish were fed freshly chopped earthworms for four hours daily, starting at 8 am. Each day, the water was drained and replaced with fresh water containing the appropriate test chemical. Unconsumed food was measured and removed to prevent organic decomposition. The food consumed (in %) was calculated as difference between the total wet weight of food provided and the food left unconsumed. The control fish consumed 100% of the food. Fish food consumption at each sublethal test concentration was compared to the control.

2.4. Chronic Toxicity Test

2.4.1. Experimental Set Up

Chronic toxicity tests were conducted over a 45-day period during the monsoon season in the laboratory, using 15 L glass aquaria containing 10 L of dechlorinated tap water. For the preparation of the *Ocimum sanctum* leaf powder, the *O. sanctum* leaves were collected from a nearby source and cleaned thoroughly with distilled water. The leaves were then dried in an oven at 45 °C for 48 h and ground to powder using the mortar and pestle. Based on the results of the acute toxicity tests (96 h LC_{50} values), three sublethal concentrations of each test chemical were determined: 10% of the 96 h LC_{50} value, 20% of the 96 h LC_{50} value, and a mixture of 20% of the 96 h LC_{50} value with dried *Ocimum sanctum* leaf powder at 1.2 mg/L per day. These three sublethal concentrations, along with a control, were used for the 45-day chronic toxicity tests. In this study, all treatments were categorized into four different groups:

(i) Group 1. Fish without toxicant;
(ii) Group 2. Fish with toxicant at 10% of 96 h LC_{50} value;
(iii) Group 3. Fish with toxicant at 20% of 96 h LC_{50} value;
(iv) Group 4. Fish with toxicant at 20% of 96 h LC_{50} value and 1.2 mg/L leaf powder of *Ocimum sanctum*/day.

Each aquarium, after appropriate preparation, was stocked with ten acclimatized *Anabas testudineus*. Twenty-four hours after stocking, the fish were treated with the test chemicals. The stocked fish were fed with white fish meal, wheat flour, shrimp meal, dried yeast, and soybean meal, supplemented with vitamins and minerals, six days a week. Initially, the food ration was set at 2–3% of the fish's stocking weight, with a 10% increase every two weeks. A separate experiment was conducted to observe changes in the reproduction of *Anabas testudineus*, with males and females stocked in a 1:1 ratio (mean body weight: 38.24 ± 5.56 g; mean total length: 12.3 ± 3.3 cm). The same management practices were followed during the rearing of male and female fish to monitor reproductive changes. Triplicates for all chronic toxicity tests were conducted in accordance with the established methods [7,8,30], with thirty fish exposed to each concentration of the test chemical.

For bioremediation, dried *Ocimum sanctum* leaf powder was administered at 1.2 mg/L per day with the fish food to mitigate the toxicity of the test chemical. During the toxicity tests, static renewal bioassay methods were employed, with 10% of the water in the test aquaria siphoned out every 24 h and replaced with fresh water containing the appropriate concentration of the test chemical. Results from the 45-day chronic toxicity tests were recorded on days 1, 15, 30, and 45. Alterations in biochemical parameters of blood serum (total glucose, protein, urea, creatinine, alanine aminotransferase-ALT, and aspartate aminotransferase-AST) and haematologicalparameters (RBC, WBC, Hb, and Hct %) were measured every 15 days. At the end of the experiment, changes in growth (including the gastrosomatic index, hepatosomatic index (HSI), weight gain, % increase in length, Specific Growth Rate, Food Conversion Ratio-FCR, and Food Conversion Efficiency-FCE), as well as reproductive parameters (gonadosomatic Index, ovary size, and fecundity), were evaluated. The physicochemical properties of test water (pH, CO_2, dissolved oxygen, alkalinity, and hardness) were also assessed every 15 days during the chronic bioassay.

2.4.2. Growth and Organo-Somatic Indices

The length and weight of the fish were noted within 24–48 h of preservation. The several growth parameters (gastrosomatic index, hepatosomatic index, percent increase in weight, percent increase in length, specific growth rate, food conversion ratio, food conversion efficiency) were evaluated from the length (mm) and weight (g) of the fish and their different tissues. The data of length and weight were transformed to log values for regression analysis. To calculate the growth parameters of the fish, the formulae were adopted from standard protocols [31–33] and they are given below:

(i) Gastrosomatic Index = $(V/W) \times 100$,
where V is the visceral weight (g) of the fish and W is the observed body weight (g) of fish;
(ii) Hepatosomatic index (HSI) = [{wet weight (g) of liver without gall bladder}/wet body weight (g)] × 100;
(iii) Percentage increase in weight = $(W_2 - W_1)/W_1 \times 100$,
where W_1 is the initial weight (g) of the fish and W_2 is the final weight (g) of the fish;
(iv) Percentage increase in length = $[(L_2 - L_1)/L_1] \times 100$
where, L_1 = initial length of fish; L_2 = final length of fish;
(v) Specific growth rate [34] (%/day) = $\{(\log_e W_2 - \log_e W_1)/T\} \times 100$,
where $\log_e W_1$ = natural logarithm of initial body weight of fish (g), $\log_e W_2$ = natural logarithm of final body weight (g) of fish and T = time interval;

(vi) Food conversion ratio (FCR) = food given/weight gain,
where weight gain = final weight of fish (g) − initial weight of fish (g);
(vii) Gonadosomatic index of female fish = (G/W) × 100;
(viii) Fecundity = total number of ripening eggs/females.

2.4.3. Haematological Biomarkers

The total count of RBC was performed following Dacie and Lewis [35]. For counting the red blood cells, whole blood from the test tube was pipetted by a hemocytometer tube up to the 0.5 mark and then diluted 200 times using Hayem's fluid. After thoroughly mixing, the diluted blood sample was taken in the Neubaur's counting chamber, covered with a special cover slip, and allowed to stand for a few minutes. The red cells were counted in the RBC counting chamber. For each sample, 5 readings were taken. The values were expressed in millions of cells/mm^3. Hayem's fluid was used as diluent for RBC, and Turk's fluid was used for WBC. Hemoglobin was estimated using the acid haematin method [36]. Haematocrit (HCT), TWBCC, TRBCC, and Mean Corpuscular Haemoglobin [37] were expressed as follows:

- HCT (%) = (length of packed erythrocytes ÷ total length of blood column) × 100;
- TWBCC (103 mm^3) = [total number of white blood cells counted in 4 squares of haemocytometer (Nwbc) × dilution factor (Df of 50)] ÷ [4 × volume factor (Vf of 0.1)];
- TRBCC (106 mm^3) = [total number of RBCs counted in 5 squares of haemocytometer (Nrbc) × dilution factor (Df of 200)] ÷ [5 × volume factor (Vf of 0.1)].

2.4.4. Biochemical Parameters of Blood Serum

Serum proteins were estimated following the methods of Lowry et al. [38]. The GOD/POD method (glucose oxidase-peroxidase) was employed for the estimation of glucose levels [39]. The enzymatic colorimetric method recommended by [40] was applied for the estimation of cholesterol. The creatinine level was estimated by following method [41]. The estimation of serum aspartate aminotransferase (AST) and serum alanine aminotransferase (ALT) was employed following the method of [42].

2.5. Scanning Electron Microscopic (SEM) Study

A heparinised syringe was used to take blood from the caudal peduncles of both control and polluted fish. Two to three blood drops were placed in vial with 2.5% glutaraldehyde produced in 0.1 M sodium cacodylate buffer. It was then centrifuged at 1500 rpm for 5 min, then washed and resuspended in distilled water. The procedure was performed 2–3 times. A thin film was decanted and applied to a cover slip after resuspension in distilled water. Then, the cover slips were air-dried and gold-coated using a JFC-1100 ion sputterer (JEOL Ltd., Tokyo, Japan). Observations were made on a JSM-6360 JEOL SEM at an accelerating voltage of 15–20 kV, using the secondary electron emission mode.

2.6. Homology Modelling and Molecular Docking

To predict the binding affinities of serum aspartate aminotransferase (AST) and alanine aminotransferase (ALT) with lead, molecular docking analysis was performed. The 3D structure of lead (PubChem CID: 5352425) was simulated using Avogadro software (version 1.2). Since the 3D structures of serum aspartate aminotransferase (AST; XP_026212619.1) and alanine aminotransferase (ALT; XP_026217554.1) were not available in the Protein Data Bank (PDB), we generated their structures through homology modeling using SWISS-MODEL [43]. A template search was conducted for these proteins, and models were built using ProMod3 [44]. The quality of the models was assessed using the QMEAN scoring algorithm at both the global and per-residue levels, and their validity was confirmed using Ramachandran plot analysis [45]. The final models were saved in PDB format.

For molecular docking, polar hydrogen atoms were incorporated into the target proteins to ensure proper ionization and tautomeric states of amino acids using the PyRx v8.0 tool [46]. Kollman united and Gasteiger charges were applied to the proteins, while the ligand was similarly prepared. The 3D structure of lead was further optimized in Open Babel, where its energy was minimized using the universal force field (UFF) with 200 steps of conjugate gradients. Universal and targeted docking simulations (50 runs each) were performed using PyRx [46] to identify potential binding sites, and the results were visualized using Discovery Studio v24.1.0.23298 [47].

2.7. Statistical Analysis

The Shapiro–Wilk test was performed to ascertain whether the data conformed to a normal distribution. All data, except those obtained from acute toxicity tests, were processed for significance of variance using one-way or two-way ANOVA (analysis of variance). Statistical analyses were performed using the SPSS package (version 16.0). The Probit Analysis [48] method has been employed for estimating LC_{50} values. The mean values of opercula movements obtained from respiratory tests were analysed by two-way analysis of variance (ANOVA), taking days of exposure and concentrations of a test chemical as independent variables. The comparison of mean values for significance of difference was performed using Dunnett's test.

3. Results and Discussion

3.1. Acute Toxicity Assessment

3.1.1. Effects on Mortality Rate

The results of acute toxicity test with Pb) to *Anabas testudineus* are shown in Table 1. The 24, 48, 72, and 96 h LC_{50} values of Pb were 1.47, 1.41, 1.15 and 1.08 mg/L, respectively. The 24, 48, 72, and 96 h LC_{50} values (with 95% confidence limits), probit regression equations and correlation coefficients (R^2 and r values) of Pb indicate an existence of a strong positive correlation between the percentage of mortality and toxicant concentration (Table 1).

Table 1. Comparison between the LC_{50} values (95% confidence limits, probit regression equation, R^2 and r values) of Pb to *Anabas testudineus* at different times of exposure.

Time of Exposure	LC_{50} (mg/L)	95% Fiducial Limits of LC_{50}		Probit Regression Equation Y = ax + b	R^2 Value	r Value
		Lower	Upper			
24 h	1.47 ± 0.22	1.28	1.70	y = 4.41x + 4.25	0.9	0.9
48 h	1.41 ± 0.28	1.19	1.69	y = 3.54x + 4.45	0.9	0.9
72 h	1.15 ± 0.28	0.96	1.37	y = 3.53x + 4.78	0.9	0.9
96 h	1.08 ± 0.34	0.86	1.36	y = 2.91x + 4.90	0.8	0.8

No mortality was observed in the control group during 96 h experiment. The mortality of *Anabas testudineus* increased significantly ($p < 0.05$) with increasing toxicant concentrations and the progression of exposure time (Figure 1).

This observation indicated dose- and time-dependent mortality. The LC_{50} values decreased significantly with increasing exposure period of the toxicant.

In the present study, the 96 h LC_{50} value of lead was found to be 1.08 mg/L, which is lower than the 96 h LC_{50} value of other fish species, such as 44 mg/mL for *Oreochromis niloticus* [49] and 34.20 mg/L for *Labeo rohita* [50]. Therefore, this variations in lead toxicity to different fish species depends on species and the test condition. The results indicate that the tested fish *A. testudineus* was facing high lead toxicity.

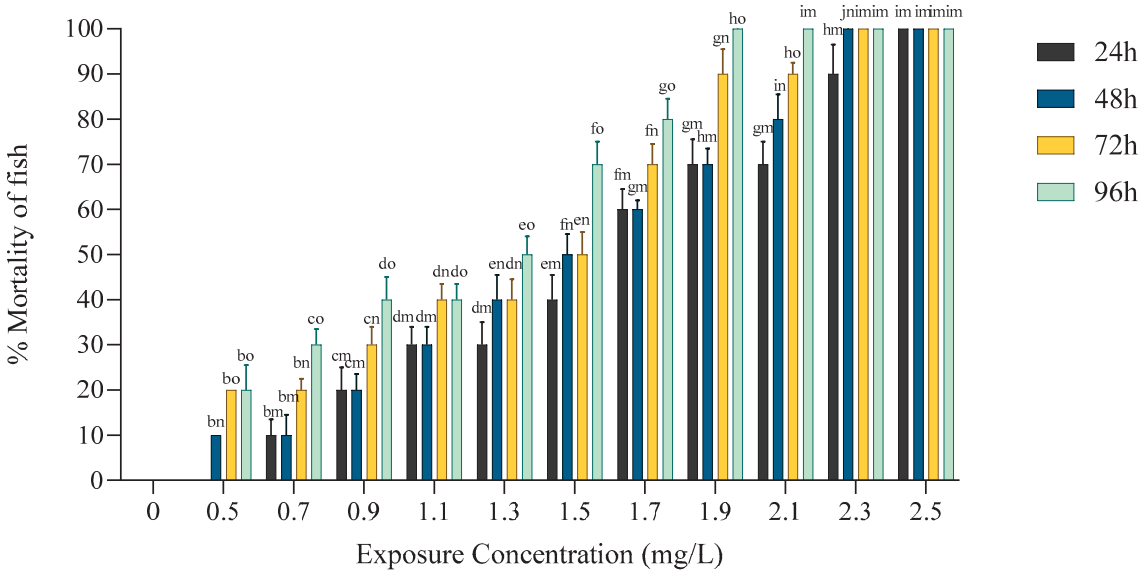

Figure 1. Mean percentage (%) values of mortality of *Anabas testudineus* exposed to different concentrations of lead over various exposure periods (24, 48, 72, and 96 h). Significant differences are denoted by b–i (columns) and m–o (rows).

3.1.2. Behavioural Changes

The increasing mucous secretion and hyper-excitability were recorded at the higher concentrations of the test chemical (1.1 mg/L) from 72 h to 96 h of exposure time. The equilibrium of fish was lost at higher concentrations of the toxicant (1.1 mg/L and above) at 72 and 96 h of exposure (Table 2).

Table 2. Impact of Pb on behaviours (MS: mucous secretion; HE: hyper-excitability; LE: loss of equilibrium) of *Anabas testudineus* at different hours (24, 47, 72, 96) of exposures; (-: absent; +: mild; ++: moderate; +++: strong).

Dose (mg/L)	MS				HE				LE			
	24 h	48 h	72 h	96 h	24 h	48 h	72 h	96 h	24 h	48 h	72 h	96 h
0	-	-	-	-	-	-	-	-	-	-	-	-
0.5	-	-	-	+	-	-	-	+	-	-	+	+
0.9	-	+	+	+	+	+	+	+	-	-	+	++
1.1	-	+	++	+++	+	+	++	+++	-	+	++	+++
1.5	-	+	+++	+++	+	+	+++	+++	-	+	+++	+++
1.9	+	++	+++	+++	+	++	+++	+++	+	+++	+++	+++

On initial exposure at higher concentration of lead, the fish showed characteristic avoidance behaviour by rapid and erratic swimming with jerky movements and hyper excitability, rapid opercula movement, jumping out from the test media, lateral swimming, and loss of equilibrium. These observations were in conformity with the findings of Murugan et al. [51], who observed characteristic restlessness, increased activity and opercular movements of fish put into hypoxic conditions. Similar abnormal behaviours were also observed in *Ctenopharyngodon idella*, *Clarias gariepinus*, and *Chanos chanos* exposed to lead nitrate [52,53].

3.1.3. Changes in Respiratory Rate

The opercular movement of fish increased significantly ($p < 0.05$) at 24 and 48 h but decreased significantly ($p < 0.05$) at 72 and 96 h with increasing toxicant concentrations. The opercular movement decreased significantly ($p < 0.05$) at all the treatments with the advancement of exposure time (Figure 2).

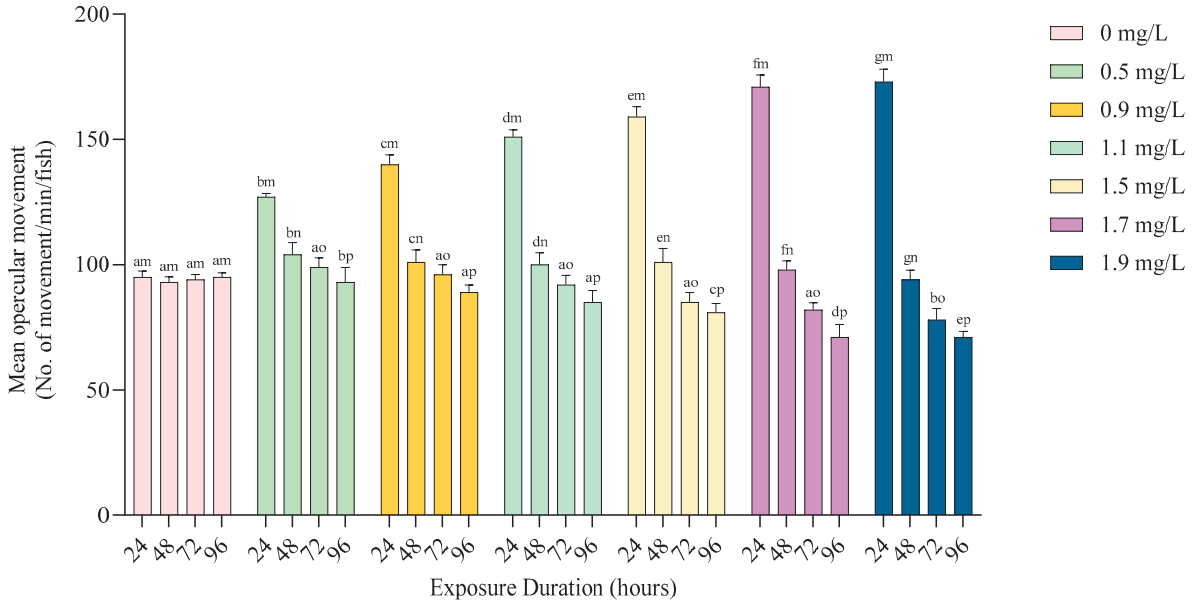

Figure 2. Mean opercular movements of *Anabas testudineus* during 96 h exposure to different exposure concentrations of Pb (mg/L). The significance levels are denoted using a–g (columns) and m–p (rows).

3.1.4. Changes in Feeding Rate

Changes in feeding rate of *Anabas testudineus* treated with different concentrations of Pb are shown in Figure 3. One-way ANOVA followed by Dunnett's test showed that the feeding rate of fish was reduced significantly ($p < 0.05$) at 10% (0.1 mg/L), 20% (0.2 mg/L), and the mixture of 20% of the LC_{50} value of Pb and leaf powder of *Ocimum sanctum*. A severe decrease in feeding rate of fish was recorded at 20% of LC_{50} value of toxicant. But the rate of feeding of fish was significantly higher exposed to the mixture of 20% of LC_{50} value and leaf powder of *Ocimum sanctum* compared to the 10% and 20% LC_{50} concentrations of Pb (Figure 3).

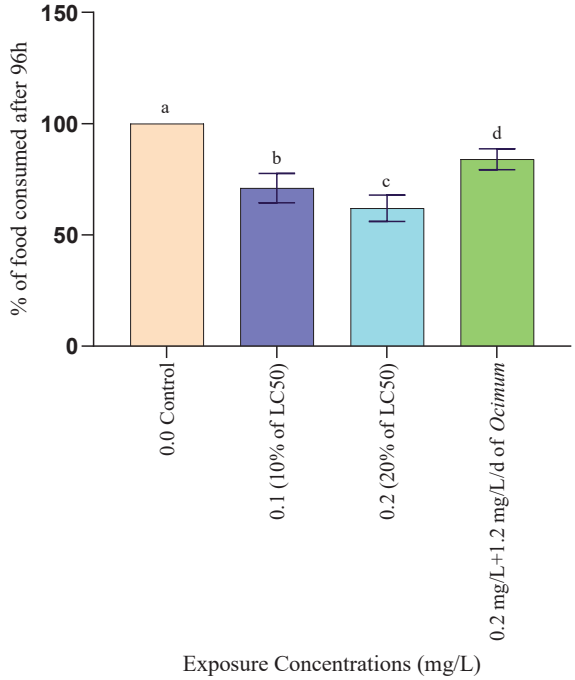

Figure 3. The proportion of food consumed by *Anabas testudineus* exposed for 96 h to different concentrations of Pb along with remediation with *Ocimum* leaf powder. Letters (a–d) indicate significant differences.

3.2. Chronic Toxicity Tests of Lead to Fish Anabas testudineus

No fish mortality was observed during the 45-day chronic toxicity bioassay. Additionally, no changes in behaviour or coloration were noted throughout the experiment. However, prolonged exposure (45 days) to sublethal concentrations of Pb resulted in significant alterations in growth rate, haematology, serum biochemistry, serum enzyme levels, and histopathology in the treated fish (Figures 4 and 5 and Tables 3 and 4).

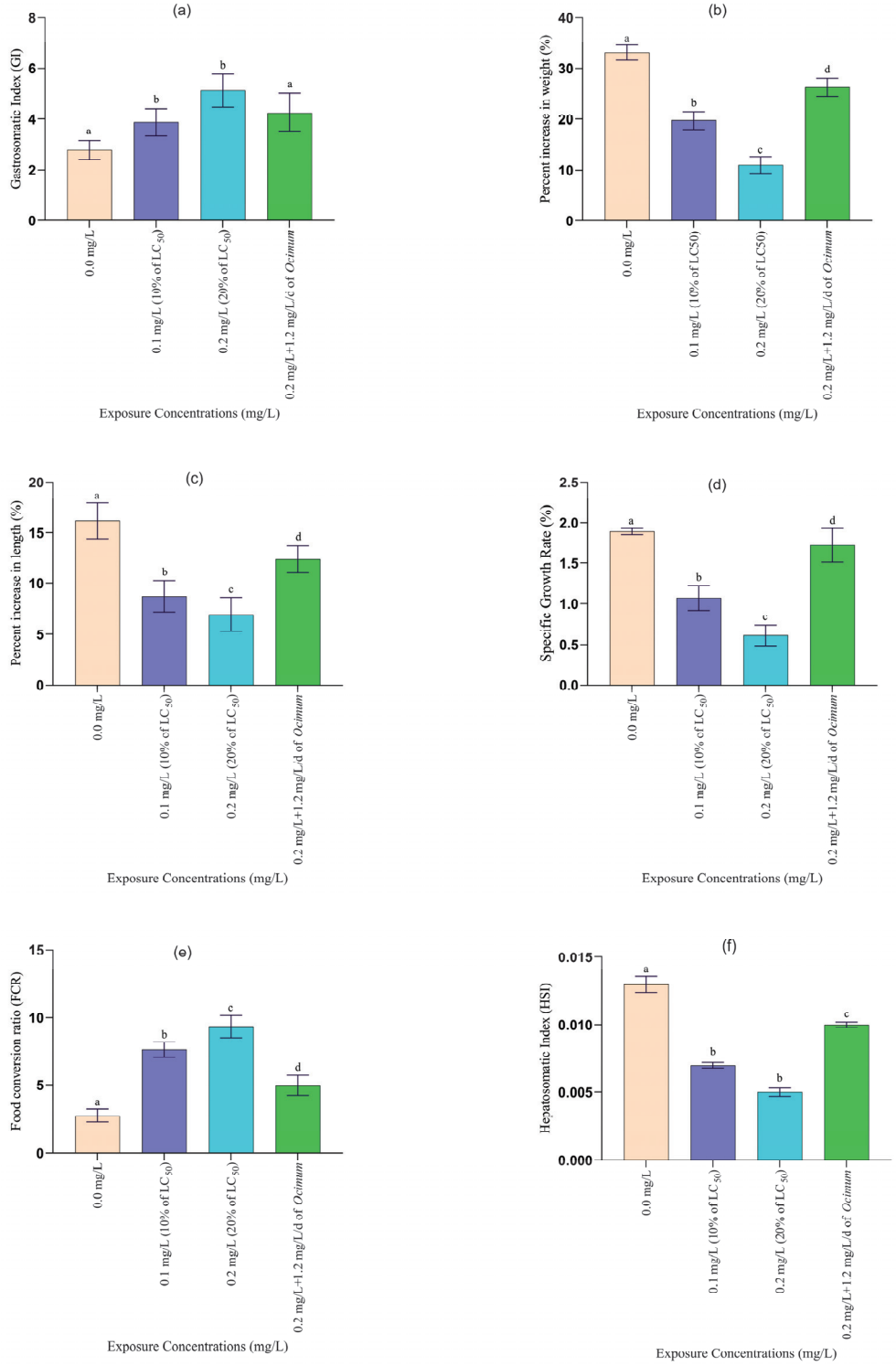

Figure 4. *Cont.*

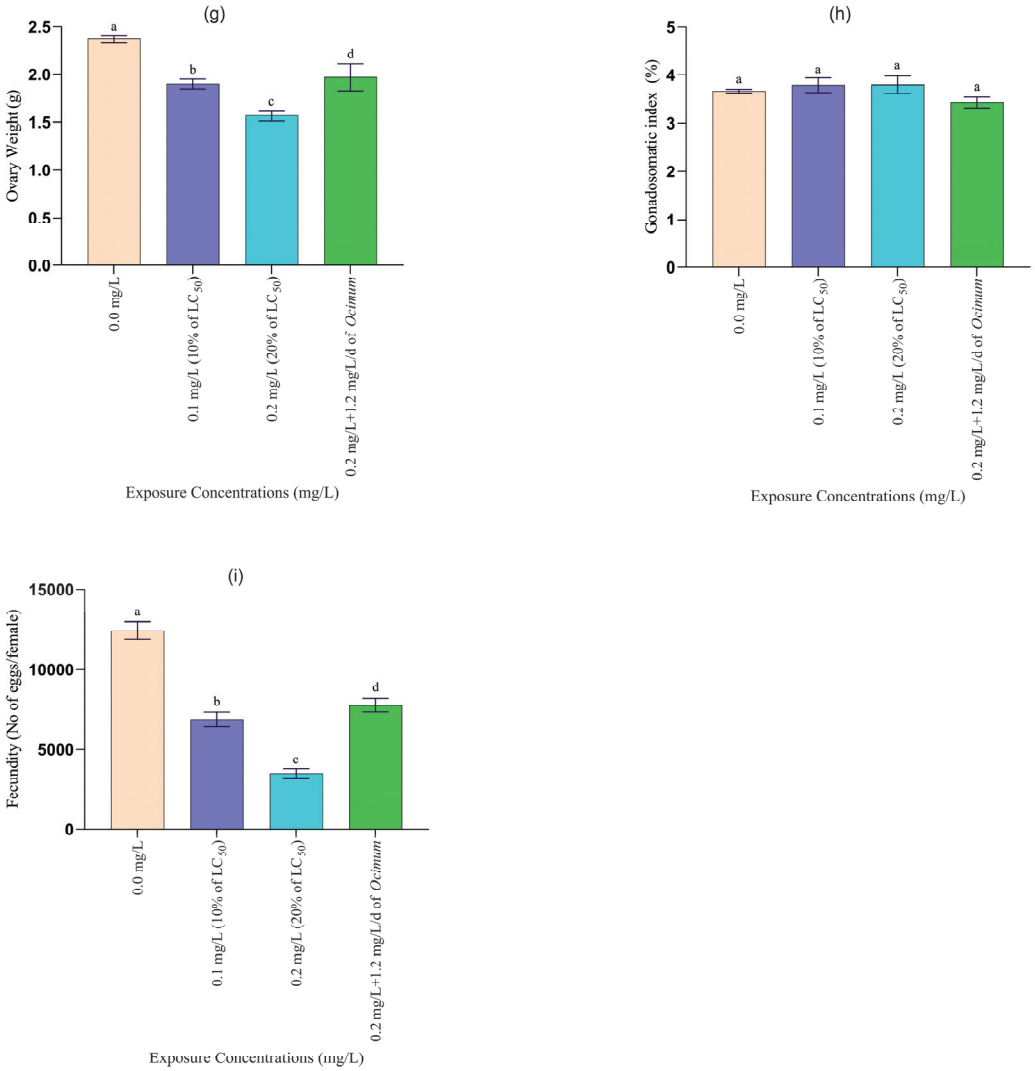

Figure 4. The (**a**) gastrosomatic index, (**b**) percentage increase in weight (**c**) percentage increase in length, (**d**) specific growth rate (% per day), (**e**) food conversion ratio (FCR), (**f**) hepatosomatic index, (**g**) gonad (ovary) weight, (**h**) gonadosomatic index (%), and (**i**) fecundity of *Anabas testudineus* exposed to sublethal concentrations of lead (mg/L) after 45 days of chronic toxicity testing are reported. Letters (a–d) indicate significant differences.

Table 3. Total RBC, total WBC, haemoglobin (g/dL) and Hct% of fish *Anabas testudineus* exposed to lead during chronic toxicity bioassay. Mean values with different superscript letters a–d within columns and m–p within rows are significantly different (two-way ANOVA followed by Dunnett's test, $p < 0.05$).

Hematological Parameter	Exposure Time (d)	Concentration of F (mg/L)			
		0.0 mg/L (Control)	**0.1 mg/L (10% of LC_{50})**	**0.2 mg/L (20% of LC_{50})**	**0.2 mg/L (20% of LC_{50}) + 1.2 mg/L/d (*Ocimum sanctum* Leaf Powder)**
Total RBC (10^6/mm^3)	1	2.83 ± 0.07^{am}	2.84 ± 0.09^{am}	2.84 ± 0.12^{am}	2.83 ± 0.08^{am}
	15	2.85 ± 0.16^{am}	2.71 ± 0.07^{bn}	2.65 ± 0.17^{bo}	2.76 ± 0.2^{bp}
	30	2.84 ± 0.16^{am}	2.62 ± 0.16^{bn}	2.53 ± 0.13^{co}	2.78 ± 0.25^{cp}
	45	2.83 ± 0.15^{am}	2.51 ± 0.05^{dn}	2.42 ± 0.16^{do}	2.80 ± 0.15^{dp}

Table 3. *Cont.*

Hematological Parameter	Exposure Time (d)	Concentration of F (mg/L)			
		0.0 mg/L (Control)	**0.1 mg/L (10% of LC_{50})**	**0.2 mg/L (20% of LC_{50})**	**0.2 mg/L (20% of LC_{50}) + 1.2 mg/L/d (*Ocimum sanctum* Leaf Powder)**
Total WBC (10^3/mm^3)	1	9.72 ± 0.34^{am}	9.71 ± 0.45^{am}	9.72 ± 0.44^{am}	9.73 ± 0.57^{am}
	15	9.69 ± 0.43^{am}	9.14 ± 0.34^{bn}	9.01 ± 0.58^{bo}	9.38 ± 0.37^{bp}
	30	9.71 ± 0.22^{am}	8.87 ± 0.43^{cn}	8.53 ± 0.57^{co}	8.59 ± 0.57^{bp}
	45	9.72 ± 0.41^{am}	8.58 ± 0.22^{dn}	7.17 ± 0.82^{do}	9.23 ± 0.48^{cp}
Haemoglobin (g/dL)	1	14.92 ± 0.52^{am}	14.91 ± 0.51^{am}	14.91 ± 0.47^{am}	14.92 ± 0.68^{am}
	15	14.90 ± 0.43^{am}	13.12 ± 0.29^{bn}	12.02 ± 0.17^{bo}	12.58 ± 0.47^{bp}
	30	14.93 ± 0.24^{am}	12.76 ± 0.58^{cn}	11.38 ± 0.37^{co}	13.44 ± 0.73^{cp}
	45	14.92 ± 0.44^{am}	11.69 ± 0.57^{dn}	9.57 ± 0.36^{co}	13.81 ± 0.27^{dp}
Hct (%)	1	24.47 ± 1.35^{am}	24.46 ± 0.96^{am}	24.45 ± 1.35^{am}	24.46 ± 0.99^{am}
	15	24.44 ± 1.46^{am}	21.52 ± 1.25^{am}	20.37 ± 1.34^{bn}	22.43 ± 1.38^{bo}
	30	24.43 ± 1.57^{am}	20.39 ± 0.94^{bn}	19.53 ± 1.52^{co}	22.87 ± 1.96^{bp}
	45	24.46 ± 1.39^{am}	18.65 ± 0.93^{cn}	17.21 ± 0.81^{co}	23.15 ± 1.01^{cm}

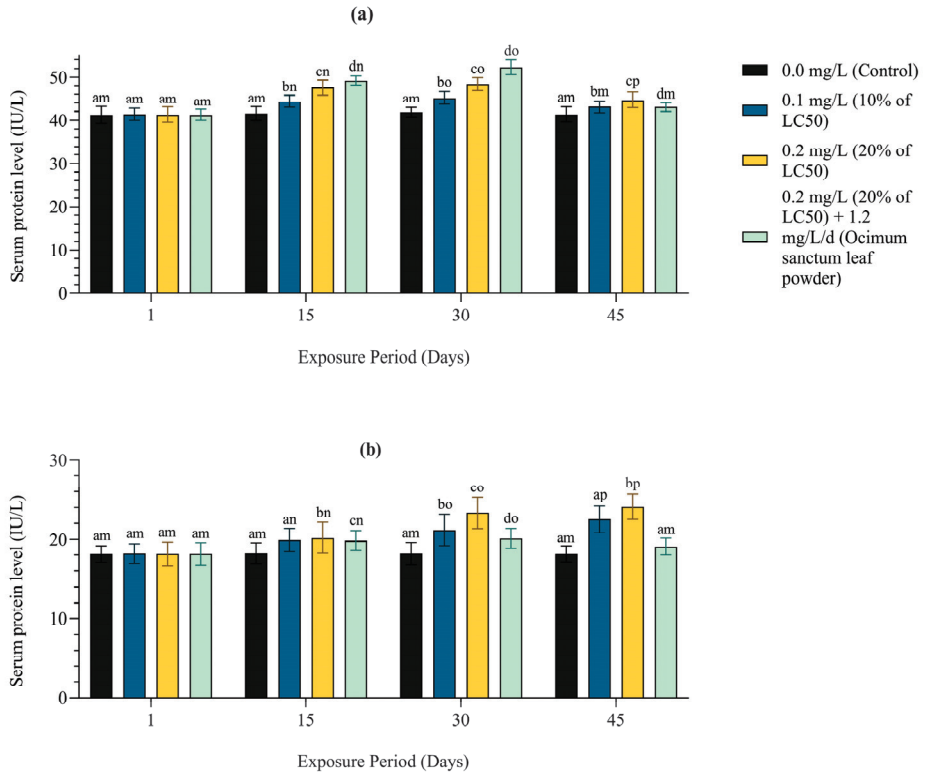

Figure 5. (**a**) Serum AST (IU/L) and (**b**) serum ALT (IU/L) level of freshwater fish *Anabas testudineus* exposed to Pb in the 45-day chronic toxicity bioassay. Letters a–g (columns) and m–p (rows) indicate significant differences.

Table 4. Plasma glucose (mg/dL), plasma protein (mg/dL), cholesterol (mg/dL) and creatinine level (mg/dL) of fish *Anabas testudineus* exposed to lead during chronic toxicity test. Mean values with different superscript letters a–d within columns and m–p within rows are significantly different (two-way ANOVA followed by Dunnett's test, $p < 0.05$).

Parameter	Exposure Time (days)	Concentration of Pb (mg/L)			
		0.0 mg/L (Control)	0.1 mg/L (10% of LC_{50})	0.2 mg/L (20% of LC_{50})	0.2 mg/L (20% of LC_{50}) + 1.2 mg/L/d (*Ocimum sanctum* Leaf Powder)
Plasma glucose (mg/dL)	1	60.23 ± 0.97^{am}	60.47 ± 0.74^{am}	60.35 ± 1.03^{am}	60.27 ± 1.02^{am}
	15	61.14 ± 0.30^{am}	62.32 ± 0.85^{bn}	63.17 ± 0.68^{bm}	62.15 ± 0.77^{bo}
	30	61.03 ± 0.98^{am}	65.83 ± 0.36^{cn}	67.29 ± 0.77^{co}	63.12 ± 1.26^{cp}
	45	60.67 ± 0.69^{am}	68.17 ± 0.51^{dn}	70.18 ± 0.75^{do}	61.74 ± 0.94^{am}
Plasma protein (mg/dL)	1	3.21 ± 0.18^{am}	3.24 ± 0.13^{am}	3.23 ± 0.04^{am}	3.22 ± 0.02^{am}
	15	3.20 ± 0.16^{am}	2.91 ± 0.06^{bn}	2.62 ± 0.13^{bo}	2.93 ± 0.15^{bp}
	30	3.19 ± 0.16^{am}	2.73 ± 0.11^{cn}	2.43 ± 0.12^{co}	2.95 ± 0.18^{cp}
	45	3.20 ± 0.17^{am}	2.62 ± 0.11^{dn}	2.19 ± 0.11^{do}	2.99 ± 0.17^{dp}
Cholesterol (mg/dL)	1	192.25 ± 1.07^{am}	191.78 ± 1.22^{am}	192.63 ± 1.84^{am}	192.12 ± 1.36^{am}
	15	191.79 ± 1.09^{am}	187.34 ± 1.43^{bn}	182.13 ± 1.38^{bo}	188.19 ± 0.96^{bp}
	30	192.13 ± 1.27^{am}	181.57 ± 1.36^{cn}	176.70 ± 1.57^{co}	183.22 ± 1.65^{bm}
	45	192.37 ± 1.58^{am}	177.72 ± 1.55^{dn}	167.58 ± 1.26^{do}	189.18 ± 1.25^{cm}
Creatinine (mg/dL)	1	0.43 ± 0.049^{am}	0.49 ± 0.074^{am}	0.49 ± 0.046^{am}	0.46 ± 0.063^{am}
	15	0.49 ± 0.067^{am}	0.69 ± 0.053^{bn}	1.06 ± 0.055^{bo}	0.88 ± 0.043^{bp}
	30	0.46 ± 0.054^{am}	0.88 ± 0.045^{cn}	1.17 ± 0.064^{co}	0.79 ± 0.062^{cp}
	45	0.49 ± 0.036^{am}	1.19 ± 0.036^{dn}	1.28 ± 0.042^{do}	0.53 ± 0.032^{dm}

3.2.1. Changes in Growth and Organo-Somatic Indices

Long-term exposure (45 days) to sublethal concentrations of lead (Pb) resulted in significant alterations in various growth parameters of the treated fish compared to the control group (Figure 4). Chronic exposure to Pb at concentrations of 0.1 mg/L and 0.2 mg/L, as well as a mixture of 0.2 mg/L Pb and *Ocimum sanctum* leaf powder (1.2 mg/L/day), led to a significant decrease in food conversion efficiency, weight gain (%), specific growth rate, and the hepatosomatic index, along with a significant increase in the gastrosomatic index and food conversion ratio (FCR), compared to the control ($p < 0.05$).

The most severe reductions in food conversion efficiency, weight gain (%), specific growth rate, and hepatosomatic index were observed in fish exposed to 20% of the LC_{50} value (122 mg/L) of Pb. However, fish treated with the mixture of 20% LC_{50} Pb and *Ocimum sanctum* leaf powder exhibited a comparatively lesser reduction in these parameters than those treated with 10% or 20% Pb alone. Fish exposed to the combination of *Ocimum sanctum* leaf powder and 0.2 mg/L Pb showed increased growth in both length and weight compared to the groups treated with 10% and 20% LC_{50} Pb concentrations.

Moreover, fish treated with the mixture of *Ocimum sanctum* leaf powder (1.2 mg/L/day) and Pb (20% LC_{50} value) showed signs of recovery from Pb toxicity. Over the 45-day period, there was a gradual improvement in food conversion efficiency, weight gain (%), specific growth rate, and the hepatosomatic index, along with a gradual reduction in the gastrosomatic index and food conversion ratio (FCR), compared to fish treated with Pb alone.

The size of ovary, gonadosomatic index [54], and fecundity of *Anabas testudineus* were reduced significantly in the fish exposed to 10% and 20% of 96 h of LC_{50} values of lead in comparison to control. The rate of reduction in the above parameters was found directly proportional to toxicant concentrations. But no negative change in the above parameters

was recorded in the mixture of 20% of 96 h of LC_{50} value of lead with 1.2 mg/L/d of leaf powder of *Ocimum sanctum* (Figure 4).

The chronic exposure of fish to 10% and 20% of LC_{50} of lead and a mixture of 20% of LC_{50} of Pb with *Ocimum sanctum* leaf powder alters the rate of weight gain (%), specific growth rate, and the hepatosomatic index. Fish performance and feed utilization, however, were significantly affected by lead concentration and exposure time. It also reported significant decrease in growth of *Channa punctatus* when exposed to heavy metal. Also, Abdel-Tawwab et al. [55] observed a significant decrease in the growth of Nile tilapia and common carp, respectively, when exposed to metal. Decreased growth in the post-larval stages of Indian prawn (*Penaeus indicus*) at 40, 80, and 160 µg/L was reported by Rajput et al. [56]. Dauble et al. [57] also observed reduced growth of fathead minnows exposed chronically to the toxicant. The hepatosomatic index is the main indicator of metabolic activity in animal organisms. In the present study, the recorded decrease of HSI values, due to lead exposure, indicates degenerative changes in the liver [58]. Bekmezciand Nevin [59] also reported that heavy metals decreased the hepatosomatic index in *Clarias gariepinus*, which was possibly due to depletion of energy reserves in liver. Stress condition developed under the effect of metals and the excess usage of energy reserves in response to increase in requirement might cause the decrease in hepatosomatic index [60].

Many heavy metals are considered essential nutrient elements that positively improve fish growth and feed utilisation; however, when these metals exceed the maximum allowable limit, they pose a risk not only to fish health but also to human consumers and disrupt ecological systems. Heavy metal toxicity has been linked to reduced gonadosomatic index [54], fecundity, hatching rate, fertilisation success, aberrant form of reproductive organs, and, ultimately, reproductive failure in fish. The rate of reduction in weight gain (%), specific growth rate, hepatosomatic index, gonadosomatic index [54], fecundity, and the rate of increase in the gastrosomatic index [54] and food conversion ratio (FCR) were the highest in fish treated with 20% of 96 h LC_{50} value of lead. The rate of change of these parameters was comparatively lower in the fish treated with a mixture of 20% of LC_{50} of lead and leaf powder of *Ocimum sanctum* over the fish treated with 10% and 20% of 96 h LC_{50} values of lead. The HSI, GSI, and fecundity were increased significantly in the mixture of 20% of 96 h of LC_{50} value of lead with 1.2 mg/L/d of leaf powder of *Ocimum sanctum* over 10% and 20% of 96 h of LC_{50} value of lead. It was probably due to the inhibitory effects of *Ocimum sanctum* reducing the oxidative stress and other toxicity from the lead during the chronic exposure of *A. testudineus* to the mixture of lead and *Ocimum sanctum* leaf powder. A similar result was also recorded by earlier researchers, such as Abdel-Tawwab et al. [61]. Similar findings were also recorded in HSI and GSI of *Heteropneustes fossilis* exposed to malathion and different metals [50]. A significant level of reduction in HSI of fish exposed to organic pollutants like PAHs was also found [62]. The HSI and GSI of *Cyprinus carpio* and *Perca fluviatilis* were also decreased during their exposure to lead and cadmium [63].

3.2.2. Haematological Changes

Chronic exposure (45 days) to sublethal concentrations of Pb caused changes in different haematological parameters of treated fish as compared to control (Table 3). The results indicated that RBC, WBC, Hb, and Ht% decreased significantly ($p < 0.05$) in the fish treated with 0.1 and 0.2 mg/L of Pb and a mixture of 0.2 mg/L of Pb and *Oscimum sanctum* leaf powder (1.2 mg/L/d) compared to the control. The effects of Pb were severe in treated fish in comparison to control. The reduction of RBC, WBC, Hb and Ht% was comparatively lower in the fish treated in the mixture of 20% of LC_{50} of Pb and leaf powder of *Ocimum sanctum* over the fish treated with 10% and 20% of Pb. There was no significant change in Ht% in the fish treated with a mixture of 20% of LC_{50} of Pb and leaf powder of *Ocimum sanctum* compared to control. The fish treated with a mixture of *Ocimum sanctum* leaf powder (1.2 mg/L/d) along with Pb (20% LC_{50} value) showed a sign of recovery from the Pb toxicity with the gradual increase in RBC, WBC count, Hb, and Ht% over a period of 45 days compared to the treated fish.

In the present investigation, the RBC, WBC, Hb, and Hct (%) values of fish were altered during chronic exposure to lead. The reduction rate was dose- and time-dependent. The hematological parameter in fishes are frequently used for the assessment of the toxic effects as well as functional status of aquatic organisms by using blood, which is an excellent indicator of toxic stress [64]. The haematological parameters, including RBC, WBC, Hct value and Hb is generally used to assess the health status of fish [65,66]. In this findings, reduction in RBC, Hb and Ht content in fish upon lead exposure, may be because of the disorder in hematopoietic processes, accelerated disintegration of RBC cell membrane [67]. Normally increased WBC count in fish exposed to lethal and chronic doses indicates leucocytosis [68]. In this study, leukocyte count decreased as dose increases which are in accordance to findings of many researchers [69,70]. Moreover, use of *Ocimum sanctum* leaf powder along with lead abridged the harmful property of the toxicant in terms of haematologicalparameters. Similar findings were observed when treated fish were exposed to toxicant [71]. Therefore, it could be useful as a protective agent against lead induced toxicity in fish.

3.2.3. Biochemical Changes of Blood Serum

Chronic exposure of fish to sublethal concentrations of Pb (0.1 mg/L, 0.2 mg/L and a mixture of 20% of LC_{50} of Pb and leaf powder of *Ocimum sanctum*) for 45 days caused noteworthy changes in different biochemical parameters (Table 4). The results indicated that serum aspartate aminotransferase (AST) and alanine aminotransferase (ALT) increased significantly ($p < 0.05$) in fish treated with 0.1 and 0.2 mg/L of Pb and a mixture of 0.2 mg/L of Pb and *Oscimum sanctum* leaf powder (1.2 mg/L/d) compared to control. The increase was dose and time dependent. There were also significant differences in serum enzyme activities between the two sublethal concentrations (0.1 and 0.2 mg/L) of Pb ($p < 0.05$). The fish treated with a mixture of *Ocimum sanctum* leaf powder (1.2 mg/L/d) along with Pb (20% LC_{50} value) showed a significant variation in the AST and ALT from 10% and 20% of LC_{50} values of Pb ($p < 0.05$), but no significant change was found compared to the control. This result may be considered as the sign of recovery from the Pb toxicity with the gradual decrease in serum ALT and AST over a period of 45 days compared to treated fish.

The utilisation of biochemical parameters in organisms as pollution indicators provides information on the adaptive or deleterious responses in organism exposed to a particular amount of chemicals. Such analyses provide early warning signals before other toxicological points, including death [72]. Among the biochemical profiles, plasma glucose has been widely used as a parameter to study stress and also used as a sensitive indicator of environmental stress in fish [73]. The hyperglycaemia recorded in the present study after lead exposure may be an indication of induced degenerative changes in the hepatopancreas [73]. The significant decrease in plasma protein levels in lead trioxide-treated fish might be due to an impaired rate of protein synthesis under metallic stress [74,75]. The variations in cholesterol level induced by heavy metals might be due to liver failure, which subsequently leads to the elevation of cholesterol concentration in the serum [76]. Various other metals also caused a decrease in the level of serum cholesterol in different fish species [77–79]. Serum creatinine is a traditional screening index for kidney function [55]. Similar results were obtained by [80], who found increased creatinine levels in Nile tilapia and common carp, respectively, due to metal toxicity.

3.2.4. Change in Blood Serum Enzymes

A notable effect of Pb was noted in the different enzyme levels of *Anabas testudineus* after 45 days of exposure to different sublethal concentration of Pb and a mixture of Pb and leaf powder in comparison to the control (Figure 5). The results showed that serum aspartate aminotransferase (AST) and alanine aminotransferase (ALT) increased significantly ($p < 0.05$) in fish treated with 0.1 and 0.2 mg/L of Pb and a mixture of 0.2 mg/L of Pb and *Oscimum sanctum* leaf powder (1.2 mg/L/d) in compare to control. The increase was dose and time dependent. There were also significant differences in serum

enzyme activities between the two sublethal concentrations (0.1 and 0.2 mg/L) of Pb ($p < 0.05$). The fish treated with a mixture of *Ocimum sanctum* leaf powder (1.2 mg/L/d) along with Pb (20% LC_{50} value) showed a significant variation in the AST and ALT from 10% and 20% of LC_{50} values of Pb ($p < 0.05$) but no significant change was found compared to the control. This result may be considered as the sign of recovery from the Pb toxicity with the gradual decrease in serum ALT and AST over a period of 45 days compared to the treated fish.

In the present study, ALT and AST levels in blood serum of the exposed fish increase with the increasing dose of lead and exposure time. Therefore, the effects of a chemical usually appear primarily in the liver [81]. Liver function tests have been used as indicators to access alterations in liver functioning following exposure to lead [81]. Several enzymes, such as ALP, GOT, and GPT, have been used to determine pollution exposure in animals and to monitor water pollution. In the present study, the significant increase in AST and ALT levels in fish exposed to lead indicates hepatic damage due to Pb accumulation, which, in turn, releases these enzymes into the bloodstream [81].

In the present study, the rate of elevation in ALT and AST levels was much higher in the fish treated with Pb and was comparatively lower in the fish treated with a mixture of 20% of LC_{50} of lead and leaf powder of *Ocimum sanctum* compared to the fish treated with 10% and 20% of lead. It indicates that the leaf powder of *Ocimum sanctum* decreases the Pb-induced toxicity of fish during their chronic exposure for a period of 45 days. In the present study, the use of leaf powder induced reversibility from abnormal levels to normal levels of ALT and AST in the blood of fish exposed to lead and may be regarded as a protective agent against toxicity. Similar findings were observed when the exposed animals were subjected to supplementation with *Moringa oleifera* extracts and spirulina [82,83].

3.2.5. Scanning Electron Microscopic (SEM) Study on the Change in RBC of Fish

Under scanning electron microscope, the erythrocytes of the treated fish showed an abnormal shape and became discoidal to elongated in shape with irregular surface (Figure 6). But the control blood cells were elliptical and discoid with normal smooth surface. Some erythrocytes of the treated fish formed lobopodian membrane protrusions. A few erythrocytes formed abnormal notches and spikes on the cell membrane.

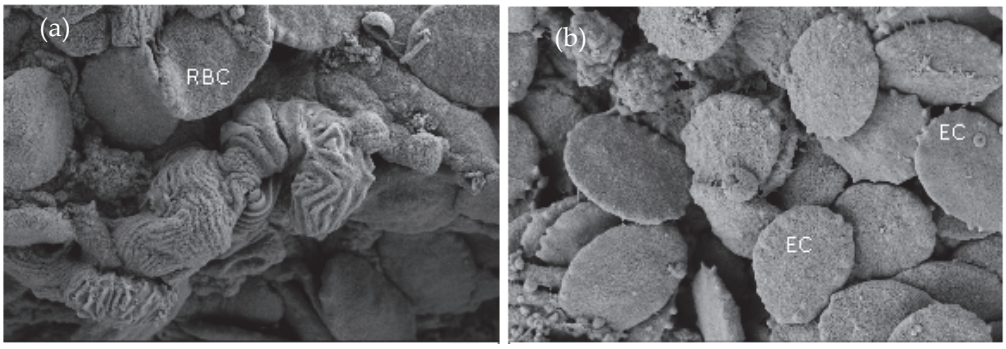

Figure 6. Scanning electron micrograph of RBC of *Anabas testudineus*: (**a**) RBC of control fish (**b**) RBC of fish treated with 0.2 mg/L (20% LC_{50} value) of lead.

The abnormally shaped RBCs of *Anabas testudineus*, exposed to lead with irregular surface, cell membrane crenation, internalization of membrane, oozed out cytoplasm, and lobopodian projections, were also found by earlier researchers in RBC of *Anabas testudineus* during chronic exposure to the pesticide cypermethrin [84]. Identical morphological changes in the RBCs of fish blood due to pesticides and heavy metal toxicity were also noted by several researchers [85,86]. The membrane internalization in mercuric chloride-exposed *Channa punctatus* was also observed [70]. The crenated RBC membrane development in fish might be due to the early echinocyte's formation. The echinocytes development cause plasma membrane expansion leading to RBC swelling before lysing [87]. The crenation of

lead-induced RBC membrane found in the present study may be associated with altered membrane surface area to cell volume ratio as stated by Naskar et al. [88] in *Clarias batrachus* exposed to aluminum. Similar types of crenations in the membrane of RBC were recorded in *Chana punctatus* exposed to mercuric chloride [70]. The formation of lobopodia and erythrocyte contraction from one side, as observed in the present study, has also been reported in *Channa punctatus* exposed to malathion and mercuric chloride [70]. Oozing cytoplasmic content and lobopodial projections were also found in the erythrocytes of *Anabas testudineus* exposed to the pesticide chlorpyrifos [84].

3.3. Homology Modelling and Docking Analysis of ALT and AST

For the modelling of ALT and AST, the templates obtained from the search have a template number of A0A3Q3AW13.1. ALT has a sequence identity of 87.37% and a GMQE score of 0.96 with 100% coverage, whereas AST has a sequence identity of 77.51% and a GMQE score of 0.92 with 100% coverage. A GMQE score above 0.7 is generally considered to be reliable [89].

The structure assessment using the Ramachandran plot also shows the model's validity. A valid protein is determined by 90–95% of its amino acids within the favoured regions of the plot, and here we obtained 97.96% amino acids in the favoured regions for ALT and 96.56% for AST. We obtained a MolProbity score of 0.65 for ALT and 1.65 for AST using MolProbity version 4.4 [90], and a clash score of 0.39 [44] for ALT and 1.39 for AST. The clash score was calculated as the number of collisions per 1000 atoms (including hydrogens) [91,92], and the MolProbity score signifies the combination of protein quality scores [44]. As the clash score and MolProbity score are low, the model can be considered suitable (Figure 7a,b). With these protein models (Figure 7a,b), we performed the docking analysis.

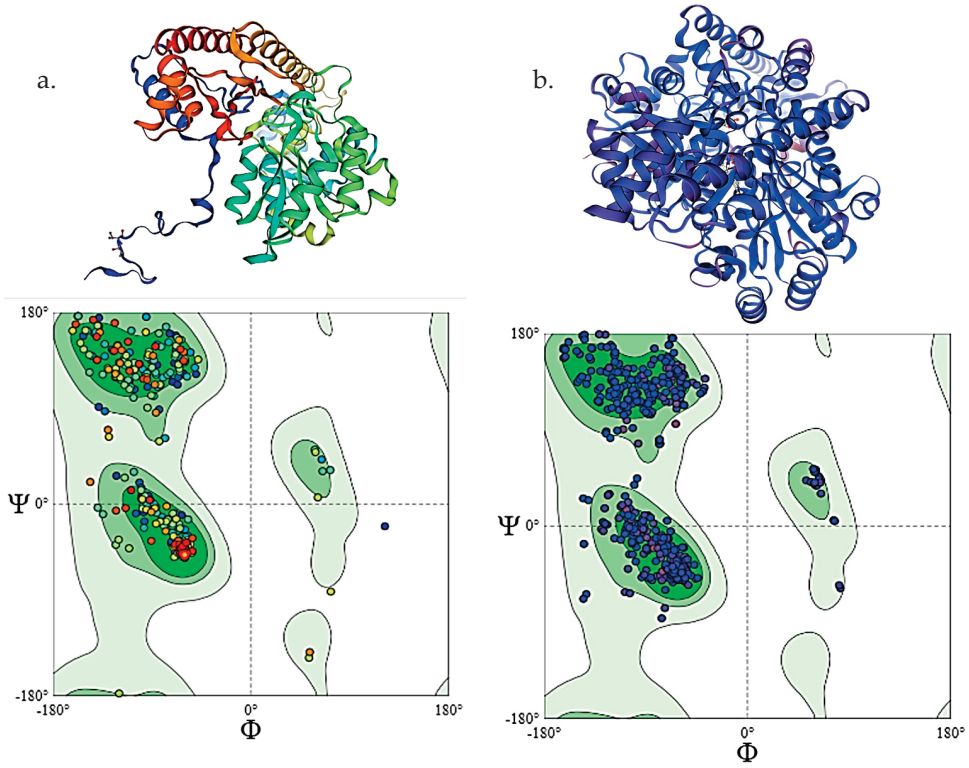

Figure 7. Homology models of ALT (**a**) and AST (**b**) with their validating Ramachandran plot below each of the models.

The docking analysis of lead with ALT shows lower affinity to AST. In Table 5, all the predicted results are mentioned regarding binding affinities. Thus, AST might interact with lead much more than ALT (Figure 8a,b).

Table 5. The binding affinities of the proteins and chemicals similar to the dimethoate obtained from docking analysis using Vina Wizard.

Sl. No.	Proteins	Binding Affinities (kcal/mol)
1.	Serum alanine aminotransferase (ALT)	−4.0
2.	Serum aspartate aminotransferase (AST)	−3.5

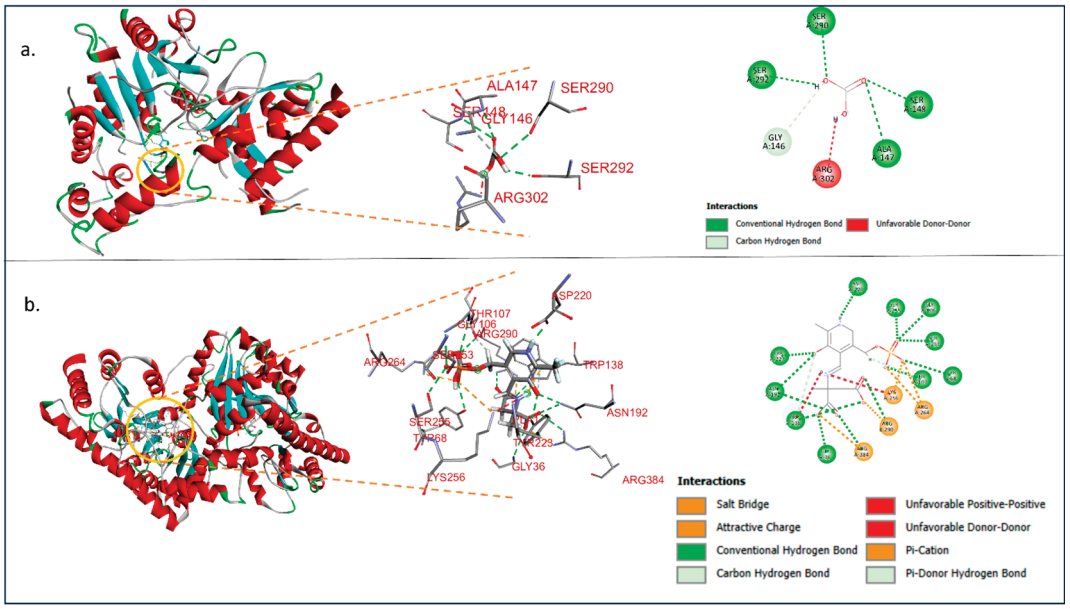

Figure 8. (**a**) Lead interacting with ALT and the 2D representation of the interaction at its left; (**b**) lead interacting with AST and the 2D representation of the interaction at its left.

4. Conclusions

The present study aimed to assess the impact of lead exposure on *Anabas testudineus* in an aquatic ecosystem, with a focus on both its toxicity and the potential mitigating effects of *Ocimum sanctum*. In addition to evaluating lead's harmful effects on *A. testudineus*, the study explored the role of *O. sanctum* in reducing this toxicity. Chronic toxicity tests revealed that lead concentrations of 0.1 mg/L (equivalent to 10% of the 96 h LC_{50}) or higher reduced feeding rate, red blood cell count (RBC), hemoglobin (Hb), hematocrit (Hct) values, plasma glucose, and plasma protein levels, while decreasing white blood cell (WBC) count and serum ALT and AST levels. These physiological alterations, along with decreased appetite, were likely the primary factors contributing to the reduced growth of the fish during prolonged lead exposure. This suggests that *O. sanctum* may play a role in mitigating oxidative stress and other toxic effects of lead, indicating a potential recovery in the fish. These findings demonstrate the significant inhibitory effect of *O. sanctum* on lead toxicity. The results of this study provide critical data on both acute and chronic lead toxicity, which could inform national and international threshold levels for lead disposal in aquatic environments. Additionally, the findings offer valuable insights into sustainable fishery management, breeding programs, and the conservation of economically important native fish species, such as *A. testudineus*, in their natural habitats.

Author Contributions: Conceptualization, N.C.S., P.P. and S.S.; data curation, N.C.S., A.C., and S.S.; formal analysis, N.C.S.; funding acquisition, N.C.S.; investigation, N.C.S., A.C., R.B., and S.S.; methodology, N.C.S., A.C., R.B. and S.S.; project administration, N.C.S.; resources, N.C.S.; software, N.C.S., P.B. and A.S.; supervision, N.C.S. and S.S.; validation, N.C.S.; visualization, N.C.S.; writing—original draft, N.C.S., A.C., P.B., R.B., A.S., and S.S.; writing—review and editing, N.C.S., A.S., P.P., and S.S. All authors have read and agreed to the published version of the manuscript.

Funding: This research received no external funding.

Institutional Review Board Statement: The test bioassay was conducted in accordance with the regulations approved by the Institutional Biosafety Committee—The University of Burdwan (BU/IBSC/22/Zo/36).

Informed Consent Statement: Not applicable.

Data Availability Statement: The datasets generated during the current study are available from the corresponding authors on reasonable request.

Acknowledgments: We appreciate the Department of Zoology of The University of Burdwan in West Bengal, India for providing the essential assistance and physical infrastructure.

Conflicts of Interest: The authors declare no conflicts of interest.

References

1. Rand, G.M.; Petrocelli, S.R. *Fundamentals of Aquatic Toxicology*; HEMISPHERE: London, UK, 1985.
2. Javed, A.; Baig, Z.; Farooqi, A.; van Geen, A. Spatial variation of arsenic in irrigation well water from three flood plains (Ravi, Chenab and Jhelum) of Punjab, Pakistan. In *Environmental Arsenic in a Changing World*; CRC Press: Boca Raton, FL, USA, 2019; pp. 235–236.
3. Joshi, U.; Balasubramanian, R. Characteristics and environmental mobility of trace elements in urban runoff. *Chemosphere* **2010**, *80*, 310–318. [CrossRef] [PubMed]
4. Ghosh, S.; Sadhu, A.; Mandal, A.H.; Biswas, J.K.; Sarkar, D.; Saha, S. Copper Oxide Nanoparticles as an Emergent Threat to Aquatic Invertebrates and Photosynthetic Organisms: A Synthesis of the Known and Exploration of the Unknown. *Curr. Pollut. Rep.* **2024**, *11*, 6. [CrossRef]
5. Alrabie, N.A.; Mohamat-Yusuff, F.; Rohasliney, H.; Zulkeflee, Z.; Amal, M.N.A.; Arshad, A.; Zulkifli, S.Z.; Wijaya, A.R.; Masood, N.; Sani, M.S.A. Preliminary evaluation of heavy metal contamination and source identification in Kuala Lumpur SMART Stormwater Pond Sediments using Pb isotopic signature. *Sustainability* **2021**, *13*, 9020. [CrossRef]
6. Azadikhah, D.; Yalsuyi, A.M.; Saha, S.; Saha, N.C.; Faggio, C. Biochemical and Pathophysiological Responses in Capoeta capoeta under Lethal and Sub-Lethal Exposures of Silver Nanoparticles. *Water* **2023**, *15*, 585. [CrossRef]
7. Dhara, K.; Chukwuka, A.V.; Saha, S.; Saha, N.C.; Faggio, C. Effects of short-term selenium exposure on respiratory activity and proximate body composition of early-life stages of Catla catla, *Labeo rohita* and *Cirrhinus mrigala*. *Environ. Toxicol. Pharmacol.* **2021**, *90*, 103805. [CrossRef]
8. Dhara, K.; Saha, S.; Chukwuka, A.V.; Pal, P.; Saha, N.C.; Faggio, C. Fluoride sensitivity in freshwater snail, Bellamya bengalensis (Lamarck, 1882): An integrative biomarker response assessment of behavioral indices, oxygen consumption, haemocyte and tissue protein levels under environmentally relevant exposure concentrations. *Environ. Toxicol. Pharmacol.* **2021**, *89*, 103789. [CrossRef]
9. Dhara, K.; Saha, S.; Saha, N.C. Toxicity of selenium on the freshwater tropical worm, Branchiura sowerbyi beddard, 1892. *BIOINFOLET Q. J. Life Sci.* **2020**, *17*, 346–354.
10. Mandal, A.H.; Ghosh, S.; Adhurjya, D.; Chatterjee, P.; Samajdar, I.; Mukherjee, D.; Dhara, K.; Saha, N.C.; Piccione, G.; Multisanti, C.R.; et al. Exploring the impact of zinc oxide nanoparticles on fish and fish-food organisms: A review. *Aquac. Rep.* **2024**, *36*, 102038. [CrossRef]
11. Velusamy, S.; Roy, A.; Sundaram, S.; Kumar Mallick, T. A review on heavy metal ions and containing dyes removal through graphene oxide-based adsorption strategies for textile wastewater treatment. *Chem. Rec.* **2021**, *21*, 1570–1610. [CrossRef]
12. Marshall, C.P.; Fairbridge, R.W. *Encyclopedia of Geochemistry*; Springer Science & Business Media: Berlin/Heidelberg, Germany, 1999.
13. Landmeyer, J.; Bradley, P.; Bullen, T. Stable lead isotopes reveal a natural source of high lead concentrations to gasoline-contaminated groundwater. *Environ. Geol.* **2003**, *45*, 12–22. [CrossRef]
14. Yurekli, Y. Removal of heavy metals in wastewater by using zeolite nano-particles impregnated polysulfone membranes. *J. Hazard. Mater.* **2016**, *309*, 53–64. [CrossRef] [PubMed]
15. Lee, J.-W.; Choi, H.; Hwang, U.-K.; Kang, J.-C.; Kang, Y.J.; Kim, K.I.; Kim, J.-H. Toxic effects of lead exposure on bioaccumulation, oxidative stress, neurotoxicity, and immune responses in fish: A review. *Environ. Toxicol. Pharmacol.* **2019**, *68*, 101–108. [CrossRef] [PubMed]

16. Peralta-Videa, J.R.; Lopez, M.L.; Narayan, M.; Saupe, G.; Gardea-Torresdey, J. The biochemistry of environmental heavy metal uptake by plants: Implications for the food chain. *Int. J. Biochem. Cell Biol.* **2009**, *41*, 1665–1677. [CrossRef] [PubMed]
17. Shahid, M.; Dumat, C.; Khalid, S.; Schreck, E.; Xiong, T.; Niazi, N.K. Foliar heavy metal uptake, toxicity and detoxification in plants: A comparison of foliar and root metal uptake. *J. Hazard. Mater.* **2017**, *325*, 36–58. [CrossRef]
18. Siddique, T.; Okeke, B.C.; Arshad, M.; Frankenberger, W.T. Biodegradation kinetics of endosulfan by Fusarium ventricosum and a Pandoraea species. *J. Agric. Food Chem.* **2003**, *51*, 8015–8019. [CrossRef]
19. Ramírez-Sandoval, M.; Melchor-Partida, G.; Muñiz-Hernández, S.; Girón-Pérez, M.; Rojas-García, A.; Medina-Díaz, I.; Robledo-Marenco, M.; Velázquez-Fernández, J. Phytoremediatory effect and growth of two species of Ocimum in endosulfan polluted soil. *J. Hazard. Mater.* **2011**, *192*, 388–392. [CrossRef]
20. APHA. *Standard Methods for the Examination of Water and Wastewater*; American Public Health Association: Washington, DC, USA, 2012; Volume 2.
21. Kaviraj, A.; Bhunia, F.; Saha, N. Toxicity of methanol to fish, crustacean, oligochaete worm, and aquatic ecosystem. *Int. J. Toxicol.* **2004**, *23*, 55–63. [CrossRef]
22. Saha, S.; Saha, N.C.; Mukherjee, D. Acute Toxicity and Behavioral Alterations of Oligochaete Worm, Branchiura sowerbyi Exposed to Diazinon. *Res. Rev. J. Life Sci.* **2018**, *8*, 1–5.
23. Saha, S.; Mukherjee, D.; Saha, N.C. Evaluation of acute toxicity and behavioral responses of *Heteropneustes fossilis* (Linn.) exposed to Captan. *Int. J. Life Sci.* **2018**, *6*, 205–208.
24. Saha, S.; Mukherjee, D.; Dhara, K.; Saha, N.C. Acute Toxicity Bioassay of a Pyrethroid Pesticide Bifenthrin to the Asian Stinging Catfish, *Heteropneustes Fossilis* (Bloch). *Curr. World Environ.* **2021**, *16*, 250–258. [CrossRef]
25. Saha, S.; Chukwuka, A.V.; Mukherjee, D.; Dhara, K.; Adeogun, A.O.; Saha, N.C. Effects of short-term sub-lethal diazinon® exposure on behavioural patterns and respiratory function in *Clarias batrachus*: Inferences for adaptive capacity in the wild. *Chem. Ecol.* **2022**, *38*, 180–194. [CrossRef]
26. Saha, S.; Banerjee, P.; Saha, N.C.; Chukwuka, A.V. Triazophos-induced Respiratory and Behavioral Effects and Development of Adverse Outcome Pathway (AOP) for short-term Exposed Freshwater Snail, Bellamya Bengalensis. *Bull. Environ. Contam. Toxicol.* **2023**, *110*, 94. [CrossRef] [PubMed]
27. Chukwuka, A.V.; Saha, S.; Mukherjee, D.; Banerjee, P.; Dhara, K.; Saha, N.C. Deltamethrin-Induced Respiratory and Behavioral Effects and Adverse Outcome Pathways (AOP) in Short-Term Exposed Mozambique Tilapia, Oreochromis mossambicus. *Toxics* **2022**, *10*, 701. [CrossRef] [PubMed]
28. Dhara, K.; Saha, S.; Saha, N.C. Sensitivity of Common Carp, *Cyprinus carpio* (Linnaeus, 1758) to the Grey List Metal, Zinc under Laboratory Condition. *Asian J. Biol. Life Sci.* **2021**, *10*, 133. [CrossRef]
29. Dhara, K.; Shubhajit, S.; Chukwuka, A.V.; Saha, N.C. Behavioural toxicity and respiratory distress in early life and adult stage of walking catfish *Clarias batrachus* (Linnaeus) under acute fluoride exposures. *Toxicol. Environ. Health Sci.* **2021**, *14*, 33–46. [CrossRef]
30. Dhara, K.; Saha, S.; Mukherjee, D.; Saha, N.C. Comparative acute toxicity of mercury to air breathing fish, Channa gachua (Ham.) and non-air breathing fish *Cyprinus carpio* (Linn.): Ethological and Haematological Consideration. *Indian J. Ecol.* **2021**, *48*, 1243–1253.
31. Le Cren, E.D. The length-weight relationship and seasonal cycle in gonad weight and condition in the perch (Perca fluviatilis). *J. Anim. Ecol.* **1951**, *20*, 201–219. [CrossRef]
32. Saha, S.; Chukwuka, A.V.; Mukherjee, D.; Dhara, K.; Pal, P.; Saha, N.C. Physiological (haematological, growth and endocrine) and biochemical biomarker responses in air-breathing catfish, *Clarias batrachus* under long-term Captan® pesticide exposures. *Environ. Toxicol. Pharmacol.* **2022**, *90*, 103815. [CrossRef]
33. Bourlière, F.; Brown, M.E. (Eds.) *The Physiology of Fishes*; Academic Press: New York, NY, USA, 1957; Volume 2.
34. Magnhagen, C.; Braithwaite, V.; Forsgren, E.; Kapoor, B. *Fish Behaviour*; Science Publishers: Enfield, NH, USA, 2008.
35. Dacie, J.V.; Lewis, S.M. Practical haematology. In *Practical Hæmatology*; Elsevier: Amsterdam, The Netherlands, 1995; p. 609.
36. Sahli, T. *Text Book of Clinical Pathology*; Williams and Willams, Co.: Baltimore, MD, USA, 1962; 35p.
37. Poet, T.S.; Kousba, A.A.; Dennison, S.L.; Timchalk, C. Physiologically based pharmacokinetic/pharmacodynamic model for the organophosphorus pesticide diazinon. *Neurotoxicology* **2004**, *25*, 1013–1030. [CrossRef]
38. Lowry, O.H.; Rosebrough, N.J.; Farr, A.L.; Randall, R.J. Protein measurement with the Folin phenol reagent. *J. Biol. Chem.* **1951**, *193*, 265–275. [CrossRef]
39. Trinder, P. Determination of glucose in blood using glucose oxidase with an alternative oxygen acceptor. *Ann. Clin. Biochem.* **1969**, *6*, 24–27. [CrossRef]
40. Kattermann, R.; Jaworek, D.; Möller, G. Multicentre study of a new enzymatic method of cholesterol determination. *Clin. Chem. Lab. Med.* **1984**, *22*, 245–252. [CrossRef] [PubMed]
41. Bowers, L.D. Kinetic serum creatinine assays I. The role of various factors in determining specificity. *Clin. Chem.* **1980**, *26*, 551–554. [CrossRef] [PubMed]
42. Reitman, S.; Frankel, S. A colorimetric method for the determination of serum glutamic oxalacetic and glutamic pyruvic transaminases. *Am. J. Clin. Pathol.* **1957**, *28*, 56–63. [CrossRef]
43. Waterhouse, A.; Bertoni, M.; Bienert, S.; Studer, G.; Tauriello, G.; Gumienny, R.; Heer, F.T.; de Beer, T.A.P.; Rempfer, C.; Bordoli, L. SWISS-MODEL: Homology modelling of protein structures and complexes. *Nucleic Acids Res.* **2018**, *46*, W296–W303. [CrossRef]

44. Studer, G.; Tauriello, G.; Bienert, S.; Biasini, M.; Johner, N.; Schwede, T. ProMod3—A versatile homology modelling toolbox. *PLoS Comput. Biol.* **2021**, *17*, e1008667. [CrossRef]
45. Muddagoni, N.; Bathula, R.; Dasari, M.; Potlapally, S.R. Homology modeling, virtual screening, prime-MMGBSA, AutoDock-identification of inhibitors of FGR protein. *Biointerface Res. Appl. Chem.* **2021**, *11*, 11088–11103.
46. Dallakyan, S.; Olson, A.J. Small-molecule library screening by docking with PyRx. *Chem. Biol. Methods Protoc.* **2015**, *1263*, 243–250.
47. Studio, D.J.A. *Discovery Studio*; Accelrys: San Diego, CA, USA, 2008; p. 420.
48. Finney, D. Statistical logic in the monitoring of reactions to therapeutic drugs. *Methods Inf. Med.* **1971**, *10*, 237–245. [CrossRef]
49. Ullah, S.; Li, Z.; Hasan, Z.; Khan, S.U.; Fahad, S.J.E.; Safety, E. Malathion induced oxidative stress leads to histopathological and biochemical toxicity in the liver of rohu (Labeo rohita, Hamilton) at acute concentration. *Ecotoxicol. Environ. Saf.* **2018**, *161*, 270–280. [CrossRef]
50. Singh, S.; Srivastava, P.K.; Kumar, D.; Tripathi, D.K.; Chauhan, D.K.; Prasad, S.M. Morpho-anatomical and biochemical adapting strategies of maize (*Zea mays* L.) seedlings against lead and chromium stresses. *Biocatal. Agric. Biotechnol.* **2015**, *4*, 286–295. [CrossRef]
51. Murugan, S.S.; Karuppasamy, R.; Poongodi, K.; Puvaneswari, S. Bioaccumulation pattern of zinc in freshwater fish *Channa punctatus* (Bloch.) after chronic exposure. *Turk. J. Fish. Aquat. Sci.* **2008**, *8*, 55–59.
52. Hesni, M.A.; Dadolahi-Sohrab, A.; Savari, A.; Mortazavi, M.S. Study the acute toxicity of lead nitrate metal salt on behavioral changes of the milkfish (Chanos chanos). *World J. Fish Mar. Sci.* **2011**, *3*, 496–501.
53. Nekoubin, H.; Gharedaashi, E.; Hatefi, S.; Sudagar, M.; Shahriari, R.; Asgharimoghadam, A. Determination of LC50 of copper sulfate and lead (II) nitrate and behavioral responses of grass carp (Ctenopharyngodon idella). *Walailak J. Sci. Technol.* **2012**, *9*, 333–340.
54. Nuraini, N.; Tanjung, A.; Warningsih, T.; Muchlisin, Z.A. Induced spawning of siban fish Cyclocheilichthys apogon using Ovaprim. *F1000 Res.* **2017**, *6*, 1855. [CrossRef]
55. Abdel-Tawwab, M.; El-Sayed, G.O.; Shady, S.H. Growth, biochemical variables, and zinc bioaccumulation in Nile tilapia, *Oreochromis niloticus* (L.) as affected by water-born zinc toxicity and exposure period. *Int. Aquat. Res.* **2016**, *8*, 197–206. [CrossRef]
56. Rajput, V.D.; Minkina, T.M.; Behal, A.; Sushkova, S.N.; Mandzhieva, S.; Singh, R.; Gorovtsov, A.; Tsitsuashvili, V.S.; Purvis, W.O.; Ghazaryan, K.A. Effects of zinc-oxide nanoparticles on soil, plants, animals and soil organisms: A review. *Environ. Nanotechnol. Monit. Manag.* **2018**, *9*, 76–84. [CrossRef]
57. Dauble, D.D.; Barraclough, S.A.; Bean, R.M.; Fallon, W.E. Chronic Effects of Coal-Liquid Dispersions on Fathead Minnows and Rainbow Trout. *Trans. Am. Fish. Soc.* **1983**, *112*, 712–719. [CrossRef]
58. Shukla, J.; Pandey, K. Effect of a sublethal concentration of zinc sulphate on the growth rate of fingerlings of *Channa punctatus* (Bloch), a freshwater murrel. *Acta Hydrochim. Hydrobiol.* **1986**, *14*, 677–680. [CrossRef]
59. Bekmezci, H.D.; Nevin, Ü. Aşağı Seyhan Ovasi Drenaj Sistemlerindeki Kirlilik Etmenlerinin Clarias gariepinus' da Toksik Etkileri. *Ç.Ü Fen ve Mühendislik Bilimleri* **2010**, *28*, 11–20.
60. Ahmed, A.S.; Sultana, S.; Habib, A.; Ullah, H.; Musa, N.; Hossain, M.B.; Rahman, M.M.; Sarker, M.S.I. Bioaccumulation of heavy metals in some commercially important fishes from a tropical river estuary suggests higher potential health risk in children than adults. *PLoS ONE* **2019**, *14*, e0219336. [CrossRef]
61. Abdel-Tawwab, M.; Mousa, M.A.; Ahmad, M.H.; Sakr, S.F. The use of calcium pre-exposure as a protective agent against environmental copper toxicity for juvenile Nile tilapia, *Oreochromis niloticus* (L.). *Aquaculture* **2007**, *264*, 236–246. [CrossRef]
62. Van der Oost, R.; Beyer, J.; Vermeulen, N.P. Fish bioaccumulation and biomarkers in environmental risk assessment: A review. *Environ. Toxicol. Pharmacol.* **2003**, *13*, 57–149. [CrossRef] [PubMed]
63. Dewi, N.K.; Prabowo, R. Determination of liver somatic index (LSI) and gonadosomatic index (GSI) value of crap (*Cyprinus carpio*) and Nile tilapia (Perca fluviatilis). *Int. J. Sci. Res. Publ.* **2017**, *7*, 220–223.
64. Bain, P.; Harr, K.E. Hematology of amphibians. *Schalm's Vet. Hematol.* **2022**, 1228–1232. [CrossRef]
65. Nussey, G.; Van Vuren, J.; Du Preez, H. Effect of copper on blood coagulation of Oreochromis mossambicus (Cichlidae). *Comp. Biochem. Physiol. Part C Pharmacol. Toxicol. Endocrinol.* **1995**, *111*, 359–367. [CrossRef]
66. Nakagawa, H.; Nakagawa, K.; Sato, T. Evaluation of erythrocyte 5-aminolevulinic acid dehydratase activity in the blood of carp *Cyprinus carpio* as an indicator in fish with water lead pollution. *Fish. Sci.* **1995**, *61*, 91–95. [CrossRef]
67. Petřivalský, M.; Machala, M.; Nezveda, K.; Piačka, V.; Svobodová, Z.; Drábek, P. Glutathione-dependent detoxifying enzymes in rainbow trout liver: Search for specific biochemical markers of chemical stress. *Environ. Toxicol. Chem.* **1997**, *16*, 1417–1421.
68. Dick, P.; Dixon, D.G. Changes in circulating blood cell levels of rainbow trout, Salmo gairdneri Richardson, following acute and chronic exposure to copper. *J. Fish Biol.* **1985**, *26*, 475–481. [CrossRef]
69. Allen, P. Changes in the haematological profile of the cichlid Oreochromis aureus (Steindachner) during acute inorganic mercury intoxication. *Comp. Biochem. Physiol. Part C Pharmacol. Toxicol. Endocrinol.* **1994**, *108*, 117–121. [CrossRef]
70. Maheshwari, S.; Dua, A. Structural analysis of the erythrocytes of *Channa punctatus* (Bloch) exposed to mercuric chloride using scanning electron microscopy. *Turk. J. Fish. Aquat. Sci.* **2016**, *16*, 865–871. [CrossRef]
71. Abdel-Hameid, N. A protective effect of calcium carbonate against arsenic toxicity on the Nile catfish, larias gariepinus. *Turk. J. Fish. Aquat. Sci.* **2008**, *12*, 143–163. [CrossRef]
72. Livingstone, D. The fate of organic xenobiotics in aquatic ecosystems: Quantitative and qualitative differences in biotransformation by invertebrates and fish. *Comp. Biochem. Physiol. Part A Mol. Integr. Physiol.* **1998**, *120*, 43–49. [CrossRef] [PubMed]

73. Kavitha, C.; Malarvizhi, A.; Kumaran, S.S.; Ramesh, M. Toxicological effects of arsenate exposure on hematological, biochemical and liver transaminases activity in an Indian major carp, Catla catla. *Food Chem. Toxicol.* **2010**, *48*, 2848–2854. [CrossRef] [PubMed]
74. Syversen, T.L. Effects of methyl mercury on protein synthesis in vitro. *Acta Pharmacol. Toxicol.* **1981**, *49*, 422–426. [CrossRef] [PubMed]
75. Nanda, P.; Behera, M.K. Nickel induced changes in some hemato-biochemical parameters of a catfish *Heteropneustes fossilis* (Bloch). *Environ. Ecol.* **1996**, *14*, 82–85.
76. Kumar, R.; Banerjee, T.K. Arsenic induced hematological and biochemical responses in nutritionally important catfish *Clarias batrachus* (L.). *Toxicol. Rep.* **2016**, *3*, 148–152. [CrossRef]
77. Canli, M. Effects of mercury, chromium and nickel on some blood parameters in the carp *Cyprinus carpio*. *Turk. J. Zool.* **1995**, *19*, 305–312.
78. Yang, J.-L.; Chen, H.-C. Effects of gallium on common carp (*Cyprinus carpio*): Acute test, serum biochemistry, and erythrocyte morphology. *Chemosphere* **2003**, *53*, 877–882. [CrossRef]
79. Parvathi, K.; Palanivel, S.; Mathan, R.; Sarasu, R. Sublethal effects of chromium on some biochemical profiles of the fresh water teleost, *Cyprinus carpio*. *Portal Reg. Da BVS* **2011**, *2*, 295–300.
80. Abdel-Tawwab, M.; El-Sayed, G.O.; Shady, S.H. Effects of dietary protein levels and environmental zinc exposure on the growth, feed utilization, and biochemical variables of Nile tilapia, *Oreochromis niloticus* (L.). *Toxicol. Environ. Chem.* **2012**, *94*, 1368–1382. [CrossRef]
81. Roy, S.; Bhattacharya, S. Arsenic-induced histopathology and synthesis of stress proteins in liver and kidney of *Channa punctatus*. *Ecotoxicol. Environ. Saf.* **2006**, *65*, 218–229. [CrossRef] [PubMed]
82. Onah, C.E.; Meludu, S.C.; Dioka, C.E.; Onuegbu, A.J.; Onah, C.F.; Ajaghaku, D.L.; Nnodim, J.K.; Ejeatuluchukwu, O. Amelioratory effect of methanolic leaf extract of Moringa oleifera on some liver and kidney function and oxidative stress markers in lead-intoxicated rats. *Eur. J. Med. Plants* **2016**, *12*, 1–12. [CrossRef]
83. Sharma, K.; Upreti, N.; Sharma, S.; Sharma, S. Protective effect of Spirulina and tamarind fruit pulp diet supplement in fish (Gambusia affinis Baird & Girard) exposed to sublethal concentration of fluoride, aluminum and aluminum fluoride. *NIScPR Online Period. Repos.* **2012**, *50*, 897–903.
84. Velmurugan, B.; Selvanayagam, M.; Cengiz, E.I.; Ugurlu, P. Scanning electron microscopy study of the gills, scales and erythrocytes of Anabas testudineus upon exposure to chlorpyrifos. *Toxicol. Environ. Chem.* **2015**, *97*, 208–220. [CrossRef]
85. Sawhney, A.; Johal, M.S. Erythrocyte alterations induced by malathion in *Channa punctatus* (Bloch). *Bull. Environ. Contam. Toxicol.* **2000**, *64*, 398–405. [CrossRef]
86. Massar, B.; Dey, S.; Barua, R.; Dutta, K. Microscopy and microanalysis of hematological parameters in common carp, *Cyprinus carpio*, inhabiting a polluted lake in North East India. *Microsc. Microanal.* **2012**, *18*, 1077–1087. [CrossRef]
87. Isomaa, B.; Hägerstrand, H.; Paatero, G.; Engblom, A.C. Permeability alterations and antihaemolysis induced by amphiphiles in human erythrocytes. *Biochim. Biophys. Acta (BBA)-Biomembr.* **1986**, *860*, 510–524. [CrossRef]
88. Naskar, R.; Veenapani, S.M.; Kumari, K.; Sen, N.S.; Ahmad, M.F. Surface ultrastructural changes in the gills of an indian stenohaline catfish, *Clarias batrachus* (Linn.) under acute acid and aluminium stress. *Ecoscan* **2009**, *3*, 221–226.
89. Gosto, R. Assessment of accuracies of protein 3-dimensional prediction software. *Southeast Eur. J. Soft Comput.* **2018**, *7*, 83–85. [CrossRef]
90. Williams, C.J.; Headd, J.J.; Moriarty, N.W.; Prisant, M.G.; Videau, L.L.; Deis, L.N.; Verma, V.; Keedy, D.A.; Hintze, B.J.; Chen, V.B. MolProbity: More and better reference data for improved all-atom structure validation. *Protein Sci.* **2018**, *27*, 293–315. [CrossRef]
91. Ramachandran, S.; Kota, P.; Ding, F.; Dokholyan, N.V. Automated minimization of steric clashes in protein structures. *Proteins Struct. Funct. Bioinform.* **2011**, *79*, 261–270. [CrossRef]
92. Sievers, C.K.; Shanle, E.K.; Bradfield, C.A.; Xu, W. Differential action of monohydroxylated polycyclic aromatic hydrocarbons with estrogen receptors α and β. *Toxicol. Sci.* **2013**, *132*, 359–367. [CrossRef]

toxics

MDPI

Article

Using Sediment Bacterial Communities to Predict Trace Metal Pollution Risk in Coastal Environment Management: Feasibility, Reliability, and Practicability

Yuanfen Xia [1], Jiayuan Liu [2,*], Xuechun Yang [2], Xiaofeng Ling [1], Yan Fang [1], Zhen Xu [1] and Fude Liu [2,*]

[1] State Power Environmental Protection Research Institute, Nanjing 210031, China; wzwfenfen@163.com (Y.X.); xygslxf@163.com (X.L.); wyl20180227@sina.com (Y.F.); alex_xuzhen@163.com (Z.X.)
[2] School of Environmental Science and Safety Engineering, Tianjin University of Technology, Tianjin 300384, China; yxcxcm@163.com
* Correspondence: ljy17695687200@163.com (J.L.); lfdsy@tjut.edu.cn (F.L.)

Abstract: The distribution of trace metals (TMs) in a continuous water body often exhibits watershed attributes, but the tidal gates of the coastal rivers may alter their transformation and accumulation patterns. Therefore, a tidal gate-controlled coastal river was selected to test the distribution and accumulation risks of Al, As, Cr, Cu, Fe, Mn, Ni, Sr, and Zn in the catchment area (CA), estuarine area (EA), and offshore area (OA). Associations between TMs and bacterial communities were analyzed to assess the feasibility of using bacterial parameters as ecological indicators. The results showed that As and Cr were the key pollutants due to the higher enrichment factor and geoaccumulation index, reaching slight to moderate pollution levels. The Nemero index was highest in EAs (14.93), indicating a higher pollution risk in sediments near tide gates. Although the TM dynamics can be explained by the metal-indicating effects of Fe and Mn, they have no linear relationships with toxic metals. Interestingly, the metabolic abundance of bacterial communities showed good correlations with different TMs in the sediment. These results highlight bacterial community characteristics as effective biomarkers for assessing TM pollution and practical tools for managing pollution control in coastal environment.

Keywords: accumulation risk; bacterial community; coastal watershed; tidal gate; trace metals

1. Introduction

At the global scale, trace metal (TM) pollution poses a significant threat to coastal ecosystems [1–4]. TMs are generally derived from natural (erosion and mineral weathering) and anthropogenic (industrial or mining activities) sources and are transferred to the coastal ecosystems through river transport and wastewater discharge [1,2,5,6]. Given their toxic, persistent, and non-releasable properties, TMs in sediments can persist in an elemental state, which disrupts food chains and threaten ecological balance [7]. Even when TM concentrations fall within regional environmental standards, their latent risks to humans and ecosystems health remain severe and require urgent attention [8,9].

TM pollution has captured the attention of many environmental scientists, due to its ability to induce bioaccumulation and disrupt the delicate ecological equilibrium, particularly in coastal river ecosystems [8,10]. TMs not only migrate over long-distances but are also influenced by the migration behavior of aquatic organisms, which can alter their distribution across different watershed zones [11]. Many studies have characterized TM pollution, toxicity, and enrichment by analyzing TM content in water bodies [12], sediments [13], and fish [14]. Additionally, source identification methods have been employed to trace the sources of TMs [15]. However, these approaches primarily focus on natural aquatic systems, neglecting the impacts of human-engineered structures like tidal gates. Tide gates, widely constructed for flood control and land management, profoundly alter

sediment transport and TM dynamics in coastal watersheds. During the tidal gate closure, sediments from the catchment accumulate in the estuary, and this continued accumulation not only leads to peak concentrations of toxic metals [16] but also complicates the variable environmental conditions in the estuary [17], which undoubtedly adds more uncertainties and restrictions in identifying pollution risk factors and establishing prevention and control strategies at the watershed scale [18,19]. Therefore, the characteristics of distribution, the source, and the accumulation of TMs in sediments and their influencing factors need further research, especially in the tidal gate-controlled coastal watersheds.

Bacterial communities in sediment play a critical role in influencing the endogenous migration or enrichment of TMs [20]. These communities influence TM distribution and transformation through mechanisms such as assimilation [21], metabolism processes [22], and the alteration of environmental conditions [23,24]. Moreover, the precipitation process of TMs is substantially affected by fundamental chemical reactions associated with bacterial activity. For example, bacteria-mediated reduction reactions involving Fe compounds have been found to determine the distribution of TMs [25]. Conversely, TMs in sediments can also cause fluctuations in bacterial communities, not only for heavy metals [26] but even for light metals derived from parent material [27]. Thus, the dynamic relationship underscores the importance of bacterial communities in TM cycling and ecosystem health. Currently, bacterial communities are being increasingly employed as an effective tool for assessing and predicting ecosystem health [28], due to their high sensitivity to environmental changes [29] and adaptive mechanisms for ecosystem succession [30]. These studies are largely based on bacterial community composition or the alpha diversity of related functional genes to estimate the quality levels of ecosystems. For example, previous studies found that soil bacterial community composition is closely associated with land use types. Within the framework of a random forest model, it was possible to accurately classify land use and predict changes in soil quality parameters with an accuracy rate of 50 to 95% [26]. Furthermore, with increasing levels of environmental pollution, the functional gene community diversity detected by the comprehensive functional gene array (GeoChip5) significantly increased, and these changes can be directly used to predict nitrate pollution and ecosystem functions [31]. While bacterial communities have shown potential as bioindicators, their application in such anthropogenic-influenced ecosystems remains limited. This gap hinders the development of effective strategies for managing TM pollution in these complex environments. In our previous study, the functional metabolic abundance of bacterial communities was applied to the classification of space units in the coastal watershed [32]. Based on this, we hypothesize that due to the high sensitivity of bacterial communities to environmental changes [32], the functional metabolic abundance of bacterial communities could serve as a reliable ecological indicator for predicting TM pollution levels compared to traditional pollutant identification methods, offering a novel approach to ecosystem health assessment in tidal gate-controlled coastal watersheds.

Tianjin, the second-largest city in the Bohai Rim urban agglomeration of China, has numerous rivers, a substantial population, and developed industry and agriculture sectors. Over the past several decades, high-intensity land reclamation and the widespread implementation of tidal gates have significantly altered the natural dynamics of coastal ecosystems. These changes have led to varying levels of TM contamination in sediments. Early reports suggest that sediment accumulation and sewage discharge play a dominant role in TM contamination in the estuary [33]. However, the continued influence of tidal gates exacerbates TM deposition, resulting in persistent pollution risks; even the Chinese government's integrated land use planning efforts have reduced direct land-based pollutant emissions [29]. Specifically, some TMs, such as Cd, As, Cr, Cu, and Zn, continue to pose potential risks in many estuarine and coastal sediments from Bohai Bay [34]. Therefore, there is an urgent need to investigate the migration mechanisms of TMs in this region, providing feasible approaches for similar tidal-gate-controlled coastal aquatic areas globally.

The Duliujian river watershed in Bohai Bay was selected as the study area due to its representative characteristics of tidal gate-controlled coastal systems. This region is

a hotspot for intensive industrial and agricultural activities, making it vulnerable to TM contamination. The presence of distinct spatial units—the catchment area (CA), estuarine area (EA), and offshore area (OA)—provides a unique opportunity to investigate TM dynamics across different environmental gradients. This paper also discusses the interrelationships of the sediments of TM contents (Al, As, Cr, Cu, Fe, Mn, Ni, Sr, and Zn), the bacterial communities, and the major physicochemical properties. The objectives of our study are as follows: (1) to assess the spatial variation in TMs and bacterial communities in sediments in different spatial units at the watershed scale; (2) to explore the potential risk of enrichment, contamination, and accumulation of TMs in sediments, identify the main influencing factors, and analyze them retrospectively; and (3) to try to determine the contamination status of TMs by using the structure, diversity, and metabolism abundance of bacterial communities, and then, to discuss the feasibility, reliability, and practicability of bacterial communities as ecological indicators in identifying TM pollution and risk in the coastal watershed management.

2. Materials and Methods

2.1. Site Description

The Duliujian river watershed is an important flood channel in Tianjin, which belongs to the Daqing watershed system and is an artificial river channel that leads floods from the Daqing and Ziya rivers to the sea. It eventually flows into Bohai Bay in Northern China, which is the second largest bay, and accounts for one fifth of the total area of Bohai Bay. Due to the weak water exchange between Bohai Bay and the Yellow Sea, the physical self-cleaning capacity of Bohai Bay is very weak [35]. Many studies have shown that Bohai Bay has been subject to varying degrees of organic pollution [34,36]. To combat the continuing pollution of Bohai Bay, 12 major rivers that flow into Bohai Bay in Tianjin were set up with tidal gates in 2011.

2.2. Sampling Collection

In this study, the sediment samples of the Duliujian river watershed were collected in September 2020. Based on the distribution of its mainstem and tributaries and the alignment of the coastal watershed, the Duliujian river watershed can be divided into three different spatial units, namely the CA, EA, and OA. The study area spans 120 km from the CA to the OA. At each sampling location, the surface sediment (0–20 cm) was collected using a mud sampler, and plant roots, shellfish, and other impurities were removed from each sediment sampling. Each sampling location was collected 3–5 times to form a comprehensive sample, thereby accurately estimating the actual situation of these sites. Some of the samples were placed in polyethylene plastic bags, transported back to the laboratory, and stored at −20 °C in a refrigerator for determination of physicochemical parameters and TM content, and the other samples were stored in dry ice buckets for the determination of 16s rRNA. A total of 41 sampling locations in the CA (20 locations), EA (12 locations), and OA (9 locations) were used to determine the physicochemical properties, and 35 sampling locations were used to determine the 16s rRNA in sediments. All sampling locations are shown in Figure 1.

2.3. Sample Processing, Sequencing, and Analysis

In this study, the physicochemical properties and TM content in sediments were determined by the following methods: air-dried samples were digested on a graphene electric heating plate for 2–3 h using a mixture of concentrated nitric acid and hydrofluoric acid, with concentrations of 1.42 g/mL (15 mL) and 1.16 g/mL (5 mL), respectively [37]. Then, the acid was removed and cooled to 2–3 mL, the cooling liquid was transferred into a 25 mL volumetric flask to ensure constant volume, and the TM contents and total P (TP) in the sediment samples were determined using inductively coupled plasma atomic emission spectrometry (VISTA-MPX, Varian, Palo Alto, CA, USA—2000) [38]. Furthermore, the air-dried samples were put into the flow analyzer to determine the content of total N (TN), the pH and salinity in sediment were determined by pH meter (Delta320, Mettler Toledo,

Greifensee, Switzerland—2007) and conductivity meter (DDSJ-308A, LEICI, Shanghai, China—2010), the moisture content (MC) in the sediment was determined by the drying weighing method, and sediment organic matter (SOM) was determined by the potassium dichromate external heating method [32]. For 16s amplicon sequencing, its experimental process and analytical methods have been published [27], and have also been supplemented in the Supplementary Method S1.

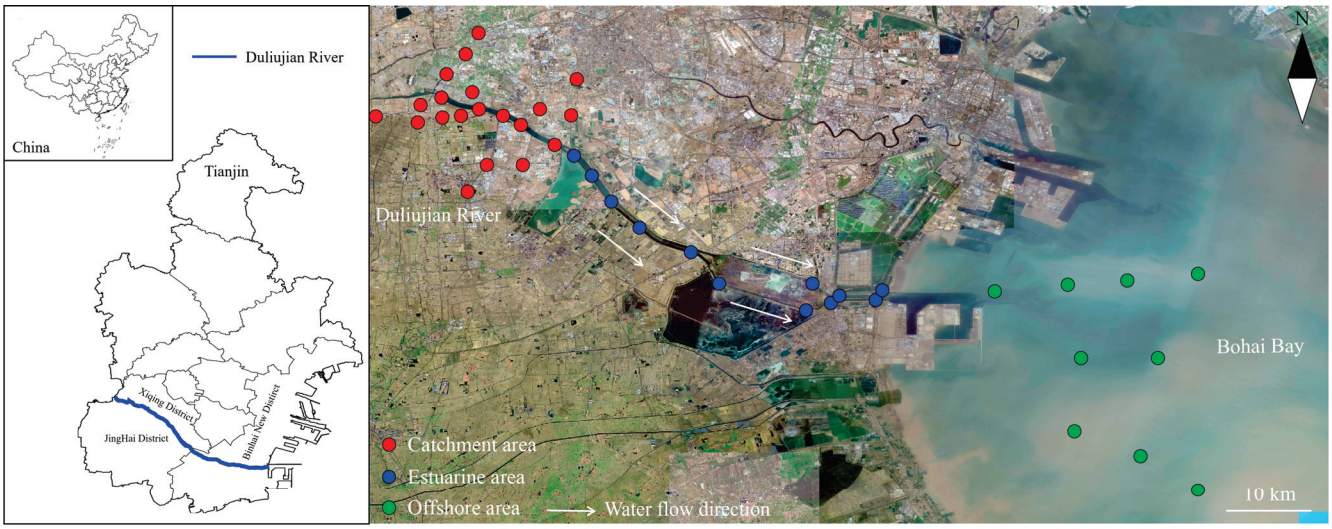

Figure 1. Sampling locations map in the catchment area (CA), estuarine area (EA), and offshore area (OA) of Duliujian river watershed in Bohai Bay (details in Table S1).

2.4. Laboratory Analysis

2.4.1. Enrichment Factor

The enrichment factor (EF) method was used to evaluate the TMs in this study [38].

$$\mathrm{EF} = \frac{\left(\frac{C_M}{C_R}\right)\mathrm{sample}}{\left(\frac{C_M}{C_R}\right)\mathrm{background}} \quad (1)$$

where $\frac{C_M}{C_R}$ is the ratio of measured and reference metals of the sediment samples and their corresponding background values. The background values of TMs in Tianjin Province were used to assess pollution levels in this study area [39]. Specifically, the background values of Al, As, Cr, Cu, Fe, Mn, Ni, Sr, and Zn are 73,200, 9.6. 84.2, 28.8, 33,500, 33.3, 200, and 79.3 mg/kg, respectively.

If EF > 1, the metal is relatively enriched and influenced by human activities. If EF ≈ 1, it originates from the weathering of the crust. In addition to the use of EF values to evaluate the TM source, the enrichment degrees of the TMs were also classified according to the following EF values: EF < 2, slight enrichment; 2 ≤ EF < 5, moderate enrichment; 5 ≤ EF < 20, moderate and high enrichment; 20 ≤ EF < 40, high enrichment; and EF ≥ 40, severe enrichment [38].

2.4.2. Geoaccumulation Index

The geoaccumulation index (I_{geo}) was used to evaluate pollution [40].

$$I_{geo} = \log_2[C_n/(k \times B_n)] \quad (2)$$

where C_n is the measured content of metal in sediments, and B_n is the geochemical background value of the TMs in sediments. The background values of the geological elements in Tianjin are described as TM background values, and K was 1.5. The pollution degree can be classified based on the following I_{geo} values: $I_{geo} < 0$, no pollution; $0 \leq I_{geo} < 1$,

no pollution-medium pollution; $1 \leq I_{geo} < 2$, medium pollution; $2 \leq I_{geo} < 3$, medium pollution-heavy pollution; and $3 \leq I_{geo} < 4$, heavy pollution [40].

2.4.3. Nemero Comprehensive Pollution Index

The Nemero comprehensive pollution index (PN) method was used to quantify the degree of TM pollution in this study [41].

$$PN = \sqrt{\frac{\left(\frac{C_i}{S_i}\right)^2_{max} + \left(\frac{1}{n}\sum_{i=1}^{n}\frac{C_i}{S_i}\right)^2}{2}} \quad (3)$$

where PN is the synthesis evaluation score, C_i is the measured content of the *i*-th element at a sampling location, and S_i is the evaluation criterion of the *i*-th element. The evaluation criterion used in this study is based on the "China Environmental Quality Standard for Sediment Metals (HJ 1315—2023)" (pH > 7.5) [37]. Al, Fe, Mn, and Sr were evaluated based on the background values of territorial sediment elements (i.e., Al, Fe, Mn, and Sr are not specified in HJ 1315—2023). The *PN* value was graded into five categories: $PN \leq 0.7$, safety; $0.7 < PN \leq 1.0$, guard; $1.0 < PN \leq 2.0$, low pollution; $2.0 < PN \leq 3.0$, moderate pollution; and $PN > 3.0$, severe pollution.

2.5. Statistical Analysis

The "ggcor" R package was used to understand the correlation between the contents and related indices of TMs and environmental factors in sediments [42,43]. Furthermore, the "vegan" R package was used for non-metric multidimensional scaling (NMDS) and principal coordinate analysis (PCoA), which determined the difference in distribution characteristics in the bacterial communities and TM contents of different spatial units [44,45]. Finally, the "ggplot2" R package was used for visualization [46,47].

The relationship between TM–TM and TM–TM-related indices is presented using linear fitting. Principal component analysis (PCA) was used to analyze the sources of different TMs in sediments [41]. SourceTracker was used to analyze the source and sink relationships of TMs across different spatial units [48]. Furthermore, redundancy analysis (RDA) was used to determine the influencing factors of environmental factors, TM contents, and bacterial community parameters [49]. Variance partitioning analysis (VPA) was used to analyze the impact of TMs and bacterial dynamics on toxic metals and TM related indices [49].

In this study, data statistics and result visualization were completed using SPSS 25, Origin 2019, R 4.10, Canoco 5, and Surfer 15.

3. Results and Discussion

3.1. Physicochemical Properties in Sediments of Duliujian River Watershed

The trends of all physicochemical properties in sediments of the CA, EA, and OA were different (Table S2). ANOVA indicated that the pH and TP have the same trend significantly, which shows that EA > OA > CA (Table S2; $p < 0.05$). Moreover, the trend of MC is shown as OA > CA > EA, which has significant differences in different spatial units (Table S2; $p < 0.05$). In addition, TN (520.42 ± 56.16 mg/kg) and SOM (12,250.33 ± 432.28 mg/kg) in the EA are significantly lower than those in the CA and OA (Table S2; $p < 0.05$). Furthermore, salinity has a signifying gradient at the watershed scale, which shows that OA > EA > CA (Table S2; $p < 0.05$).

In terms of elemental cycling, N and P in the sediment show opposite trends. P is a sedimentary cycle [31], and more P accumulates in the EA probably due to the closure of the tidal gates. In contrast, N undergoes frequent ion exchange at the sediment water interface [49,50]. The closure of the tidal gates facilitates the release of N from the sediment into the overlying water. This process is likely to lead to the migration of N in the form of ions, consequently contributing to an elevated presence of nitrogen in offshore sediments [32]. Thus, the tidal gates in coastal rivers may have altered the habitat characteristics of the coastal watershed.

3.2. Distribution of TMs in Sediments of Duliujian River Watershed

As expected, the content of TMs in the sediments varied considerably between the different spatial units affected by the tidal gates (Figure 2), as recorded by CA, EA, and OA as: 27,037.15, 17,489.76, and 33,943 mg/kg for Al; 37.30, 49.65, and 17.43 mg/kg for As; 90.81, 410.52, and 101.29 mg/kg for Cr; 27.64, 12.28, and 33.96 mg/kg for Cu; 20,006.09, 22,079.61, and 27,871.60 mg/kg for Fe; 443.75, 339.27, and 551.93 mg/kg for Mn; 29.39, 79.28, and 60.73 mg/kg for Ni; and 105.63, 75.27, and 119.42 mg/kg for Sr. In addition, PCoA showed that the TM content in the different spatial units did not show clear boundary characteristics (Figure S2), suggesting that the tidal gates may change the distribution and enrichment status of TMs in sediments and that the delineation of control units by TM content in sediments alone may become more complicated.

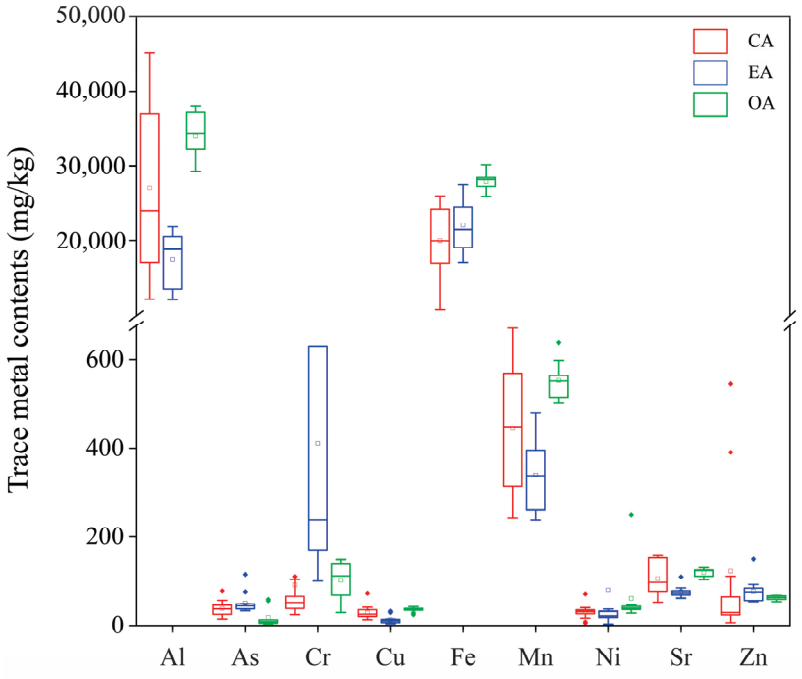

Figure 2. TM contents in the sediments of the CA, EA, and OA of Duliujian river watershed in Bohai Bay.

In the natural watershed, the TM distribution will show a clear gradient effect [51,52]. In this study, only Fe fulfilled the natural characteristics, with the remaining TMs showing enrichment at the EA or migration to the OA, indicating that the tidal gates at the EA may have altered the spatial distribution of TMs in sediments [53]. Moreover, there is a considerable distance from the CA to the OA. During the river's long-distance transport, spatial differences arising from variations in sediment environmental parameters and human activities may be one of the factors influencing the changes in TM concentrations. This study further compares the results with those from other studies (Table S3). The results show that the concentrations of As and Cr have exceeded the average levels of rivers in China and globally. Moreover, the concentrations of As and Cr are clearly higher than those in the sediments of coastal rivers that are not influenced by tidal gates. Notably, this issue has been observed in other aquatic regions affected by tidal gates [54–56]. As toxic metals, high contents of As and Cr commonly occur in factories, farms, or livestock farms. Their levels are exacerbated by anthropogenic factors such as industrial pollution, effluent discharge, and human activities, with minimal occurrences in natural environments [57]. Furthermore, our previous studies have confirmed that the CA is the most anthropogenically disturbed ecological zone [32], but that high levels of locations in the sediment still occur in the EA. Therefore, we speculate that the As and Cr originating from the CA may have undergone migration to the EA through either water or sediment transport mechanisms. Owing to the strong retention effect of the tidal gates, it caused long periods of accumulation in the EA,

which enhanced its sorption capacity, causing elevated levels in the sediment. However, the EA–OA is a complex interlacing zone of freshwater and saltwater where sediment 'resuspension' events, influenced by the water salt movement, may also be a major cause of the uneven distribution of TMs in sediments [58]. Therefore, the source of TMs needs to be further determined.

3.3. Pollution and Enrichment Indices of TMs in Sediments

Several studies have shown that the I_{geo} is a reliable parameter to reflect the accumulation degree and pollution status of TMs in sediments based on a pollution intensity classification [59,60]. The I_{geo} values are compared in Figure 3A. Except for the values of As and Cr in the EA, and Ni in the EA and OA, the values of the other TMs in the three areas are less than 0, which can be characterized as a pollution-free state. The I_{geo} of As is grade 2 (medium pollution) in the CA and EA and grade 1 (non-medium pollution) in the OA. The I_{geo} of Cr in the EA is grade 2 (moderate pollution). The I_{geo} of Ni is grade 1 (medium pollution) in the EA and OA. The findings indicate that the I_{geo} for different metals have significant differences. In particular, the impact on As and Cr enrichment remains notably high in the EA. ANOVA shows significant differences in As, Cr, Al, Fe, and Mn in the three regions ($p < 0.05$). The I_{geo} of As and Cr in the EA are significantly higher than those in the other two regions ($p < 0.05$), suggesting a certain degree of accumulation of As and Cr and potential ecological risks. In addition, the I_{geo} of Al, Fe, and Mn in the OA are significantly higher than those in the other two regions ($p < 0.05$), which may be related to the varied sources of the TMs.

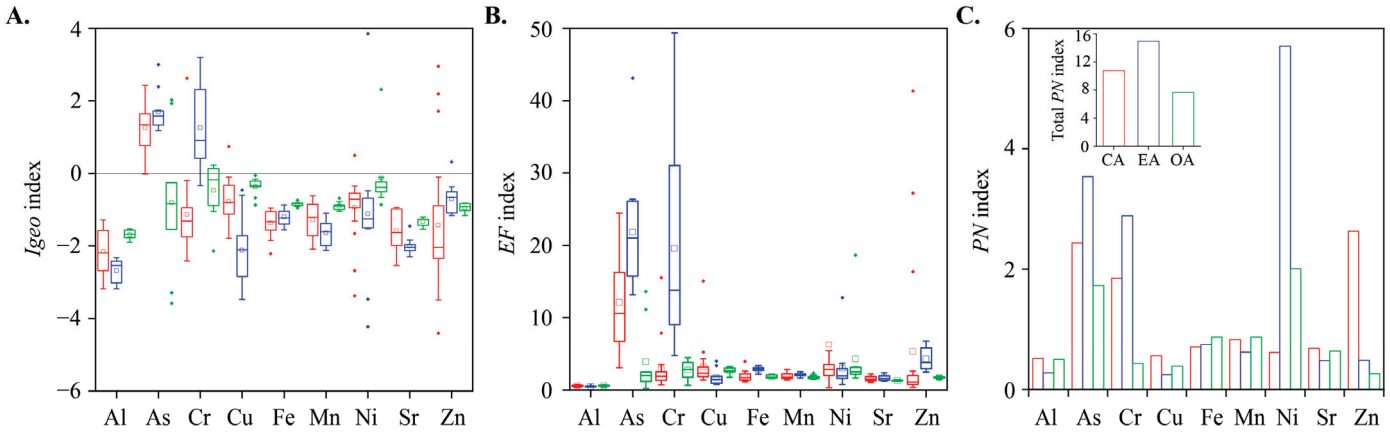

Figure 3. (**A**) Geoaccumulation index (I_{geo}), (**B**) enrichment factors (EF), and (**C**) Nemerow pollution index of TMs in the sediments of the CA, EA, and OA of the Duliujian river watershed in Bohai Bay.

Except for the patterns for Al, Cu, and Zn, the EF of other TMs in the EA are higher than those in the other two regions (Figure 3B). According to the classification of EF values, As is highly enriched in the CA and EA, and moderately enriched in the OA. The EF value was easily affected by human factors, such as the petroleum industry and river regulation, which may lead to the accumulation of As in sediments of different watersheds [61]. The EF of Cr in the EA belongs to the medium and high enrichment levels and it belongs to the medium enrichment level in the CA and OA. The EF values of Cr, Cu, Ni, and Zn are higher than in the CA, which belongs to moderate enrichment. Among them, As and Cr are potential toxic metal pollution sources. When the exogenous input or bioaccumulation release enters the overlying water, the precipitation process will occur. Furthermore, when the physical and chemical properties in the sediment change, the accumulated TMs will also be released into the overlying water, making the sediment an endogenous pollution source and causing a large degree of endogenous pollution [62]. Therefore, great attention should be paid to the As and Cr pollution in the whole study area.

The PN was used to evaluate the TM pollution degree in the study area and Figure 3C illustrates the PN of each TM in the three different regions. The PN of Al, Cu, Fe, Mn,

and Sr in three regions are all lower than 1, indicating that no pollution was found for these TMs. The PN of As, Cr, and Ni in the EA all exceed 2, indicating severe pollution. This is suggestive of potential influences arising from human activities, atmospheric factors, acid deposition, and bioaccumulation in the vicinity of the EA. Consequently, there is a pressing need for targeted monitoring to identify and address specific sources of sediment pollution in the EA. The PN of Zn in the CA is 2.6, indicating moderate pollution, which may be attributed to wetland reclamation and agricultural activity control (i.e., fertilization and sewage irrigation). Furthermore, the PN of Fe and Mn is approximately 0.7, indicating a pollution-free state. A possible explanation is that Fe and Mn mainly originate from parent materials. In addition, the total PN values at the watershed show EA (14.93) > CA (10.75) > OA (7.64), suggesting that the tidal gates would significantly mitigate the potential risk of TMs in sediments in the OA, but have the potential to exacerbate TMs pollution in the EA.

3.4. Source Analysis for TMs and Their Abiotic Influencing Factors

The accumulation risk level of TMs is not only related to their concentrations but also their sources [63]. PCA is usually used to identify the pollutant source [64–66]. The results showed that the first two principal components can explain 55.61% of the variable changes (Figure 4A; Table S4). The first principal component (PC1) represents the natural factors [67], and is mainly loaded by Mn (0.96), Al (0.95), Sr (0.79), and Fe (0.78) in this study, explaining 39.2% of the common variance (Figure 4A; Table S4). Furthermore, Al, Fe, Mn, and Sr show a significant positive correlation (Figure 4E; $p < 0.001$), indicating a similar source of these TMs. The presence of Al, Fe, Sr, and Mn suggests an association of these elements with rock weathering, lithology, or particle size characteristics [68–70]. PC1 appears to delineate the gradient between continental and oceanic realms or particle-size distribution [41]. Therefore, it can be inferred that Al, Fe, and Mn likely originated primarily from parent materials. However, due to wastewater discharge and industrial production, the influence of human activities may contribute to the elevated correlation between these TMs in certain regions. Future studies need to incorporate additional data of anthropogenic influences to clarify this aspect.

The second principal component (PC2) represents human factors [67] and is negatively correlated with As and Cr but positively correlated with Zn and Ni (Figure 4A; Table S4) in this study. The concentrations of these four TMs are predominantly shaped by anthropogenic disturbance, with minimal natural occurrences. The findings highlight the association of these TMs with human interference. However, it is noteworthy that the origins of the paired trace metals (As and Cr; Zn and Ni) exhibit divergence, indicating that these metal pairs have a different source. First, Zn and TN have a significant positive correlation (Figure 4B; $p < 0.001$), indicating that Zn may have originated from wetland reclamation or agricultural activity control (i.e., fertilization and sewage irrigation), while Ni and Zn have a similar origin. Therefore, coastal wetland management should perhaps be strengthened. Second, for As and Cr, our above speculations were verified, and the source of As and Cr may be due to anthropogenic activities at the CA that increase the entry of these two TMs into the overlying water. In addition, As and Cr are the TMs that account for the largest proportion of sediment in the various indices calculated for TM content (Figure 4D). Combined with SourceTracker analysis (Figure 4C), when the CA and OA serve as TM sources and the EA acts as a sink, the potential for the spatial transport of TMs from source to sink is clearly greater than that were EA to be the source. Furthermore, TMs show the least migration potential from the CA to OA or from the OA to CA (Figure 4C). These results suggest that the presence of tidal gates may alter the spatial distribution of TMs, particularly, As and Cr. There are two possible explanations for this phenomenon. First, the operation of tidal gates affects the redox environment of the water. Closing the gates may cause water retention, creating a higher redox environment, which can lead to the increase in TM concentrations in the sediments. For example, studies have shown that the cycling of As at the groundwater surface water interface in tidal

channels is controlled by hydrological conditions, with redox conditions varying across tidal and seasonal timescales, affecting the mobility of As [71]. Second, tidal gates control the mixing of freshwater and seawater, altering salinity gradients. Changes in salinity affect the solubility and adsorption behavior of TMs, thereby influencing their distribution in the sediments. Research has found that TMs exhibit a clear response pattern at the tidal and salinity interfaces in estuarine areas, with the salinity effect significantly impacting the partition coefficients of metals such as As and Cr [72].

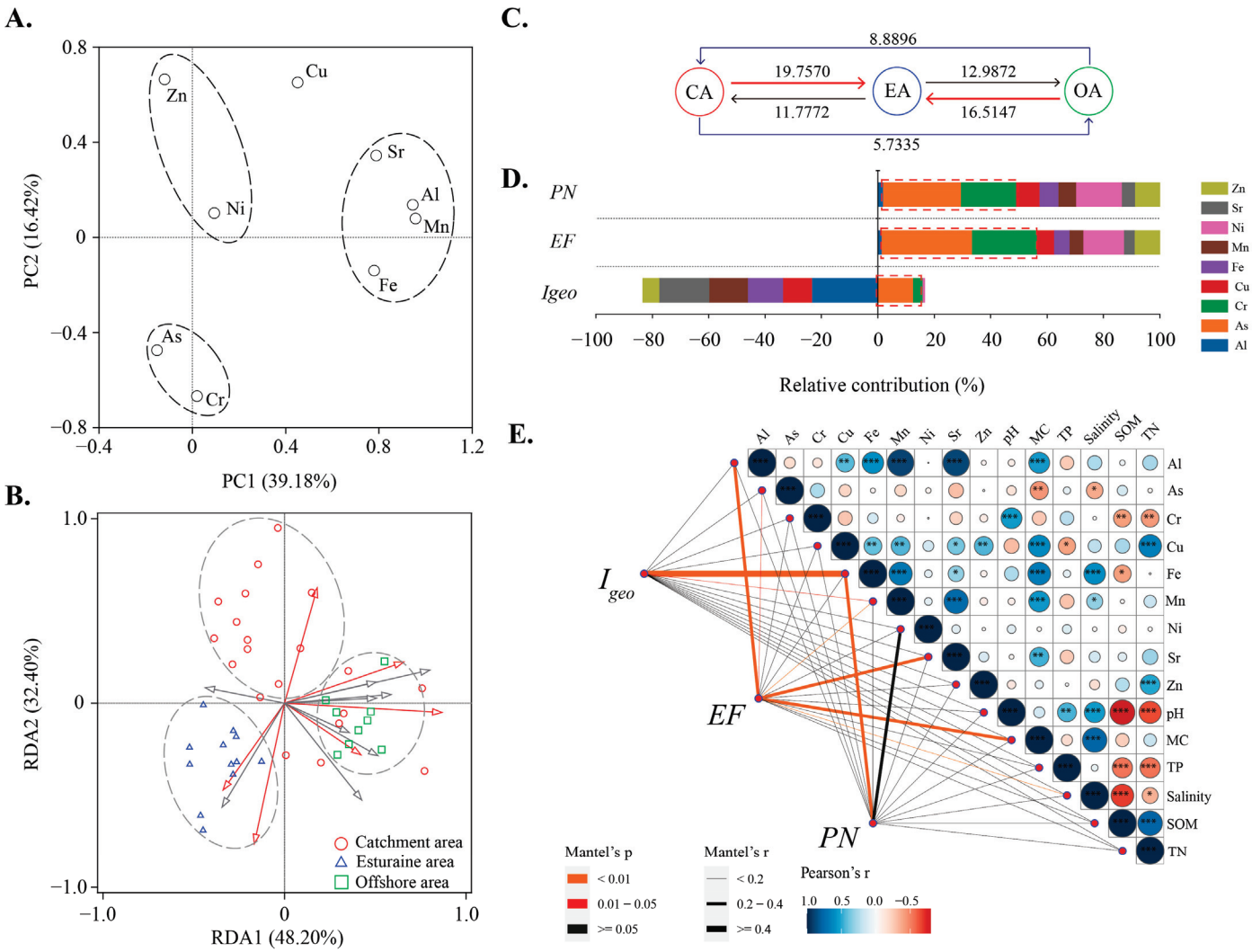

Figure 4. (**A**). Principal component analysis of TMs in the different spatial units. (**B**) RDA of TM with environmental factors. (**C**) SourceTracker analysis of the sink and source relationships of TMs in different spatial units. The values represent the total exchange potential. (**D**) The degree of contribution of TMs in sediments to each index. The red box represents the degree of contributions of As and Cr. (**E**) Paired comparison of environmental factors and TMs with the TM related indices. The color gradient and circle size represent the Spearman correlation coefficients; the width of the line represents the degree of correlations among potential risks, TMs, and environmental factors. Asterisks denote statistically significant differences (***, $p < 0.001$; **, $p < 0.01$; *, $p < 0.05$).

Incorporating environmental factors and TM into the RDA framework, it can be seen that different aquatic regions have distinct boundary features between them, suggesting that different environmental factors may be the main reasons influencing the distribution of TMs (Figure 4B; Table S5). Next, the correlation heatmap revealed the relationship between the contents of TMs and the physicochemical properties in sediments at the coastal watershed (Figure 4E). TMs will be affected by various physical and chemical

properties [73], with varying degrees of environmental factors affecting their transport rates. For As, there was a significant negative correlation with salinity (Figure 4E; $p < 0.05$). In this study, there was a gradual increase in salinity from the CA to the OA, and its increase may have inhibited the migration ability of As. Salinity is the most important factor and an increase in salinity usually means a decrease in the rate of migration and sedimentation of metal ions, as it can alter the free metal ion activity and, thus, the bioavailability and toxicity of TMs in coastal systems [74]. For example, previous studies have found that as salinity increased, the uptake of TMs by brackish water organisms became less efficient, resulting in TMs being less likely to be deposited in coastal systems [75]. Some scholars have specified TM ions (Cd^{2+}) and saline organisms (*Bahia pigmentia*) to study the effect of salinity on uptake efficiency, and morphological modeling revealed a 25% reduction in the percentage of free ions [76]. Furthermore, for Cr, there was a positive correlation with pH (Figure 4E; $p < 0.05$), with elevated pH causing the accumulation of TMs in the sediment [77]. Therefore, the influence given by the environment of the estuary may be the main cause of potential As and Cr pollution in the sediments.

3.5. Correlation Analysis Between Potential Risks and Environmental Factors

The correlation coefficients, such as I_{geo}, EF, and the PN of TMs, were used as variables to test their correlations with environmental factors and individual TMs. Al, Fe, and Mn were found to have significant correlations with those indices. In this study, Al was used as the reference TM for geochemical normalization because its geochemistry was like that of many TMs and its natural content tended to be stable [78]. Then, taking Al as a reference coefficient to calculate the *EF* in sediments might be the main reason for the significant correlation between EF and Al. Furthermore, iron-manganese oxides are the main forms of Fe and Mn in sediments and can improve the effectiveness of metal pollutants under certain redox changes in nature [79]. It can even be considered a key metal that indicates the pollution and enrichment status of TM in sediment [13]. In this study, Fe and Mn are generally derived from parent material (Figure 4A), the main constituents of which are primary minerals (such as quartz, feldspar, and mica), and their formation is largely dependent on the composition of the sediment and other TMs in the environment [80]. Furthermore, this study attempts to use Fe and Mn as monitoring factors for the pollution and enrichment of TM, and to linearly fit the correlation indices of TM. The results indicate that Fe and Mn have good relationships with different indices of TM (Figure 5A), indicating that the content of Fe and Mn in sediment may monitor sediment metals status to some extent. Next, this study made an in-depth attempt to investigate the ability of Fe and Mn as monitoring factors. In theory, they can characterize the occurrence states of As and Cr in sediments. The oxides of the Fe and the Mn had strong oxidation and adsorption capacities for As and Cr. Under oxidation conditions, they can effectively oxidize dissolved Cr^{3+} and As^{3+}, while most of the newly formed Cr^{6+} and As^{5+} will be adsorbed on the metal surface and fixed [81–83]. Furthermore, EA was affected by the tide, and some sediments would be exposed to the air for a long time, resulting in the adsorption of exogenous As and Cr on the surface of Fe and Mn aboveground oxide. However, the correlation between pairs of TMs did not reach the desired results (Figure 5B). It is easy to see that some locations in EA have strayed, resulting in a shift in the fitting results, suggesting that the construction of tidal gates in EA has altered the natural characteristics of toxic metals in the coastal watershed, which may complicate the monitoring efforts. In addition, As and Cr, as high-concentration toxic metals, pose potential ecological and human health risks due to the unique environmental characteristics at EA. The increase in As and Cr content in the EA indicates that the presence of tidal gates has severely affected the spatial distribution characteristics of toxic metals. As is a known carcinogen and exhibits the highest toxicity in its inorganic As. Under the reducing conditions, it can be desorbed from sediment particles, thereby increasing its bioavailability and toxicity in aquatic systems. Research has shown that an increase in As content in sediments can cause toxic effects on aquatic organisms through food chain bioaccumulation, while also increasing the risk

of human exposure through drinking water [84]. Moreover, Cr exhibits high toxicity and mobility in an oxidizing environment. Its accumulation through the food chain in aquatic systems may pose a severe risk to the growth of aquatic organisms [85]. Therefore, there is an urgent need for innovative methods to identify TM pollution affected by tidal gates in coastal watersheds.

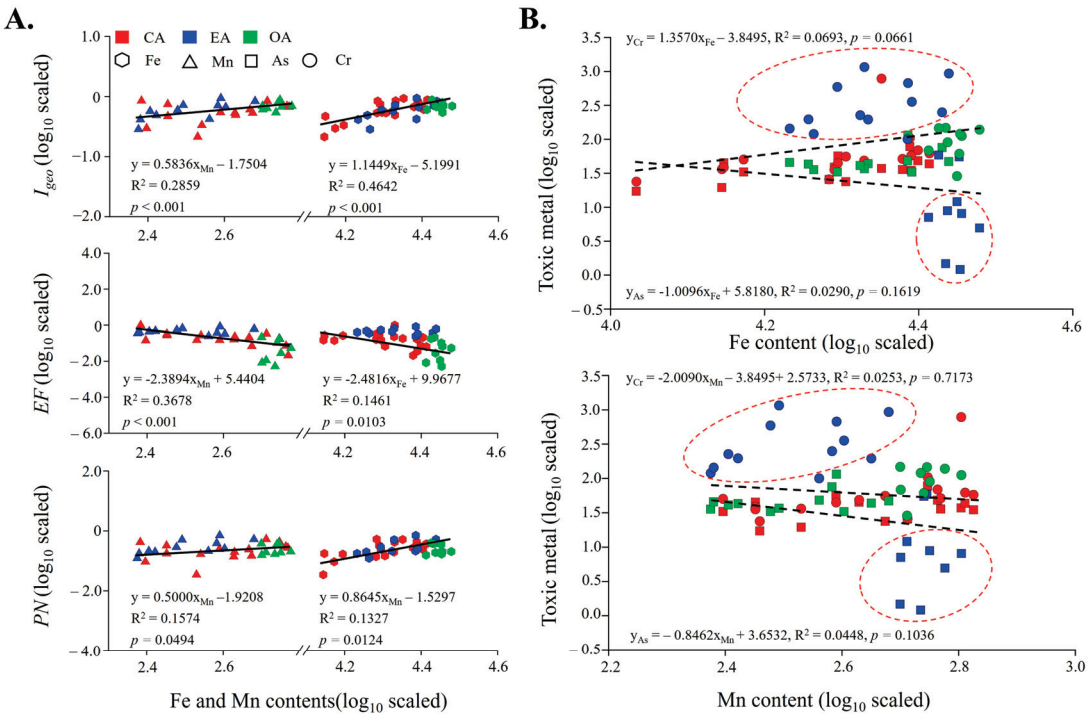

Figure 5. (**A**) Regression analysis for pairwise combination of Fe and Mn with TM correlation indices, and (**B**) pairwise combination of Fe and Mn with toxic metals (As and Cr). Axes are $\log_{10}$ scaled.

3.6. Bacterial Communities and Their Influencing Factors at the Coastal Watershed

As the four most dominant phyla at the watershed scale, the relative abundance of *Proteobacteria*, *Actinobacteria*, *Chloroflexi*, and *Epsilombacteraeot* collectively represent over 70% of the total relative abundance (Figure 6A and Table S6). Moreover, the bacterial community's alpha diversity and functional abundance exhibited distinct characteristics across the basin, gradually decreasing from the CA to the OA (Figures 6B and S2; $p < 0.05$).

Additionally, the NMDS results revealed clear boundary distinctions among bacterial communities across the coastal watershed, indicating variations in their composition across different spatial units (Figure 6C). Furthermore, RDA was used to determine the influence of different variables in the sediment of the different spatial units on the structure, diversity, and metabolism abundance of the bacterial community (Figure S3); it showed that salinity (57.7% and 64.2%), MC (53.9 and 48.2%), SOM (27.3 and 33.1%), and pH (18.9 and 21.0%) were found to be most influential (Tables S7–S9).

There is considerable variation in the pattern of bacterial communities in different spatial units, and the diversity and metabolism abundance of bacterial communities have clear watershed characteristics. In general, bacterial community structure is highly sensitive, with changes in the local environment shaping the structure of similar bacterial communities [32]. In this study, the EA was the most heavily contaminated area by the accumulation and pollution of TMs, such as As and Cr. However, the diversity and metabolism abundance of the bacterial community were much higher in the CA than in the EA. Could this be due to the higher contamination level in the CA compared to the EA? There are two possible reasons for this phenomenon. First, the changing characteristics of the overlying water environment need to be considered; previous studies have confirmed that CA-overlying waters are more eutrophic than EA waters [32] and that high eutrophic

levels drive the enhanced functionality and primary productivity of bacterial communities, possibly creating new bacterial ecological niches [86]. Second, salinity is a major driver in structuring bacterial communities. Previous studies have compared changes in microbial diversity from freshwater to marine salinity trajectories and found that microbial diversity was progressively lower moving from the freshwater end of the river to the coast [87]. It is worth noting that the EA is a complex dynamic area subject to tidal action resulting in the alternation of fresh and salty water. Although the variation in bacterial communities in coastal river sediments is manipulated by salinity, it is not systematic, with a greater abundance of genes encoding heterotrophic processes compared to the river and marine genes, and certain groups of bacteria may exhibit greater abundance profiles [88].

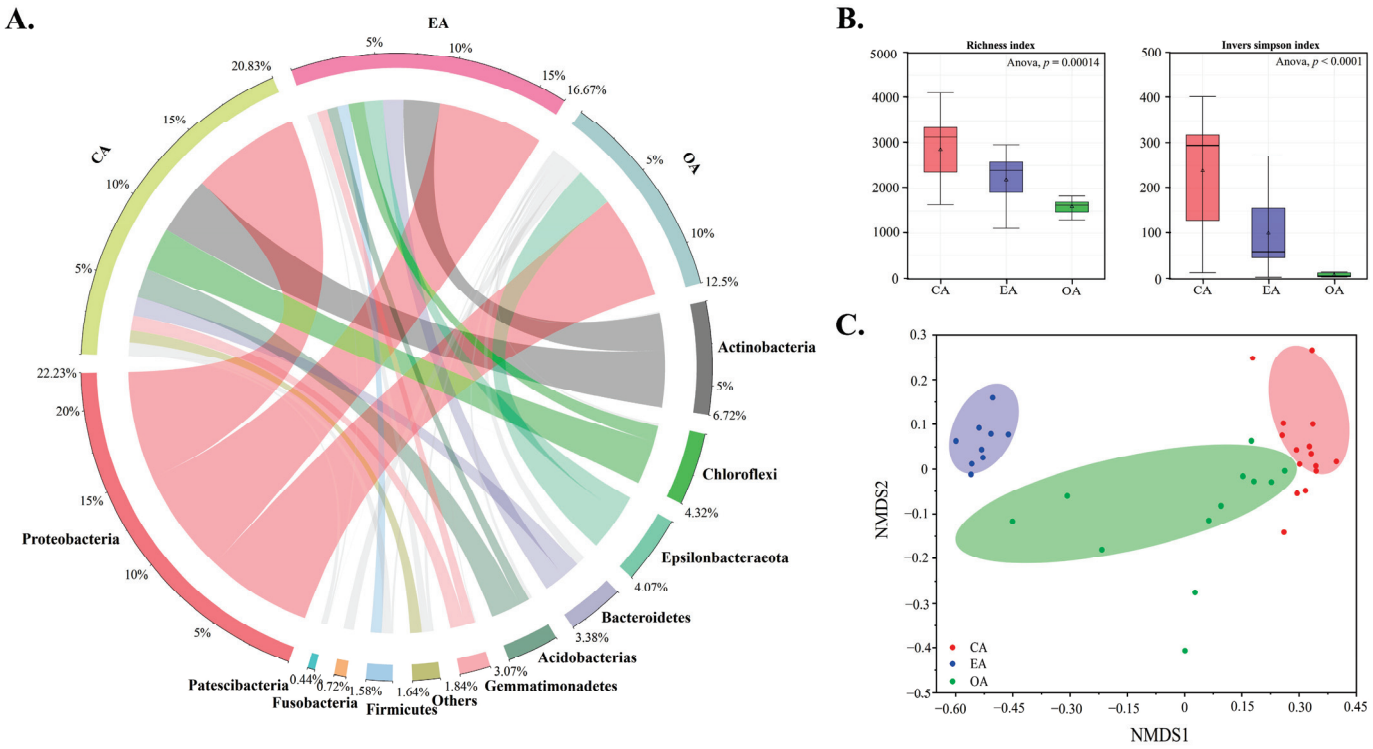

Figure 6. Changes in community composition (**A**) and diversity (**B**) of bacterial communities and NMDS analysis (**C**) for determining differences in bacterial communities at the watershed scale.

3.7. The Indicative Role of Bacterial Community on TMs in Duliujian River Watershed

Within the framework of RDA, the response relationship between bacterial community structure, diversity, and metabolism abundance in different spatial units was investigated by using nine trace metals as influencing factors. The results showed that RDA1 and RDA2 explained 58.31, 57.19, and 64.95% (Figure 7A–C) of bacterial community structure, diversity, and metabolic abundance. Notably, Fe and Mn were the key TMs influencing changes in structure, diversity, and metabolism abundance as analyzed by Monte Carlo (Tables S10–S12), suggesting that the dynamics of bacterial communities at the coastal watershed can be influenced by the mediating effects of Fe and Mn from the parent material. It is worth noting that only the metabolic abundance of bacterial communities is correlated with As and Cr. Furthermore, this study further compares the accuracy of bacterial metabolic abundance and traditional pollutant identification methods in the framework of VPA (Figure 8). The results showed that bacterial metabolic abundance could explain 23.9 (Figure 8A; $p < 0.01$) and 59.7% (Figure 8B; $p < 0.05$) of the changes in toxic metals and TM related indices, respectively. However, Fe and Mn can only significantly explain the changes in TM related indices ($p < 0.05$), but they do not seem to fully explain the changing trends of toxic metals ($p > 0.05$). These results indicate that dynamic changes in the metabolic abundance of bacterial communities as a monitoring factor for assessing

the state of contamination, accumulation, and enrichment of TM in sediments are a better approach in tidal gate-influenced coastal river.

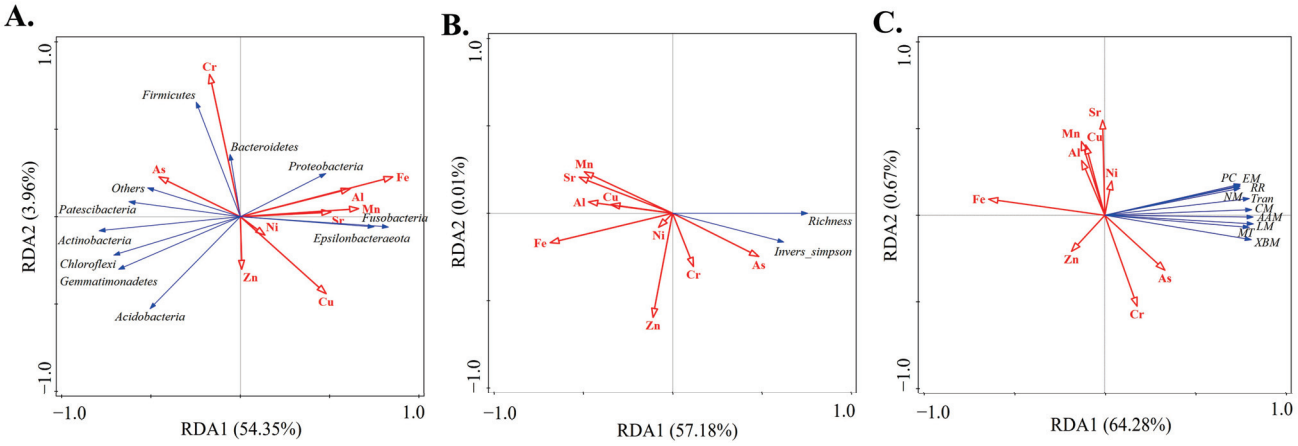

Figure 7. RDA of TM with bacterial dynamics. (**A**) TM with dominant abundance of bacterial community; (**B**) TM with bacterial diversity; (**C**) TM with bacterial metabolism abundance. Among them, PC represents the poorly characterized; EM represents the energy metabolism; RR represents the replication and repair; NM represents the nucleotide metabolism; Tran represents the translation; CM represents the carbohydrate metabolism; AAM represents the amino acid metabolism; LM represents the lipid metabolism; MT represents the membrane transport; XBM represents the xenobiotics biodegradation and metabolism.

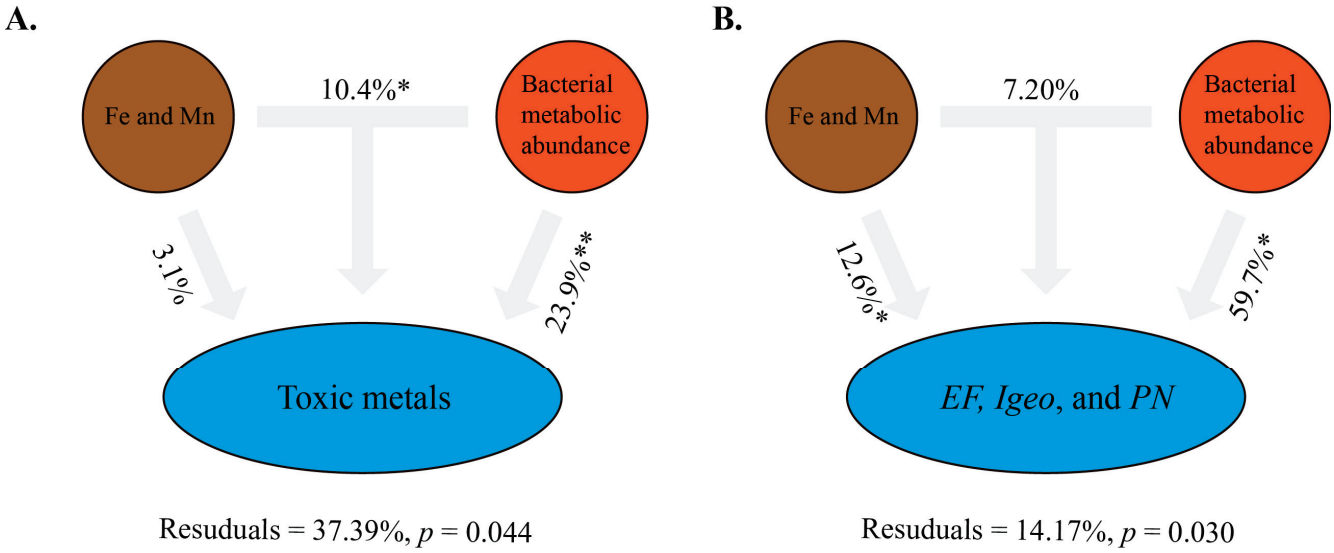

Figure 8. VPA of traditional TM identification (Fe and Mn) and bacterial metabolic abundance for toxic metals (**A**) and TM-related indices (**B**). Among them, * and ** represent $p < 0.05$ and $p < 0.01$, respectively. Toxic metals contain As and Cr.

Introducing bioindicators into future river monitoring processes to better estimate TM pollution in aquatic regions is feasible, because of two factors. First, the construction of gates may lead to instability in water levels and tidal variations, which may affect the distribution and transport of TMs in the sediments [89,90]. However, the synchronized adaptations exhibited by bacterial communities allow them to quickly adapt and respond to ecosystem health [91]. Bacteria inevitably encounter various elements in the natural environment. Mn^{4+}, Fe^{2+}, and Fe^{3+} can act as biological donors or acceptors and can participate at the same time. With the participation of bacterial communities, Fe^{2+} and Mn^{2+} will be oxidized into Fe^{3+} and Mn^{3+}, and other bound colloids are deposited in

the substrate, increasing the content of Fe and Mn in the substrate. Biological reduction has always been regarded as an important metabolic process. It controls the migration and transformation of TMs in sediments. At the same time, in the natural environment, TMs are sufficient to meet the physiological needs of bacteria at lower concentrations [58], and when TMs accumulate and contaminate, they may undergo the same changes as sediment contamination to better adapt to the environment. Second, given the heightened sensitivity of bacterial communities to environmental changes, their metabolic activity is inevitably impacted when their habitat faces stress from specific pollutants. In cases where these pollutants are decomposable by community members, the metabolic abundance increases to meet the heightened energy demands required for pollutant breakdown. However, if the concentration of pollutants exceeds the decomposition capabilities of the community, some bacteria may diminish in number or vanish entirely, leading to the loss of specific functional metabolic pathways. Despite this, members with greater adaptability may counter environmental disturbances through mechanisms like dormancy, evolving new metabolic pathways to restore their original activity levels. These functional pathway changes can still be rapidly detected. Therefore, during regional pollution assessments, especially in the preliminary background investigation and final evaluation phases, we strongly advocate for the use of bacterial metabolic abundance as a critical biological indicator. By analyzing the metabolic dynamics of bacterial communities, not only can the effectiveness of project implementations be assessed, but targeted management strategies can also be developed based on the accumulation of pollutants. Nevertheless, we must acknowledge that the conclusion of this study may have certain limitations. In particular, the concentration of TMs is significantly influenced by seasonal variations in aquatic areas. Previous research has shown that TM concentrations are typically lower during the dry season compared to the rainy season, both in overlying water and sediments [92]. Therefore, this study may have time constraints, which could bias the findings. To address these limitations, future studies should conduct long-term monitoring across different seasons and establish additional sampling sites along coastal rivers regulated by tidal gates for experimental analysis. This approach will facilitate a more comprehensive understanding of TM behavior and distribution, thereby enhancing the scientific rigor and applicability of the results.

4. Conclusions

This study highlighted the intricate dynamics between TMs and bacterial communities in tidal gate-affected coastal watersheds. It revealed that the EA exhibited the highest TM pollution risk, particularly with As and Cr, a situation exacerbated by the blocking effects of tidal gates, which promotes sediment accumulation. This issue may also reflect challenges faced by many tidal gate-controlled coastal rivers globally. In such complex environments, traditional pollutant identification methods may struggle to accurately monitor toxic metals. Fortunately, this study identified that the functional metabolic abundance of bacterial communities serves as a reliable indicator of TM contamination levels, making it a key ecological indicator for ecosystem health assessment and pollution management in future coastal watershed management. This underscores the feasibility and reliability of incorporating bacterial community dynamics into environmental management practices to more effectively track and monitor TM pollution, especially where traditional chemical monitoring proves insufficient. In addition, we recommend that future studies focus on the resilience and functional adaptability of bacterial communities under different TM loads and environmental conditions, which could provide new insights into ecosystem recovery and management strategies. Overall, this finding provides a foundational understanding of TM–bacteria interactions, paving the way for more targeted and efficient environmental management practices in coastal ecosystems.

Supplementary Materials: The following supporting information can be downloaded at: https://www.mdpi.com/article/10.3390/toxics12120839/s1, Method S1. Details in 16S rRNA sequencing

and analysis. Table S1. The details of latitude and longitude information from different groups in the study area [29,93,94]. Table S2. The physicochemical properties of sediments in the CA, EA, and OA of Duliujian coastal watershed in Bohai Bay. Table S3. Comparison of TM concentration in sediments between this study and other studies (mg/kg) [54–56,95–98]. Table S4. Rotated component matrix and initial eigenvalues of principal component analysis of TMs in the CA, EA, and OA of Duliujian coastal watershed in Bohai Bay. Table S5. Important ranking for physicochemical properties and TM in different space units at the watershed scale. Table S6. Average relative abundance of dominant bacteria phylum in sediment samples. Table S7. Importance ranking of environmental factors in sediment to explain the overall characteristics of dominant phylum abundance of bacterial communities in different watershed spatial units. Table S8. Importance ranking of environmental factors in sediment to explain the overall characteristics of bacterial diversity in different watershed spatial units. Table S9. Importance ranking of environmental factors in sediment to explain the overall characteristics of bacterial metabolism abundance in different watershed spatial units. Table S10. Importance ranking of trace metals in sediment to explain the change in the dominant phylum abundance of bacterial community in different spatial units at the watershed scale. Table S11. Importance ranking of trace metals in sediment to explain the change in the diversity of bacterial community in different spatial units at the watershed scale. Table S12. Importance ranking of trace metals in sediment to explain the change in the metabolism abundance of bacterial community in different spatial units at the watershed scale. Figure S1. PCoA of the variability between TMs contents in sediments from different spatial units at the watershed scale. Figure S2. Metabolic abundance of bacterial communities on KEGG database in different spatial. Among them, one-way ANOVA was used to test for variability in metabolic abundance at the watershed scale. Figure S3. RDA of environmental factors with bacterial community dynamics. A. Effect of environmental factors on the dominant community abundance; B. effect of environmental factors on the diversity; C. effect of environmental factors on the metabolism abundance.

Author Contributions: Conceptualization, F.L.; Data Curation, Y.X. and X.Y.; Formal Analysis, J.L., X.Y., X.L., Y.F., Z.X. and F.L.; Funding Acquisition, F.L. and Z.X.; Investigation, X.Y., X.L., Y.F., Z.X. and F.L.; Project Administration, F.L. and X.Z; Visualization, Y.X.; Writing—Original Draft, Y.X., J.L. and F.L.; Writing—Review and Editing, Y.X., J.L. and F.L. All authors have read and agreed to the published version of the manuscript.

Funding: This work is financially supported by the Research on Ecological and Environmental Risk Management for CHN Energy (HBHZ2024Y01) and the Tianjin Research Program of Application Foundation and Advanced Technology (14JCYBJC23000).

Institutional Review Board Statement: Not applicable.

Informed Consent Statement: Not applicable.

Data Availability Statement: The data that support the findings of this study are available from the corresponding author upon reasonable request.

Acknowledgments: The authors are grateful to Yan Zhang from Tianjin Academy of Eco-environmental Science and Desheng Li from Tianjin University of Technology for their help in the field work.

Conflicts of Interest: The authors declare no conflicts of interest.

References

1. Goyette, J.O.; Bennett, E.M.; Maranger, R. Low buffering capacity and slow recovery of anthropogenic phosphorus pollution in watersheds. *Nat. Geosci.* **2018**, *11*, 921–925. [CrossRef]
2. Goyette, J.O.; Bennett, E.M.; Maranger, R. Differential influence of landscape features and climate on nitrogen and phosphorus transport throughout the watershed. *Biogeochemistry* **2019**, *142*, 155–174. [CrossRef]
3. Raj, P.R.S.; Viswanathan, P.M. Occurrence and distribution of geochemical elements in Miri estuary, NW Borneo: Evaluating for processes, sources and pollution status. *Chemosphere* **2023**, *316*, 137838. [CrossRef]
4. Uzairu, A.; Harrison, G.F.S.; Balarabe, M.L.; Nnaji, J.C. Concentration levels of trace metals in fish and sediment from Kubanni River, Northern Nigeria. *Bull. Chem. Soc. Ethiopia* **2009**, *23*, 9–17. [CrossRef]
5. Ardila, P.A.R.; Alonso, R.Á.A.; Valsero, J.J.D.; García, R.M.; Cabera, F.Á.; Cosío, E.L.; Laforet, S.D. Assessment of heavy metal pollution in marine sediments from southwest of Mallorca island, Spain. *Environ. Sci. Pollut. Res.* **2023**, *30*, 16852–16866. [CrossRef] [PubMed]

6. Ardila, P.A.R.; Alonso, R.Á.; Árcega-Cabrera, F.; Valsero, J.J.D.; García, R.M.; Lamas-Cosío, E.; Oceguera-Vargas, I.; DelValls, A. Assessment and review of heavy metals pollution in sediments of the Mediterranean Sea. *Appl. Sci.* **2024**, *14*, 1435. [CrossRef]
7. Lordache, A.M.; Nechita, C.; Voica, C.W.; Pluháček, T.; Schug, K.A. Climate change extreme and seasonal toxic metal occurrence in Romanian freshwaters in the last two decades—Case study and critical review. *Npj Clean Water* **2022**, *5*, 2. [CrossRef]
8. Pejman, A.; Bidhendi, G.N.; Ardestani, M.; Saeedi, M.; Baghvand, A. A new index for assessing heave metals contamination in sediments: A case study. *Ecol. Indic.* **2015**, *58*, 365–373. [CrossRef]
9. Yu, H.; Ni, S.J.; He, Z.W.; Zhang, C.J.; Nan, X.; Kong, B.; Weng, Z.Y. Analysis of the spatial relationship between heavy metals in soil and human activities based on landscape geochemical interpretation. *J. Geochem. Explor.* **2014**, *46*, 136–148. [CrossRef]
10. Maanan, M.; Saddik, M.; Maanan, M.; Chaibi, M.; Assobhei, O.; Zourarah, B. Environmental and ecological risk assessment of heavy metals in sediments of Nador lagoon, Morocco. *Ecol. Indic.* **2015**, *48*, 616–626. [CrossRef]
11. Li, P.F.; Hua, P.; Zhang, J.; Krebes, P. Ecological risk and machine learning based source analyses of trace metals in typical surface water. *Sci. Total Environ.* **2022**, *838*, 155944. [CrossRef] [PubMed]
12. Wu, J.; Ge, Y.X.; Li, J.; Lai, X.Y.; Chen, R.H. A PMF-SSD based approach for the source apportionment and source-specific ecological risk assessment of Le'an river in Jiangxi Province, China. *Environ. Res.* **2023**, *219*, 115027. [CrossRef] [PubMed]
13. Bervoets, L.; Solis, D.; Romero, A.M.; Van Damme, P.A.; Ollevier, F. Trace metal levels in chironomid larvae and sediments from a Bolivian river: Impact of mining activities. *Ecotox Environ. Safe* **1998**, *41*, 275–283. [CrossRef] [PubMed]
14. Li, D.B.; Pan, B.Z.; Han, X.; Lu, Y.; Wang, Y.X. Toxicity risks associated with trace metals call for conservation of threatened fish species in heavily sediment-laden Yellow River. *J. Hazard. Mater.* **2023**, *448*, 130928. [CrossRef] [PubMed]
15. Thuong, N.T.; Yoneda, M.; Shimada, Y.; Matsui, Y. Assessment of trace metal contamination and exchange between water and sediment systems in the To Lich River in inner Hanoi, Vietnam. *Environ. Earth Sci.* **2015**, *73*, 3925–3936. [CrossRef]
16. Chakraborty, P.; Jayachandran, S.; Raghynadh Babu, P.V.; Karri, S.; Tyadi, P.; Yao, K.M.; Sharma, B.M. Intra-annual variations of arsenic totals and species in tropical estuary surface sediments. *Chem. Geol.* **2012**, *322*, 172–180. [CrossRef]
17. Young, S.M.; Ishiga, H. Assessment of dam removal from geochemical examination of Kuma River sediment, Kyushu, Japan. *Environ. Monit. Assess.* **2014**, *186*, 8267–8289. [CrossRef]
18. Müller-Karulis, B.; Poikāne, R.; Segliņš, V. Heavy metals in the Ventspils Harbour: Normalization based on a multi-parameter dataset. *Environ. Geol.* **2003**, *43*, 445–456. [CrossRef]
19. Shulkin, V.; Zhang, J. Trace metals in estuaries in the Russian Far East and China: Case studies from the Amur River and the Changjiang. *Sci. Total Environ.* **2014**, *499*, 196–211. [CrossRef]
20. Gillan, D.C.; Baeyens, W.; Bechara, R.; Billon, G.; Denis, K.; Grosjean, P.; Leermakers, M.; Lesven, L.; Pode, A.; Sabbe, K.; et al. Links between bacterial communities in marine sediments and trace metal geochemistry as measured by in situ DET/DGT approaches. *Mar. Pollut. Bull.* **2012**, *64*, 353–362. [CrossRef]
21. Schlekat, C.E.; Decho, A.W.; Chandler, G.T. Bioavailability of particle-associated silver, cadmium, and zinc to the estuarine amphipod Leptocheirus plumulosus through dietary ingestion. *Limnol. Oceanogr.* **2000**, *45*, 11–21. [CrossRef]
22. Barton, L.L.; Goulhen, F.; Bruschi, M.; Woodards, N.A.; Plunkett, R.M.; Rietmeijer, F.J.M. The bacterial metallome: Composition and stability with specific reference to the anaerobic bacterium Desulfovibrio desulfuricans. *Biometals* **2007**, *20*, 291–302. [CrossRef] [PubMed]
23. Bai, J.H.; Huang, L.B.; Yan, D.H.; Wang, Q.G.; Gao, H.F.; Xiao, R.; Huang, C. Contamination characteristics of heavy metals in wetland soils along a tidal ditch of the Yellow River Estuary, China. *Stochastic Environ. Res. Risk Assess.* **2011**, *25*, 671–676. [CrossRef]
24. Yin, Y.; Impellitteri, C.A.; You, S.J.; Allen, H.E. The importance of organic matter distribution and extract soil: Solution ratio on the desorption of heavy metals from soils. *Sci. Total Environ.* **2002**, *287*, 107–119. [CrossRef]
25. Cifuentes, G.R.; Jiménez-Millán, J.; Quevedo, C.P.; Gálvez, A.; Castellanos-Rozo, J.; Jiménez-Espinosa, R. Trace element fixation in sediments rich in organic matter from a saline lake in tropical latitude with hydrothermal inputs (Sochagota Lake, Colombia): The role of bacterial communities. *Sci. Total Environ.* **2021**, *762*, 143113. [CrossRef]
26. Pal, A.; Bhattacharjee, S.; Saha, J.; Sarkar, M.; Mandal, P. Bacterial survival strategies and responses under heavy metal stress: A comprehensive overview. *Crit. Rev. Microbiol.* **2021**, *37*, 17603–17624. [CrossRef]
27. Lian, T.X.; Ma, Q.B.; Shi, Q.H.; Cai, Z.D.; Zhang, Y.T.; Cheng, Y.B.; Nian, H. High aluminum stress drives different rhizosphere soil enzyme activities and bacterial community structure between aluminum-tolerant and aluminum-sensitive soybean genotypes. *Plant Soil.* **2019**, *440*, 409–425. [CrossRef]
28. Hermans, S.M.; Buckley, H.L.; Case, B.S.; Curran-Cournane, F.; Taylor, M.; Lear, G. Using soil bacterial communities to predict physico-chemical variables and soil quality. *Microbiome* **2020**, *8*, 79. [CrossRef] [PubMed]
29. Liu, J.Y.; Feng, Y.; Zhang, Y.; Liang, N.; Wu, H.L.; Liu, F.D. Allometric releases of nitrogen and phosphorus from sediments mediated by bacteria determines water eutrophication in coastal river basins of Bohai Bay. *Ecotox Environ. Safe* **2022**, *235*, 113426. [CrossRef]
30. Ghate, S.D.; Shastry, R.P.; Arun, A.B.; Rekha, P.D. Unraveling the bacterial community composition across aquatic sediments in the Southwestern coast of India by employing high-throughput 16S rRNA gene sequencing. *Reg. Stud. Mar. Sci.* **2021**, *46*, 101890. [CrossRef]
31. He, Z.L.; Zhang, P.; Wu, L.W.; Rocha, A.W.; Tu, Q.C.; Shi, Z.; Wu, B.; Qin, T.J.; Wang, J.J.; Yan, Q.Y.; et al. Microbial functional gene diversity predicts groundwater contamination and ecosystem functioning. *MBIO* **2018**, *9*, e02435-17. [CrossRef] [PubMed]

32. Liu, J.Y.; Feng, Y.; Yang, X.C.; Zhang, Y.; Li, D.E.; Liu, F.D. Identification of bacterial flora and metabolic function of sediment in different channels of Duliujian River Basin, Tianjin. *Environ. Sci.* **2022**, *43*, 3635–3644. (In Chinese) [CrossRef]
33. Sun, C.H.; Wei, Q.; Ma, L.X.; Li, L.; Wu, G.H.; Pan, L. Trace metal pollution and carbon and nitrogen isotope tracing through the Yongdingxin River estuary in Bohai Bay, Northern China. *Mar. Pollut. Bull.* **2017**, *115*, 451–458. [CrossRef]
34. Wang, X.J.; Fu, R.L.; Li, H.L.; Zhang, Y.; Lu, M.Q.; Xiao, K.; Zhang, X.L.; Zheng, C.M.; Xiong, Y. Heavy metal contamination in the surface sediments: A comprehensive, large-scale evaluation for the Bohai Sea, China. *Environ. Pollut.* **2020**, *260*, 113986. [CrossRef] [PubMed]
35. Tao, J.H. Numerical simulation of aquatic Eco-environment of Bohai bay. *J. Hydrodyn.* **2006**, *18*, 34–42. [CrossRef]
36. Feng, H.; Jiang, H.Y.; Gao, W.S.; Weinstein, M.P.; Zhang, Q.F.; Zhang, W.G.; Yu, L.Z.; Yuan, D.Y.; Tao, J.H. Metal contamination in sediments of the western Bohai Bay and adjacent estuaries, China. *J. Environ. Manag.* **2011**, *92*, 1185–1197. [CrossRef] [PubMed]
37. *HJ 1315–2023*; Soil and Sediment—Determination of 19 Total Metal Elements—Inductively Coupled Plasma Mass Spectrometry. Ministry of Ecology and Environment of the People's Republic of China: Beijing, China, 2023.
38. Zahra, A.; Hashmi, M.Z.; Malik, R.N.; Ahmed, Z. Enrichment and geo-accumulation of heavy metals and risk assessment of sediments of the Kurang Nallah-Feeding tributary of the Rawal Lake Reservoir, Pakistan. *Sci. Total Environ.* **2014**, *470–471*, 925–933. [CrossRef]
39. China National Environmental Monitoring Centre. *Background Values of Elements in Soils of China*; China Environmental Science and Technology Press: Beijing, China, 1990; p. 501.
40. Muller, G. Index of geoaccumulation in sediments of the Rhine River. *Geo J.* **1969**, *2*, 108–118.
41. Liu, F.D.; Zheng, B.W.; Zheng, Y.; Mo, X.; Li, D.S. Accumulation risk and sources of heavy metals in supratidal wetlands along the west coast of the Bohai Sea. *RSC Adv.* **2019**, *9*, 30615–30627. [CrossRef]
42. Liu, J.Y.; Lu, B.H.; Liu, Y.H.; Wang, L.X.; Liu, F.D.; Chen, Y.X.; Mustafa, G.; Qin, Z.R.; Lv, C.Q. Role of BP-ANN in simulating greenhouse gas emissions from global aquatic ecosystems via carbon component-environmental factor coupling. *Sci. Total Environ.* **2024**, *930*, 172722. [CrossRef]
43. Li, Y.B.; Zhang, M.M.; Xu, R.; Lin, H.Z.; Sun, X.X.; Xu, F.Q.; Gao, P.; Kong, T.; Xiao, E.Z.; Yang, N.; et al. Arsenic and antimony co-contamination influences on soil microbial community composition and functions: Relevance to arsenic resistance and carbon, nitrogen, and sulfur cycling. *Environ. Int.* **2021**, *153*, 106522. [CrossRef] [PubMed]
44. Kenya, E.; Kinyanjui, G.; Kipnyargis, A.; Kinyua, F.; Mwangi, M.; Khamis, F.; Mwirichia, R. Amplicon-based assessment of bacterial diversity and community structure in three tropical forest soils in Kenya. *Heliyon* **2022**, *8*, e11577. [CrossRef] [PubMed]
45. Swamy, C.T.; Gayathri, D. High throughput sequencing study of foliose lichen-associated bacterial communities from India. *Mol. Biol. Rep.* **2021**, *48*, 2389–2394. [CrossRef] [PubMed]
46. Hamilton, N.E.; Ferry, M. ggtern: Ternary diagrams using ggplot2. *J. Stat. Softw.* **2019**, *87*, 1–17. [CrossRef]
47. Zhang, G.L.; Bai, J.H.; Tebbe, C.C.; Huang, L.B.; Jia, J.; Wang, X.; Yu, L.; Zhao, Q.Q. Plant invasion reconstructs soil microbial assembly and functionality in coastal salt marshes. *Mol. Ecol.* **2022**, *31*, 4478–4494. [CrossRef]
48. Knights, D.; Kuczynski, J.; Charlson, E.S.; Zaneveld, J.; Mozer, M.C.; Collman, R.G.; Bushman, F.D.; Knight, R.; Kelley, S.T. Bayesiam community-wied culture-independent microbial source tracking. *Nat. Methods* **2011**, *8*, 761–763. [CrossRef]
49. Zhang, G.Z.; Bai, J.H.; Tebbe, C.C.; Zhao, Q.Q.; Jia, J.; Wang, W.; Wang, X.; Yu, L. Salinity controls soil microbial community structure and function in coastal estuarine wetlands. *Environ. Microbiol.* **2021**, *23*, 1020–1037. [CrossRef]
50. Zhou, F.X.; Gao, X.L.; Zhang, Y.; Yuan, H.M.; Song, J.M.; Liu, K.; Yang, B.; Zhang, W. Potential mobility of inorganic nutrients and its controls at the sediment water interface in the main path of Kuroshio Current off eastern Taiwan. *Mar. Pollut. Bull.* **2017**, *119*, 270–276. [CrossRef] [PubMed]
51. Gao, X.L.; Zhou, F.X.; Chen, C.T.A. Pollution status of the Bohai Sea: An overview of the environmental quality assessment related trace metals. *Environ. Int.* **2014**, *62*, 12–30. [CrossRef]
52. Wang, Y.; Ling, M.; Liu, R.H.; Yu, P.; Tang, A.K.; Luo, X.X.; Ma, Q.M. Distribution and source identification of trace metals in the sediment of Yellow River Estuary and the adjacent Laizhou Bay. *Phys. Chem. Earth* **2017**, *97*, 62–70. [CrossRef]
53. Li, H.J.; Gao, X.L.; Gu, Y.B.; Wang, R.R.; Xie, P.F.; Liang, M.; Ming, H.X.; Su, J. Comprehensive large-scale investigation and assessment of trace metal in the coastal sediments of Bohai Sea. *Mar. Pollut. Bull.* **2018**, *129*, 126–134. [CrossRef] [PubMed]
54. Artigas, F.; Loh, J.M.; Shin, J.Y.; Grzyb, J.; Yao, Y. Baseline and distribution of organic pollutants and heavy metals in tidal creek sediments after Hurricane Sandy in the Meadowlands of New Jersey. *Environ. Earth Sci.* **2017**, *76*, 293. [CrossRef]
55. Zhou, X.H.; Liu, L.M.; Chen, X.; Chen, Z.G.; Zhang, J.P.; Li, Y.M.; Liu, B. Heavy metals distribution characteristics and ecological risk evaluation in surface sediments of Dammed Jinshan Lake. *Environ. Sci.* **2014**, *35*, 4127–4134. (In Chinese)
56. Xia, Y.F.; Ling, X.F.; Fang, Y.; Xu, Z.; Liu, J.Y.; Liu, F.D. Effects of tidal dikes on the distribution and accumulation risk of trace metals in the coastal wetlands of Laizhou Bay, China. *Water* **2024**, *16*, 3230. [CrossRef]
57. Wu, H.H.; Xu, C.B.; Wang, J.H.; Xiang, Y.; Ren, M.; Qie, H.T.; Zhang, Y.J.; Yao, R.H.; Li, L.; Lin, A.J. Health risk assessment based on source identification of heavy metals: A case study of Beiyun River, China. *Ecotox Environ. Safe* **2021**, *213*, 112046. [CrossRef]
58. Jroundi, F.; Martinez-Ruiz, F.; Merroun, M.L.; Gonzalez-Muñoz, M.T. Exploring bacterial community composition in Mediterranean deep-sea sediments and their role in heavy metal accumulation. *Sci. Total Environ.* **2020**, *712*, 135600. [CrossRef] [PubMed]

59. Aiman, U.; Mahmood, A.; Waheed, S.; Malik, R.N. Enrichment, geo-accumulation and risk surveillance of toxic metals for different environmental compartments from Mehmood Booti dumping site, Lahore city, Pakistan. *Chemosphere* **2016**, *20*, 356. [CrossRef]
60. Huang, S.H.; Yang, Y.; Yuan, C.Y.; Ouyang, K.; Wang, B.; Wang, Z.X. Pollution evaluation of heavy metals in soil near smelting area by index of geoaccumulation (Igeo). *IOP Conf. Ser. Earth Environ. Sci.* **2017**, *52*, 012095. [CrossRef]
61. Zhang, G.L.; Bai, J.H.; Zhao, Q.Q.; Lu, Q.Q.; Jia, J.; Wen, X.J. Heavy metals in wetland soils along a wetland-forming chronosequence in Yellow River Delta of China: Levels, sources and toxic risks. *Ecol. Indic.* **2016**, *69*, 331–339. [CrossRef]
62. Ngatia, L.W.; De Oliveira, L.M.; Betiku, O.C.; Fu, R.; Moriasi, D.N.; Steiner, J.L.; Verser, J.A.; Taylor, R.W. Relationship of arsenic and chromium availability with carbon functional groups, aluminum and iron in Little Washita River Experimental Watershed Reservoirs, Oklahoma, USA. *Ecotox Environ. Safe* **2021**, *207*, 111468. [CrossRef]
63. Liu, F.D.; Zhang, S.; Dong, Y.F.; Zheng, Y.; Li, D.S.; Wang, M.H. The distribution and enrichment of trace metals in the rainfall-driven supratidal wetlands of Tianjin, China. *Clean-Soil. Air Water* **2017**, *45*, 1700200. [CrossRef]
64. Chai, Y.; Guo, J.; Chai, S.L.; Cai, J.; Xue, L.F.; Zhang, Q.W. Source identification of eight heavy metals in grassland soils by multivariate analysis from the Baicheng-Songyuan area, Jilin Province, Northeast China. *Chemosphere* **2015**, *134*, 67–75. [CrossRef] [PubMed]
65. Facchinelli, A.; Sacchi, E.; Mallen, L. Multivariate statistical and GIS-based approach to identify heavy metal sources in soils. *Environ. Pollut.* **2001**, *114*, 313–324. [CrossRef] [PubMed]
66. Franco-Uría, A.; López-Mateo, C.; Roca, E.; Fernández-Marcos, M.L. Source identification of heavy metals in pastureland by multivariate analysis in NW Spain. *J. Hazard. Mater.* **2009**, *165*, 1008–1015. [CrossRef]
67. Chen, D.Q.; Xie, Z.Y.; Zhang, Y.J.; Luo, X.L.; Guo, Q.R.; Yang, J.J.; Liang, Y.J. Source apportionment of soil heavy metals in Guangzhou Based on the PCA/APCS Model and Geostatistics. *Ecol. Environ. Sci.* **2016**, *25*, 1014–1022. (In Chinese)
68. Bataille, C.P.; Willis, A.; Yang, X.; Liu, X.M. Continental igneous rock composition: A major control of past global chemical weathering. *Sci. Adv.* **2017**, *3*, e1602183. [CrossRef]
69. Carrero, S.; Slorznick, S.P.; Fakra, S.C.; Sitar, M.C.; Bone, S.E.; Mauk, J.L.; Manning, A.H.; Swanson-Hysell, N.L.; Williams, K.H.; Banfield, J.F.; et al. Mineralogical, magnetic and geochemical data constrain the pathways and extent of weathering of mineralized sedimentary rocks. *Geochim. Cosmochim. AC* **2023**, *343*, 180–195. [CrossRef]
70. Peng, B.; Piestrzynski, A.; Pieczonka, J.; Xiao, M.; Wang, Y.Z.; Xie, S.R.; Tang, X.Y.; Yu, C.X.; Song, Z. Mineralogical and geochemical constraints on environmental impacts from waste rock at Taojiang Mn-ore deposit, central Hunan, China. *Environ. Geol.* **2007**, *52*, 1277–1296. [CrossRef]
71. Yu, X.; LeMonte, J.J.; Li, J.X.; Stuckey, J.W.; Sparks, D.L.; Cargill, J.G.; Russoniello, C.J.; Michael, H.A. Hydrologic control on arsenic cycling at the groundwater—Surface water interface of a tidal channel. *Environ. Sci. Technol.* **2023**, *57*, 222–230. [CrossRef]
72. Liu, J.; Zheng, B.H.; Liu, L.S.; Ma, Y.Q.; Lin, K.X.; Wang, X.; Xia, Y. Response behaviors of heavy metals at tidal currents interface and salinity interface in the estuary area. *Environ. Sci.* **2016**, *37*, 2989–3000. (In Chinese)
73. Zhang, H.J.; Liu, Y.G.; Wang, Y.; Hou, L. Spatial distribution of heavy metals in the sediments of Yangzonghai lake wetland. *J. Hydroecol.* **2017**, *38*, 44–50. (In Chinese) [CrossRef]
74. Verslycke, T.; Vangheluwe, M.; Heijerick, D.; Schamphelaere, K.D.; Sprang, P.V.; Janssen, C.R. The toxicity of metal mixtures to the estuarine mysid Neomysis integer (Crustacea: Mysidacea) under changing salinity. *Aquat. Toxicol.* **2003**, *64*, 307–315. [CrossRef] [PubMed]
75. Blust, R.; Kockelbergh, E.; Baillieul, M. Effect of salinity on the uptake of cadmium by the brine shrimp Artemia franciscana. *Mar. Ecol. Prog. Ser.* **1992**, *84*, 245–254. [CrossRef]
76. Roast, S.D.; Widdows, J.; Jones, M.B. Effects of salinity and chemical speciation on cadmium accumulation and toxicity to two mysid species. *Environ. Toxicol. Chem.* **2001**, *20*, 1078–1084. [CrossRef]
77. Santos Bermejo, J.C.; Beltrán, R.; Gómez, A. Spatial variations of heavy metals contamination in sediments from Odiel river (Southwest Spain). *Environ. Int.* **2003**, *29*, 69–77. [CrossRef] [PubMed]
78. Augustynowicz, J.; Sitek, E.; Latowski, D.; Wolowski, K.; Kowalczyk, A.; Przejczowski, R. Unique biocenosis as a foundation to develop a phytobial consortium for effective bioremediation of Cr(VI)-polluted waters and sediments. *Environ. Pollut.* **2021**, *273*, 116506. [CrossRef]
79. Tan, W.F.; Liu, F.; Feng, X.H.; Huang, Q.Y.; Li, X.Y. Adsorption and redox reactions of heavy metals on Fe-Mn nodules from Chinese soils. *J. Colloid. Interf. Sci.* **2005**, *284*, 600–605. [CrossRef]
80. Gasparatos, D. Sequestration of heavy metals from soil with Fe-Mn concretions and nodules. *Environ. Chem. Lett.* **2013**, *11*, 1–9. [CrossRef]
81. An, B.; Zhao, D.Y. Immobilization of As (III)in soil and groundwater using a new class of polysaccharide stabilized Fe-Mn oxide nanoparticles. *J. Hazard. Mater.* **2012**, *211*, 332–341. [CrossRef]
82. Hai, J.; Liu, L.H.; Tan, W.F.; Hao, R.; Qiu, G.H. Catelytic oxidation and adsorption of Cr(III) on iron-manganese nodules under oxic conditions. *J. Hazard. Mater.* **2020**, *390*, 122166. [CrossRef]
83. Zhang, G.S.; Qu, J.H.; Liu, H.J.; Liu, R.P.; Wu, R.C. Preparation and evaluation of novel Fe-Mn binary oxide adsorbent for effective arsenite removal. *Water Res.* **2007**, *41*, 1921–1928. [CrossRef] [PubMed]

84. Xu, Z.Y.; Zhao, Y.X.; Xu, Z.; Chen, X.; Zhang, X.L.; Chen, Z.B.; Ban, Y.H. Arbuscular mycorrhizal fungi enhanced the drinking water treatment residue-based vertical flow constructed wetlands on the purification of arsenic-containing wastewater. *J. Hazard. Mater.* **2023**, *465*, 133241. [CrossRef] [PubMed]
85. Uddin, M.M.; Zakeel, M.C.M.; Zavahir, J.S.; Marikar, F.M.M.T.; Jahan, I. Heavy metal accumulation in rice and aquatic plants used as human food: A general review. *Toxics* **2021**, *9*, 360. [CrossRef] [PubMed]
86. Alexander, T.J.; Vonlanthen, P.; Seehausen, O. Does eutrophication-driven evolution change aquatic ecosystems? *Philos. Trans. R. Soc. B* **2017**, *372*, 1712. [CrossRef]
87. Fortunato, C.S.; Herfort, L.; Zuber, P.; Baptista, A.M.; Crump, B.C. Spatial variability overwhelms seasonal patterns in bacterioplankton communities across a river to ocean gradient. *ISME J.* **2011**, *6*, 554–563. [CrossRef]
88. Satinsky, B.M.; Fortunato, C.S.; Doherty, M.; Smith, C.B.; Sharma, S.; Ward, N.D. Metagenomic and metatranscriptomic inventories of the lower Amazon River, May 2011. *Microbiome* **2015**, *3*, 39. [CrossRef]
89. Pan, K.; Wang, W.X. Trace metal contamination in estuarine and coastal environments in China. *Sci. Total Environ.* **2012**, *421–422*, 3–16. [CrossRef]
90. Zhang, J.; Liu, C.L. Riverine composition and estuarine geochemistry of particulate metals in China-Weathering features, anthropogenic impact and chemical fluxes. *Estuar. Coast. Shelf Sci.* **2002**, *54*, 1051–1070. [CrossRef]
91. Sun, M.Y.; Dafforn, K.A.; Brown, M.V.; Johnston, E.L. Bacterial communities are sensitive indictors of contaminant stress. *Mar. Pollut. Bull.* **2012**, *64*, 1029–1038. [CrossRef]
92. Martin, A.J.; Calvert, S.E. Hydrological and geochemical controls governing the distribution of trace metals in a mine-impacted lake. *Environ. Geol.* **2003**, *43*, 408–418. [CrossRef]
93. Yuan, J.; Wen, T.; Zhang, H.; Zhao, M.L.; Pen, C.R.; Thomashow, L.S.; Shen, Q.R. Predicting disease occurrence with high accuracy based on soil macroecological patterns of Fusarium wilt. *ISME J.* **2020**, *14*, 2936–2950. [CrossRef] [PubMed]
94. Chen, T.; Liu, Y.X.; Huang, L.Q. ImageGP: An easy-to-easy-use data visualization web server for scientific researchers. *iMeta* **2022**, *1*, e5. [CrossRef] [PubMed]
95. Jeong, H.; Ra, K. Pollution and ecological risk assessments for heavy metals in coastal, river, and road-deposited sediments from Apia city in Upolu Island, Samoa. *Mar. Pollut. Bull.* **2023**, *188*, 114596. [CrossRef] [PubMed]
96. Liu, X.Z.; Sheng, Y.Q.; Liu, Q.Q.; Li, Z.R. Ecological and environmental risks of heavy metals in sediments in Dingzi Bay, South Yellow Sea. *Mar. Pollut. Bull.* **2023**, *188*, 114683. [CrossRef]
97. Wu, Z.; Liu, L.L.; Zhang, X.X.; Jiang, S.H.; Gao, J.F.; Zhang, S.J. Distribution and pollution assess of heavy metals in surface sediments along the Weihai coast, China. *Mar. Pollut. Bull.* **2023**, *190*, 114885. [CrossRef]
98. Tong, L. Element abundances of China's continental crust and its sedimentary layer and upper continental crust. *Chin. J. Geochem.* **1995**, *14*, 26–32. [CrossRef]

toxics

MDPI

Article

Characteristics and Mechanism of Hematite Dissolution and Release on Arsenic Migration in Heterogeneous Materials

Zheying Li [1,2], Huimei Shan [1,2,*], Wanyue Rong [1,2], Zhicheng Zhao [1,2], Kexin Ma [1,2], Sanxi Peng [3] and Song Wei [1,2,*]

[1] Guangxi Key Laboratory of Environmental Pollution Control Theory and Technology, Guilin University of Technology, Guilin 541004, China; 15837571133@163.com (Z.L.); ke-xma2002@163.com (K.M.)
[2] Collaborative Innovation Center for Water Pollution Control and Water Safety in Karst Area, Guilin University of Technology, Guilin 541004, China
[3] College of Earth Sciences, Guilin University of Technology, Guilin 541004, China
* Correspondence: shanhuimei@glut.edu.cn (H.S.); weis@glut.edu.cn (S.W.)

Abstract: The migration of arsenic in groundwater is influenced by the heterogeneity of the medium, and the presence of iron minerals adds complexity and uncertainty to this effect. In this study, a stratified heterogeneous sand column with an embedded hematite lens at the coarse-to-medium sand interface was designed. We introduced an arsenic-laden solution and controlled groundwater flow to investigate the spatiotemporal characteristics of arsenic migration and the impact of hematite dissolution. The results showed that the medium structure significantly influenced the arsenic migration and distribution within the lens-containing sand column. The clay layers directed the lateral migration of arsenic, and the arsenic concentrations in deeper layers were up to seven times greater than those on the surface. The extraction experiments of solid-phase arsenic revealed that the main adsorption modes on quartz sand surfaces were the specific adsorption (F2) and adsorption on weakly crystalline iron–aluminum oxides (F3), correlating to the specific and colloidal adsorption modes, respectively. Monitoring the total iron ions (Fe(aq)) revealed rapid increases within the first 14 days, reaching a maximum on day 15, and then gradually declining; these results indicate that hematite did not continuously dissolve. This study can aid in the prevention and control of arsenic contamination in groundwater.

Keywords: arsenic; heterogeneity; hematite; migration; dissolution

1. Introduction

Arsenic (As) is found in groundwater worldwide [1,2]. The World Health Organization stipulates that the As concentration in drinking water should not exceed 10 μg/L [3]. Drinking groundwater contaminated with As can cause cancer and diseases of the lungs, liver, kidneys, and skin [4,5]. As often occurs in groundwater, and its migration and distribution are affected by iron minerals, medium heterogeneity, and human activities [6–8]. Recent studies have shown that the heterogeneity of the medium affects the temporal and spatial variations in groundwater arsenic concentrations [9,10]. Hematite is a common natural mineral and adds complexity to arsenic migration in heterogeneous media. Hematite dissolves into hydrated iron oxides that adsorb arsenic [11] and directly adsorb arsenic through inner-sphere complexation [12]. Therefore, the effects of the medium heterogeneity on As migration and transformation have received increasing attention.

Currently, the effect of medium heterogeneity on As migration is still unclear. During the groundwater flow process, the migration rate of arsenic may be influenced by mineral adsorption, particularly the adsorption of minerals such as clays and oxides/hydroxides of iron, aluminum, and manganese [13]. Due to the varying distribution of these minerals in sediments, they can retain arsenic to different extents, thereby affecting the migration and distribution of arsenic [14]. Duan (2020) [15] combined experimental work with sand

columns and data simulations to determine that pumping enhances groundwater flow and arsenic migration along preferred pathways. They discovered that both physical and chemical heterogeneities jointly influenced these processes. Their results showed that physical heterogeneity alone could not fully explain the findings, highlighting the significant impact of medium heterogeneity on arsenic migration. Duan (2022) [16] conducted an in-depth study on the desorption of arsenic by using a heterogeneous sand tank and competitive adsorption ions. They reported that arsenic desorption was driven not only by the competitive adsorption of phosphate irons (PO_4^{3-}), but also occurred in the preferential flow channels. This study highlighted the significant role of medium heterogeneity in influencing arsenic migration and transformation. Although the heterogeneity and competitive adsorption of ions have been proven to be very important, the impact of natural hematite on arsenic migration in heterogeneous systems has yet to receive adequate attention.

The characteristics of arsenic adsorption by iron minerals have been extensively studied. For example, iron and aluminum minerals affect arsenic adsorption and desorption through dissolution processes [17–19]. Specifically, hematite, which is a typical iron mineral in high-arsenic areas, not only adsorbs arsenic on its surface or within its crystal structure but also dissolves due to river water infiltration, leading to the release of arsenic. This process further influences the speciation of arsenic [20,21]. In their study of West Bengal's groundwater, Nath (2005) [22] reported that arsenic-rich areas had sandy aquifers mixed with fine sediments rich in arsenic and iron. These findings indicated that iron oxides in groundwater were crucial in controlling arsenic migration in shallow aquifers. Fendorf (2010) [23] noted from their examination of groundwater wells in the Himalayan region that the reduction and dissolution of iron oxides such as hematite not only released arsenic but also converted As(V) to the more mobile As(III). This process was influenced by groundwater movement and altered the concentration and distribution of arsenic. Due to the crucial role of hematite in arsenic migration, investigating the impacts of medium heterogeneity and the dissolution of hematite on arsenic mobility is essential.

Based on the aforementioned scientific issues, in this study, a heterogeneous sand column was designed, different-sized quartz sand was layered in the reactor, strips of clay were embedded to simulate lenses, and hematite spheres were incorporated at the coarse-to-medium sand interface. An arsenic-laden solution was introduced, and the groundwater flow was controlled by pumping to investigate the spatiotemporal characteristics of arsenic migration and the impact of hematite dissolution. Here, characterization analysis was combined with the changes in the iron concentration to determine the mechanisms involved. The aims of this study are (1) to assess the impact and characteristics of pumping and hematite on arsenic migration and (2) to explore the dissolution and release patterns of hematite under the influence of pumping. This study deepens our understanding of arsenic migration and transformation in contaminated areas and can provide a scientific basis for arsenic pollution control.

2. Experimental Materials and Analytical Methods

2.1. Sand Trough Structure and Operation Mode

A sand tank experimental device is used to characterize the migration and transformation of pollutants in the aquifer and includes the tank body, fixed rod, PVC pipe, semipermeable board, positioning plate, water level controller, water inlet pipe, drainage pipe, and sampling device, as illustrated in Figure 1a. The tank body is a rectangular block sealed using acrylic plates, with support rods inside to prevent deformation, semipermeable baffles at both ends, positioning plates, and water level controllers outside. The simulated liquid storage tank and the waste liquid collection bucket are connected through the water inlet and drainage pipes. A total of 25 sampling holes are located on the front, and a simulated pumping well is installed. Please refer to the Supporting Information (Text S1 and Figure S1) for detailed information on the sand tank structure. The hematite sand column was filled with quartz sand, clay, and a hematite lens body, as illustrated in Figure 1b. Based on a profile of an actual aquifer structure from the field, different particle

sizes of quartz sand (from 50 to 200 mesh) and clay were proportionally and sequentially loaded into the sand tank. The column was set to a height of approximately 30 cm, with the first 21 cm consisting of sand layers, followed by a clay layer from 21 to 29 cm and large quartz particles from 29 to 30 cm to prevent the clay from floating during the experiment.

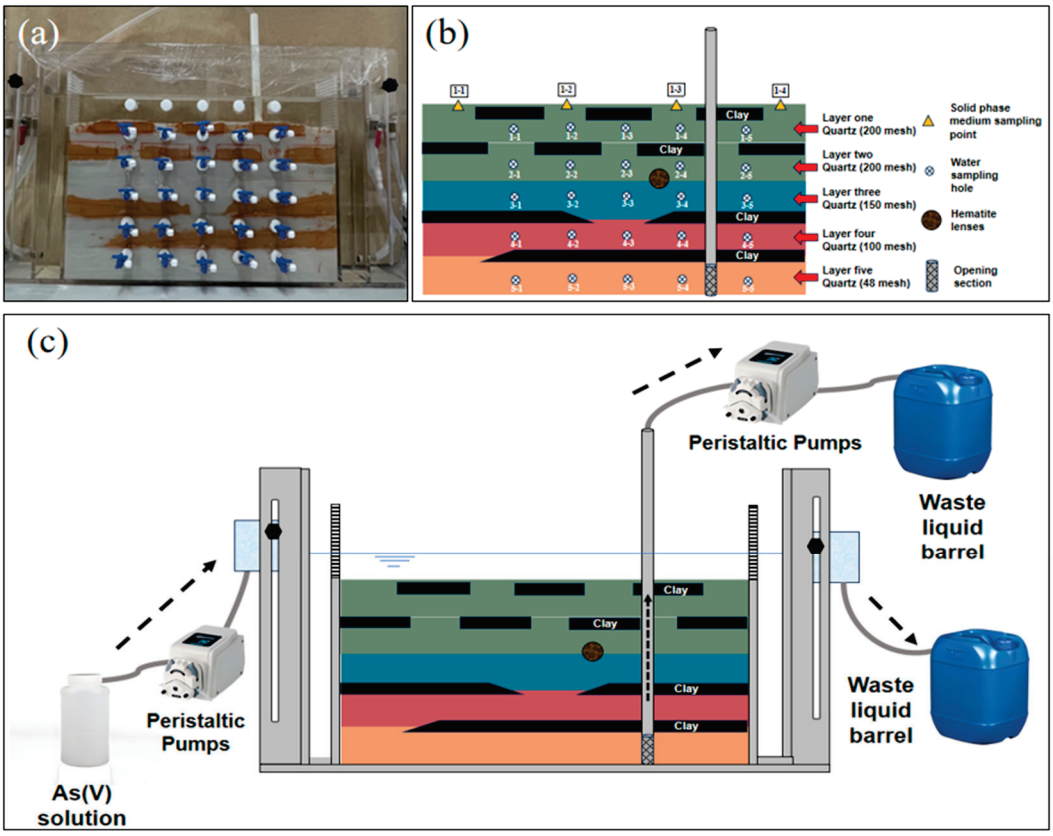

Figure 1. Experimental device. (**a**) Actual image; (**b**) medium structure; (**c**) device operation.

Before the experiment, the flow rate of the peristaltic pump for the water supply was adjusted to 2.0 mL/min, and the flow rate of the peristaltic pump for the water extraction was adjusted to 1.0 mL/min. As shown on the left side of Figure 1c, the water level at the inlet is 3–4 mm higher than that at the outlet; this provides a horizontal hydraulic gradient of 4.6×10^{-3} to 6.2×10^{-3}. The arsenic-containing simulated fluid is pumped into the system, and the liquid level in the tank gradually increases until it maintains an approximate 2 cm free water layer (top layer) during the experiment. The channel is stabilized for 5 days to achieve local chemical equilibrium between the minerals and the injected water. During the pumping phase, the liquid is drawn from the bottom sand layer at a 1.0 mL/min rate through the "well", driving the oxidized water at the top to flow downward through the heterogeneous layer system. The water supply rate at the inlet exceeds the pumping rate at the well; this causes excess water to flow directly over the top water layer toward the outlet side rather than seep into the quartz sand medium.

2.2. Reagents and Samples

In the experiment, quartz sand was used as the reaction medium and underwent multiple cycles of soaking and rinsing with deionized water until the conductivity reached a stable value of approximately 30 μS/cm. Afterwards, the sand was subjected to drying in a forced-air oven at a temperature of 50 °C and was then set aside for future utilization. Hematite was purchased from the Hubei Exi Geological Industry and Trade Co., Hubei, China Ltd., Shiyan, China. The experimental water was ultrapure (conductivity < 18 μS/cm) and was used to prepare a 10.9203 mg/L $Na_2HAsO_4 \cdot 7H_2O$ simulation solution.

The experiment utilized analytical quality reagents, including $Na_2HAsO_4 \cdot 7H_2O$, $NaAsO_2$, H_2NCSNH_2, and $C_6H_8O_6$. Additionally, KOH, NaOH, and HCl were used. The 1000 μg/mL arsenic standard solution was acquired from the National Nonferrous Metals and Electronic Materials Analysis and Testing Center. Analytical-grade reagents were used.

2.3. Tests and Methods

The concentrations of As(V) in the solution were measured using atomic fluorescence spectroscopy (AFS-933/SA-20, Beijing Jitian Instruments, Beijing, China; detection limit $\leq$ 0.01 mg/L). The elemental lamp used was an atomic fluorescence hollow cathode lamp (HAF-2) with a current of 36 mA. The dissolved iron (Fe(aq)) concentrations were determined using a microplate reader (SPARK, TECAN, Männedorf, Switzerland).

The main phases and crystallinity of the quartz sand samples were analyzed using an X'Pert3 Powder multifunctional X-ray diffractometer (PANalytical, BV, The Netherlands, Cu target, λ = 1.54056 Å). The scan step was set at 0.026°, with a scanning speed of 0.65(°)/s and a range from 5° to 90°. Fourier transform infrared spectroscopy (FTIR, iS 10, Thermo Fisher Scientific, Waltham, MA, USA) was used to determine the functional groups and chemical bond vibrations. The surface morphology and elemental composition were examined using scanning electron microscopy and energy dispersive spectroscopy (SEM-EDS, JSM-7900F, JEOL Ltd., Tokyo, Japan). The composition of the arsenic bound to the surface of the quartz sand was analyzed using an improved Wenzel extraction method [24], as shown in Table 1.

Table 1. Wenzel extraction method.

Chemical Form	Extraction Method	Water–Sand Ratio (mL:g)
Nonspecifically adsorbed state (F1)	0.05 mol/L $(NH4)_2SO_4$, 25 °C, shaking 4 h	25:1
Specifically adsorbed state (F2)	0.05 mol/L $NH_4H_2PO_4$, 25 °C, shaking 16 h	25:1
Amorphous iron-aluminum oxide-bound state (F3)	First time: 0.2 mol/L ammonium oxalate buffer (pH = 3.5), 25 °C, shaking 4 h Second time: 0.2 mol/L ammonium oxalate buffer (pH = 3.5), 25 °C, shaking 10 min	First time 25:1 Second time 12.5:1
Crystalline iron-aluminum oxide-bound state (F4)	First time: ammonium oxalate (0.2 mol/L) + ascorbic acid (0.1 mol/L), pH = 3.5, 96 °C, shaking 30 min Second time: ammonium oxalate (0.2 mol/L) + ascorbic acid (0.1 mol/L), pH = 3.5, 96 °C, shaking 10 min	First time 25:1 Second time 12.5:1

2.4. Statistical Analysis and Plotting Software

All data were statistically analyzed using Excel 2016, and all figures were generated using Origin 2021.

3. Results and Discussion

3.1. Migration Characteristics of As

Figure 2a shows that the As(V) concentrations in sections 1-2 and 1-4 are significantly higher than those in sections 1-1, 1-3, and 1-5. As shown in Figure 2b, the concentrations in the second layer at points 2-1, 2-2, and 2-3 are notably higher. These results are in agreement with existing research; this research has revealed that the clay layers are impermeable, leading to higher flow rates in more permeable quartz sand layers and the formation of preferential flow channels [25]. Thus, by forming preferential flow pathways, the clay layer facilitates the rapid migration of As(V) in samples 1-2, 1-4, 2-1, 2-2, and 2-3.

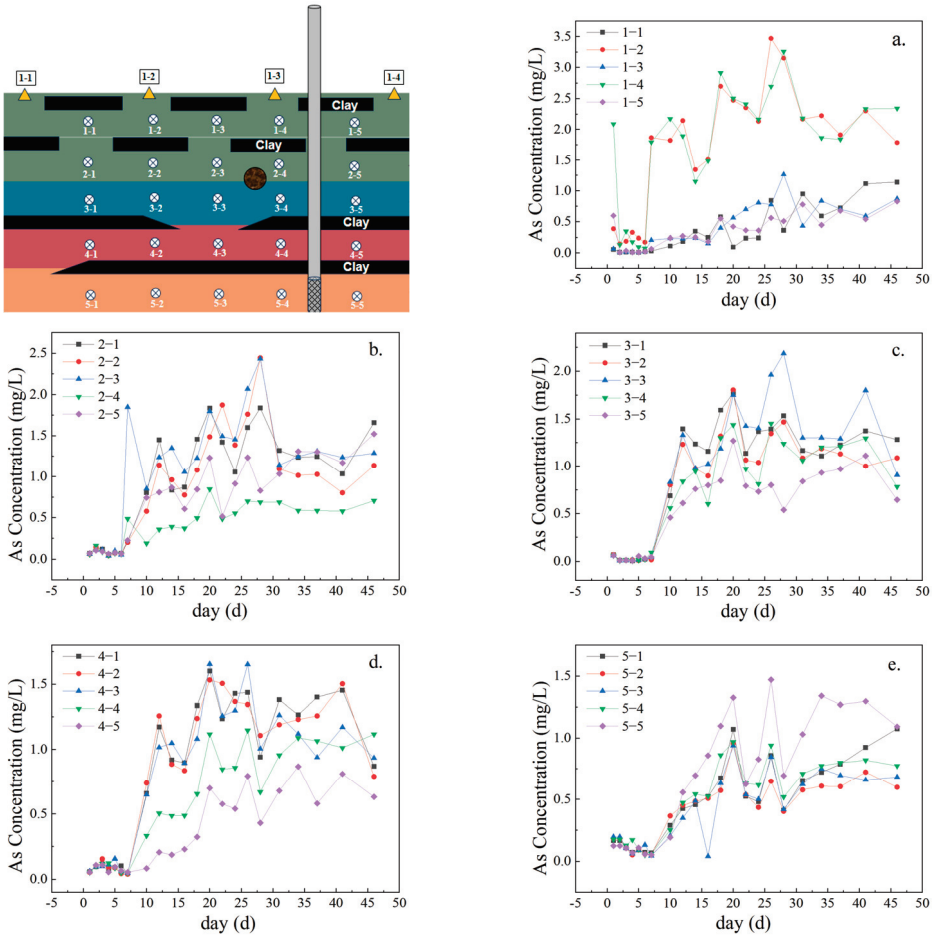

Figure 2. As(V) migration curve. (**a**) Arsenic concentration changes in layer one; (**b**) Arsenic concentration changes in layer two; (**c**) Arsenic concentration changes in layer three; (**d**) Arsenic concentration changes in layer four; (**e**) Arsenic concentration changes in layer five.

Figure 2c,d show that the As(V) concentrations are significantly greater in the third layer at points 3-1, 3-2, and 3-3 and in the fourth layer at points 4-1, 4-2, and 4-3. These results indicate that the clay within the sand layers significantly affects the migration of As(V) in the third and fourth layers; thus, under the vertical pressure induced by pumping, the clay layers force As(V) to migrate horizontally. Duan [15] and Close [26] also reported that clay layers without hematite promoted the horizontal migration of As(V). However, their sampling points with the highest concentrations differed from ours; their highest concentrations were found at points 3-4, 3-5, 4-4, and 4-5. These results indicate that the hematite lens bodies influenced As(V) migration at locations 3-4 and 3-5, primarily through the dissolution and release of hematite and the formation of iron–aluminum oxide colloids. As water flows, hematite gradually dissolves and continuously releases Fe(aq) into the water. This released Fe(aq) is a key source of iron–aluminum oxides and contributes to the formation of new iron–aluminum oxides that adsorb As(V). This resulted in significantly lower As(V) concentrations at locations 3-4 and 3-5 than at the other sampling sites.

Figure 2e illustrates the migration pattern of As(V) in the fifth-layer medium. As pumping progresses, the As(V) concentrations are similar across most sampling points, except for a higher concentration at sample points 5-5. These results align with the studies by Duan [15] and Qin [27]; their studies indicated that the distribution of As(V) was relatively uniform in the bottom layer, with rapid horizontal flow and stable flow rates. This result also shows that the distribution of As(V) is relatively uniform in relatively closed groundwater spaces.

Notably, the equilibrium concentrations of As(V) in each layer are inversely proportional to depth. As the depth increases, the maximum concentration of As(V) gradually decreases from 3.5 mg/L to 1.5 mg/L. Thus, the As distribution in heterogeneous media is highly uneven, indicating that the low permeability of clay layers impedes the diffusion and migration of As(V). Based on a comparison of the changes in As(V) concentrations at different depths between days 10 and 15, the As concentrations in various media layers decreased to varying extents. The most significant decreases were in the first and fourth layers, which decreased from 2.3 mg/L and 1.3 mg/L to 1.2 mg/L and 0.82 mg/L, respectively. These results indicate that diffusion cannot solely explain the migration of As(V) in the heterogeneous sand column. Adsorption by Fe(aq) and quartz sand also plays a crucial role in controlling the movement of As(V). The content of As(III) remains extremely low, and its concentration shows minimal fluctuation, indicating that the change in total As concentration is primarily due to As(V).

3.2. Fe Ion Release and Migration Characteristics

As shown in Figure 3, during the test period, the concentration of Fe(aq) in the surface layer (1-2 layers) minimally changed, and after 40 days of pumping, the concentration of Fe(aq) remained above 0.65 mg/L. Figure 3a,b show that the surface concentration of Fe(aq) reaches a maximum on day 18; thus, pumping creates preferential flow paths, and Fe(aq) diffuses against the direction of pumping along these pathways [28]. Previous research has also shown that extracting high-arsenic groundwater for irrigation activities causes groundwater levels to rise, promoting the reductive dissolution of iron oxides [29–31]. Therefore, from 0 to 18 days, pumping promotes the reductive dissolution of hematite, leading to a rapid increase in the concentration of Fe(aq).

Figure 3c,d show that the Fe(aq) concentration rapidly increases to its maximum before day 16 and then decreases to 0 mg/L after 25 days. Existing research indicates that the release process of minerals such as hematite involves two stages: a rapid dissolution and release phase followed by a dissolution equilibrium phase [32,33]. Thus, hematite is initially released quickly and then reaches concentration equilibrium later. Although Figure 3c,d also show two stages, unlike existing studies, the concentration of Fe(aq) does not remain stable after rapid growth but quickly decreases. Moreover, the peak concentration of Fe(aq) in layer 3 is much higher than that in layer 4, indicating that water pumping can cause only part of the Fe(aq) to diffuse downward. In summary, although pumping leads to a rapid release of hematite, once it reaches the release equilibrium phase, Fe(aq) participates in the adsorption process of As(V), resulting in a rapid decrease in Fe(aq) levels.

In addition, as shown in Figure 3a,b,e, the maximum Fe(aq) concentrations in layers 1, 2, and 5 all appeared after 18 days; the amount of time needed to reach this maximum was significantly longer with respect to that in layers 3 and 4 (their maximum Fe(aq) concentrations were reached at 16 days). Previous studies have shown that after pollutants (as solutes) enter the underground saturated zone, they mainly exist in the groundwater in the form of ions and dissolved substances and migrate with the groundwater through advection and diffusion [34,35]. However, due to the low permeability of the clay layers, they are often considered impermeable in field studies. In layers 1, 2, and 5, the clay layer barrier effect restricted the solution's advection and diffusion, hindering the migration of Fe(aq). Thus, the time to reach the maximum concentrations of Fe(aq) in these layers was extended.

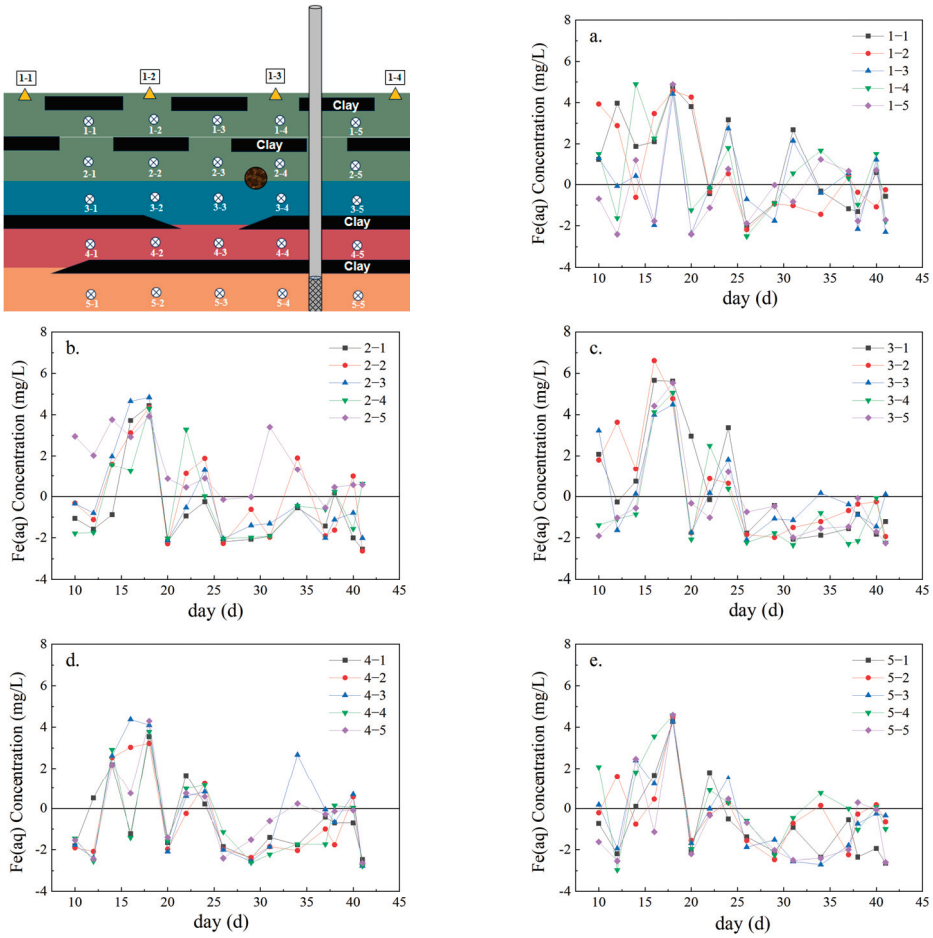

Figure 3. Fe(aq) migration curve. (**a**) Change of Fe(aq) concentration in the first layer; (**b**) Change of Fe(aq) concentration in the second layer; (**c**) Change of Fe(aq) concentration in the third layer; (**d**) Change of Fe(aq) concentration in the fourth layer; (**e**) Change of Fe(aq) concentration in the fifth layer.

3.3. Morphology and Distribution Characteristics of Solid As

Figure 4a displays the total adsorption of As. The results show that the adsorption levels at points 1-2 and 1-3 are significantly greater than those at points 1-1 and 1-4, and the order is as follows: 1-2 > 1-3 > 1-1 > 1-4. Moreover, the highest content of As in the F3 binding state is found at points 1-2 and 1-3. A comparison of these sampling locations at points 1-2 and 1-3, which are located on the preferential flow channels, shows greater As adsorption. These findings highlight the importance of the preferential flow channels in enhancing As adsorption.

To further analyze the mechanism by which Fe(aq) adsorbs As, we compared the content of As in different binding states. Figure 4b shows that the predominant forms of As(V) adsorbed by quartz sand are F2 and F3, which together account for 77% to 82% of the total As. Thus, quartz sand primarily adsorbs As(V) as amorphous and weakly crystalline iron–aluminum oxides. Evidence from prior studies indicates that hematite primarily adsorbs As in the F1 and F2 forms [36,37] rather than in the F2 and F3 forms. This difference indicates that Fe(aq) no longer adsorbs As(V) on quartz sand surfaces in the form of hematite after the hematite dissolves. Zhong [38] reported that adding hematite to arsenic-containing soil significantly increased As adsorption in the F3 binding state.

Additionally, the oxidation of iron with atmospheric oxygen and the subsequent precipitation of iron minerals can cause a decrease in the As concentrations [39]. This result indicates that after hematite dissolves and releases Fe(aq), Fe(aq) forms hematite on the surface of quartz sand, further adsorbing As(V). Thus, weakly crystalline iron–aluminum

oxides are the primary forms for As adsorption. Therefore, hematite can facilitate the adsorption of As onto quartz sand surfaces in the form of weakly crystalline iron–aluminum oxides [40,41].

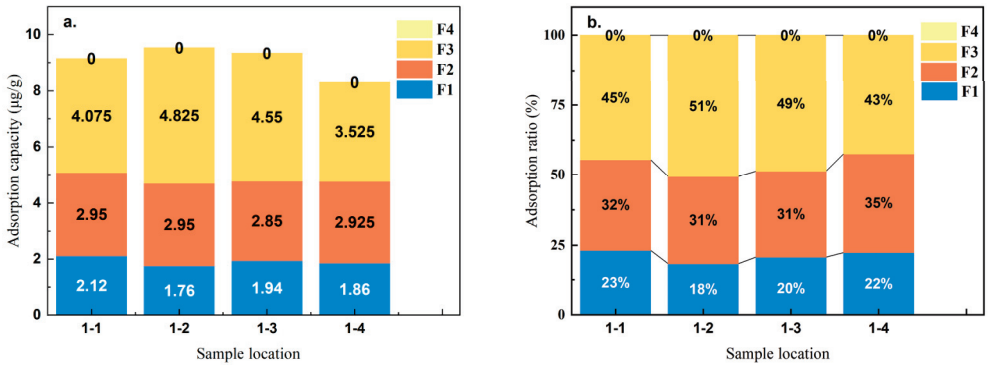

Figure 4. Contents and percentages of arsenic in its different adsorbed states. (**a**) Amount of arsenic adsorbed in each adsorbed state (μg/g); (**b**) Proportion of arsenic in each adsorbed state (%).

Notably, Figure 4 shows no presence of crystalline iron–aluminum oxide-bound As (F4) at any of the sampling points from 1-1 to 1-4. This means that Fe(aq) cannot directly form crystalline iron oxides. Additionally, the As contents in samples 1-2 and 1-3 (9.535 μg/g and 9.340 μg/g) are significantly greater than those in samples 1-1 and 1-4 (9.145 μg/g and 8.310 μg/g). However, the proportions and amounts of F1 and F2 in samples 1-2 and 1-3 are lower than those in samples 1-1 and 1-4. Zhong's research [38] showed that adding limonite and hematite to arsenic-containing soil did not significantly change the F4 content in the soil after the reaction. However, the F1 content decreased to varying degrees. Similarly, studies have shown that weakly crystalline iron minerals could effectively adsorb As [42–44]. Based on these results and studies, iron minerals adsorb As mainly by dissolving to form amorphous Fe-Al oxides. Zheying [45] reported that when the Fe(aq) concentration was lower than 1 mg/L, the adsorption of As by quartz sand was inhibited. After the dissolution of hematite released Fe(aq), Fe(aq) inhibited the adsorption of F1 and F2 while promoting the adsorption of F3. Thus, although some Fe(aq) was directly adsorbed by quartz sand at lower concentrations and occupied the F1 nonspecific adsorption sites, the dissolution of hematite released more Fe(aq). The quartz sand then adsorbed this excess Fe(aq), forming amorphous iron–aluminum oxides, which greatly increased the As(V) adsorption by the quartz sand.

4. Reaction Mechanism Analysis

4.1. Surface Morphology and Element Distribution

As shown in Figure 5, the surface of the quartz sand was relatively smooth, with few particles present before the reaction. After the experiment, the surface of sample 1-1 contained numerous particles and mineral crystals, along with a few very small pores. Samples 1-2 and 1-3 also contain a lot of particulate matter. It should be noted that the surface of sample 1-2 exhibits ridge-like structures, with particles uniformly distributed along these ridges. The surface of sample 1-3 contained microporous structures, with some particles aggregating into more significant crystalline substances. The surface of sample 1-4 contained uniformly distributed particles and a few microporous structures.

Additionally, some particles had aggregated into moss-like crystalline substances. These results were consistent with those from Du [46]; in their study, the surface of river sand exhibited numerous grooves and flaky structures after adsorbing As. Other studies have also revealed that the surface of quartz sand had pore structures [47], and these pore structures facilitated the adsorption of As. Clearly, the surface of the quartz sand had few impurities before the reaction. Thus, the crystalline substances on the quartz sand surface after the reaction were likely to be iron and aluminum oxides.

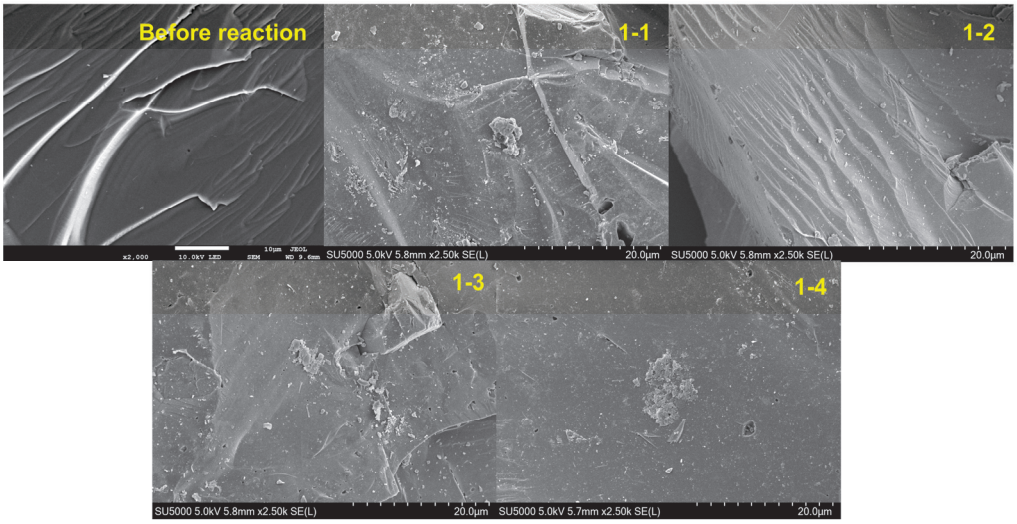

Figure 5. Microscopic morphology of sand before and after reaction.

To further investigate the composition of the crystalline substances on the quartz sand surface after the reaction, EDS was performed. As shown in Figure 6, while Al is enriched, the Fe and As are relatively dispersed. Additionally, a comparison of the distribution of Al reveals that it is concentrated in the mineral crystals, indicating that the crystals on the quartz sand surface are aluminum oxides. Additionally, no As enrichment is observed at the locations where aluminum is concentrated, indicating that aluminum oxides on the quartz sand surface do not effectively adsorb As. Thus, the Fe (hydro)oxides on the quartz sand surface provide adsorption sites for As [48,49], enhancing its adsorption.

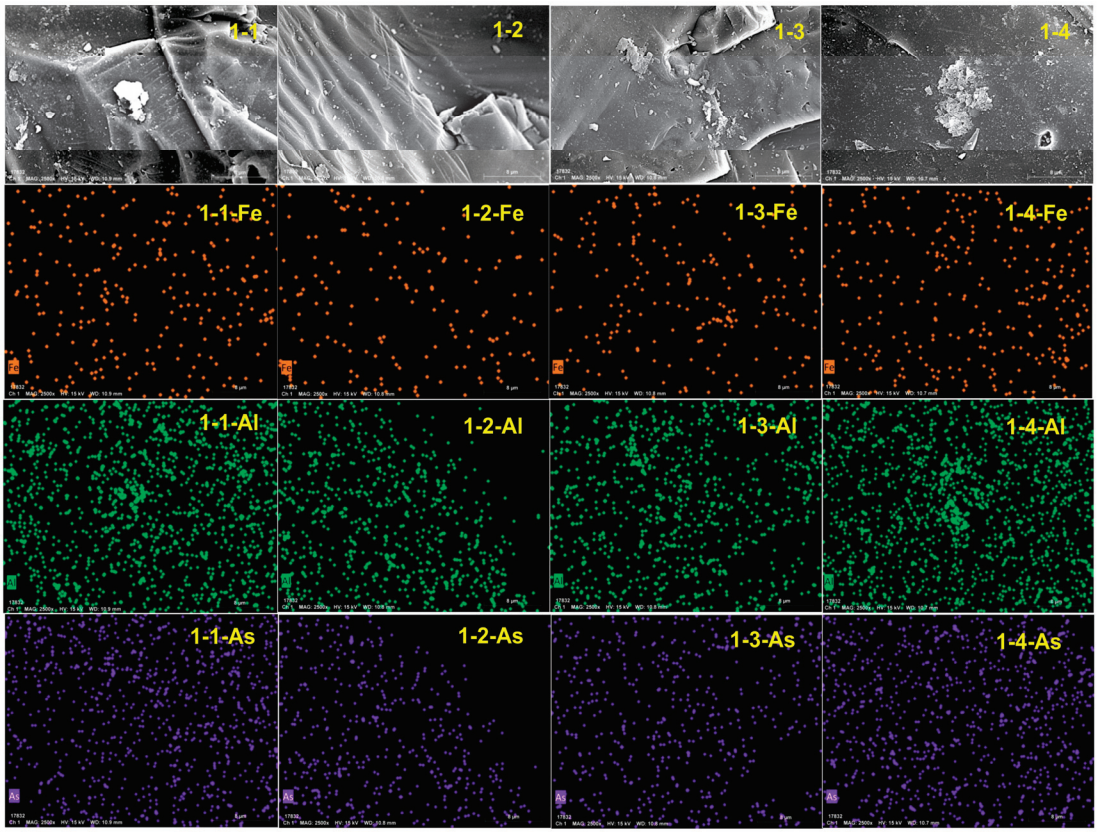

Figure 6. Surface energy spectrum of sand before and after the reaction.

Based on the data in Table 2, minimal amounts of iron oxides are effective for arsenic adsorption in samples 1-2 and 1-3. This demonstrates the ability of iron oxides to bind arsenic efficiently. Conversely, no arsenic was detected in samples 1-1 and 1-4, where iron oxides are absent. Notably, a comparison of the percentages of Fe and As on the surfaces of samples 1-2 and 1-3 reveals significantly lower Fe (0.08) and As (0.01) contents in sample 1-2 with respect to Fe (0.31) and As (0.02) in sample 1-3. These results indicate that the adsorption capacity of river sand for As increases after Fe (hydro)oxides attach to the surface of quartz sand. Thus, Fe (hydro)oxides can effectively enhance the adsorption of As [50].

Table 2. Elemental contents of sand before and after reaction with As and Fe (unit: %).

Condition	C	O	Si	Al	Fe	As
Before reaction	4.47	52.14	42.45	0.21	0.73	0
1-1	5.97	41.66	52.13	0.23	0	0
1-2	4.81	44.49	50.05	0.04	0.08	0.01
1-3	5.07	38.89	55.63	0.07	0.31	0.02
1-4	6.38	43.30	50.25	0.07	0	0

4.2. Main Crystalline Phase on the Surface

The XRD patterns of the quartz samples before and after the reaction at different locations are shown in Figure 7. The results indicate that the main component of the river sand surface was SiO_2. Trace amounts of As compounds were detected on the surface of the quartz sand. After the pumping test, the quartz sand spectra revealed several distinct characteristic peaks. The peak at $2\theta = 26.75^\circ$ corresponded to SiO_2, indicating that SiO_2 was the dominant component in all samples. Based on previous studies, regardless of the presence of organic matter in riparian sediments, the main phase detected by XRD after the adsorption reaction remained SiO_2 [51]. After the pumping test reached equilibrium, the peak intensity at $2\theta = 21^\circ$ in the XRD pattern slightly increased. This was potentially caused by As adsorbing onto the quartz sand surface as As_2O_3. The peak intensity at $2\theta = 68^\circ$ significantly increased. Compared with standard reference cards (PDF85-1712 and PDF15-0778), this was likely the result of the combined effects of As and As_2O_3. The peak intensity of 1-2 at $2\theta = 50^\circ$ significantly increased. Compared with the standard card (PDF85-1712), the As on the surface of the quartz sand mainly existed in the form of an As acid salt [52].

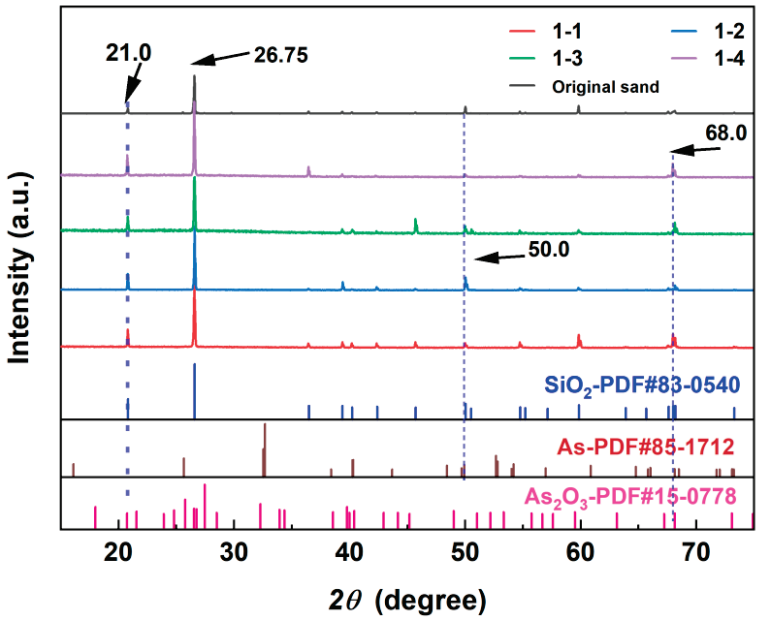

Figure 7. Physical phase of sand after reaction.

4.3. Changes in the Surface Functional Groups

The FTIR spectra of the quartz sand after the reaction at different locations are shown in Figure 8. No significant differences were observed between the FTIR spectra of quartz sand before and after As adsorption at the different locations. Under high-concentration conditions (Fe(aq) = 20 mg/L), a characteristic absorption peak for SiO_2 appears at 690 cm^{-1} [53]. Thus, the main component is SiO_2; this result is consistent with the results from the EDS and XRD analyses. Previous studies have shown that characteristic vibrational absorption peaks of Si–O are present at 463.06, 797.49, and 1084.72 cm^{-1} [54]. Si–O bond stretching vibrations cause peaks at 463.06 and 797.49 cm^{-1}, whereas the peak at 1084.72 cm^{-1} is due to the antisymmetric stretching vibration of Si–O–Si [45]. The characteristic absorption peaks observed between 950 and 1250 cm^{-1} are attributed primarily to the stretching vibrations of Si–OH and the antisymmetric stretching vibrations of Si–O–Si [55]. After the reaction, the surface of the quartz sand did not show the characteristic peaks of Fe minerals such as α-FeOOH (889, 795 cm^{-1}) [56], γ-FeOOH (1020 cm^{-1}) [57], Fe_2O_3 (559, 427 cm^{-1}) [58], and Fe_3O_4 (586 cm^{-1}) [59]. These results indicate that no new iron-containing functional groups were formed during the reaction. In addition, under low-concentration conditions (Fe(aq) = 0.1 mg/L), characteristic absorption peaks of aldehydes were found at 2815 and 2803 cm^{-1} in all samples. The stretching vibrations of the C–H bond caused these peaks. The 1632 and 1346 cm^{-1} peaks were attributed to the C=O stretching vibrations and –OH bending vibrations, respectively. These absorption peaks were formed by a small number of water molecules [60].

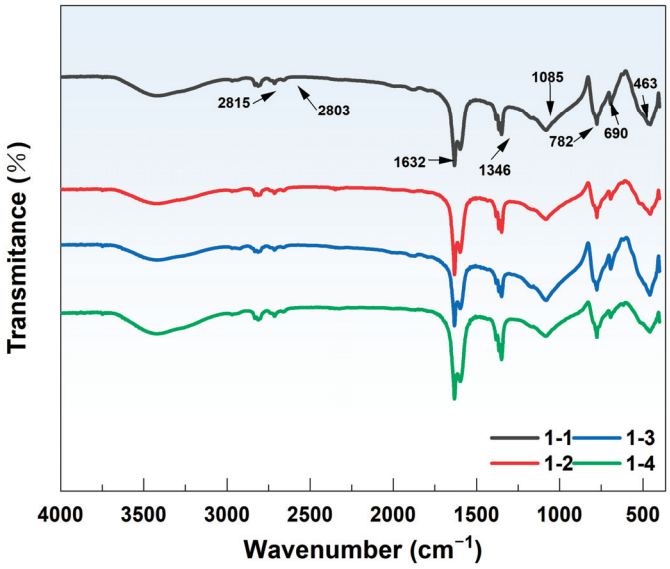

Figure 8. Crown group of sand after reaction.

5. Conclusions

In this study, the migration and distribution behaviors of As(V) and aqueous iron (Fe(aq)) in a groundwater environment were examined using a sand column experiment embedded with hematite lenses. Solid-phase extraction and characterization analysis was applied to investigate the control mechanisms of the As(V) migration. Our study reveals the intricate dynamics of As migration and distribution within different geological substrates, highlighting the role of the medium structure, particularly the arrangement of clay layers and quartz sand. These substrates distinctly affected the As concentrations. In the case of hematite, dissolution initially occurred at a rapid pace, and Fe(aq) was released into the system. However, this release rate notably diminished once a certain concentration threshold was reached, showing a crucial factor in the As distribution. Furthermore, our findings on solid-phase As indicated varying binding states, and that an amorphous iron–aluminum oxide-bound state and specifically adsorbed state were predominant under

the influence of preferential flow channels, which facilitated the enhanced As adsorption. Hematite dissolution releases Fe(aq). Fe(aq) subsequently reduces the migration of As(V) by modifying its adsorption and binding on quartz sand. These insights are critical for developing robust strategies for groundwater As pollution management, providing a theoretical foundation for the development of effective As mitigation approaches.

Supplementary Materials: The following supporting information can be downloaded at: https://www.mdpi.com/article/10.3390/toxics12090687/s1, Figure S1: Sand tank structure diagram; Table S1: Chemical compositions of medium (%). Text S1: Detailed information for sand tank.

Author Contributions: Conceptualization, Z.L. and H.S.; methodology, H.S.; validation, Z.Z. and W.R.; formal analysis, Z.L., H.S. and K.M.; investigation, Z.L., Z.Z. and W.R.; resources, H.S. And S.W.; data curation, Z.L., Z.Z., W.R. and S.P.; writing—original draft preparation, Z.L., H.S. and S.P.; writing—review and editing, Z.L., H.S., K.M. and S.W.; visualization, Z.L., Z.Z. and W.R.; supervision, Z.L.; project administration, Z.L., Z.Z. and W.R.; funding acquisition, H.S. and S.W. All authors have read and agreed to the published version of the manuscript.

Funding: Funding for this research was provided by the Natural Science Foundation of Guangxi (2022GXNSFBA035600), and the National Natural Science Foundation of China (Nos. 42167026, 42062015, and 42207063).

Institutional Review Board Statement: Not applicable.

Informed Consent Statement: Not applicable.

Data Availability Statement: The original contributions presented in the study are included in the article material, further inquiries can be directed to the corresponding authors.

Acknowledgments: We would like to thank Peng San-xi, from Guilin University of Technology, for editing the English text of a draft of this manuscript.

Conflicts of Interest: The authors declare that they have no conflicts of interest.

References

1. Podgorski, J.; Berg, M. Global threat of arsenic in groundwater. *Science* **2020**, *368*, 845–850. [CrossRef] [PubMed]
2. Cao, W.; Fu, Y.; Cheng, Y.; Zhai, W.; Sun, X.; Ren, Y.; Pan, D. Modeling potential arsenic enrichment and distribution using stacking ensemble learning in the lower Yellow River Plain, China. *J. Hydrol.* **2023**, *625*, 129985. [CrossRef]
3. WHO (World Health Organization). *Guidelines for Drinking Water Quality: Fourth Edition Incorporating the First Addendum*; World Health Organization: Geneva, Switzerland, 2017.
4. Guo, J.; Cao, W.; Lang, G.; Sun, Q.; Nan, T.; Li, X.; Ren, Y.; Li, Z. Worldwide Distribution, Health Risk, Treatment Technology, and Development Tendency of Geogenic High-Arsenic Groundwater. *Water* **2024**, *16*, 478. [CrossRef]
5. Sinha, D.; Prasad, P. Health effects inflicted by chronic low-level arsenic contamination in groundwater: A global public health challenge. *J. Appl. Toxicol.* **2020**, *40*, 87–131. [CrossRef] [PubMed]
6. Xu, N.; Zhang, F.; Xu, N.; Li, L.; Liu, L. Chemical and mineralogical variability of sediment in a quaternary aquifer from Huaihe River Basin, China: Implications for groundwater arsenic source and its mobilization. *Sci. Total Environ.* **2023**, *865*, 160864. [CrossRef]
7. Yuan, R.; Li, Z.; Guo, S. Health risks of shallow groundwater in the five basins of Shanxi, China: Geographical, geological and human activity roles. *Environ. Pollut.* **2023**, *316*, 120524. [CrossRef]
8. Biswas, T.; Pal, S.C.; Saha, A.; Ruidas, D. Arsenic and fluoride exposure in drinking water caused human health risks in coastal groundwater aquifers. *Environ. Res.* **2023**, *238*, 117257. [CrossRef]
9. McArthur, J.M.; Nath, B.; Banerjee, D.M.; Purohit, R.; Grassinea, N. Palaeosol control on groundwater flow and pollutant distribution: The example of arsenic. *Environ. Sci. Technol.* **2011**, *45*, 1376–1383. [CrossRef]
10. Brikowski, T.H.; Neku, A.; Shrestha, S.D.; Smith, L.S. Hydrologic control of temporal variability in groundwater arsenic on the Ganges floodplain of Nepal. *J. Hydrol.* **2014**, *518*, 342–353. [CrossRef]
11. Wang, J.; Li, Z.; Zhu, Q.; Wang, C.; Tang, X. Review on arsenic environment behaviors in aqueous solution and soil. *Chemosphere* **2023**, *333*, 138869. [CrossRef]
12. Fischel, M.H.H.; Clarke, C.E.; Sparks, D.L. Arsenic sorption and oxidation by natural manganese-oxide-enriched soils: Reaction kinetics respond to varying environmental conditions. *Geoderma* **2024**, *441*, 116715. [CrossRef]
13. Li, C.; Bundschuh, J.; Gao, X.; Li, Y.; Zhang, X.; Luo, W.; Pan, Z. Occurrence and behavior of arsenic in groundwater-aquifer system of irrigated areas. *Sci. Total Environ.* **2022**, *838*, 155991. [CrossRef] [PubMed]
14. Cheng, H.; Hu, Y.; Luo, J.; Xu, B.; Zhao, J. Geochemical processes controlling fate and transport of arsenic in acid mine drainage (AMD) and natural systems. *J. Hazard. Mater.* **2009**, *165*, 13–26. [CrossRef] [PubMed]

15. Duan, Y.; Li, R.; Gan, Y.; Yu, K.; Tong, J.; Zeng, G.; Ke, D.; Wu, W.; Liu, C. Impact of physico-chemical heterogeneity on arsenic sorption and reactive transport underwater extraction. *Environ. Sci. Technol.* **2020**, *54*, 14974–14983. [CrossRef]
16. Duan, Y.; Li, R.; Yu, K.; Zeng, G.; Liu, C. Effects of geochemical and hydrodynamic transiency on desorption and transport of As in heterogeneous systems. *Sci. Total Environ.* **2022**, *835*, 155381. [CrossRef]
17. Zou, Q.; Wei, H.; Chen, Z.; Ye, P.; Zhang, J.; Sun, M.; Huang, L.; Li, J. Soil particle size fractions affect arsenic (As) release and speciation: Insights into dissolved organic matter and functional genes. *J. Hazard. Mater.* **2023**, *443*, 130100. [CrossRef]
18. Aftabtalab, A.; Rinklebe, J.; Shaheen, S.M.; Niazi, N.K.; Moreno-Jiménez, E.; Schaller, J.; Knorr, K.H. Review on the interactions of arsenic, iron (oxy)(hydr) oxides, and dissolved organic matter in soils, sediments, and groundwater in a ternary system. *Chemosphere* **2022**, *286*, 131790. [CrossRef]
19. Cai, X.; Yin, N.; Liu, X.; Wang, P.; Du, H.; Cui, Y.; Hu, Z. Biogeochemical processes of arsenic transformation and redistribution in contaminated soils: Combined effects of iron, sulfur, and organic matter. *Geoderma* **2022**, *422*, 115948. [CrossRef]
20. Lu, S.; Su, X.; Feng, X.; Sun, C. Study on the formation and influencing factors of arsenic in nearshore groundwater during river water infiltration. *Earth Sci. Front.* **2022**, *29*, 455–467. (In Chinese with English abstract)
21. Zhang, D.; Guo, H.; Xiu, W.; Ni, P.; Zheng, H.; Wei, C. In-situ mobilization and transformation of iron oxides-adsorbed arsenate in natural groundwater. *J. Hazard. Mater.* **2017**, *321*, 228–237. [CrossRef]
22. Nath, B.; Berner, Z.; Mallik, S.B.; Chatterjee, D.; Charlet, L.; Stueben, D. Characterization of aquifers conducting groundwaters with low and high arsenic concentrations: A comparative case study from West Bengal, India. *Mineral. Mag.* **2005**, *69*, 841–854. [CrossRef]
23. Fendorf, S.; Michael, H.A.; Van Geen, A. Spatial and temporal variations of groundwater arsenic in South and Southeast Asia. *Science* **2010**, *328*, 1123–1127. [CrossRef] [PubMed]
24. Wenzel, W.W.; Kirchbaumer, N.; Prohaska, T.; Stingeder, G.; Lombi, E.; Adriano, D.C. Arsenic fractionation in soils using an improved sequential extraction procedure. *Anal. Chim. Acta* **2001**, *436*, 309–323. [CrossRef]
25. Shepley, M.G.; Schmidt, N. Utility trench water level recessions in an aquitard: Findings from analytical and numerical analyses. *Hydrogeol. J.* **2022**, *30*, 2495–2507. [CrossRef]
26. Glose, T.J.; Zipper, S.; Hyndman, D.W.; Stingeder, G.; Lombi, E.; Adriano, D.C. Quantifying the impact of lagged hydrological responses on the effectiveness of groundwater conservation. *Water Resour. Res.* **2022**, *58*, e2022WR032295. [CrossRef]
27. Qin, R.; Wu, Y.; Xu, Z.; Xie, D.; Zhang, C. Numerical modeling of contaminant transport in a stratified heterogeneous aquifer with dipping anisotropy. *Hydrogeol. J.* **2013**, *21*, 1235. [CrossRef]
28. Wu, Q.; Zhang, J.; Lin, W.; Wang, G. Dye tracing of soil water flow pattern and evaluation of preferential flow degree. *Trans. Chin. Soc. Agric. Eng.* **2014**, *30*, 82–90. (In Chinese with English abstract)
29. Yan, Y.; Xie, X.; Zheng, W.; Chi, Z.; Liu, Y. Effects of irrigation activities on arsenic migration in surface soil of Datong Basin. *Geol. Sci. Technol. Inf.* **2017**, *36*, 235–241. (In Chinese with English abstract)
30. Li, H.; Ding, S.; Song, W.; Wang, X.; Ding, J.; Lu, J. The degradation of dissolved organic matter in black and odorous water by humic substance-mediated Fe (II)/Fe (III) cycle under redox fluctuation. *J. Environ. Manag.* **2022**, *321*, 115942. [CrossRef]
31. Xu, F.; Li, P. Biogeochemical mechanisms of iron (Fe) and manganese (Mn) in groundwater and soil profiles in the Zhongning section of the Weining Plain (northwest China). *Sci. Total Environ.* **2024**, *939*, 173506. [CrossRef]
32. Zhang, Q.; Wang, X.; Chen, J.; Zhuang, G. Heterogeneous reaction mechanism of SO_2 and Fe_2O_3 to form Fe(II)(aq) and sulfate. *J. Chem. Univ.* **2006**, 1347–1350. (In Chinese with English abstract)
33. Peng, X.; Yang, B.; Li, X.; Dai, X.; Wei, C.; Lu, Z.; Deng, Z.; Li, M.; Fan, G. Dissolution behavior of hematite in H_2SO_4 solution: A kinetic analysis and its importance on the zinc hydrometallurgical hematite process. *Miner. Eng.* **2024**, *215*, 108811. [CrossRef]
34. Zeng, J.; Tabelin, C.B.; Gao, W.; Tang, L.; Luo, X.; Ke, W.; Jiang, J.; Xue, S. Heterogeneous distributions of heavy metals in the soil-groundwater system empowers the knowledge of the pollution migration at a smelting site. *Chem. Eng. J.* **2023**, *454*, 140307. [CrossRef]
35. Yao, Y.; Mi, N.; He, C.; Yin, L.; Zhou, D.; Zhang, Y.; Sun, H.; Yang, S.; Li, S.; He, H. Transport of arsenic loaded by ferric humate colloid in saturated porous media. *Chemosphere* **2020**, *240*, 124987. [CrossRef] [PubMed]
36. An, L.; Liu, M.; Zhang, J.; Huang, L.; Chen, Z. Research progress on the sources of arsenic in soil and factors affecting its migration and release. *Soils* **2020**, *52*, 234–246. (In Chinese with English abstract)
37. Zhang, Y.; Xie, X.; Sun, S.; Wang, Y. Arsenic transformation and redistribution in groundwater induced by the complex geochemical cycling of iron and sulfur. *Sci. Total Environ.* **2023**, *894*, 164941. [CrossRef]
38. Zhong, S.; Yin, G.; He, H.; Huang, R.; Chen, Z.; Lin, Q.; Peng, H.; Wang, K. Stabilization effect and mechanism of different iron minerals on arsenic in paddy soil. *J. Environ. Sci.* **2017**, *37*, 1931–1938. (In Chinese with English abstract)
39. Park, J.H.; Han, Y.S.; Ahn, J.S. Comparison of arsenic co-precipitation and adsorption by iron minerals and the mechanism of arsenic natural attenuation in a mine stream. *Water Res.* **2016**, *106*, 295–303. [CrossRef]
40. Yang, Z.; Zeng, X.; Sun, B.; Su, S.; Wang, Y.; Zhang, N.; Zhang, Y.; Wu, C. Research progress on fixation of soil heavy metals by iron oxides. *Soil Bull.* **2021**, *52*, 728–735. (In Chinese with English abstract)
41. Yao, D.; Shi, Y.; Pan, H.; Zhong, D.; Hou, H.; Wu, X.; Chen, J.; Wang, L.; Hu, Y.; Crittenden, J.C. Promotion mechanism of natural clay colloids in the adsorption of arsenite on iron oxide particles in water. *Chem. Eng. J.* **2020**, *392*, 123637. [CrossRef]
42. Inchaurrondo, N.; Di Luca, C.; Haure, P.; Žerjav, G.; Pintar, A.; Palet, C. Evaluation of low-cost geo-adsorbents for As (V) removal. *Environ. Technol. Innov.* **2021**, *21*, 101341. [CrossRef]

43. Wang, H.; Tsang, Y.F.; Wang, Y.; Sun, Y.; Zhang, D.; Pan, X. Adsorption capacities of poorly crystalline Fe minerals for antimonate and arsenate removal from water: Adsorption properties and effects of environmental and chemical conditions. *Clean Technol. Environ. Policy* **2018**, *20*, 2169–2179. [CrossRef]
44. Zhang, D.; Wu, S.; Wei, Y.; Zhou, L. Schwertmannite modified with ethanol: A simple and feasible method for improving As (III) adsorption capacity. *J. Environ. Chem. Eng.* **2022**, *10*, 107412. [CrossRef]
45. Li, Z.; Peng, S.; Shan, H.; Liao, Q.; Zhou, H.; Zhao, Z. The Influence of Aqueous Iron on River Sand's Arsenic Adsorption: Characteristics and Mechanisms. *Water* **2024**, *16*, 1107. [CrossRef]
46. Du, H.; Shan, H.; Huang, J.; Zeng, C.; Zhang, X.; Liu, Y. Experimental study on the effects of flow velocity and medium particle size on As(III) migration. *Earth Sci.* **2024**, *49*, 1459–1469. (In Chinese with English abstract)
47. Itamiya, H.; Sugita, R.; Sugai, T. Analysis of the surface microtextures and morphologies of beach quartz grains in Japan and implications for provenance research. *Prog. Earth Planet. Sci.* **2019**, *6*, 43. [CrossRef]
48. Ding, K.; Ruan, L.; Wang, H.; Deng, X.; Yang, W.; Jiang, N.; Zhang, J. Research progress on the application of FeOOH in adsorption of water pollutants. *Appl. Chem. Ind.* **2024**, *53*, 894–899. (In Chinese with English abstract)
49. Zhang, Y.; Hou, Z.; Fu, P.; Wang, X.; Xue, T.; Chen, Y. Simultaneous stabilization of arsenic and antimony co-contaminated mining soil by Fe(II) activated-Fenton sludge: Behavior and mechanisms. *Environ. Pollut.* **2023**, *337*, 122538. [CrossRef]
50. Li, J.; Zhan, M.; Zhong, X.; Wang, Y.; Ou, Y.; Zhao, X. Accumulation characteristics and influencing factors of heavy metals in soil-crop systems in typical karst areas of Guangxi. *J. Environ. Sci.* **2021**, *41*, 597–606. (In Chinese with English abstract)
51. Nguyen, K.T.; Navidpour, A.H.; Ahmed, M.B.; Mojiri, A.; Huang, Y.; Zhou, J.L. Adsorption and desorption behavior of arsenite and arsenate at river sediment-water interface. *J. Environ. Manag.* **2022**, *317*, 115497. [CrossRef]
52. Hou, Q.; Zhang, Y.; Yu, K.; Han, D.; Chen, J. Dynamic transformation of soil arsenic binding forms driven by flooding-drying cycles. *Sci. Technol. Eng.* **2023**, *23*, 9728–9736. (In Chinese with English abstract)
53. Chen, H.S.; Sun, Z.Y.; Shao, J.C. Investigation on FT-IR Spectroscopy for Eight Different Sources of SiO_2. *Bull. Chin. Ceram. Soc.* **2011**, *30*, 934–937. (In Chinese with English abstract)
54. Sun, S.Y.; Wen, K.; Yang, B.; Zhou, Q.; Dong, F.; Nie, X.; Liu, L.; Fan, S. The preparation and adsorption properties of novel active carbon/diatomite. *Acta Petrol. Mineral.* **2013**, *32*, 941–946. (In Chinese with English abstract)
55. Wang, Y.; Yu, W.; Chang, Z.; Gao, C.; Yang, Y.; Zhang, B.; Wang, Y.; Xing, B. Effects of dissolved organic matter on the adsorption of norfloxacin on a sandy soil (fraction)from the Yellow River of Northern China. *Sci. Total Environ.* **2022**, *848*, 157495. [CrossRef]
56. Zhang, L.; Song, L.T.; Zheng, X.D.; Teng, Y.; Wang, J. The remobilization of heavy metals influenced by interaction of DOM and iron oxides. *Chin. J. Ecol.* **2014**, *33*, 2193–2198. (In Chinese with English abstract)
57. Adames-Montero, Y.; López-Guerra, S.; Marrero-Águila, R.; Cueli-Corugedo, A.; Davis-Harriett, J. Transformaciones físico-químicas de productos de corrosión el hierro en instalaciones petroleras. *Tecnol. Química* **2020**, *40*, 627–639.
58. Wang, H.M.; Ma, Y.P.; Chen, X.Y.; Xu, S.; Chen, D.; Zhang, L.; Zhao, B.; Ning, P. Promoting effect of SO_4^{2-} functionalization on the performance of Fe_2O_3 catalyst in the selective catalytic reduction of NOx with NH_3. *J. Fuel Chem. Technol.* **2020**, *48*, 584–593. (In Chinese with English abstract) [CrossRef]
59. Zulfikar, M.A.; Utami, A.R.; Handayani, N.; Wahyuningrum, D.; Setiyanto, H.; Azis, M.Y. Removal of phthalate ester compound from PVC plastic samples using magnetic molecularly imprinted polymer on the surface of superparamagnetic Fe_3O_4 (Fe_3O_4@ MIPs). *Environ. Nanotechnol. Monit. Manag.* **2022**, *17*, 100646. [CrossRef]
60. Kefirov, R.; Ivanova, E.; Hadjiivanov, K.; Dzwigaj, S.; Che, M. FTIR characterization of Fe^{3+}–OH groups in Fe–H–BEA zeolite: Interaction with, CO and NO. *Catal. Lett.* **2008**, *125*, 209–214. [CrossRef]

toxics

MDPI

Article

Bioaccumulation of Arsenic, Cadmium, Chromium, Cobalt, Copper, and Zinc in *Uroteuthis edulis* from the East China Sea

Mengqi Li [1], Baihao Zhang [1] and Zhou Fang [1,2,3,4,5,*]

[1] College of Marine Living Resource Sciences and Management, Shanghai Ocean University, Shanghai 201306, China; m220200735@st.shou.edu.cn (M.L.); baihao_zhang@163.com (B.Z.)
[2] National Engineering Research Center for Oceanic Fisheries, Shanghai Ocean University, Shanghai 201306, China
[3] Key Laboratory of Sustainable Exploitation of Oceanic Fisheries Resources, Ministry of Education, Shanghai Ocean University, Shanghai 201306, China
[4] Key Laboratory of Oceanic Fisheries Exploration, Ministry of Agriculture and Rural Affairs, Shanghai 201306, China
[5] Scientific Observation and Experimental Station of Oceanic Fishery Resources, Ministry of Agriculture and Rural Affairs, Shanghai 201306, China
* Correspondence: zfang@shou.edu.cn; Tel.: +86-021-61900166

Abstract: In this study, the concentrations of trace elements (TEs) in *Uroteuthis edulis* caught from the East China Sea were determined. There were significant differences between TE concentrations in different body parts. Cu, Zn, and Cd were the most concentrated in the digestive glands and the concentrations of Cr and Co were highest in the gills. No significant differences in concentrations were shown between these tissues. In the four tissues analyzed, the mantle recorded the highest proportion of elemental load, while the digestive glands and gills had the lowest proportions. After maturity, TEs in the mantle showed no significant differences. In the digestive gland, the concentrations of all elements, except Zn, were significantly increased. The gonads illustrated apparent increases in the concentrations of Cr, Cu, and As. In the gills, the concentrations of Co and As were markedly increased.

Keywords: squids; trace elements; distribution in tissues

1. Introduction

Trace elements (TEs) are defined as metallic elements with a density greater than 5.0 g/cm^3 [1]. From the perspective of environmental pollution, TEs include certain non-metallic elements such as Arsenic (As) and Selenium (Se) [1]. Approximately 45 types of TEs exist in nature. According to the requirements for physiological function, they can be classified into two categories. The first category includes essential elements and micronutrients such as Copper (Cu) and Zinc (Zn), which are usually necessary for physiological functions [2,3]. The deficiency of these elements affects individual growth, but an excessive intake also has adverse effects. The second category includes nonessential elements, such as Cadmium (Cd) and Lead (Pb), which are nonessential for physiological function and have obvious toxicity. They may be transferred to the food chain in various ways and via different media.

Seawater and marine sediments are significant sources of the pollutants that accumulate in marine organisms. Toxic TE pollutants are absorbed from seawater and marine sediments through terrestrial and aerial pathways. TEs accumulate in marine organisms and are then combined with proteins and enzymes to form toxic substances. In addition, TEs can be transferred to organisms at higher nutritional levels and to human beings via the food chain [4,5], thus posing serious threats to marine ecosystems and humans. Above-standard TE pollutants have led to serious public health incidents such as the "Itai-Itai disease" event caused by Cd poisoning in 1931 and the "Minamata disease" event

caused by Hg poisoning in 1956 [6–9]. According to previous studies, Hg, Cd, Pb, and the semi-metallic element As are the main TEs that have serious impacts on marine life and humans. These elements are certified as important indicators for the detection of "limited toxic and harmful substances" in drinking water products [6,10]. Therefore, it is important to investigate the accumulation of TEs in important economic species in the ocean.

The East China Sea (ECS) is located in the south of the estuary of the Yangtze River and the east of Eurasia. As a marginal sea on the western side of the Pacific Ocean, it covers approximately 700,000 square kilometers [11,12]. Its complex ocean current circulation system supports the reproduction of various fish species; hence, it is one of the most important fishing grounds in China [13]. The inshore fishing grounds of ECS are adjacent to developed regions like Shanghai, Jiangsu, Zhejiang, and Fujian. Consequently, the sediments in the region are influenced by both the Yangtze River and human activities [14–16], resulting in high contents of trace elements and severe pollution [15]. However, as one of the most important fishing grounds in China, the ECS is a habitat for many marine organisms and is abundant in nutrients. The pollutants entering the ocean affect the growth and development of marine organisms to a certain degree and ultimately change human health via the food chain.

The squid, *Uroteuthis edulis* (*U. edulis*), is a coastal warm-temperate shallow-water species widely distributed in the northwestern Pacific Ocean and along the eastern coast of Africa [17,18]. In the East China Sea, *U. edulis* is one of the most important economic species; thus, it is important to explore the accumulation of TEs in *U. edulis*. The concentrations of trace elements in fish and shellfish in most seas have been investigated in recent years; however, a similar study on cephalopods in the ECS has seldom been reported [19,20]. A cephalopod is a type of invertebrate with a fast growth rate and a short lifespan and is extremely sensitive to trace element pollutants [21,22]. *U. edulis* prey mainly on crustaceans and small fishes and easily accumulate TEs. *U. edulis* is in the intermediate nutritional level [23], so it is a significant species in food chains. Studies on trace element accumulation have increased in recent years and have mostly focused on food science or environmental aspects. In food science research [24], the concentrations of TEs in the muscular tissues of the target organism were used to assess their edibility. In environmental science research, different cephalopods, including those from Loliginidae across different marine areas, were explored to analyze the effect of location on TE concentrations in the tissues of target organisms [24,25]. *U. edulis* is one of the most important economic species, with an annual catch of 5000~15,000 tons; therefore, understanding the distribution of microelements in *U. edulis* can facilitate effective response to risks and help maintain social stability [21,22]. The concentrations of TEs in the muscular tissues of cephalopods have been measured in most studies; however, other tissues such as gonads and internal organs with significant accumulation of TEs and potential correlation with the enrichment pattern of muscles have not been explored [26,27]. Additionally, the accumulation, transfer, and factors influencing TEs in different tissues of squids from Loliginidae are seldom reported.

This study aims to analyze the distribution of trace elements in different tissues of *U. edulis* and explore the correlation between trace elements in various tissues. This study will provide crucial data and a scientific basis for a better understanding of the enrichment characteristics of TEs in cephalopod species.

2. Materials and Methods

2.1. Sample Collection

Sampling areas were located in the East China Sea (123° E–127.5° E, 28° N–31.5° N). The samples were caught by the trawler "Zhejiang Lingyu 23860" (Figure 1) and about 50 samples were obtained each month. In this study, 289 samples of *U. edulis* were obtained. All the samples were immediately frozen, transported to the laboratory, and stored at −20 °C.

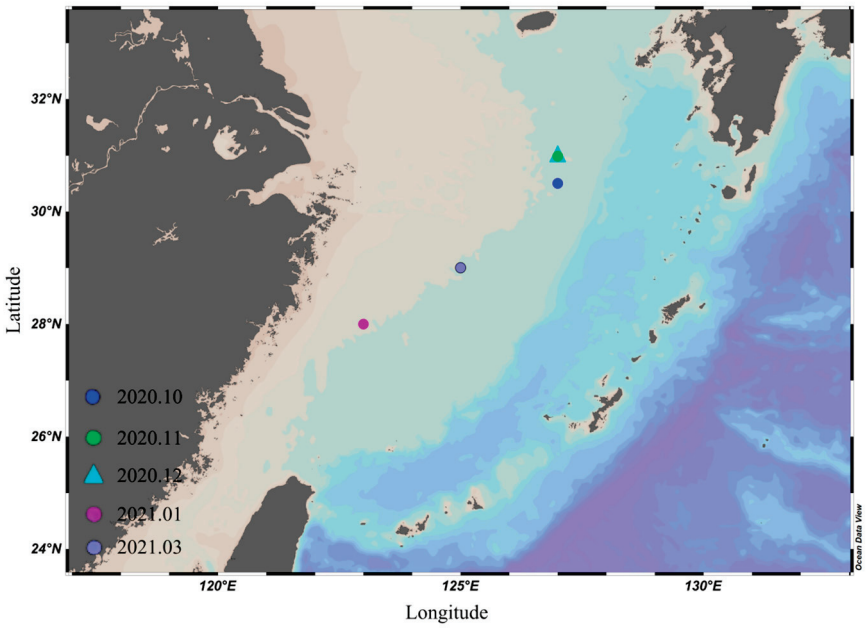

Figure 1. Sampling locations of *Uroteuthis edulis* in the East China Sea. The blue point represents the sampling locations in October 2020; the green point represents the sampling locations in November 2020; the cyan triangle represents the sampling locations in December 2020; the pink point represents the sampling locations in January 2021; the purple point represents the sampling locations in March 2021.

2.2. Sample Processing

The samples of *U. edulis* were thawed at room temperature in the laboratory. All samples were numbered, arranged in the trays, and photographed, and the mantle length and body weight of samples were measured [28]. After the biological data were recorded, the samples were dissected to obtain various tissues including mantle, digestive gland, gonad, and gill. In each month, 8 samples were randomly selected, including 4 mature individuals and 4 immature individuals. After the same treatment, the differences in the contents of trace elements in the tissues of *U. edulis* before and after gonad maturation were analyzed. Finally, the samples were stored in a −20 °C freezer for the subsequent analysis of trace elements [28].

2.3. Materials and Methods

Prior to the formal experiment, the scallop standard (GBW10024) was used to finish the pre-experiment, which was utilized to determine the trace elements. The ratio of HNO3 to H2O2, the heating program, and the duration were adjusted, and the experiment was repeated six times to compare recovery rates. The scheme with the highest recovery rate was ultimately selected for the experimental plan. The recovery rates of the six trace elements were all within the norms of chemical testing methods (Table 1). Unfortunately, due to the limited number of samples, the samples were not available in duplicates or triplicates.

Table 1. Concentration of heavy metals (μg/g) in scallop (GBW10024) obtained in the present study, showing the certified values and the recovery% (mean ± SD, n = 6).

Element	Certified	Determined	Recovery%
As	3.6 ± 0.6	3.35 ± 0.5	93.1
Co	0.047 ± 0.006	0.043 ± 0.12	91.5
Cu	1.34 ± 0.18	1.24 ± 0.09	92.5
Cd	1.06 ± 0.10	1.00 ± 0.03	94.3
Cr	0.28 ± 0.07	0.28 ± 0.1	99.9
Zn	75 ± 3	68 ± 4	90.7

2.3.1. Sample Collection

To reduce the interferences from the external environment and residues in the digestion tube, all containers such as polytetrafluoroethylene beakers and digestion tubes had to be washed with acids and rinsed with ultra-pure water. Firstly, containers were soaked in 20% nitric acid (GR grade) for 72 h; then, they were washed repeatedly with clean water; finally, they were rinsed with ultra-pure water. Afterward, containers were dried at 180 °C in a drying oven for 3 h and then cooled to room temperature for use.

2.3.2. Tissue Pre-Treatment

After the samples of *U. edulis* were thawed at room temperature in the laboratory, an appropriate amount of four different tissue samples were weighed and placed in a cryogenic vial for 72 h freeze-drying at −80 °C. After freeze-drying, the samples were ground with agate mortar and then a portion of samples (0.5 ± 0.0005 g) were weighed in an analytical balance with an accuracy of 0.0001 g.

Before the measurements of the trace elements were conducted, the samples were digested to destroy the organic matters and remove the interfering compounds according to the Chinese National Standard GB5009.268-2016 "Food Safety National Standard Determination of Multi-elements in Food" (GB 5009.268-2016). The HNO_3(65%)-H_2O_2(30%) digestion and microwave solver digestion methods were used.

A high concentration of HNO_3 might damage measurement instruments, so it was necessary to carry out acid-reducing operations. After digestion, all the organic matters were decomposed, but some insoluble substances, such as silicon dioxide, remained, particularly those in the gills. These impurities had to be removed from the solution so as to prevent the blockage of the nebulizer during detection. Subsequently, the samples were filtered through a 25 mm polyvinylidene fluoride (PVDF) 0.22 μm filter membrane, transferred into 2 mL centrifuge tubes, and stored at room temperature for elemental analysis. Detailed information, sample usage, and operation steps are shown in GB 5009.268-2016.

2.3.3. Instrumental Detection of Trace Elements in Tissue Samples

After the pre-treatments, the samples were analyzed with inductivity-coupled plasma–mass spectrometry (ICP-MS) at the trace element detection laboratory of Shanghai Ocean University. The elements analyzed include Chromium (Cr), Cobalt (Co), Copper (Cu), Zinc (Zn), Arsensic (As), and Cadmium (Cd), leading to a total of six elements in this study. Before testing, a proper concentration of the mixed standard solution for multi-element ICP-MS was required to formulate the standard curve. In this study, the concentrations of the standard substance were selected to be 0.01, 0.05, 0.1, 0.5, 1, 2, 5, 10, 50, 100, and 500 ppm. HNO_3 solution (1%) was used as a blank sample.

Based on the comparison of the signal intensity of elements from both the test solution and the standard solution, the contents of the trace elements in the specimens (ppm) were calculated as follows:

$$\text{Heavy mental concentration} = \frac{(C - C_0) \times V}{W \times 1000} \quad (1)$$

where C indicates the concentration of a trace elements in the measured liquid obtained from the standard curve (μg/mL); Co indicates trace elements concentration in the blank detection liquid obtained from the standard curve (μg/mL); V indicates the final volume of the substance (mL) (in this study, it was 25 mL); W indicates the weight of the *U. edulis* sample (g, dry weight) (in this study, it was 0.5 g).

Finally, the outliers in the results were removed and the data analysis was performed.

2.3.4. Data Analysis

The concentrations of Cr, Co, Cu, Zn, As, and Cd in the mantle, digestive glands, gonads, and gills were displayed in box–scatter composite plots. The Shapiro–Wilk test method and variance homogeneity test (F-test) were used to test the data. If both tests

were satisfied, then a one-way ANOVA (one-way analysis of variance) was used to analyze the differences among elements in each tissue and the differences of a single element in different tissues. If the data did not follow a normal distribution or meet the condition of variance homogeneity, the Kruskal–Wallis H method was used to test the data. For the correlational analysis among different elements in each tissue and the individual elements in the different tissues, the Spearman rank correlation coefficient was employed. In order to analyze trace elements concentrations before and after gonad maturation, two sample groups were set. Therefore, if the data did not follow a normal distribution or meet the condition of variance homogeneity, then the Mann–Whitney U-test method was chosen to test the differences in the concentration of each element in various tissues before and after maturity. Data analysis and plotting were performed with R language, Excel 2020, and Origin 2021.

3. Results

3.1. TEs Concentrations

In this study, the mantle length, body weight, and sexual maturity showed significant differences among the samples caught in the same month. Therefore, the box-and-dot composite plot was used to fully depict the distribution differences in trace elements concentrations in the tissue samples of *U. edulis*. The results of Cr, Co, Cu, Zn, As, and Cd in the mantle, digestive gland, gonads, and gills of *U. edulis* are shown in Figure 2.

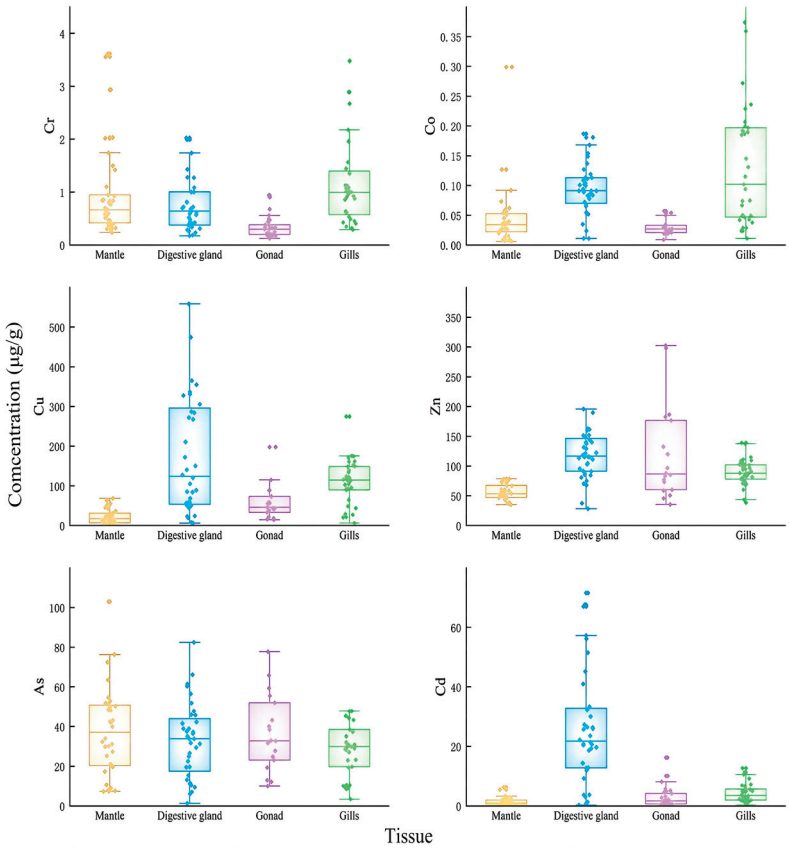

Figure 2. Contents (μg/g (μg/g dry weight)) of selected metals in the tissues of *Uroteuthis edulis*. Yellow represents the mantle; blue represents the digestive gland; purple represents the gonads; green represents gills.

The concentrations of Cu and Zn were significantly higher than those of other elements (Figure 2). The concentration of Cu was the highest and exceeded 600 μg/g in the digestive gland of one sample. The concentration of As was slightly lower than those of Cu and Zn. The concentration of As in four tissues was around 40 μg/g. The concentration of Cd

exceeded 5 μg/g in four tissues and was approximately 20 μg/g in the digestive glands. The concentration of Cr in the four tissues was below 1 μg/g and the concentration of Co was around 0.1 μg/g. The concentrations of Cr and Co were the highest in the gills in comparison with the other tissues. The concentration of As in the four types of tissue was basically the same, except that the concentration of As in the mantle was slightly higher than that in the other tissues.

The results of the Shapiro–Wilk test and the variance homogeneity test (F-test) indicated that the concentrations of the six elements in each tissue did not follow a normal distribution, nor did they meet the condition of variance homogeneity. Therefore, Kruskal–Wallis H test was performed. The distributions of Cr, Co, Cu, Zn, and Cd across the four tissues showed significant differences ($p < 0.05$). The distribution of As across the four tissues showed no significant difference.

3.2. Trace Elements Load Level in Each Tissue and Correlation of Trace Elements Distribution

The proportions of the trace elements' loads in each tissue of *U. edulis* were calculated (Figure 3). TEs were mainly accumulated in the mantle. The loads of Cr, Co, As, and Zn in the mantle accounted for more than 50% of the corresponding total loads and displayed the most significant enrichment, followed by those in the gonads. The proportions of the trace elements' loads in the digestive glands were lower. The loads of Cu and Cd in the digestive glands were higher. Especially, the Cd load in the digestive glands was much higher than that in the other tissues and was significantly higher than the loads of the other elements in the digestive glands. The load proportions of all elements in the gills were the lowest.

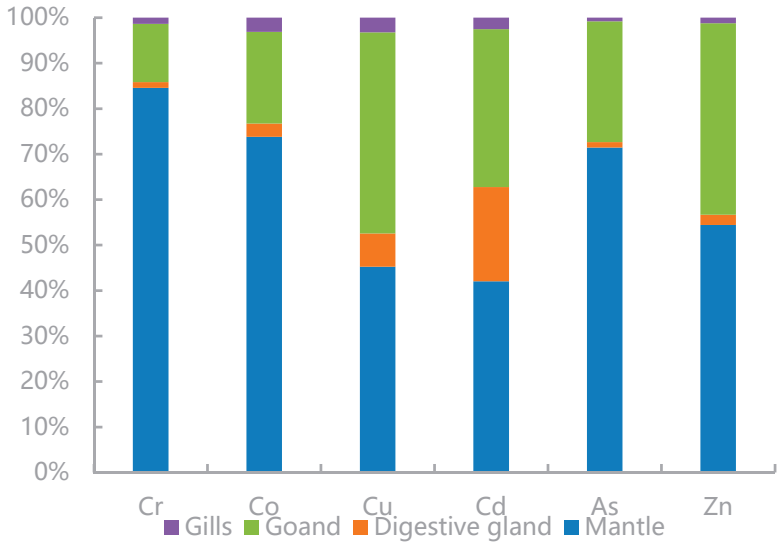

Figure 3. Total body burdens of Cr, Co, Cu, Cd, As, and Zn in the mantle, digestive gland, gonads, and gills of *Uroteuthis edulis*.

A correlation coefficient between 0.3 and 0.5 indicates a weak correlation. A correlation coefficient between 0.5 and 0.8 indicates a moderate correlation; a correlation coefficient above 0.8 indicates a strong correlation. The absolute values of the correlation coefficients of Cr in the four tissues were all less than 0.3, indicating that the concentrations of Cr in the four tissues had no correlation. The correlation coefficient of Co in the digestive gland and gills was 0.459, which indicated a moderate correlation. The correlation coefficients of Cu among different tissues (mantle and gonads; mantle and gills; digestive gland and gills; gonads and gills) were, respectively, 0.381, 0.623, 0.531, and 0.388, which were all positive correlations. Cd only showed a medium correlation between mantle and gills, and the correlation coefficient was 0.566. The distribution of As in various tissues was quite uniform and remains stable (Table 2). The distribution of As in the four tissues showed moderate positive correlations.

Table 2. Trace element correlations among the tissues of *Uroteuthis edulis*.

Elements	Correlations
Cr	-
Co	+D and Gi ^{**b}
Cu	+M and Go ^{*c} +M and Gi ^{***b} +D and Gi ^{***b} +Go and Gi ^{*c}
Zn	+D and Gi ^{***b}
As	+M and D ^{***b} +M and Go ^{**b} +M and Gi ^{***b} +D and Go ^{**b} +D and Gi ^{***b} +Go and Gi ^{**b}
Cd	+M and Gi ^{***b}

Notes: "+" denotes a positive correlation; *: $p < 0.05$; **: $p < 0.01$; ***: $p < 0.001$; M: mantle; D: digestive gland; Go: gonads; Gi: gills; ^{b}: middle correlation; ^{c}: weak correlation.

Through Spearman's correlation analysis, we found correlations between the concentrations of different elements in the same tissue (Figure 4). In the mantle, with the exception where Cr showed no correlation with Cu, Zn, As, or Cd, the elements showed positive correlations with each other. In addition, Co showed a strong correlation with Cu and Cd; Cu also had a strong correlation with Cd. Their correlation coefficients were all above 0.8. In the digestive gland, strong positive correlations were found among the following TEs: Co and Zn; Co and As; Co and Cd; Cr and Zn. But the correlations among the other elements were not significant. The correlations of all the elements in the gonads and gills were not strong. In the gonads, Cu showed a significant positive correlation with Co and Cd. In the gills, significantly positive correlations were found among the following TEs (Cr and Co; Cu and As; Cu and Cd). The possibility that the correlations between the elements suggests that they have a common origin has not been confirmed.

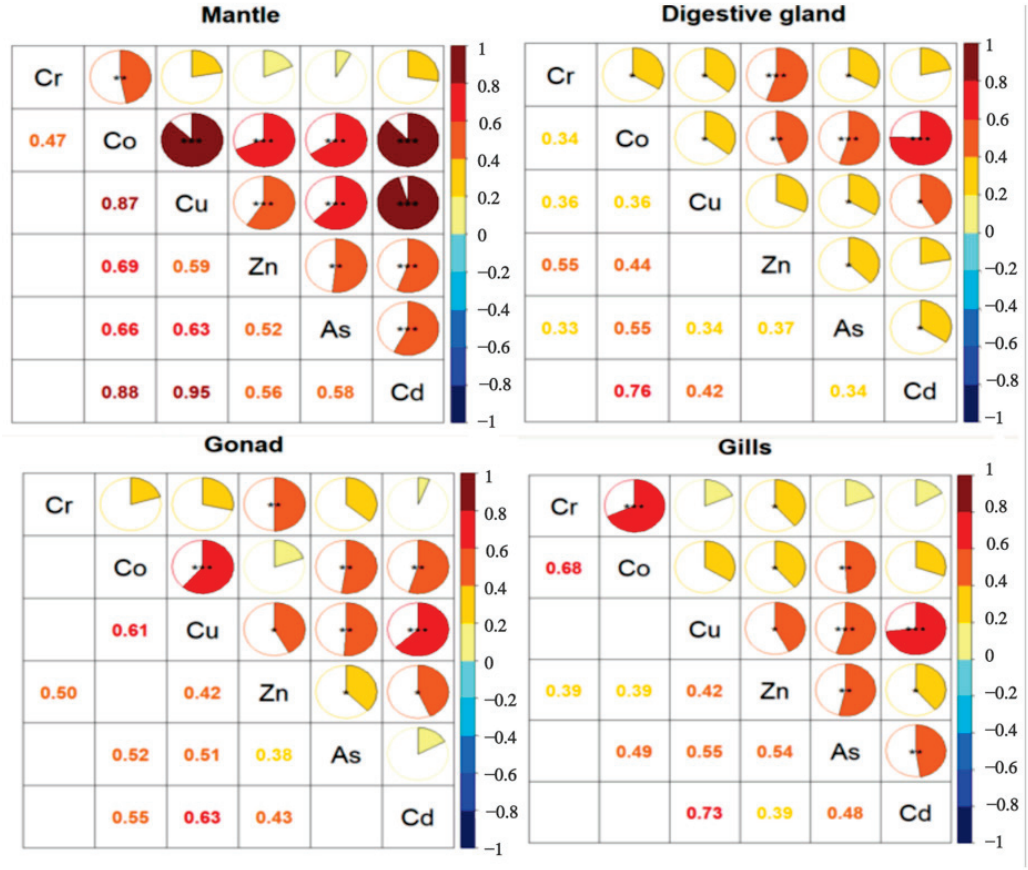

Figure 4. Correlation analysis of TEs concentration in various tissues of *Uroteuthis edulis*. Notes: *: $p < 0.05$; **: $p < 0.01$; ***: $p < 0.001$.

3.3. Transfer Characteristics and Influencing Factors of Trace Elements in U. edulis

The concentrations of Cr in all four tissues except the mantle slightly decreased after maturity. The concentration of Co stayed almost constant in the mantle and the gonads and decreased in the digestive glands and the gills. The concentrations of Cu in the four tissues decreased after maturity. The decrease was the smallest in the mantle and gills and more significant in the digestive glands. Similarly, the concentration of Zn significantly decreased in the digestive glands, remained stable in the mantle and gonads, and decreased in the gills. The concentrations of As in all tissues decreased after maturity. The concentrations of As in both the digestive glands and the gonads greatly decreased. The concentration of Cd was the highest in the digestive glands in comparison with the other tissues and decreased after maturity.

The Shapiro–Wilk test and variance homogeneity test (F-test), carried out to determine the concentrations of the trace elements in various tissues of *U. edulis*, indicated that the concentrations of the six elements in the tissues did not follow a normal distribution, nor did they meet the condition of variance homogeneity. Additionally, for the two sample groups (immature and mature gonads), the Mann–Whitney U test was performed to test the differences (Table 3). In the mantle muscle, the concentrations of all the elements showed no significant differences after maturity ($p > 0.05$). However, in the digestive glands, all the elements except Zn showed no significant difference ($p < 0.05$). The correlations of the concentrations of all the elements in the gonads were rather complex. The concentrations of Cr, Cu, and As showed significant differences, but the concentrations of Co, Zn, or Cd showed no significant difference. In gills, the concentrations of Co and As showed significant differences, whereas the concentration of Cr, Cu, Zn, or Cd showed no significant difference.

Table 3. Mann–Whitney U test of trace elements concentrations in mature and immature *Uroteuthis edulis*.

Groups	Tissues	Cr	Co	Cu	Zn	As	Cd
Mature	mantle	0.51 (0.38~1.50)	0.03 (0.02~0.04)	20.82 (8.25~27.16)	52.69 (45.31~61.78)	35.58 (22.95~48.34)	0.93 (0.40~1.29)
Immature		0.76 (0.49~0.90)	0.04 (0.02~0.06)	16.58 (7.13~33.87)	53.41 (46.86~66.46)	36.83 (20.39~52.29)	0.93 (0.47~2.17)
Z		−0.371	−0.591	−0.644	−0.124	−0.237	−0.241
p		0.725	0.569	0.534	0.915	0.827	0.825
Mature	digestive gland	0.91 (0.67~1.32)	0.1 (0.09~0.13)	209.08 (111.48~297.3)	136.03 (94.54~153.90)	38.31 (33.9~50.95)	29.13 (18.40~46.77)
Immature		0.44 (0.28~0.69)	0.08 (0.05~0.11)	68.67 (34.36~258.41)	115.15 (77.97~133.51)	19.67 (10.8~40.3)	19.72 (12.31~26.43)
Z		−3.199	−2.326	−2.102	−1.749	−2.904	−2.045
p		0.001	0.019	0.036	0.083	0.003	0.049
Mature	gonads	0.34 (0.30~0.47)	0.03 (0.02~0.03)	46.69 (43.59~88.75)	85.46 (73.35~186.43)	40.12 (32.28~59.37)	1.76 (0.46~2.73)
Immature		0.21 (0.18~0.32)	0.02 (0.02~0.03)	35.55 (18.03~71.71)	90.34 (59.69~131.06)	23.95 (11.32~32.85)	1.45 (0.64~4.25)
Z		−2.700	−1.102	−2.069	−1.115	−3.413	−0.084
p		0.006	0.283	0.047	0.285	0.000	0.948
Mature	gills	1.18 (0.82~1.57)	0.14 (0.07~0.21)	112.88 (94.30~123.70)	97.98 (82.32~103.36)	34.73(29.69~46.02)	4.1 (2.58~5.21)
Immature		0.96 (0.47~1.10)	0.05 (0.03~0.19)	113.64 (36.51~149.25)	85.69 (71.97~94.47)	28.26 (10.28~31.61)	2.66 (1.92~6.76)
Z		−0.976	−2.320	−0.973	−1.550	−2.451	−0.541
p		0.345	0.020	0.345	0.127	0.013	0.606

In this paper, the transfer of trace elements in the gonads of *U. edulis* is mainly to verify the transfer efficiency of trace elements to offspring and their potential impact, which still requires further research in the future.

4. Discussion

4.1. Arsenic

Arsenic enrichment is unique. Arsenic is a nonessential element in human beings [29,30]. However, in aquatic species, Arsenic is a component of arsenobetaine, which has a similar structure to trimethylglycine and allows an organism to remain unaffected by changes in water salinity. As a result, Arsenic is a vital nutrient for the majority of aquatic species [30–34]. Arsenic is a component of arsenobetaine; therefore, it is essential in all tissues of *U. edulis*. As a result, the distribution of As in the tissues of *U. edulis* demonstrated that the As concentrations in four tissues was similar and showed no significant difference among the different tissues. In addition, the distribution of As was related to the size and growth state of *U. edulis*. In this experiment, the distribution of As in all tissue samples followed a normal distribution, as reported by other experts [30]. The correlation analysis of As concentration in various tissues revealed strong correlations of As concentrations in different tissues. The concentration of As in tissues showed no significant difference and its load proportion in four tissues was almost equal to the proportion of wet weights of four tissues. However, due to the large mass of torso, its proportion was much higher. The correlations between As and other elements were weak and the correlation between Co and Cu in mantle was strong. Arsenic showed a specific maternal transmission pattern [30]. According to the variations in As concentrations in all tissues after the maturity of the gonads of *U. edulis*, the concentrations of As in four tissues decreased. With the exception of the mantle, the other three tissues showed considerable changes in the concentration of As during gonadal maturation. As a result, it was difficult to determine whether it could be transferred with the parent material after maturity.

The concentration of As in *U. edulis* in this study was higher than that in previous studies and close to that which has been found for other cephalopods in the East China Sea [34], such as *Sepia longipes*. It was much higher than that in giant marine cephalopods like *S. pteropus* and benthic octopuses like *O. hubbsorum* due to the sampling locations of *U. edulis*.

4.2. Chromium

The concentrations of Cr in the muscle, digestive gland, gonads, and gills were 1.11 ± 1.18 μg/g, 0.89 ± 0.70 μg/g, 0.34 ± 0.21 μg/g, and 1.44 ± 1.42 μg/g, respectively. In the previous study (Koyama et al., 2000), the gills were identified as the primary concentration tissue of TEs, as confirmed by the variance in Cr concentrations found in this experiment. The concentration of Cr in *U. edulis* in this study was significantly lower than that which has been found in some oceanic species (Table 4), such as *Sthenoteuthis pteropus* (Lischka et al., 2018), *Loligo sanpaulensis* [28], and *Nototodarus gouldi* [29]. The concentration of Cr *U. edulis* was slightly higher than that in octopuses and some oceanic species due to the differences in the distribution areas of the species. For example, *S. pteropus* was widely found in the marginal zone of Cape Verde [30], where subtropical circulation and recirculation intersected. The marine conditions in this area made it easier for nutrients in water to bind to Cd. Similarly, *N. gouldi* accumulated around upwind flow areas in southeast Australia. Ocean currents transported Cr from adjacent seas to their habitat and a large quantity of Cr accumulated in their bodies. The concentration of Cr was the highest in gills, although the proportion of Cr load in gills was negligible in terms of trace elements load in the four tissues. The proportion of Cr load in mantle was the highest among the four tissues and exceeded 80%, whereas that in gills and digestive glands was less than 5%. The difference was related to tissue mass. The higher the mass was, the larger the proportion of TEs load was. In this investigation, the concentrations of Cr in gonads and digestive glands decreased dramatically after maturity, indicating that Cr could be passed to offspring from mother. Le also discovered that Cr in squid juveniles was primarily derived from the maternal source [31]. The results demonstrated the significant correlation between Cr and Zn in digestive glands, as well as the significant correlation between Cr and Co in gills. Many studies suggested that Co was largely absorbed and stored via gills in seawater [31,32].

Table 4. Concentration of TEs (μg/g) of cephalopods.

Species	Tissues	Cr	Co	Cu	Zn	As	Cd	Location	Reference
Uroteuthis edulis	Mantle	1.11 ± 1.18	0.05 ± 0.05	37.01 ± 72.74	58.45 ± 19.05	36.99 ± 20.78	2.51 ± 5.54	East China Sea	This paper
	Digestive gland	0.89 ± 0.7	0.12 ± 0.17	295.78 ± 677.7	142.81 ± 154.21	43.37 ± 65.12	35.7 ± 59.63		
	Gonads	0.34 ± 0.21	0.03 ± 0.01	64.28 ± 56.77	120.8 ± 86.83	31.81 ± 17.57	2.98 ± 3.46		
	Gills	1.44 ± 1.42	0.15 ± 0.13	109.91 ± 55.04	89.07 ± 21.28	28.78 ± 12.75	4.44 ± 3.00		
Todarodes pacificus	Digestive gland	-	-	858	160	27	80.3		
Sepia longipes	Digestive gland	-	-	48	320	113	34.3		[29]
Sepia madokai	Digestive gland	0.60	-	1870	480	99	110.8		
Ommastrephes pteropus	Digestive gland	1.75 ± 2.13	19.9 ± 15.4	152.00 ± 206.0	187.00 ± 111.00	18.30 ± 11.70	748.00 ± 279.00	Eastern Tropical Atlantic	[25]
Moroteuthopsis ingens	Mantle (male)	0.13 ± 0.06	0.07 ± 0.04	11.79 ± 7.46	69.16 ± 15.05	12.48 ± 2.58	0.99 ± 0.75	Chatham Rise	[30]
	Digestive gland (male)	0.12 ± 0.03	0.17 ± 0.11	28.38 ± 34.92	42.65 ± 12.25	12.59 ± 2.03	116.00 ± 267.00		
	Mantle (female)	0.15 ± 0.13	0.06 ± 0.02	8.37 ± 4.05	66.88 ± 12.30	13.66 ± 3.40	0.57 ± 0.51		
	Digestive gland (female)	0.11 ± 0.03	0.15 ± 0.13	29.84 ± 63.76	44.55 ± 26.80	11.10 ± 1.71	52.90 ± 103		
Nototodarus gouldi	Mantle	0.26 ± 0.13	0.50 ± 0.65	25.4 ± 18.3	64.2 ± 8.89	29.9 ± 17.7	0.81 ± 0.51	New Zealand waters	[30]
	Digestive gland	5.00	1.99 ± 1.31	1185 ± 1008	351 ± 307	29.4 ± 14.3	194 ± 214		
Nototodarus sloanii	Mantle	0.32 ± 0.36	0.36 ± 0.56	23.3 ± 18	55.4 ± 11.8	11.9 ± 9.54	0.65 ± 0.46		
	Digestive gland	0.35 ± 0.26	0.89 ± 0.87	352 ± 581	77.7 ± 68.6	11.3 ± 5.08	89.3 ± 86.3		
Gonatus fabricii	Mantle (male)	0.28	0.03	18.80	54.00	26.30	-	Disko Island	[30]
	Digestive gland (male)	0.12	0.12	138.00	56.50	10.25	31.79		
	Mantle (female)	0.32	0.04	26.30	90.60	22.31	-		
	Digestive gland (female)	0.10	0.17	124.00	74.00	10.18	31.57		
	Mantle (young)	0.99	0.06	11.50	91.70	6.06	-		
	Digestive gland (young)	1.68	0.29	14.10	136.00	6.68	41.60		
Uroteuthis sibogae	Mantle	-	-	-	-	1.10 ± 0.43	0.187 ± 0.30	Manaar Bay	[32]
	Digestive gland	-	-	-	-	2.66 ± 1.56	7.33 ± 9.00		
	Gills	-	-	-	-	2.02 ± 0.80	0.754 ± 0.80		
Sepia pharaonis	Mantle	-	-	-	-	9.19 ± 10.6	0.055 ± 0.03		
	Digestive gland	-	-	-	-	8.02 ± 6.61	69.9 ± 30.8		
	Gills	-	-	-	-	7.17 ± 4.93	0.295 ± 0.19		

Table 4. *Cont.*

Species	Tissues	Cr	Co	Cu	Zn	As	Cd	Location	Reference
Octopus hubbsorum	Mantle	<0.12	<0.15	25	58	37	<0.13	Santa Rosalia	[34]
	Digestive gland	0.24	50	3296	877	43	76.00		
	Gills	0.28	2.20	136	87	33	0.70		
	Mantle	<0.12	<0.15	20	64	65	<0.13	La Paz	
	Digestive gland	0.49	6.00	2104	802	46	53.00		
	Gills	0.24	0.2	130	80	47	0.40		
Sepia officinalis	Mantle	-	-	0.115 ± 0.03	15.409 ± 3.9	-	0.153 ± 0.019	Gabes Bay, Gilbert Island	[35]
	Digestive gland	-	-	3.538 ± 0.7	2.7 ± 0.5	-	0.043 ± 0.02		
	Gonads	-	-	0.732 ± 0.2	10.724 ± 1.9	-	0.101 ± 0.04		
	Gills	-	-	3.041 ± 0.7	1.04 ± 0.2	-	0.032 ± 0.01		
	Mantle	-	-	0.45 ± 0.03	20.814 ± 7.6	-	0.185 ± 0.06	Gabes Bay, Gargour	
	Digestive gland	-	-	12.144 ± 2.4	4.397 ± 1.1	-	-		
	Gonads	-	-	0.82 ± 0.5	27.048 ± 7.3	-	0.272 ± 0.04		
	Gills	-	-	2.06 ± 0.63	1.646 ± 0.4	-	0.091 ± 0.02		

4.3. Cobalt

The concentration of Co was the lowest among the six elements detected in this experiment. Among the four tissues, the gills contained the highest concentration of Co, at 0.15 ± 0.013 μg/g. The concentration of Co in the digestive glands was 0.12 ± 0.17 μg/g. The concentrations of Co in the mantle and gonads were relatively low, at only 0.05 ± 0.05 μg/g and 0.03 ± 0.01 μg/g, respectively. The gills were found to be the primary Co enrichment tissue due to their direct interaction with seawater, containing Copper. Bustamante discovered that the concentration of Co in the tissues directly in contact with Co-rich seawater significantly decreased after 6 days of contact with purified seawater [33], further demonstrating that squids interacted with Co through a mechanism involving seawater, and that the digestive gland was the primary organ of Co uptake. Due to potent retention capacity of this organ, the Co concentration in the digestive glands was found to be relatively high. Additionally, the digestive gland in adult squids was responsible for 91% to 95% of the total Co load in the body [33]. The findings of previous studies were significantly different from the findings in the present study because various species have differently sized digestive glands.

The concentration of Co in *U. edulis* was comparable to that in *Gonatus fabricii* and *Moroteuthopsis ingens* [30], but significantly lower than that in the pelagic cephalopods *S. pteropus* and Nototodarus sloanii [25,30]. The highest concentration of Co in the digestive gland of the benthic cephalopod *Octopus hubbsorum* reached 50 μg/g [34], which was significantly higher than the results in this experiment. In the sampling process of the above study, the *O. hubbsorum* was obtained in seriously polluted areas. As a benthic organism, *O. hubbsorum* was influenced not only by crustaceans and shellfish, with a strong TE-accumulation capacity, but also by Co pollutants in sediments; thus, the body contained an abnormally high concentration of Co. In other words, cephalopods are potentially at a risk of accumulating and absorbing Co through sediment.

Co showed a significant correlation with several elements (Cu, Cd, Cr, Zn, and As) in various tissues, particularly in the mantle. Co exhibited a high correlation with Cd in the digestive glands. The correlation might be ascribed to the relationship between Co and metallothionein [31]. Similar to Cu, Zn, and Cd, Co also induced metallothionein. As a result, in the mantle, a protein-rich tissue, Co was correlated strongly with some metals such as Cu, Zn, and Cd, which triggered metallothionein. This correlation could also be interpreted by the Co accumulation function of digestive glands. The digestive glands were found to contain a high concentration of metallothionein; Co can bind to metallothionein to perform its detoxifying function. Therefore, the concentration of Co in the digestive glands was found to be much higher than that in other tissues.

4.4. Copper

Cu, one of the most significant necessary elements in cephalopods, is abundant in all tissues. This is especially the case in the digestive glands, where the concentration of Cu was the highest. The concentrations of Cu in the tissues of different cephalopod species in different seas varied substantially. In this study, the Cu concentration in the digestive glands was 295.78 ± 677.72 μg/g, but the concentration of Cu in the digestive glands of squids found in the Gulf of Gabes, Tunisia, was only 3.538 ± 0.7 μg/g [35]. The concentration of Cu in the digestive glands of *O. hubbsorum* found in the Santa Rosalia region was the highest and reached 3296 μg/g [34]. As a result, regional pollutants and species' habits have a significant impact on Cu concentration. Cu, as a component of hemocyanin, is a vital element for cephalopods. The digestive gland, as a digestive organ of cephalopods, also processes aged hemocytes. The hemocytes of cephalopods finally converge and are broken down in the digestive gland, thus resulting in a large quantity of Cu. Therefore, the determined concentration of Cu in the digestive gland was exceptionally high. The concentration of Cu in the gills was close to that in the digestive glands because they were both tissues (organs) through which a huge number of hemocytes passed.

The concentration of Cu in gills was significantly positively correlated with that in the digestive glands.

In addition, only two Cu-containing proteins are involved in the transfer of nutrients from the carcass to the gonads: hemocyanin and metalloproteins. During the development phase of the gonads, the mantle delivers most of the nutrients to the gonads, but the concentration of Cu in the nutrients was found to be low. Therefore, the correlation between the mantle and the gonads was not significant.

Compared to the Cu accumulation exhibited by cephalopods in other seas, the concentration of Cu in the digestive glands of *U. edulis* in this study was higher; however, it was found to be lower than that in the benthic cephalopod, *O. hubbsorum*, in dense industrial areas, and *N. gouldi* in New Zealand waters. Compared to the findings of TEs accumulation in other cephalopods, the concentration of Cu in the digestive glands in this study was the highest due to the features of *U. edulis*. The mass proportion of the digestive gland in *U. edulis* was substantially less than that of other cephalopods. The correlation analysis of Cu and other elements in the four tissues revealed a strong correlation between Cu and Cd due to metallothionein features. Cu caused metallothionein to participate in Cd detoxification, thus resulting in a positive correlation.

4.5. Cadmium

In this study, Cd is the only nonessential element for aquatic organisms. Cephalopods feed on crustaceans and shellfish, both of which can enrich a large quantity of Cd, so the concentration of Cd in cephalopods was high. The concentration of Cd in the digestive glands of *U. edulis* was the highest (35.7 can c μg/g). The concentrations of Cd in the other tissues were similar. In related studies, the concentration of Cd in digestive glands was the highest regardless of the species or environmental conditions of the habitat. Cephalopods interacted with Cd mainly through ingestion. As a result, the concentration of Cd was directly related to the ingestion structure of cephalopods, changes in ingestion behaviors, and amounts of Cd in the habitat.

In comparison to previous studies, the Cd concentration in this study was lower than that of cephalopods in the East China Sea such as *Todarodes pacificus* and *Sepia madokai*, but higher than that of Gonatopsisborealis. The concentration of TEs in digestive glands was lower than in that in other seawater samples and the highest values were found in digestive glands of S. pteropus in the tropical eastern Atlantic. The concentrations of Cd in benthic cephalopods (*O. hubbsorum*) were higher than those in non-benthic cephalopods (*Sepia officinalis* and Gonatopsisborealis) because benthic cephalopods fed on more crustaceans and bivalves than non-benthic cephalopods. In addition, Cd adsorbed via different pathways had different retention durations in various tissues. Cd that was encountered via seawater had a biological half-life of around two months and TEs accumulated through foods had a half-life in tissues of several years.

Cd had a significant correlation with Cu and Co, particularly in the mantle. Cd had a moderate correlation with Zn. In previous studies, the correlations with the three elements were ascribed to metallothionein induction. However, Charles demonstrated that Zn was significantly correlated with Cd because Zn could more easily engage in the metallothionein reaction [31]. This viewpoint was contradictory with the correlation analysis results in this study. Cd load in four tissues was unique. The concentration of Cd in digestive glands was 5–15 times higher than in that in other tissues. Even though the mass fraction of a digestive gland was low, Cd load remained relatively high and reached approximately 20%. Cd load in the digestive gland of *Sthenoteuthis oualaniensis* was 72.18 ± 6.47% and Cd load in the digestive gland of *Nautilus macromphalus* in New Caledonia might reach 90%. The above results were significantly different from our study due to the differences in the mass of the digestive glands between various mollusk species.

4.6. Zinc

Both Cu and Zn are vital elements that are required during the growth process, so the concentration of Zn is higher than that of the other four elements. Different from Cu, Zn is most concentrated in the digestive glands and exists in the gonads (Figure 2). Zn is closely related to hemocyanin, which is abundant in the digestive glands, but the content of hemocyanin in the gonads is much lower, resulting in a significant difference between the two tissues. In comparison to previous studies on cephalopods in other oceans, the concentration of Zn in this study was in the medium–high level. The concentration of Zn in the digestive glands of *U. edulis* in the study was much lower than that in the benthic octopus due to the feeding patterns of benthic creatures. The concentration of Zinc in the gonads was much higher than that in other studies. Zn load in the gonads of *U. edulis* was only slightly lower than that in the mantle, indicating that the high concentration of Zn in the gonads was related to the proportion of nutrition transfer in different cephalopods.

4.7. Transfer Characteristics of TEs after Maturity

The mariculture conditions of *U. edulis* are not possible to study in the laboratory, so it was impossible to investigate the transfer characteristics of TEs in *U. edulis* with isotope tracing technology. As a result, the only feasible choice was to choose the samples of *U. edulis* in different life cycle stages and investigate the variations in TEs concentrations in various tissues. The Mann–Whitney U test was performed to investigate the factors that exhibited substantial differences in various tissues between mature and immature individuals (Figure 5).

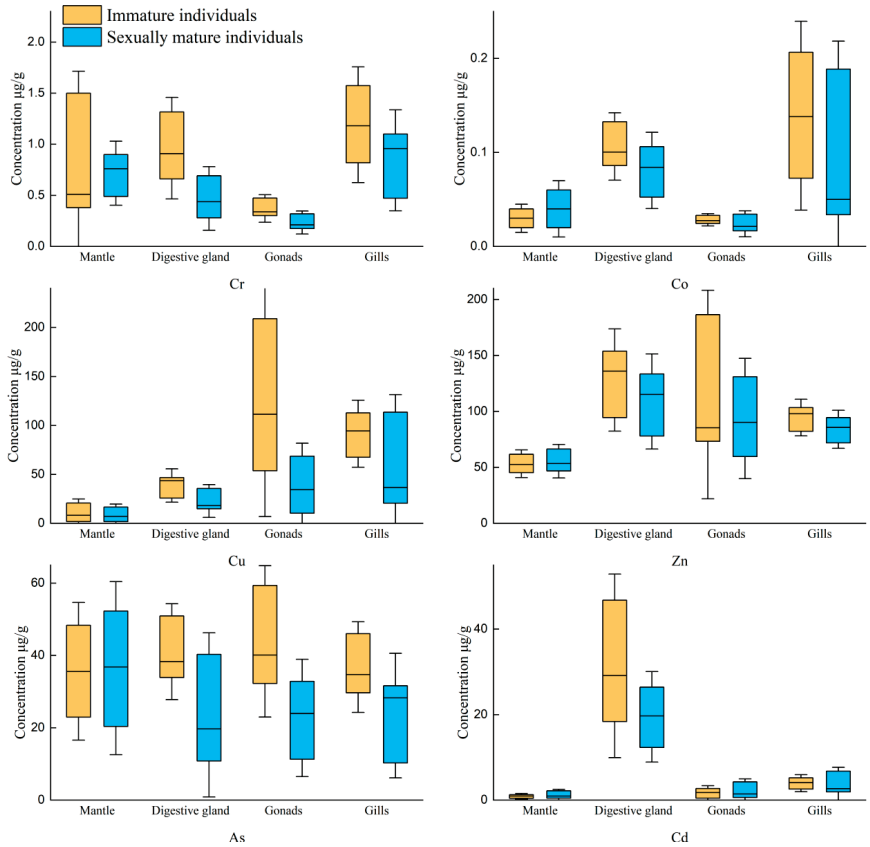

Figure 5. Comparison of the concentration changes of six TEs elements in various tissues of squid before and after gonadal maturation.

Unexpectedly, the concentrations of various elements in the mantle showed no significant difference after gonadal maturity. As the tissue with the highest proportion of TEs load, the mantle should receive the most nutrients given by the muscles, thus resulting in a

significant reduction in TEs. In *U. edulis*, more nutrients were externally obtained and the decrease in the concentrations of TEs in mantle was insignificant. In addition, the muscle mass was quite high. Even if more nutrients were transferred from muscle to gonads, the decreases in the concentrations of TEs were not significant. Furthermore, among various TEs, only As had the highest concentration in the mantle. The other elements had only slight concentrations in the mantle. As a result, the overall loss of TEs during transfer was reduced, and the decreased concentrations were too small to be detected by our instruments. Therefore, the decreases in the concentrations were insignificant.

In the digestive glands, the changes in the concentrations of TEs, with the exception of Zn, were found to be significantly increased due to the increase in the intake and the trophic level during the ingestion process of the nutrients. As the intake increased, the exposure to TEs also increased, and more nutrients were transferred to the gonads. TEs were more enriched in the digestive glands. Therefore, the concentrations of Cr, Co, Cu, As, and Cd were significantly increased. In the gonads, the concentrations of Cr, Cu, and As were significantly increased after gonadal maturity. The essential elements for *U. edulis* were closely related to growth and development, so these elements showed higher accumulation. Although Zn is an essential element, its concentration did not change significantly after gonadal maturity. This phenomenon requires further analysis and research. Some scholars have hypothesized that Cr and As are maternally transferred. The present study theoretically supports this view because TEs could be transferred from other tissues to the gonads. Isotope tracing techniques are recommended in subsequent studies.

Co and As concentrations in the gills showed significant differences between mature and immature individuals and significantly increased after gonadal maturity. It was verified that Co was enriched by the gills, so its concentration significantly increased during the ingestion process. The main accumulation pathways of As in cephalopods included seawater, so the concentration of As increased after gonadal maturity, similar to the concentration of Co.

Cephalopods cannot be cultured or continuously observed. Therefore, we only assessed the concentrations of TEs in the samples from different life cycle stages and then predicted TEs transfer features based on the comparison. In addition, some cultivable species can also be used to create a toxicological model to investigate the transfer properties of different tissues. In the future, we will explore the enrichment of TEs in *U. edulis* from prey after gonadal development and investigate the role of ingestion in the changes in TEs concentrations.

5. Conclusions

This study focuses on *U. edulis* in the East China Sea and aims to investigate TEs accumulation characteristics and influencing factors. The distribution, inter-element, and inter-tissue correlations of Cr, Co, Cu, Zn, As, and Cd in the mantle, the digestive glands, the gonads, and the gills were investigated. TEs accumulation characteristics, transfer characteristics, and influencing factors in the tissues of *U. edulis* in the East China Sea were determined. The key findings of this paper are summarized here.

The distribution of TEs in the tissues of *U. edulis* showed considerable heterogeneity. The digestive glands contained the highest concentrations of Cu, Zn, and Cd; thus, it was confirmed that the three metals accumulated mostly through consumption. The concentrations of Cr and Co were the highest in the gills, indicating that they mostly accumulated through the seawater. The concentration of As showed no significant difference among tissues. The TEs load was the highest in the mantle, followed by the gonads, whereas TEs loads in the digestive glands and gills were the lowest.

Some TEs found in the tissues of *U. edulis* differed significantly between mature and immature individuals. After sexual maturity, TEs in mantle decreased slightly. The concentrations of TEs except Zn in digestive glands increased dramatically. After maturity, gonads showed significant increases in the concentrations of Cr, Cu, and As. The concentrations of Co and As in gills increased significantly after maturity. Considerable specific components

were transported from digestive glands and gills to gonads after maturity. In this study, we investigated the distribution of six trace elements in *U. edulis* samples and assessed their transfer before and after gonadal maturation, providing basic data for food health risk assessment, which is beneficial for social stability. In the future, more species should be subjected to long-term monitoring.

Author Contributions: M.L.: Writing—Original Draft Preparation, Data curation, Formal analysis, Visualization, Investigation, and Validation; Z.F.: Resources, Supervision, Writing—Review and Editing, Funding acquisition, and Project administration; B.Z.: Conceptualization and Methodology. All authors have read and agreed to the published version of the manuscript.

Funding: This work was funded by the National Key R&D Program of China (2019YFD0901404), National Nature Foundation of China (NSFC41876141), and Funding for the Opening of Key Laboratories for Offshore Fishery Development by the Ministry of Agriculture (LOF 2021-01).

Institutional Review Board Statement: No applicable.

Informed Consent Statement: No applicable.

Data Availability Statement: The data presented in this study are available on request from the corresponding author due to data disclosure is at the discretion of the author of the communication.

Acknowledgments: Thanks to my mentor' guidance on this article. And thanks to the reviewers for their constructive comments of this manuscript.

Conflicts of Interest: The authors declare no conflicts of interest.

References

1. Krishna, A.; Mohan, K.; Murthy, N. Assessment of Heavy Metal Contamination in Sediments using Multivariate Statistical Techniques in an Abandoned Mining Site: A Case Study from Kolar Gold Fields Area, Karnataka, India. *Int. J. Earth Sci. Eng.* **2011**, *4*, 1052–1058. Available online: https://www.researchgate.net/publication/233782312 (accessed on 2 April 2024).
2. Bai, Z.; Wu, F.; He, Y.; Han, Z. Pollution and risk assessment of heavy metals in Zuoxiguo antimony mining area, southwest China. *Environ. Pollut. Bioavailab.* **2023**, *35*, 2156397. [CrossRef]
3. Sun, F.; Yu, G.; Han, X.; Chi, Z.; Lang, Y.; Liu, C. Risk assessment and binding mechanisms of potentially toxic metals in sediments from different water levels in a coastal wetland. *J. Environ. Sci.* **2023**, *129*, 202–212. [CrossRef] [PubMed]
4. Cao, L.; Liu, J.; Dou, S.; Huang, W. Biomagnification of methylmercury in a marine food web in Laizhou Bay (North China) and associated potential risks to public health. *Mar. Pollut. Bull.* **2020**, *150*, 110762. [CrossRef] [PubMed]
5. Wei, L.L.; Zhou, Q.; Xei, C.X.; Wang, J.; Li, J. Bioaccumulation and Biomagnification of Heavy Metals in Three Gorges Reservoir and Effect of Biological Factors. *Huan Jing Ke Xue* **2016**, *37*, 325–334. [CrossRef]
6. Bi, B.S.; Yu, H.C.; Zhang, Y.; Tang, W. Content characteristics and ecological risk assessment of heavy metals in surface sediment of Dongfeng Xisha Reservoir, Shanghai, China. *J. Shanghai Ocean Univ.* **2020**, *29*, 709–719. [CrossRef]
7. Aoshima, K. Itai-itai disease: Lessons from the investigations of environmental epidemiology conducted in the 1970's, with special reference to the studies of the Toyama Institute of Health. *Nippon. Eiseigaku Zasshi Jpn. J. Hyg.* **2017**, *72*, 149–158. [CrossRef]
8. Noda, M.; Yasuda, M.; Kitagawa, M. Iron as a possible aggravating factor for osteopathy in itai-itai disease, a disease associated with chronic cadmium intoxication. *J. Bone Miner. Res.* **1991**, *6*, 245–255. [CrossRef]
9. Jarup, L. Hazards of heavy metal contamination. *Br. Med. Bull.* **2003**, *68*, 167–182. [CrossRef]
10. Clemens, S.; Ma, J.F. Toxic Heavy Metal and Metalloid Accumulation in Crop Plants and Foods. *Annu. Rev. Plant Biol.* **2016**, *67*, 489–512. [CrossRef]
11. Ning, X.R.; Liu, Z.L.; Shi, J.X. Assessment of primary productivity and potential fishery production in the Bohai, Yellow and East China Seas. *Acta Oceanolog. Sin.* **1995**, *17*, 72–84. [CrossRef]
12. Liu, M.; Wang, J.; Yu, K.; Jiang, R.; Liu, X.; Wang, S.; Liu, X. Community structure and geographical distribution of bacterial on surface layer sediments in the East China Sea. *Oceanol. Limnol. Sin.* **2015**, *46*, 1119–1131. [CrossRef]
13. Li, G.; Chen, X.J. Study on the relationship between catch of mackerel and environmental factors in the East China Sea in sum-mer. *J. Mar. Sci.* **2009**, *27*, 1–8. [CrossRef]
14. Yang, X.H.; Jin, A.M. Heavy Metal Geochemistry of Surface Sediments in the Northern East China Sea. *Bull. Sci. Technol.* **2019**, *35*, 32–40.
15. Zhuang, W.; Zhou, F. Distribution, source and pollution assessment of heavy metals in the surface sediments of the Yangtze River Estuary and its adjacent East China Sea. *Mar. Pollut. Bull.* **2021**, *164*, 112002. [CrossRef] [PubMed]
16. Xu, F.; Hu, B.; Yuan, S.; Zhao, Y.; Dou, Y.; Jiang, Z.; Yin, X. Heavy metals in surface sediments of the continental shelf of the South Yellow Sea and East China Sea: Sources, distribution and contamination. *CATENA* **2018**, *160*, 194–200. [CrossRef]

17. Li, N.; Fang, Z.; Chen, X.J. Study on microstructure and growth characteristics of Uroteuthis edulis statolith in East China Sea. *South China Fish. Sci.* **2020**, *16*, 21–31. [CrossRef]
18. Yamaguchi, T.; Takayama, K.; Hirose, N.; Matsuyama, M. Relationship between empirical water temperature and spring characteristics of swordtip squid (*Uroteuthis edulis*) caught in the eastern Tsushima Strait. *Mar. Biol. Res.* **2020**, *16*, 93–102. [CrossRef]
19. Yuan, Y.; Sun, T.; Wang, H.; Liu, Y.; Pan, Y.; Xie, Y.; Huang, H.; Fan, Z. Bioaccumulation and health risk assessment of heavy metals to bivalve species in Daya Bay (South China Sea): Consumption advisory. *Mar. Pollut. Bull.* **2019**, *150*, 110717. [CrossRef]
20. Hao, Z.; Chen, L.; Wang, C.; Zou, X.; Zheng, F.; Feng, W.; Zhang, D.; Peng, L. Heavy metal distribution and bioaccumulation ability in marine organisms from coastal regions of Hainan and Zhoushan, China. *Chemosphere* **2019**, *226*, 340–350. [CrossRef]
21. Wang, K.-Y.; Chang, K.-Y.; Liao, C.-H.; Lee, M.-A.; Lee, K.-T. Growth Strategies of the Swordtip Squid, Uroteuthis Edulis, in Response to Environmental Changes in the Southern East China Sea—A Cohort Analysis. *Bull. Mar. Sci.* **2013**, *89*, 677–698. [CrossRef]
22. Alavian Petroody, S.S.; Hamidian, A.H.; Ashrafi, S.; Eagderi, S.; Khazaee, M. Study on age-related bioaccumulation of some heavy metals in the soft tissue of rock oyster (*Saccostrea cucullata*) from Laft Port–Qeshm Island, Iran. *Iran. J. Fish. Sci.* **2017**, *16*, 897–906. [CrossRef]
23. Lin, D.; Zhu, K.; Qian, W.; Punt, A.E.; Chen, X. Fatty acid comparison of four sympatric loliginid squids in the northern South China Sea: Indication for their similar feeding strategy. *PLoS ONE* **2020**, *15*, e0234250. [CrossRef] [PubMed]
24. Koyama, J.; Nanamori, N.; Segawa, S. Bioaccumulation of Waterborne and Dietary Cadmium by Oval Squid, Sepioteuthislessoniana, and its Distribution Among Organs. *Mar. Pollut. Bull.* **2000**, *40*, 961–967. [CrossRef]
25. Lischka, A.; Lacoue-Labarthe, T.; Hoving, H.; JavidPour, J.; Pannell, J.; Merten, V.; Churlaud, C.; Bustamante, P. High cadmium and mercury concentrations in the tissues of the orange-back flying squid, *Sthenoteuthis pteropus*, from the tropical Eastern Atlantic. *Ecotoxicol. Environ. Saf.* **2018**, *163*, 323–330. [CrossRef] [PubMed]
26. Zhang, L.; Shi, Z.; Jiang, Z.; Zhang, J.; Wang, F.; Huang, X. Distribution and bioaccumulation of heavy metals in marine organisms in east and west Guangdong coastal regions, South China. *Mar. Pollut. Bull.* **2015**, *101*, 930–937. [CrossRef] [PubMed]
27. Ridame, C.; Le Moal, M.; Guieu, C.; Ternon, E.; Biegala, I.C.; L'Helguen, S.; Pujo-Pay, M. Nutrient control of N2 fixation in the oligotrophic Mediterranean Sea and the impact of Saharan dust events. *Biogeosciences* **2011**, *8*, 2773–2783. [CrossRef]
28. Vilches, F.O.; Bobinac, M.A.; Labudía, A.C.; Viola, M.N.P.; Marcovecchio, J.E.; Cappozzo, H.L.; Panebianco, M.V. Metals concentration and bioaccumulation in the marine-coastal trophic web from Buenos Aires province southern coast, Argentina. *Chem. Ecol.* **2019**, *35*, 501–523. [CrossRef]
29. Tanaka, M.; Yamaguchi, Y.; Harada, Y.; Tsuchiya, K.; Takaku, Y. As, Cd and Hg in the organs of Todarodes pacificus, Sepia longipes and Sepia madokai in the East China Sea. *Ecotoxicol. Environ. Saf.* **2017**, *145*, 103–110. [CrossRef]
30. Lischka, A.; Braid, H.; Cherel, Y.; Bolstad, K.; Lacoue-Labarthe, T.; Bustamante, P. Influence of sexual dimorphism on stable isotopes and trace element concentrations in the greater hooked squid Moroteuthopsis ingens from New Zealand waters. *Mar. Environ. Res.* **2020**, *159*, 104976. [CrossRef]
31. Le Pabic, C.; Caplat, C.; Lehodey, J.-P.; Milinkovitch, T.; Koueta, N.; Cosson, R.P.; Bustamante, P. Trace metal concentrations in post-hatching cuttlefish *Sepia officinalis* and consequences of dissolved zinc exposure. *Aquat. Toxicol.* **2015**, *159*, 23–35. [CrossRef] [PubMed]
32. Shalini, R.; Jeyasekaran, G.; Shakila, R.J.; Sundhar, S.; Arisekar, U.; Jawahar, P.; Aanand, S.; Sivaraman, B.; Malini, A.H.; Surya, T. Dietary intake of trace elements from commercially important fish and shellfish of Thoothukudi along the southeast coast of India and implications for human health risk assessment. *Mar. Pollut. Bull.* **2021**, *173 Pt A*, 113020. [CrossRef]
33. Bustamante, P.; Cherel, Y.; Caurant, F.; Miramand, P. Cadmium, copper and zinc in octopuses from Kerguelen Islands, Southern Indian Ocean. *Polar Biol.* **1998**, *19*, 264–271. [CrossRef]
34. Roldán-Wong, N.T.; Kidd, K.A.; Marmolejo-Rodríguez, A.J.; Ceballos-Vázquez, B.P.; Shumilin, E.; Arellano-Martínez, M. Bioaccumulation and biomagnification of potentially toxic elements in the octopus *Octopus hubbsorum* from the Gulf of California. *Mar. Pollut. Bull.* **2018**, *129*, 458–468. [CrossRef] [PubMed]
35. Ajala, M.; Ben Ameur, W.; Annabi, A. First evidence of the utility of cephalopods for biomonitoring program in the field: Case of Sepia officinalis south west of Mediterranean Sea (Gulf of Gabes, Tunisia). *Environ. Sci. Pollut. Res.* **2022**, *29*, 28675–28687. [CrossRef] [PubMed]

toxics

MDPI

Article

Effects of 17β-Estradiol Pollution on Microbial Communities and Methane Emissions in Aerobic Water Bodies

Zihao Gao [1,2], Yu Zheng [1,2], Zhendong Li [1,2] and Aidong Ruan [1,3,*]

[1] The National Key Laboratory of Water Disaster Prevention, Hohai University, Nanjing 210098, China; 211301020001@hhu.edu.cn (Z.G.); 211301010120@hhu.edu.cn (Y.Z.); 231301020003@hhu.edu.cn (Z.L.)
[2] College of Hydrology and Water Resources, Hohai University, Nanjing 210098, China
[3] College of Geography and Remote Sensing, Hohai University, Nanjing 210098, China
* Correspondence: adruan@hhu.edu.cn; Tel.: +86-133-8276-5166

Abstract: 17β-Estradiol (E2) is a widely present trace pollutant in aquatic environments. However, its impact on microbial communities in aerobic lake waters, which are crucial for methane (CH_4) production, remains unclear. This study conducted an E2 contamination experiment by constructing laboratory-simulated aerobic microecosystems. Using 16S rRNA high-throughput sequencing, the effects of E2 on bacterial and archaeal communities were systematically examined. Combined with gas chromatography, the patterns and mechanisms of E2's impact on CH_4 emissions in aerobic aquatic systems were uncovered for the first time. Generally, E2 contamination increased the randomness of bacterial and archaeal community assemblies and weakened microbial interactions. Furthermore, changes occurred in the composition and ecological functions of bacterial and archaeal communities under E2 pollution. Specifically, two days after exposure to E2, the relative abundance of *Proteobacteria* in the low-concentration (L) and high-concentration (H) groups decreased by 6.99% and 4.01%, respectively, compared to the control group (C). Conversely, the relative abundance of *Planctomycetota* was 1.81% and 1.60% higher in the L and H groups, respectively. E2 contamination led to an increase in the relative abundance of the *methanogenesis* functional group and a decrease in that of the *methanotrophy* functional group. These changes led to an increase in CH_4 emissions. This study comprehensively investigated the ecotoxicological effects of E2 pollution on microbial communities in aerobic water bodies and filled the knowledge gap regarding aerobic methane production under E2 contamination.

Keywords: aquatic pollutant; bacterial and archaeal community; aerobic methane production; aquatic environment

1. Introduction

According to reports, 17β-Estradiol (E2) is considered one of the most potent natural estrogens [1]. Its widespread presence in various aquatic environments has sparked global concerns as it can have significant impacts on aquatic organisms and human health, even at extremely low concentrations [2–5].

Current research has primarily focused on exploring the impacts of estrogens on higher organisms, while comparatively less attention has been given to investigating the ecotoxicological effects of estrogens on microorganisms. However, recent studies have confirmed that E2 has significant impacts on microbial communities in various environments. For instance, Chun et al. [6] conducted E2 contamination experiments in laboratory soil, revealing that E2 can alter the soil microbial community, with effects correlating with soil properties. Zhang et al. [7] suggested that E2 in soil may act as a nutrient for microbes, thereby stimulating the growth of certain bacteria. In river water, E2 concentrations ranging from 1 to 100 ng/L were found to significantly enhance the growth of heterotrophic nitrifying bacteria [8]. Additionally, the growth characteristics of *Enterobacteriaceae* were observed to change under E2 pollution [9]. However, information

regarding the influence of E2 on microbial communities in aerobic lake waters remains extremely limited.

Water microbial communities play a crucial role in driving elemental biogeochemical cycles, facilitating the cycling of carbon, nitrogen, sulfur, phosphorus, and other essential elements [10,11]. Lakes, due to their capacity for storage, transport, and transformation of substantial carbon quantities [12], have emerged as focal points for carbon cycling dynamics and greenhouse gas emissions. Despite covering less than 4% of the Earth's surface, lake ecosystems significantly contribute to methane (CH_4) emissions, exerting pivotal influences on the global carbon cycle [13]. CH_4 is not only a primary component of greenhouse gases but can also accumulate substantially in lakes, potentially leading to gas eruptions that cause significant human and animal fatalities. For instance, Lake Kivu in East Africa, known for its high CH_4 content in deep, anoxic waters, is considered one of the most dangerous freshwater lakes [14]. Traditionally, CH_4 production in lakes has been attributed primarily to methanogens in anaerobic environments. However, in recent years, evidence has been accumulating regarding CH_4 production in aerobic water bodies [15,16], a phenomenon known as the "methane paradox". Early studies on the "methane paradox" primarily focused on marine environments, proposing various hypotheses based on mechanisms involving methanogenic microorganisms to explain CH_4 supersaturation in the presence of oxygen [17–19]. Recent research suggests that aerobic microbial conversion of methylphosphonate (MPn) may be a significant contributor to CH_4 production in marine and freshwater environments [20–22], providing direct evidence for the existence of aerobic methanogenic microorganisms. Our previous studies showed that E2 significantly influenced CH_4 emission rates in both simulated natural and anaerobic systems, with its effects being constrained by major environmental factors [23–25]. However, the influence of E2 on CH_4 emissions in aerobic lake waters remains unclear.

Based on these considerations, this study established aerobic simulated microecosystems in the laboratory. Different concentrations of E2 were added to the systems to conduct pollution experiments aiming to: (1) investigate the impact of E2 pollution on CH_4 emissions in aerobic lake waters; (2) assess the ecotoxicological effects of E2 pollution on microbial communities in aerobic lake waters; and (3) elucidate the microbiological mechanisms by which E2 affects CH_4 emissions. These findings will provide a theoretical basis for future water pollution control and aid in more accurately predicting and assessing methane emissions in lake water bodies.

2. Materials and Methods

2.1. Experimental Design

The sediment and overlying water samples used in this study were obtained from Longxu Lake in Anhui Province, China, an ecologically protected area where no estrogen was detected. The sediment samples underwent a series of treatments including air-drying, grinding, sieving (100 mesh), and homogenization. Methylphosphonic acid was added to the water samples to achieve a final concentration of 1 mmol/L. Approximately 100 g of treated sediment and 150 mL of treated overlying water were placed in 500 mL conical flasks. Subsequently, these flasks were covered with membranes (air flux: 1020 $m^3/m^2 \cdot h$ at 0.01 MPa) with a pore size of 0.2–0.3 μm, ensuring system aeration while preventing the introduction of external microbes. Nine laboratory-simulated aerobic microecosystems were established using the described method and were placed in constant temperature incubators at 30 °C, shielded from light, well-ventilated, and agitated at 100 rpm. After three days, the gas emission rates of each system stabilized and exhibited uniformity; this was followed by the initiation of E2 pollution treatment on the systems. Stock solutions of E2 were prepared by dissolving E2 (99%, CAS 50-28-2, Thermo Scientific, Waltham, MA, USA) in ethanol. Volumes of 30 μL of these stock solutions were added at different concentrations to the systems to achieve final E2 concentrations of 0 ng/L (control group, C), 100 ng/L (low-concentration group, L), and 10,000 ng/L (high-concentration group, H). Each group consisted of three replicate samples.

2.2. Sample Collection and Measurement

The date of E2 solution addition was designated as Day 0. Prior to E2 contamination, gas and slurry–water mixture samples were collected once. Subsequently, gas samples were collected every 24 h, and slurry–water mixture samples were collected every 48 h. The specific collection method involved using a sterile syringe to puncture the septum and collect 5 mL of headspace gas samples, followed by sealing the system for incubation. After 2.5 h of incubation, another 5 mL of headspace gas samples were collected using a sterile syringe. Then, each system was thoroughly mixed, and 10 mL of slurry–water mixture samples were collected and stored in a −80 °C freezer.

The experimental period lasted for 7 days. Gas samples collected daily were analyzed for CH_4 concentration using gas chromatography (GC-7890B, Agilent Technologies, Santa Clara, CA, USA). A total of 36 slurry–water mixture samples collected on the 0th, 2nd, 4th, and 6th days were subjected to high-throughput sequencing.

2.3. DNA Extraction, Amplification, and Sequencing

The DNA from the slurry–water mixture samples was extracted using the TGuide S96 Magnetic Soil/Stool DNA Kit (Tiangen Biotech (Beijing) Co., Ltd., Beijing, China). Subsequently, the DNA concentration of the samples was measured using the Qubit dsDNA HS Assay Kit and Qubit 4.0 Fluorometer (Invitrogen, Thermo Fisher Scientific, Waltham, MA, USA). The V4-V5 region of the 16S rRNA gene was amplified in each sample using the 515F primer (5′-GTGYCAGCMGCCGCGGTAA-3′) and the 926R primer (5′-CCGYCAATTYMTTTRAGTTT-3′). Sequencing adapters were attached to the ends of the primers for PCR amplification, and the resulting products underwent purification, quantification, and normalization to create sequencing libraries. After passing quality control assessment, the libraries were sequenced using Illumina Novaseq 6000 (Illumina, Santiago, CA, USA). Additionally, raw data have been uploaded to the NCBI SRA database (No. PRJNA1097048).

2.4. Bioinformatic Analysis

The raw reads obtained from sequencing were filtered using Trimmomatic (version 0.33). Primer sequences were identified and removed to obtain clean reads using Cutadapt (version 1.9.1). Subsequently, the clean reads underwent feature classification using dada2, resulting in the generation of amplicon sequence variants (ASVs) [26]. ASVs with relative abundances of less than 0.005% were filtered out. Taxonomic annotation of the filtered ASVs was conducted using the Naive Bayes classifier [27] based on the Silva.138 reference database [28].

Alpha diversity indices of the samples were calculated using the QIIME2 software [27]. Beta diversity was evaluated through Principal Coordinates Analysis (PCoA) based on the Bray–Curtis distance [29]. The relative importance of microbial community assembly processes was determined using the iCAMP model [30]. Molecular Ecological Networks (MENs) were established using Random Matrix Theory (RMT), and subsequent analysis was carried out with the Molecular Ecological Network Analysis Pipeline (MENAP, http://mem.rcees.ac.cn:8081 accessed on 1 May 2023) [31]. Gephi (version 0.9.2) was utilized for visualizing all networks. Functional groups within the samples were predicted using FAPROTAX [32], and the results were visualized with the R package pheatmap to generate heat maps. Redundancy analysis (RDA) was conducted using vegan (version 2.3-0), with significance tested via Monte Carlo permutation tests (permu = 999).

2.5. Analysis of Methane Emission Rates

The specific formula for calculating CH_4 emission rates is as follows:

$$v = ((c_2 - c_1) \times V_h \times 1/22.4 \times 273/(273 + T) \times P/101325)/(V_s \times t), \quad (1)$$

v: the CH_4 emission rate ($\mu mol \cdot L^{-1} \cdot h^{-1}$);
c_1: the CH_4 volume concentration before sealing (ppm);
c_2: the CH_4 volume concentration after 2.5 h of sealing (ppm);
V_h: the headspace volume (mL);
T: the gas temperature (°C);
P: the gas pressure (Pa);
V_s: the sample volume (mL);
t: the sealing time (h).

2.6. Statistical Analysis

Permutational Multivariate Analysis of Variance (PERMANOVA) was utilized to examine disparities in microbial community structures among different groups. The Student's *t*-test was employed to assess the statistical significance of differences between two samples. Differences were considered statistically significant if the *p*-value was less than 0.05.

3. Results

3.1. The Impact of 17β-Estradiol Pollution on Methane Emission Patterns

The study tracked the changes in CH_4 emission rates within each treatment group over 7 days post E2 pollution (Figure 1A). The results revealed differences in CH_4 emission rates among the groups only during the first 2 days, with the low-concentration group significantly higher than the control group on day 2 ($p = 0.0013$). Subsequently, from days 3 to 7, all groups showed a gradual decline in CH_4 emissions without significant discrepancies. To further investigate the inter-group disparities, an analysis of CH_4 emission rate increments was performed (Figure 1B). Within the first 2 days, fluctuations were observed in the rate increments across all treatment groups. Notably, on day 1, both pollution groups had higher rate increments compared to the control group, with particularly the low-concentration group displaying a significant increase over the control group ($p = 0.047$). By days 3 to 7, CH_4 emissions had stabilized in all groups, with rate increments approaching zero. In conclusion, E2 was found to stimulate short-term CH_4 production in aerobic water systems.

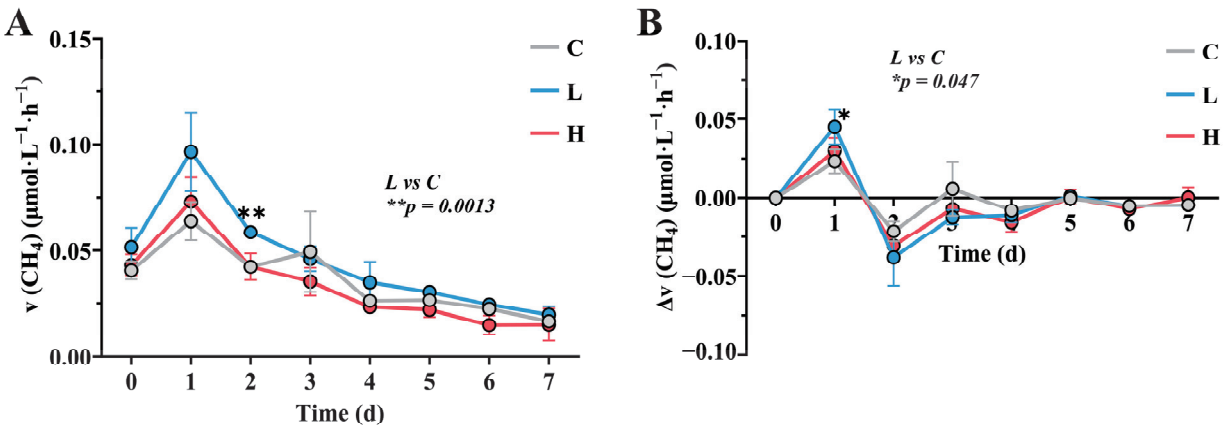

Figure 1. Temporal changes in methane emission rate (**A**) and rate increment (**B**). The rate increment is calculated by subtracting the previous day's rate from the current day's rate. C represents the control group, L represents the low-concentration group, and H represents the high-concentration group. The significance markers in Figure 1A and 1B represent the results of the Student's *t*-test comparing the C and L groups on day 2 and day 1, respectively.

3.2. Response of Bacterial and Archaeal Community Diversity to 17β-Estradiol Pollution

Sequencing of 36 samples yielded a total of 562 ASVs, classified into 25 phyla, 133 families, and 186 genera. Bacteria accounted for 82.55–99.54%, archaea for 0.04–8.94%, and unassigned organisms for 0.42–17.29% of the community. The study treated bacterial and

archaeal communities as a unified entity. Following E2 pollution, there were no significant differences in Chao1 and Shannon indices of bacterial and archaeal communities among the three treatment groups (Figure 2A,B). This indicates that E2 pollution did not significantly impact the species richness and diversity of bacterial and archaeal communities within the system.

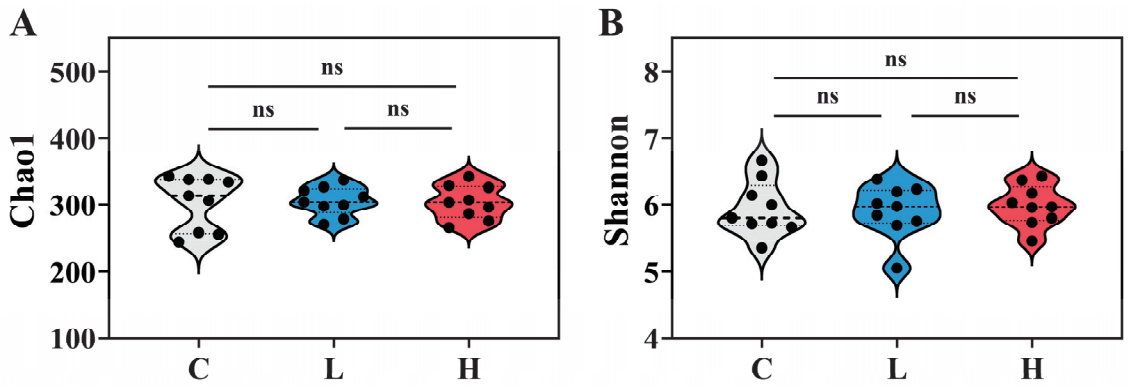

Figure 2. Chao1 (**A**) and Shannon (**B**) indices of bacterial and archaeal communities in each group after E2 contamination. C represents the total of samples from the control group collected on days 2, 4, and 6; L represents the total of samples from the low-concentration group collected on days 2, 4, and 6; H represents the total of samples from the high-concentration group collected on days 2, 4, and 6. "ns" indicates no significant difference.

To evaluate the impact of E2 on bacterial and archaeal community structure, we conducted Principal Coordinate Analysis (PCoA) on the community compositions of the three treatment groups on different dates. The results showed no significant differences in community structures among the three treatment groups on day 0 (Figure 3A), indicating homogeneity before E2 pollution. However, on day 2, a significant difference emerged between the control group and the two pollution groups (PERMANOVA, p = 0.0497) (Figure 3B), suggesting a notable effect of E2. On days 4 and 6, the community structures of all three groups were similar, showing no significant differences (Figure 3C,D). Overall, these findings suggest that under aerobic conditions, the influence of E2 on bacterial and archaeal communities may be transient.

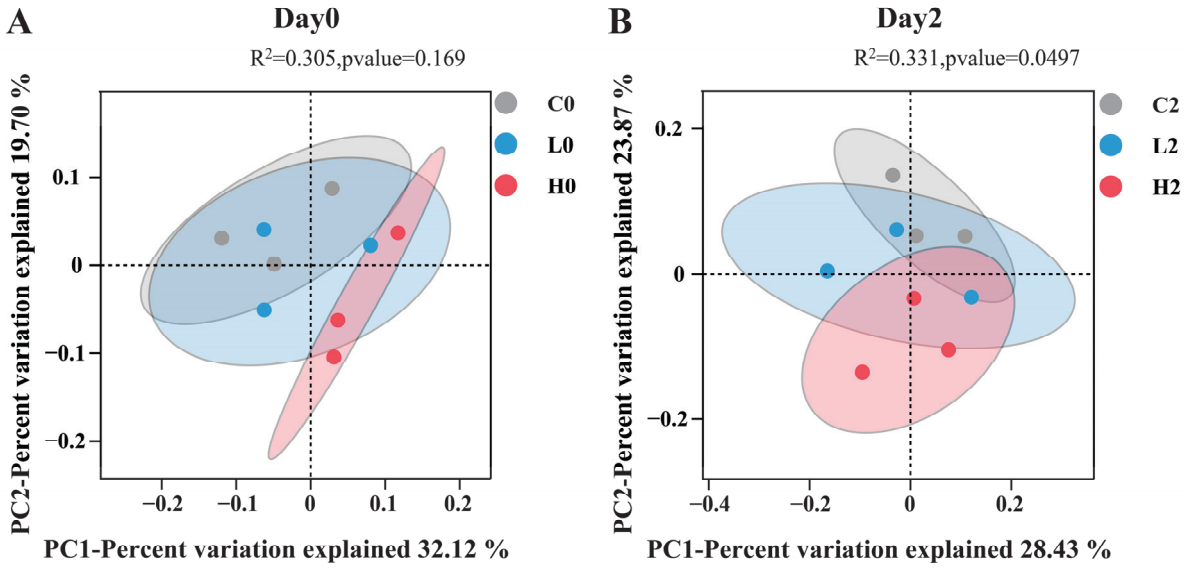

Figure 3. *Cont.*

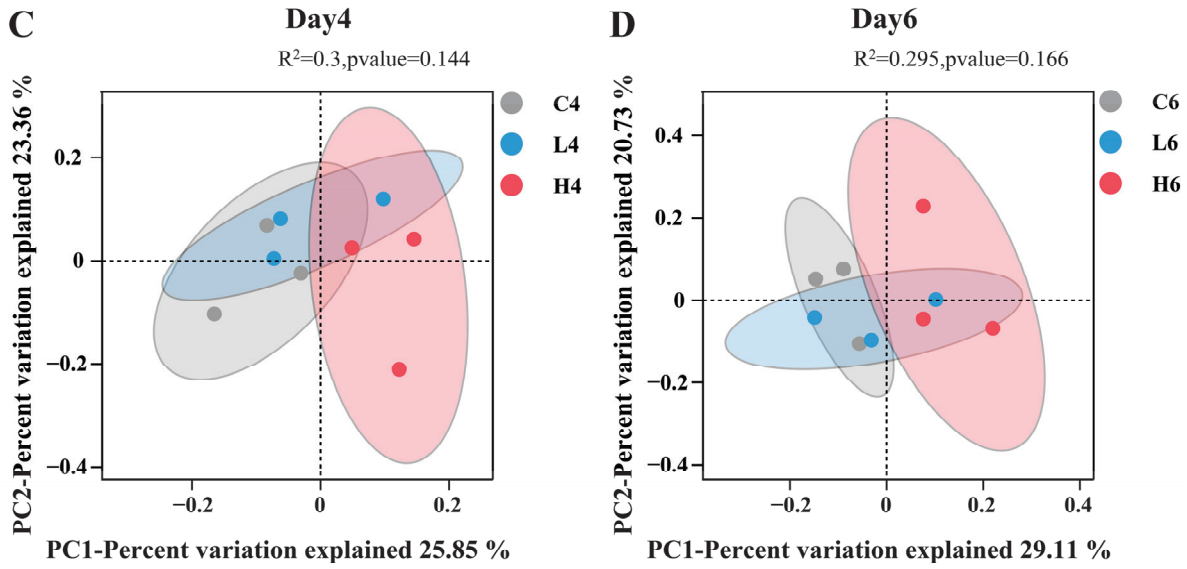

Figure 3. The Principal Coordinate Analysis (PCoA) of bacterial and archaeal communities on days 0 (**A**), 2 (**B**), 4 (**C**), and 6 (**D**). Sample labeling rule: Letters represent groups, and numbers represent dates. For example, C0 represents samples from the control group on day 0.

3.3. Exposure to 17β-Estradiol Alters Taxonomic Composition of Bacterial and Archaeal Communities

Exposure to E2 significantly impacted the composition of bacterial and archaeal communities. During E2 pollution, *Proteobacteria* (29.3–39.0%) and *Bacteroidota* (18.3–38.3%) were dominant in all three treatment groups (Figure 4A). However, the relative abundance of these dominant phyla gradually decreased over the incubation period. To compare the differences in community compositions among the three groups, particular attention was given to analyzing the second day, where significant differences in community structure were observed. Analysis of variance (ANOVA) revealed that on day 2, three phyla among the top ten in relative abundance showed significant differences among the groups. In the two pollution groups, the relative abundance of *Proteobacteria* was lower than that of the control group, especially with the low-concentration group showing a significant decrease compared to the control group (Figure 4C). This suggests that the addition of E2 reduced the dominance of *Proteobacteria*. Furthermore, in the pollution groups, the relative abundances of *Planctomycetota* and *Bdellovibrionota* were higher than those in the control group, especially with *Planctomycetota* in the low-concentration group and *Bdellovibrionota* in the high-concentration group showing significantly higher relative abundances than in the control group. Therefore, E2 significantly increased the relative abundances of *Planctomycetota* and *Bdellovibrionota* in aerobic water bodies.

At the genus level, *Flavisolibacter* was consistently the most abundant genus in both the control group and low-concentration group throughout the experiment (12.1–27.3%, 15.8–26.5%), followed by *Ideonella* (7.9–11.0%, 5.2–9.2%) (Figure 4B). In the high-concentration group, *Flavisolibacter* remained dominant in relative abundance (9.4–25.1%), but *Ideonella* dropped to fourth and seventh place on day 4 and day 6, indicating a threat to the dominance of *Ideonella* posed by high concentrations of E2. Particularly noteworthy is that on day 2, *Ideonella* in the low-concentration group was significantly lower than in the control group (Figure 4D), suggesting that even low concentrations of E2 reduced the dominance of *Ideonella*. Additionally, in both pollution groups, *Ellin6067*, *Bryobacter*, and *Gemmata* had higher relative abundances compared to the control group, with this difference being more pronounced in the high-concentration group (Figure 4D). Conversely, *Massilia* and *Novosphingobium* had lower relative abundances in both pollution groups, with a more significant decrease observed in the high-concentration group (Figure 4D). This indicates that E2 significantly increased the relative abundances of *Ellin6067*, *Bryobacter*,

and *Gemmata* while markedly decreasing those of *Massilia* and *Novosphingobium*, particularly under high-concentration conditions. Furthermore, *Pseudolabrys* and *Pajaroellobacter* showed no significant differences in relative abundance compared to the control group in the low-concentration group but exhibited significantly higher relative abundances in the high-concentration group (Figure 4D), indicating that E2 only promotes the growth of *Pseudolabrys* and *Pajaroellobacter* at high concentrations.

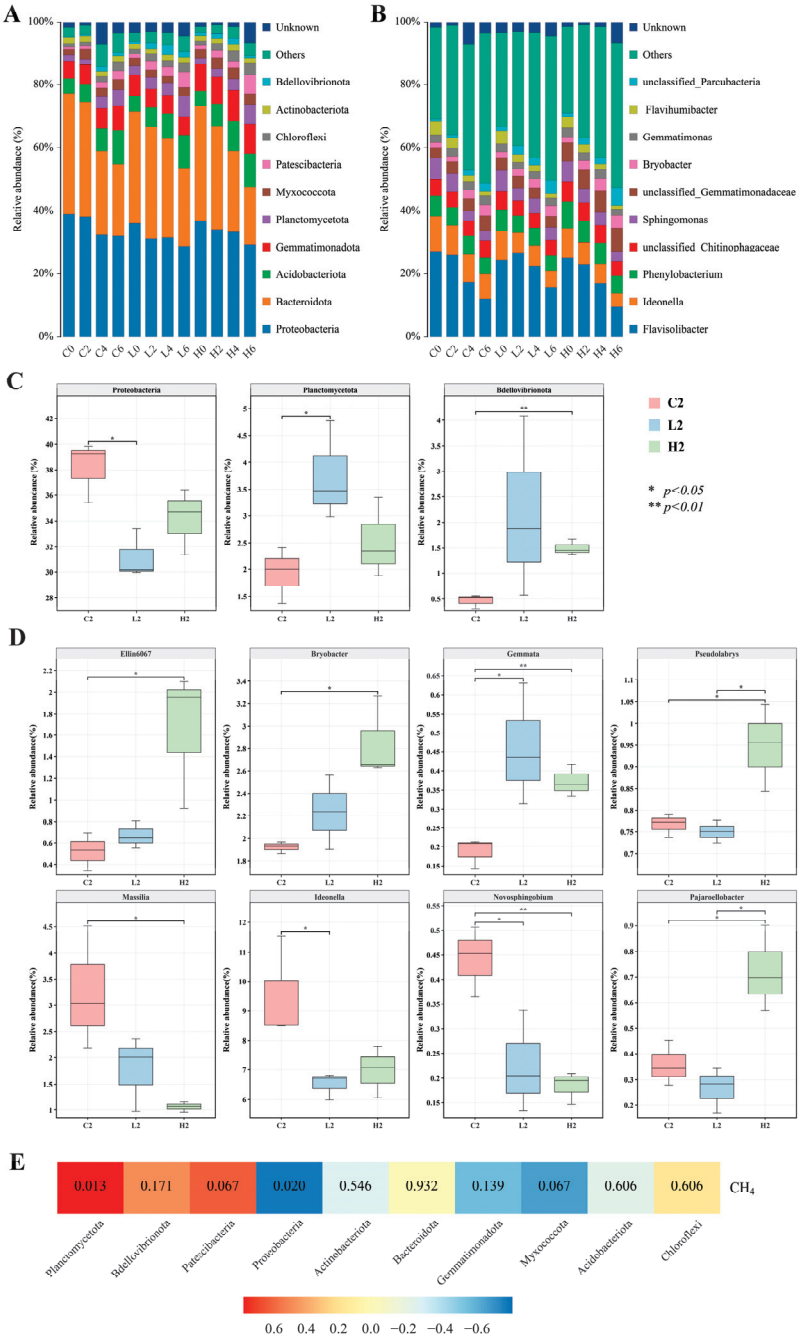

Figure 4. Taxonomic composition of bacterial and archaeal communities at the phylum (**A**) and genus (**B**) levels, and relative abundance of differential phyla (**C**) and genera (**D**) on day 2. C2, L2, and H2 represent samples from the control group, low-concentration group, and high-concentration group, respectively, on day 2. (**E**) Heatmap of the correlation between major phyla and CH_4 emission rates on day 2.

3.4. The Influence of 17β-Estradiol Pollution on Community Assembly

iCAMP was used to quantify the assembly of bacterial and archaeal communities after adding E2 solution. The dominant process across all three treatment groups was drift (DR, 68.3–81.3%) in stochastic processes, followed by homogeneous selection (HoS, 11.4–18.4%) in deterministic processes (Figure 5A). Consequently, the assembly of bacterial and archaeal communities in all groups was primarily governed by stochastic processes. Nevertheless, variations were observed among the ecological processes within the three treatment groups. Specifically, in the low-concentration group, HoS was significantly lower compared to the control group (Cohen's d = 3.53, $p = 0.0004$), while DR was significantly higher (Cohen's d = −4.27, $p = 0.002$) (Figure 5B). Similarly, in the high-concentration group, HoS and DR displayed comparable trends to the control group, although the differences were not statistically significant. These findings suggest that E2 significantly impacts the principal ecological processes of bacterial and archaeal communities within the system, leading to a notable increase in the stochasticity of community assembly (Cohen's d = −3.57, $p = 0.0004$) (Figure 5B).

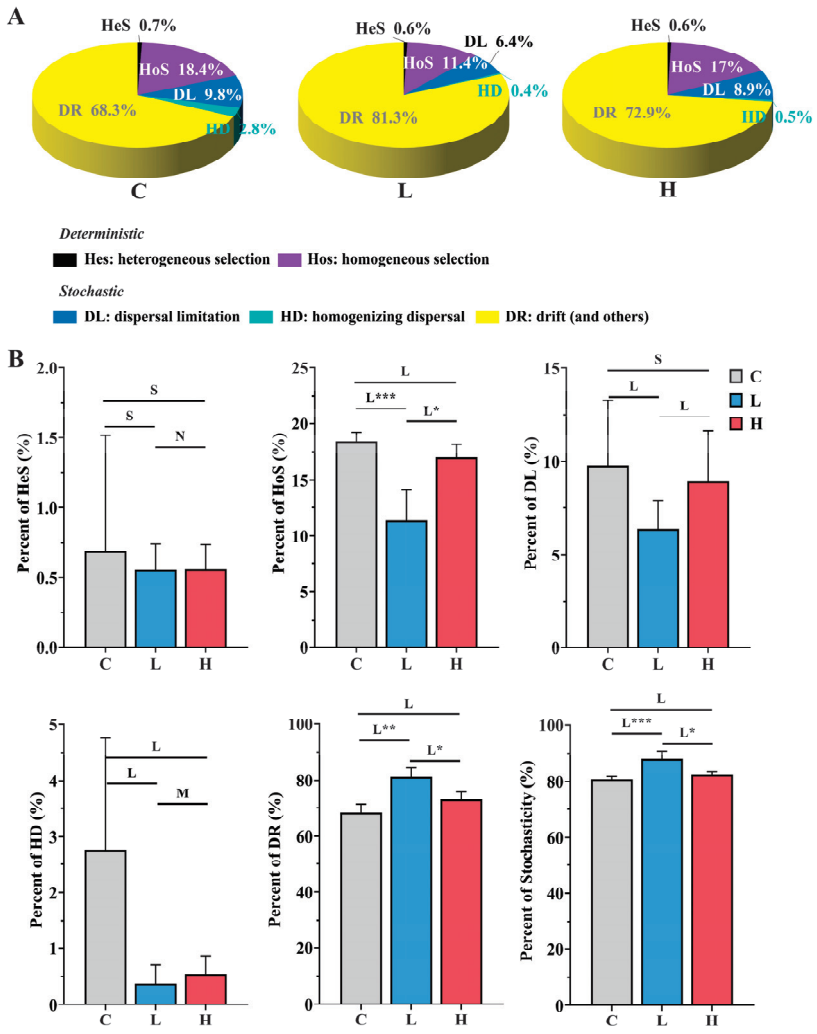

Figure 5. Relative importance of various ecological processes within each group (**A**) and differences in ecological processes among groups (**B**) after E2 pollution. C represents the total of samples from the control group collected on days 2, 4, and 6; L represents the total of samples from the low-concentration group collected on days 2, 4, and 6; H represents the total of samples from the high-concentration group collected on days 2, 4, and 6. *** $p < 0.001$; ** $p < 0.01$; * $p < 0.05$. L, M, S, and N represent large ($|d| > 0.8$), medium ($0.5 < |d| \leq 0.8$), small ($0.2 < |d| \leq 0.5$), and negligible ($|d| \leq 0.2$) effect sizes of E2 pollution based on Cohen's d.

3.5. Molecular Ecological Network Analysis

The impact of E2 on microbial interactions within bacterial and archaeal communities was revealed through molecular ecological network analysis (MENs). The visualization of networks before and after E2 pollution is shown in Figure 6, with specific network properties detailed in Table S1. The node connectivity of the four networks conformed to a power-law distribution (R^2 = 0.89–0.95), indicating that these networks were all scale-free networks. Additionally, with average path lengths ranging from 6.39 to 6.92 and close approximation of the logarithm of the total number of nodes, the networks exhibited typical small-world characteristics. Furthermore, all the networks demonstrated modularity values between 0.774 and 0.804, significantly higher than those of corresponding random networks, indicating the presence of modular features in the constructed networks.

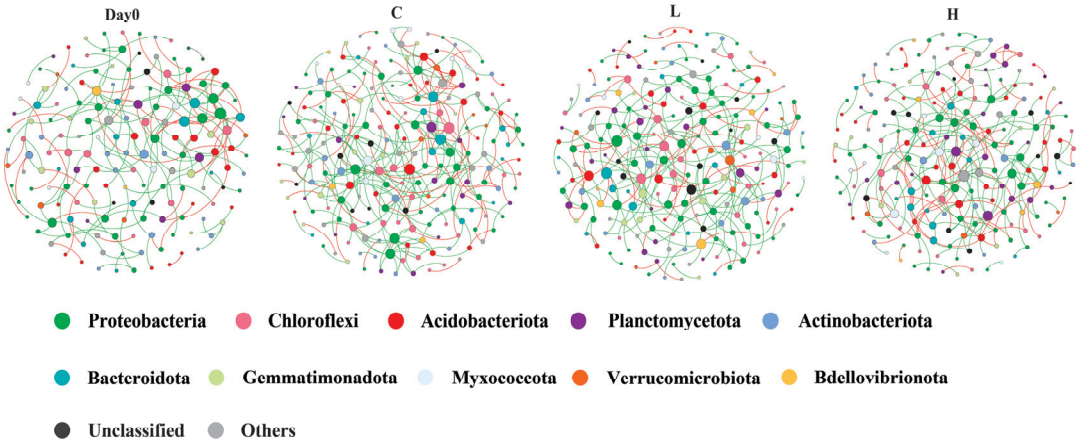

Figure 6. Molecular ecological networks (MENs) before and after E2 pollution. Node size represents the node degree. Edge color represents positive (red) and negative (green) correlations. Day 0 represents the total of samples from three groups collected on day 0; C represents the total of samples from the control group collected on days 2, 4, and 6; L represents the total of samples from the low-concentration group collected on days 2, 4, and 6; H represents the total of samples from the high-concentration group collected on days 2, 4, and 6.

Compared to the initial state, the three treatment groups exhibited a significant increase in network nodes and links following the addition of E2 solution, indicating an enhancement in network complexity. This improvement may be attributed to ethanol acting as a solvent, resulting in more nutrients being provided to bacteria and archaea, thereby boosting microbial activity and diversity and, consequently, enhancing network complexity. In contrast to the control group, the two pollution groups showed notably fewer links, suggesting simpler network structures. Furthermore, both pollution groups had lower average degree (avgK) and average clustering coefficient (avgCC) values than the control group, indicating weaker node connectivity and reduced closeness and clustering among nodes in pollution networks. These results suggest that E2 could reduce the complexity and stability of bacterial and archaeal community networks in aerobic water bodies.

Based on the within-module connectivity (Zi) and among-module connectivity (Pi), nodes are categorized into network hubs, module hubs, connectors, and peripherals [33]. The first three types are regarded as keystone taxa, playing a pivotal role in the system's resilience against external disturbances or species invasions [34]. Each network has distinct connectors and module hubs (Figure S1). Before pollution, the network had three connectors. Following E2 contamination, the control group showed four module hubs and three connectors, the low-concentration group had four module hubs and eight connectors, and the high-concentration group had four module hubs and four connectors. Therefore, the introduction of E2 led to an increase in the number of keystone taxa within the network. The specific classification of these keystone ASVs is detailed in Table S2. In the control group, over half of the keystone ASVs belonged to *Proteobacteria*, indicating their potential

importance as the predominant phylum in the system. However, in the low-concentration group, only two keystone ASVs were from *Proteobacteria*, accounting for 16.7% of the total keystone ASVs, while two keystone ASVs were identified as *Planctomycetota*, which were absent among the keystone taxa in the control group. In the high-concentration group, 50% of the keystone ASVs belonged to *Planctomycetota*. This suggests that with increasing E2 concentration, the interactions between *Proteobacteria* and other microorganisms gradually weaken, while the significance of *Planctomycetota* in the network increases. At the family level, both pollution groups had keystone ASVs belonging to *Gemmatimonadaceae*, *Gemmataceae*, and *Isosphaeraceae*. However, in the control group, there were no keystone ASVs from these three families. Therefore, the addition of E2 could enhance the interactions between *Gemmatimonadaceae*, *Gemmataceae*, *Isosphaeraceae*, and other microorganisms.

3.6. The Influence of 17β-Estradiol Contamination on Ecological Functions

Functional predictions were conducted using Faprotax for bacterial and archaeal communities on day 2. Out of 562 ASVs, 83 were assigned to at least one functional group. The most abundant functional groups in all three treatment groups were *chemoheterotrophy* (26.3–28.5%), followed by *aerobic_chemoheterotrophy* (23.4–25.5%) and *nitrate_reduction* (20.4–25.9%) (Figure 7). Significant variations in the relative abundances of major functional groups were observed among the three treatment groups. Both pollution groups exhibited higher levels of *aerobic_chemoheterotrophy* and *chemoheterotrophy* compared to the control group, while *nitrate_reduction* was lower in the pollution groups (Figure S2). Moreover, functional groups associated with methane production, such as *methanogenesis*, *methanogenesis_by_CO_2_reduction_with_H_2*, and *hydrogenotrophic_methanogenesis*, were most abundant in the high-concentration group, followed by the low-concentration group. The methane oxidation functional group, *methanotrophy*, was enriched in the control group (Figure S2). Hence, E2 has the potential to influence microbial carbon and nitrogen cycling within the system.

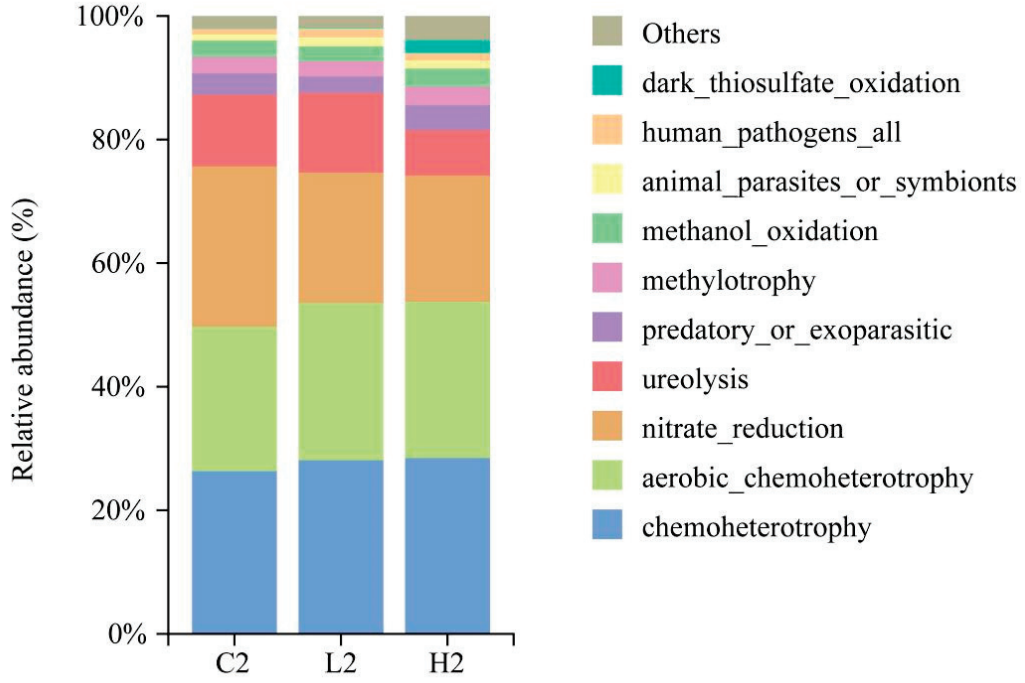

Figure 7. Relative abundance of functional groups in different treatment groups on day 2.

4. Discussion

4.1. Ecological Toxicological Effects of 17β-Estradiol on Bacterial and Archaeal Communities

Based on the findings, E2 has disrupted the original structure of bacterial and archaeal communities in aerobic water bodies. The molecular ecological network analysis

revealed that both pollution groups exhibited lower links, avgK, and avgCC compared to the control group. This indicates that the introduction of E2 weakened interactions among microorganisms, impacting information flow and material cycling within the ecosystem, and consequently, reducing ecosystem stability. Additionally, the iCAMP analysis demonstrated a significant increase in the proportion of stochasticity in community assembly due to E2 pollution, suggesting heightened uncertainty in the formation and evolution of microbial community structures. This could be attributed to variations in species' adaptability to E2. The introduction of E2 decreased the dominance of the major phylum *Proteobacteria*, providing additional resources and available space for other microorganisms, and thereby amplifying the randomness in community assembly [35]. Overall, within aerobic water bodies, E2 contamination led to microbial communities becoming more unpredictable and unstable.

However, the impact is only effective in the short term. Beta diversity analysis revealed significant differences in the bacterial and archaeal community structures of the three treatment groups only on the second day after E2 contamination, with no notable variances on the fourth and sixth days. This suggests that the influence of E2 contamination on the structure of bacterial and archaeal communities is transient. Over time, the community structure may gradually revert to its original state. This recovery capability could be attributed to keystone taxa within the community [31]. The number of keystone taxa in the pollution groups was notably higher than that in the control group, indicating that under the pressure of E2 contamination, specific microbial taxa began to assume more critical roles, exerting essential regulatory effects on maintaining the structure and function of the entire community [36]. Notably, the significance of *Planctomycetota* in the network increased gradually, with two family-level members, *Gemmataceae* and *Isosphaeraceae*, identified as specific keystone taxa in the pollution groups. These bacterial families exhibit robust hydrolytic potential, enabling them to utilize a broad spectrum of organic substances [37,38] and potentially participate in E2 degradation. Therefore, *Planctomycetota* may exhibit higher adaptability, enabling it to play a dominant role under E2 contamination and facilitate the community's recovery towards a relatively stable state by degrading E2.

Moreover, E2 contamination altered the composition of bacterial and archaeal communities. Specifically, E2 significantly increased the relative abundance of *Ellin6067* and *Bryobacter*, with a more pronounced effect observed at higher concentrations. Additionally, high concentrations of E2 notably stimulated the growth of *Pseudolabrys*. *Bryobacter* exhibits chemoheterotrophic activity, enabling it to degrade organic compounds [39,40]. Research by Liu et al. has indicated that *Ellin6067* is capable of degrading organic pollutants [41]. Additionally, *Pseudolabrys* demonstrates strong adaptability to extreme environments [42] and possesses significant potential in removing nitrogen compounds, and degrading organic pollutants like chlorinated alkanes, chlorinated alkenes and benzoic acid [43]. These findings suggest that these three genera may participate in aerobic pathways for E2 degradation in aquatic environments. Overall, following E2 contamination, the relative abundance of bacteria associated with E2 degradation significantly increased, with a more pronounced effect observed at higher E2 concentrations. This indicates that E2 may be degraded by microorganisms as an organic pollutant in the system, thereby impacting bacterial and archaeal community structures.

4.2. Mechanism of 17β-Estradiol in Promoting Methane Emission

Traditionally, CH_4 production was attributed primarily to anaerobic methanogenic archaea. However, evidence accumulated over the past three decades suggests that CH_4 can also be generated in aerobic environments [15,16], a phenomenon termed the "methane paradox". The "methane paradox" has been extensively documented and is considered to contribute significantly to the biogeochemical cycle of CH_4 [44]. Currently, two main perspectives prevail regarding CH_4 production under aerobic conditions: (1) Methanogens can survive in aerobic conditions by utilizing their self-synthesized antioxidant pathways, leading to the production of CH_4 [45,46]. (2) Certain bacteria and fungi can metabolize

methylphosphonic acid under aerobic conditions, producing CH_4 through demethylation processes [20–22].

In the aerobic microecosystems, both the CH_4 emission rate and the structure of the bacterial and archaeal communities were significantly affected within two days after E2 pollution. Therefore, CH_4 emissions may be influenced by changes in the composition of bacterial and archaeal communities. This hypothesis was validated through Redundancy analysis (RDA), as depicted in Figure S3. The Monte Carlo test results indicate that both the CH_4 emission rate and E2 concentration were significantly correlated with the structure of bacterial and archaeal communities ($p < 0.05$) (Table S3). This suggests that E2 has a noteworthy impact on the bacterial and archaeal communities, thereby affecting CH_4 production.

The functional prediction results suggest that E2 increased the relative abundance of the *methanogenesis* functional group. The ASVs assigned to *methanogenesis* belonged to the genus *Methanoregula*. *Methanoregula* are hydrogenotrophic methanogens whose growth is inhibited even under low oxygen levels [47]. Additionally, studies have indicated that small molecular heat shock proteins play a crucial role in tolerating oxidative stress. The absence of these genes resulted in lower oxygen tolerance in *Methanoregula* [48]. Therefore, the presence of *Methanoregula* in the system could be attributed to anaerobic microenvironments created by sediment facilitating their survival. The higher relative abundance of the *methanogenesis* functional group in the pollution groups might suggest that E2 or its metabolites promoted the growth of *Methanoregula*, thus enhancing CH_4 production.

To investigate the correlation between bacteria and CH_4 production in aerobic systems, we utilized a heatmap to visualize the relationship between the relative abundance of the top ten phyla and CH_4 emission rates (Figure 4E). The results demonstrated a significant positive correlation between *Planctomycetota* and CH_4 emission rates. Methylphosphonic acid could be utilized by microorganisms through various pathways, but only the C-P cleavage pathway could release CH_4 [49]. In *Escherichia coli*, the C-P cleavage pathway was encoded by 14 genes *(phnC-phnP*) [50,51]. Zhi et al. [52] found that *Planctomycetota* carried key genes involved in organic phosphonate metabolism, such as *phnM* and *phnI*. Therefore, *Planctomycetota* might have the potential to produce CH_4 from methylphosphonic acid under aerobic conditions. The promoting effect of E2 pollution on the growth of *Planctomycetota* contributed to increased CH_4 production in the system.

The emission of CH_4 is the result of the combined processes of CH_4 production and CH_4 oxidation. The *methanotrophy* functional group, which is capable of consuming CH_4, was enriched in the control group, indicating that the addition of E2 reduced the relative abundance of methanotrophic bacteria in the system, thereby decreasing CH_4 consumption. The ASVs assigned to *methanotrophy* all belonged to *Proteobacteria*, and *Proteobacteria* exhibited a significant negative correlation with CH_4 emission rates (Figure 4E). Additionally, E2 significantly decreased the dominance of *Proteobacteria*. Hence, the inhibitory effect of E2 on methanotrophic bacteria is also a key factor contributing to the higher CH_4 emissions in the pollution groups.

5. Conclusions

In conclusion, E2 contamination significantly disrupted the community structure of bacteria and archaea in aerobic water bodies, leading to a reduction in microbial interactions and a notable increase in the stochasticity of community assembly. This resulted in heightened unpredictability and instability within the communities. Specifically, the most dominant *Proteobacteria* phylum experienced a decline in its advantageous position due to E2 pollution. Conversely, *Planctomycetota* demonstrated a strong adaptability to E2 contamination, as evidenced by a marked increase in relative abundance, and played a crucial role in community recovery. At the genus level, there was a substantial rise in the relative abundance of bacteria associated with E2 degradation, including *Ellin6067*, *Bryobacter*, and *Pseudolabrys*. Furthermore, E2 contamination promoted CH_4 emissions through three pathways: stimulating the growth of *Methanoregula* in anaerobic microenvironments; boosting

the abundance of *Planctomycetota* capable of utilizing methylphosphonate for methane production; and inhibiting the growth of methanotrophic bacteria. This study filled the theoretical gap between E2 metabolism and methane metabolism in aerobic waters and contributed to enriching the ecotoxicological theory of E2.

Supplementary Materials: The following supporting information can be downloaded at: https://www.mdpi.com/article/10.3390/toxics12050373/s1. Figure S1: Zi-Pi plots for each network; Figure S2: Functional group abundance heatmap of bacterial and archaeal communities in different treatment groups on day 2; Figure S3: Redundancy analysis (RDA) of the correlation between ASVs of bacterial and archaeal communities and properties on day 2; Table S1: Topological properties of empirical networks and random networks; Table S2: Taxonomic classification of keystone ASVs; Table S3: Results of Monte Carlo permutation test.

Author Contributions: Z.G.: Conceptualization, Data curation, Formal analysis, Investigation, Methodology, Visualization, Writing—original draft. Y.Z.: Formal analysis, Supervision, Writing—review and editing. Z.L.: Data curation, Visualization. A.R.: Funding acquisition, Supervision, Writing—review and editing, Project administration. All authors have read and agreed to the published version of the manuscript.

Funding: This research was funded by the National Natural Science Foundation of China (42077221). The APC was funded by Zihao Gao.

Institutional Review Board Statement: Not applicable.

Informed Consent Statement: Not applicable.

Data Availability Statement: Raw data have been uploaded to the NCBI SRA database (No. PRJNA1097048).

Acknowledgments: We thank the National Key Laboratory of Water Disaster Prevention for supplying the experimental platform.

Conflicts of Interest: The authors declare no conflicts of interest.

References

1. LaFleur, A.D.; Schug, K.A. A Review of Separation Methods for the Determination of Estrogens and Plastics-Derived Estrogen Mimics from Aqueous Systems. *Anal. Chim. Acta* **2011**, *696*, 6–26. [CrossRef] [PubMed]
2. Nelles, J.L.; Hu, W.-Y.; Prins, G.S. Estrogen Action and Prostate Cancer. *Expert Rev. Endocrinol. Metab.* **2011**, *6*, 437–451. [CrossRef] [PubMed]
3. Li, X.; Liu, X.; Jia, Z.; Wang, T.; Zhang, H. Screening of Estrogenic Endocrine-Disrupting Chemicals in Meat Products Based on the Detection of Vitellogenin by Enzyme-Linked Immunosorbent Assay. *Chemosphere* **2021**, *263*, 128251. [CrossRef] [PubMed]
4. Marlatt, V.L.; Bayen, S.; Castaneda-Cortès, D.; Delbès, G.; Grigorova, P.; Langlois, V.S.; Martyniuk, C.J.; Metcalfe, C.D.; Parent, L.; Rwigemera, A.; et al. Impacts of Endocrine Disrupting Chemicals on Reproduction in Wildlife and Humans. *Environ. Res.* **2022**, *208*, 112584. [CrossRef] [PubMed]
5. Moore, S.C.; Matthews, C.E.; Ou Shu, X.; Yu, K.; Gail, M.H.; Xu, X.; Ji, B.-T.; Chow, W.-H.; Cai, Q.; Li, H.; et al. Endogenous Estrogens, Estrogen Metabolites, and Breast Cancer Risk in Postmenopausal Chinese Women. *JNCI J. Natl. Cancer Inst.* **2016**, *108*, djw103. [CrossRef] [PubMed]
6. Chun, S.; Lee, J.; Radosevich, M.; White, D.; Geyer, R. Influence of Agricultural Antibiotics and 17β-Estradiol on the Microbial Community of Soil. *J. Environ. Sci. Health Part B Pestic. Food Contam. Agric. Wastes* **2006**, *41*, 923–935. [CrossRef] [PubMed]
7. Zhang, X.; Li, Y.; Liu, B.; Wang, J.; Feng, C. The Effects of Estrone and 17β-Estradiol on Microbial Activity and Bacterial Diversity in an Agricultural Soil: Sulfamethoxazole as a Co-Pollutant. *Ecotoxicol. Environ. Saf.* **2014**, *107*, 313–320. [CrossRef]
8. Dong, Z.; Xiao, C.; Zeng, W.; Zhao, J. Impact of 17β-Estradiol on Natural Water's Heterotrophic Nitrifying Bacteria. *GEP* **2020**, *8*, 230–241. [CrossRef]
9. Viancelli, A.; Avalos, D.; Reis, P.; Málaga, P.; Shah, M.; Dwivedi, N.; Michelon, W. The Impact of 17β-Estradiol (E2) on the Growth Profile of Environmental Enterobacteriaceae. *Water Air Soil Pollut.* **2022**, *234*, 20. [CrossRef]
10. Battin, T.J.; Kaplan, L.A.; Findlay, S.; Hopkinson, C.S.; Marti, E.; Packman, A.I.; Newbold, J.D.; Sabater, F. Biophysical Controls on Organic Carbon Fluxes in Fluvial Networks. *Nat. Geosci.* **2008**, *1*, 95–100. [CrossRef]
11. Liu, Y.; Zhang, J.; Zhao, L.; Zhang, X.; Xie, S. Spatial Distribution of Bacterial Communities in High-Altitude Freshwater Wetland Sediment. *Limnology* **2014**, *15*, 249–256. [CrossRef]
12. Sun, H.; Yu, R.; Liu, X.; Cao, Z.; Li, X.; Zhang, Z.; Wang, J.; Zhuang, S.; Ge, Z.; Zhang, L.; et al. Drivers of Spatial and Seasonal Variations of CO2 and CH4 Fluxes at the Sediment Water Interface in a Shallow Eutrophic Lake. *Water Res.* **2022**, *222*, 118916. [CrossRef] [PubMed]

13. Gao, J.; Xie, D.; Cao, L.; Zhao, Z.; Zhou, J.; Liao, W.; Xu, X.; Wang, Q.; He, F. The Ratio but Not Individual of Fragile to Refractory DOM Affects Greenhouse Gases Release in Different Trophic Level Lakes. *J. Environ. Manag.* **2024**, *351*, 119914. [CrossRef] [PubMed]
14. Descy, J.-P.; Darchambeau, F.; Schmid, M. Lake Kivu: Past and Present. In *Lake Kivu: Limnology and Biogeochemistry of a Tropical Great Lake*; Descy, J.-P., Darchambeau, F., Schmid, M., Eds.; Springer: Dordrecht, The Netherlands, 2012; pp. 1–11. ISBN 978-94-007-4243-7.
15. Bizic, M. Phytoplankton Photosynthesis: An Unexplored Source of Biogenic Methane Emission from Oxic Environments. *J. Plankton Res.* **2021**, *43*, 822–830. [CrossRef]
16. Tang, K.W.; McGinnis, D.F.; Ionescu, D.; Grossart, H.-P. Methane Production in Oxic Lake Waters Potentially Increases Aquatic Methane Flux to Air. *Environ. Sci. Technol. Lett.* **2016**, *3*, 227–233. [CrossRef]
17. Ditchfield, A.; Wilson, S.; Hart, M.; Purdy, K.; Green, D.; Hatton, A. Identification of Putative Methylotrophic and Hydrogenotrophic Methanogens within Sedimenting Material and Copepod Faecal Pellets. *Aquat. Microb. Ecol.* **2012**, *67*, 151–160. [CrossRef]
18. Bianchi, M.; Marty, D.; Teyssie, J.-L.; Fowler, S. Strictly Aerobic and Anaerobic Bacteria Associated with Sinking Particulate Matter and Zooplankton Fecal Pellets. *Mar. Ecol. Prog. Ser.* **1992**, *88*, 55–60. [CrossRef]
19. Oremland, R.S. Methanogenic Activity in Plankton Samples and Fish Intestines A Mechanism for in Situ Methanogenesis in Oceanic Surface Waters. *Limnol. Oceanogr.* **1979**, *24*, 1136–1141. [CrossRef]
20. Wang, Q.; Dore, J.E.; McDermott, T.R. Methylphosphonate Metabolism by *Pseudomonas* Sp. Populations Contributes to the Methane Oversaturation Paradox in an Oxic Freshwater Lake. *Environ. Microbiol.* **2017**, *19*, 2366–2378. [CrossRef]
21. Yao, M.; Henny, C.; Maresca, J.A. Freshwater Bacteria Release Methane as a By-Product of Phosphorus Acquisition. *Appl. Environ. Microbiol.* **2016**, *82*, 6994–7003. [CrossRef]
22. Repeta, D.J.; Ferrón, S.; Sosa, O.A.; Johnson, C.G.; Repeta, L.D.; Acker, M.; DeLong, E.F.; Karl, D.M. Marine Methane Paradox Explained by Bacterial Degradation of Dissolved Organic Matter. *Nat. Geosci.* **2016**, *9*, 884–887. [CrossRef]
23. Ruan, A.; Zhao, Y.; Liu, C.; Wang, Y.; Xie, X. Effect of Low Concentration 17β-Estradiol on the Emissions of CH4 and CO2 in Anaerobic Sediments. *Environ. Toxicol. Chem.* **2013**, *32*, 2672–2677. [CrossRef] [PubMed]
24. Ruan, A.; Liu, C.; Zhao, Y.; Zong, F.; Jiang, S.; Yu, Z. Effects of 17β-Estradiol on Typical Greenhouse Gas Emissions in Aquatic Anaerobic Ecosystem. *Water Sci. Technol.* **2015**, *71*, 1815–1822. [CrossRef] [PubMed]
25. Ruan, A.; Zhao, Y.; Liu, C.; Zong, F.; Yu, Z. Effects of 17β-Estradiol on Emissions of Greenhouse Gases in Simulative Natural Water Body. *Environ. Toxicol. Chem.* **2015**, *34*, 977–982. [CrossRef] [PubMed]
26. Callahan, B.J.; McMurdie, P.J.; Rosen, M.J.; Han, A.W.; Johnson, A.J.A.; Holmes, S.P. DADA2: High-Resolution Sample Inference from Illumina Amplicon Data. *Nat. Methods* **2016**, *13*, 581–583. [CrossRef] [PubMed]
27. Bolyen, E.; Rideout, J.R.; Dillon, M.R.; Bokulich, N.A.; Abnet, C.C.; Al-Ghalith, G.A.; Alexander, H.; Alm, E.J.; Arumugam, M.; Asnicar, F.; et al. Reproducible, Interactive, Scalable and Extensible Microbiome Data Science Using QIIME 2. *Nat. Biotechnol.* **2019**, *37*, 852–857. [CrossRef] [PubMed]
28. Quast, C.; Pruesse, E.; Yilmaz, P.; Gerken, J.; Schweer, T.; Yarza, P.; Peplies, J.; Glöckner, F.O. The SILVA Ribosomal RNA Gene Database Project: Improved Data Processing and Web-Based Tools. *Nucleic Acids Res.* **2013**, *41*, D590–D596. [CrossRef] [PubMed]
29. Gower, J.C. Some Distance Properties of Latent Root and Vector Methods Used in Multivariate Analysis. *Biometrika* **1966**, *53*, 325–338. [CrossRef]
30. Ning, D.; Yuan, M.; Wu, L.; Zhang, Y.; Guo, X.; Zhou, X.; Yang, Y.; Arkin, A.P.; Firestone, M.K.; Zhou, J. A Quantitative Framework Reveals Ecological Drivers of Grassland Microbial Community Assembly in Response to Warming. *Nat. Commun.* **2020**, *11*, 4717. [CrossRef]
31. Feng, K.; Peng, X.; Zhang, Z.; Gu, S.; He, Q.; Shen, W.; Wang, Z.; Wang, D.; Hu, Q.; Li, Y.; et al. iNAP: An Integrated Network Analysis Pipeline for Microbiome Studies. *iMeta* **2022**, *1*, e13. [CrossRef]
32. Louca, S.; Parfrey, L.W.; Doebeli, M. Decoupling Function and Taxonomy in the Global Ocean Microbiome. *Science* **2016**, *353*, 1272–1277. [CrossRef] [PubMed]
33. Olesen, J.M.; Bascompte, J.; Dupont, Y.L.; Jordano, P. The Modularity of Pollination Networks. *Proc. Natl. Acad. Sci. USA* **2007**, *104*, 19891–19896. [CrossRef] [PubMed]
34. Hu, Q.; Tan, L.; Gu, S.; Xiao, Y.; Xiong, X.; Zeng, W.; Feng, K.; Wei, Z.; Deng, Y. Network Analysis Infers the Wilt Pathogen Invasion Associated with Non-Detrimental Bacteria. *npj Biofilms Microbiomes* **2020**, *6*, 8. [CrossRef] [PubMed]
35. Feng, Y.; Chen, R.; Stegen, J.C.; Guo, Z.; Zhang, J.; Li, Z.; Lin, X. Two Key Features Influencing Community Assembly Processes at Regional Scale: Initial State and Degree of Change in Environmental Conditions. *Mol. Ecol.* **2018**, *27*, 5238–5251. [CrossRef] [PubMed]
36. Yuan, M.M.; Guo, X.; Wu, L.; Zhang, Y.; Xiao, N.; Ning, D.; Shi, Z.; Zhou, X.; Wu, L.; Yang, Y.; et al. Climate Warming Enhances Microbial Network Complexity and Stability. *Nat. Clim. Change* **2021**, *11*, 343–348. [CrossRef]
37. Ivanova, A.A.; Naumoff, D.G.; Kulichevskaya, I.S.; Meshcheriakova, A.A.; Dedysh, S.N. Paludisphaera Mucosa Sp. Nov., a Novel Planctomycete of the Family Isosphaeraceae from a Boreal Fen. *Microbiology* **2023**, *92*, 483–492. [CrossRef]
38. Rakitin, A.L.; Naumoff, D.G.; Beletsky, A.V.; Kulichevskaya, I.S.; Mardanov, A.V.; Ravin, N.V.; Dedysh, S.N. Complete Genome Sequence of the Cellulolytic Planctomycete Telmatocola Sphagniphila SP2T and Characterization of the First Cellulolytic Enzyme from Planctomycetes. *Syst. Appl. Microbiol.* **2021**, *44*, 126276. [CrossRef]

39. Li, Q.; Zhang, D.; Zhang, J.; Zhou, Z.; Pan, Y.; Yang, Z.; Zhu, J.; Liu, Y.; Zhang, L. Crop Rotations Increased Soil Ecosystem Multifunctionality by Improving Keystone Taxa and Soil Properties in Potatoes. *Front. Microbiol.* **2023**, *14*, 1034761. [CrossRef]
40. Pertile, M.; Sousa, R.M.S.; Mendes, L.W.; Antunes, J.E.L.; Oliveira, L.M.D.S.; De Araujo, F.F.; Melo, V.M.M.; Araujo, A.S.F. Response of Soil Bacterial Communities to the Application of the Herbicides Imazethapyr and Flumyzin. *Eur. J. Soil Biol.* **2021**, *102*, 103252. [CrossRef]
41. Liu, C.; Han, Y.; Teng, C.; Ma, H.; Tao, B.; Yang, F. Residue Dynamics of Florpyrauxifen-Benzyl and Its Effects on Bacterial Community Structure in Paddy Soil of Northeast China. *Ecotoxicol. Environ. Saf.* **2023**, *249*, 114390. [CrossRef]
42. Zhang, M.; Liang, G.; Ren, S.; Li, L.; Li, C.; Li, Y.; Yu, X.; Yin, Y.; Liu, T.; Liu, X. Responses of Soil Microbial Community Structure, Potential Ecological Functions, and Soil Physicochemical Properties to Different Cultivation Patterns in Cucumber. *Geoderma* **2023**, *429*, 116237. [CrossRef]
43. Manucharova, N.A.; Bolshakova, M.A.; Babich, T.L.; Tourova, T.P.; Semenova, E.M.; Yanovich, A.S.; Poltaraus, A.B.; Stepanov, A.L.; Nazina, T.N. Microbial Degraders of Petroleum and Polycyclic Aromatic Hydrocarbons from Sod-Podzolic Soil. *Microbiology* **2021**, *90*, 743–753. [CrossRef]
44. Wang, Q.; Alowaifeer, A.; Kerner, P.; Balasubramanian, N.; Patterson, A.; Christian, W.; Tarver, A.; Dore, J.E.; Hatzenpichler, R.; Bothner, B.; et al. Aerobic Bacterial Methane Synthesis. *Proc. Natl. Acad. Sci. USA* **2021**, *118*, e2019229118. [CrossRef] [PubMed]
45. Bogard, M.J.; Del Giorgio, P.A.; Boutet, L.; Chaves, M.C.G.; Prairie, Y.T.; Merante, A.; Derry, A.M. Oxic Water Column Methanogenesis as a Major Component of Aquatic CH4 Fluxes. *Nat. Commun.* **2014**, *5*, 5350. [CrossRef] [PubMed]
46. Angle, J.C.; Morin, T.H.; Solden, L.M.; Narrowe, A.B.; Smith, G.J.; Borton, M.A.; Rey-Sanchez, C.; Daly, R.A.; Mirfenderesgi, G.; Hoyt, D.W.; et al. Methanogenesis in Oxygenated Soils Is a Substantial Fraction of Wetland Methane Emissions. *Nat. Commun.* **2017**, *8*, 1567. [CrossRef] [PubMed]
47. Yashiro, Y.; Sakai, S.; Ehara, M.; Miyazaki, M.; Yamaguchi, T.; Imachi, H. Methanoregula Formicica Sp. Nov., a Methane-Producing Archaeon Isolated from Methanogenic Sludge. *Int. J. Syst. Evol. Microbiol.* **2011**, *61*, 53–59. [CrossRef]
48. Kwon, M.J.; Tripathi, B.M.; Göckede, M.; Shin, S.C.; Myeong, N.R.; Lee, Y.K.; Kim, M. Disproportionate Microbial Responses to Decadal Drainage on a Siberian Floodplain. *Glob. Change Biol.* **2021**, *27*, 5124–5140. [CrossRef] [PubMed]
49. Karl, D.M.; Beversdorf, L.; Björkman, K.M.; Church, M.J.; Martinez, A.; Delong, E.F. Aerobic Production of Methane in the Sea. *Nat. Geosci.* **2008**, *1*, 473–478. [CrossRef]
50. Huang, J.; Su, Z.; Xu, Y. The Evolution of Microbial Phosphonate Degradative Pathways. *J. Mol. Evol.* **2005**, *61*, 682–690. [CrossRef]
51. White, A.K.; Metcalf, W.W. Microbial Metabolism of Reduced Phosphorus Compounds. *Annu. Rev. Microbiol.* **2007**, *61*, 379–400. [CrossRef]
52. Zhi, R.; Deng, J.; Xu, Y.; Xu, M.; Zhang, S.; Han, X.; Yang, G.; Ren, C. Altered Microbial P Cycling Genes Drive P Availability in Soil after Afforestation. *J. Environ. Manag.* **2023**, *328*, 116998. [CrossRef] [PubMed]

toxics

MDPI

Review

Methods Using Marine Aquatic Photoautotrophs along the Qatari Coastline to Remediate Oil and Gas Industrial Water

Roda F. Al-Thani and Bassam T. Yasseen *,†

Department of Biological and Environmental Sciences, College of Arts and Sciences, Qatar University, Doha P.O. Box 2713, Qatar; ralthani@qu.edu.qa

* Correspondence: qumcc@qu.edu.qa; Tel.: +44-7505901992

† Current address: Independent Researcher, 8 James Court, Dunstable Road, Luton LU4 0HN, UK.

Abstract: Qatar and other Gulf States have a diverse range of marine vegetation that is adapted to the stressful environmental conditions of seawater. The industrial wastewater produced by oil and gas activities adds further detrimental conditions for marine aquatic photosynthetic organisms on the Qatari coastlines. Thus, these organisms experience severe stress from both seawater and industrial wastewater. This review discusses the biodiversity in seawater around Qatar, as well as remediation methods and metabolic pathways to reduce the negative impacts of heavy metals and petroleum hydrocarbons produced during these activities. The role of microorganisms that are adjacent to or associated with these aquatic marine organisms is discussed. Exudates that are released by plant roots enhance the role of microorganisms to degrade organic pollutants and immobilize heavy metals. Seaweeds may have other roles such as biosorption and nutrient uptake of extra essential elements to avoid or reduce eutrophication in marine environments. Special attention is paid to mangrove forests and their roles in remediating shores polluted by industrial wastewater. Seagrasses (*Halodule uninervis*, *Halophila ovalis*, and *Thalassia hemprichii*) can be used as promising candidates for phytoremediation or bioindicators for pollution status. Some genera among seaweeds that have proven efficient in accumulating the most common heavy metals found in gas activities and biodegradation of petroleum hydrocarbons are discussed.

Keywords: heavy metals; macroalgae; mangrove; microorganisms; phycoremediation; seagrasses; seaweeds

1. Introduction

The State of Qatar is on a peninsula located on the north-eastern coast of the Arabian Peninsula. It extends from the Arabian Desert as an outcrop in the Western Arabian Gulf in an area that is warm and humid, although the land area is arid or semi-arid and highly saline. Hence, this part of the Arabian Gulf and the marine vegetation are influenced by warm waters and the high salinity of the seawater of the Gulf. The common type of landscape comprises rocky desert, depressions, and salt marshes, and in general, it is flat to undulating. Seawater surrounds the Qatari peninsula except at the southern part, which borders the Kingdom of Saudi Arabia.

The Qatari peninsula and other Gulf States have a diverse range of marine vegetation, and the seawater is rich in many species of marine organisms that are adapted to the unique environmental conditions of the region [1]. In general, the marine aquatic photoautotrophs include higher plants, algae (micro- and macro-algae), fungi, and bacteria. Notably, the prominent marine vegetation found at the coastline of the peninsula includes (1) mangrove plants and associated microorganisms, (2) seagrasses, (3) seaweeds, and (4) phytoplankton. During the last decades, many reports have discussed the mechanisms of bioremediation, phytoremediation, and phycoremediation using various types of bacteria, fungi, algae, and plants in Qatari ecosystems. This review discusses the biodiversity in seawater around

Qatar, as well as remediation methods and metabolic pathways to reduce the negative impacts of heavy metals and petroleum hydrocarbons produced during these activities.

2. Metabolic Reactions and Modern Biotechnology

Van Aken et al. [2] examined the uptake of organic compounds that result from anthropogenic and industrial oil and gas activities. These compounds are classified in different ways. For example, Kamath et al. [3] classified petroleum hydrocarbons using two main groups: (1) gasoline range organics (GROs) and (2) diesel range organics (DROs). GROs include mono-aromatic hydrocarbons such as benzene, toluene, ethylbenzene, and xylenes (BTEX), as well as short-chain alkanes (C6-C10), while DROs include longer-chain alkanes (C10-C40) and hydrophobic chemicals such as polycyclic aromatic hydrocarbons (PAHs). Wang et al. [4] classified petroleum hydrocarbons as follows: (1) n-alkanes, (2) iso-alkanes, (3) cycloalkanes, and (4) aromatics. The most biodegradable groups among petroleum hydrocarbons are n-alkanes (saturated hydrocarbons, C_nH_{2n+2}). Other chemical compounds have also been reported as organic pollutants in soils and waters, including 1,1,1-trichloro-2–2-bis-(4′-chlorophenyl) ethane (DDT), benzo[α] pyrene, pesticides, chlorinated solvents, explosives, PAHs, dioxins, and polychlorinated biphenyls (PCBs) [5–9].

Notably, not many plants are able to metabolize these compounds, as their actions on them are limited. Thus, large-scale degradation is not possible unless microorganisms actively contribute to these reactions. Catabolic enzymes that can achieve complete metabolism of these compounds in plants are either inefficient or unavailable. Partial degradation of these compounds could result in some organic components that can be stored in the vacuoles of these plants [4,10]. Reports have described some metabolic reactions of the degradation of petroleum hydrocarbons. The degradation of n-alkanes could lead to some useful metabolites such as acetyl-Co A and fumaric acid, which readily contribute to Krebs-cycle reactions, fatty-acid biosynthesis, and amino-acid interconversions. These reactions are considered as crucial events in plant metabolic pathways because they convert dangerous toxic compounds to useful metabolites.

Complete degradation of petroleum hydrocarbons is affected by many factors, including environmental conditions, the cooperation between plants and their associated microorganisms, and the expression of genetic materials in the soil–microbe–plant system. During the last decade, numerous studies have discussed the impact of these factors on the degradation of pollutants produced by oil and gas activities. For example, Gkorezis et al. [11] examined plant-associated bacteria systems in detail to phytoremediate petroleum hydrocarbons and restore polluted sites. They attributed the ability of bacteria to degrade petroleum hydrocarbons to genes that control the productions of enzymes that catalyze and enhance the biodegradation processes. The cooperation between bacteria and plants is decisive in achieving complete metabolism of petroleum hydrocarbons as plants provide some exudates, while bacteria synthesize plant hormones while suppressing ethylene production and the mobilization of essential elements.

Many studies have discussed the impact of environmental factors on the degradation of these compounds. The optimum temperatures may vary according to the microbial species and the compound being biodegraded [12], while pH affects the microbial growth and enzyme activity that control the biodegradation of petroleum hydrocarbons. Furthermore, these reactions have different pH optima for growth and degradation [13], and biodegradation rates may decrease under alkaline conditions [14].

Nutrient availability is another factor that might affect the growth of bacteria. Essential elements such as nitrogen, phosphorus, and some trace elements are reported to have great impact on the degradation speed and can result in complete or partial degradation [15,16] Oxygen is also a limiting factor, especially in anaerobic environments. As most biodegradation processes are aerobic, oxygen is required for microbial metabolism [17]. Adequate moisture is also necessary for microbial growth and activity, and extreme moisture content can inhibit the process of biodegradation [18].

Microbial activity is negatively affected by salinity. Some halophilic bacteria that are recognized in Qatari sabkhas could be biologically active in such habitats. These bacteria perform various roles and activities in supporting native plants to resist salinity and have applications in biotechnology and the pharmaceutical industry, as well as the production of some useful compatible solutes [9,19–23]. Another factor is the composition of petroleum hydrocarbons. High concentrations can cause some toxicity to the microbial activity and could lead to a great reduction in the rate of biodegradation. Moreover, some other organic components are added during oil and gas activities, such as mono-, di-, and tri-ethylene glycol (MEG, DEG, and TEG, respectively) and kinetic hydrate inhibitors (KHIs). These compounds are present in the wastewater and might have negative impacts on the growth of plants when they are irrigated with such wastewater [10,21,24–26].

The internal factors in the soil biota might play important roles in the biodegradation of organic pollutants and stabilization of inorganic components such as heavy metals. These factors encompass the cooperation between plants and their associated microorganisms and the genetic features of these living organisms. In this respect, native plants or algae (as autotrophic living organisms) might play roles that are independent of the microorganisms' actions, but in nature, it is difficult to separate the impact of plants from their associated microorganisms in degrading petroleum hydrocarbons. These microorganisms include rhizospheric, phyllospheric, and endophytic bacteria and fungi that interact with the secretions of plants.

Many native plants secrete and release substances into the rhizosphere, and these exudates may help in encouraging microorganisms to degrade organic compounds of various types, as well as stabilizing heavy metals in the soil adjacent to the root systems of plants. Some interrelated activities and conditions take place at the rhizosphere. For example, plant roots exude various substances that can stimulate microbial growth and activity, and the microbes can degrade various toxic organic compounds completely or partially [21,27,28].

Furthermore, some plants absorb these organic compounds, and inside the plant tissues, these compounds might be further degraded into useful metabolites. Otherwise, toxic compounds are stored in the vacuoles to avoid their detrimental impacts on the plant metabolism [10,21,29]. Plants or microorganisms alone are also less efficient in metabolizing organic compounds than when they work together [30]. Thus, microbes play crucial roles in alleviating the impact of organic contaminants on the plant and human health by degrading toxic organic compounds into less toxic or into useful metabolites that can be absorbed by the plant and contribute to the metabolic pathways [21,31].

Plants and microorganisms cannot work alone in bio-transforming complex organic compounds of industrial wastewater into simpler units. Numerous studies have confirmed the active cooperation between plants and their associated and/or adjacent microorganisms, as such a combination could provide some resistance against various environmental conditions, including pollution. Notably, plant roots release various substances such as exudates, secretions, lysates, plant mucilage, and mucigel that might have significant roles in remediation of extreme environmental conditions such as pollutions [22]. Moreover, the work of Alves et al. [32] confirmed the role of the microorganisms associated with plants in immobilization of heavy metals. Some successful studies have elucidated the influence of separation of plants from associated microorganisms using hydroponic systems, sterile plant roots, and inoculating some bacteria to remove organic compounds such as phenol [33].

There are many possibilities of such relationships. Symbiotic relationships with microorganisms such as mycorrhizal fungi and nitrogen-fixing bacteria can support the plant's ability to transform contaminants [34]. Relationships may also be synergistic. For example, certain microbes can break down complex organic contaminants into simpler compounds that can be absorbed readily and metabolized inside plant tissues [35,36]. Plants and microorganisms also produce enzymes that can degrade petroleum hydrocarbons, but these groups of enzymes are different, and distinguishing between plant-derived

enzymes and microbial enzymes is very difficult unless advanced molecular techniques are used [4,37–42].

Plants can also enhance microbial activity by adding some nutrients that stimulate indigenous microbes or introduce specific microorganisms. This situation further complicates the attribution of each group of living organisms alone in the degradation of petroleum hydrocarbons. Sterile conditions may be exploited by designing experiments to distinguish the role of plants from microorganisms separately. Using sterile hydroponic systems for plant growth to avoid the interference of associated microorganisms can solve the issue of the difficulty of separating the effects of each group alone. Furthermore, the isolation of a pure culture of a microorganism can be used to test the ability of each microbial species to transform organic petroleum hydrocarbons into simpler compounds [33,43].

3. Genetic Factors and Modern Biotechnology

The genetic factors involved in the bioremediation of petroleum hydrocarbons cover a wide range of aspects involving different microbial communities, genetic adaptation, and the expression of genes involved [4,44]. Many microorganisms contain genes that control the degradation of petroleum hydrocarbons [45], and numerous microorganisms (bacteria and fungi) in Qatari soils are activated when irrigated with industrial wastewater and its various components. During the last decade, studies have identified many microorganisms in Qatari lands and seawater of the Arabian Gulf. For example, Al-Sulaiti et al. [25] identified many bacteria and fungi species using modern techniques, the VITEK system (bioMerieux-Vitek, Hazelwood, MO, USA) and the API 20 C AUX identification system (REF 20 210 of bioMerieux SA) for bacteria and fungi (yeast), respectively. Bacteria species included (1) *Staphylococcus* spp. such as *Staphylococcus sciuri* and *Staphylococcus lentus*; (2) *Lactococcus lactis;* (3) *Micrococcus luteus;* (4) *Kocuria kristinae;* (5) *Bacillus megaterium;* (6) *Pseudomonas* spp. such as *Pseudomonas aeruginosa*, *Pseudomonas stutzeri,* and *Pseudomonas putida*; (7) *Stenotrophomonas maltophilia;* (8) *Sphingomonas paucimobilis*; (9) *Burkholderia* spp. such as *Burkholderia cepacia* and *Burkholderia pseudomallei*; and (10) *Enterobacter cloacae*. Soils exposed to various changes in their compositions, abiotic factors, and biotic factors, including petroleum hydrocarbon pollution from oil and gas activities, might activate these species and others, such as *Bacillus* spp., *Pseudomonas geniculata,* and *Achromobacter xylosoxidans* [21,46,47].

Yeast species that were identified in such soils showed changes under the same conditions facing bacteria. The following yeast species were the most common in all soil and sand cultures: (1) *Candida* spp. such as *Candida tropicalis*, *Candida famata,* and *Candida guilliermondii*; (2) *Trichosporon mucoides*; and (3) *Cryptococcus* spp. such as *Cryptococcus humicola* and *Cryptococcus albidus*. These microorganisms could contribute to activities in the soil biota in Qatari lands, especially when polluted with industrial wastewater. Therefore, microorganisms might be promoted to play significant roles in the polluted soil, but the conditions of seawater from the Arabian Gulf are completely different from those of the lands. It is very difficult to distinguish the influence of microorganisms (bacteria and fungi) from that of seaweed, seagrass, and phytoplankton.

Findings suggest that such activation of microorganisms to degrade spilled petroleum hydrocarbons might occur in seawater as well. Using modern biotechnology and phylogenetic analysis, numerous bacteria species have been identified, including Proteobacteria (*Cobetia marina*, *Halobacillus profundi*, *Pseudoalteromonas agarivorans*, *Pseudoalteromonas piscicida*, *Pseudoalteromonas rubra*, *Pseudoalteromonas prydzensis*, *Ruegeria mobilis*, *Shewanella loihica*, *Virgibacillus dokdonensis*, *Vibrio harveyi*, *Vibrio nereis*, *Vibrio nigripulchritudo*, *Vibrio parahaemolyticus*), Cytophaga–Flavobacterium–Bacteroides (CFB) bacteria (*Tenacibaculum mesophilum*), and Firmicutes (GC) (*Bacillus boroniphilus*) [48]. Infectious *Vibrio* bacteria species have also been recognized and investigated in terms of their roles [22,49,50].

Microorganisms of marine sediments contribute significantly to the functions related to the degradation of organic compounds of anthropogenic and industrial origin [51,52]. Notably, few works and baseline investigations have examined the potential of microorgan-

isms to degrade industrial wastewater pollution in the seawater of the Arabian Gulf since few comparisons have been made between ecosystems, especially regarding the microbial ecology and functions in the marine sediments surrounding the Qatari peninsula. However, microbial communities either decrease or increase in response to pollution with petroleum hydrocarbons from industrial wastewater [53].

Regarding solutions to the environmental issues, three strategies have been suggested and applied during the last four decades to improve the efficiency of living organisms to restore polluted soil and water, including plants, algae, and microorganisms. These strategies are environmental, genetic, and biological approaches. Environmental manipulation has been adopted earlier for the reclamation of saline lands and to remove toxic ions from agricultural lands. However, the environmental approaches have many drawbacks and are not always an applicable option, especially for seawater [54].

Genetic approaches have been suggested as promising options to solve many biotic and abiotic problems [21,55]. Modern biotechnology and genetic engineering programs have been considered as future solutions for many problems related to agriculture, health, economy, and pollution. Modern biotechnological and biological options could be applied together to solve many pollution issues. For example, transgenic plants and microorganisms might be more efficient in the de-toxification of pollutants, remediation of heavy metals, and metabolism of petroleum hydrocarbons [21,54,56–60].

4. Mangrove Plants and Associated Microorganisms

Mangrove forests are found on the eastern and north-eastern coastlines of Qatar, with large stands in Al-Dhakhira, Fewairet, Al-Reweis, Al-Khor, and Al-Wakra (Figure 1). These forests cover an area of about 981 ha and represent most of the existing stands in Qatar [61]. Only one species, *Avicennia marina*, is represented in the mangrove forests in Qatar. This species is internationally known as grey mangrove and is an evergreen dark green tree or shrub that does not exceed 4 m in height. It also produces propagules (Figure 2) and a cable network of breathing roots called pneumatophores (Figure S1).

Notably, mangrove forests are common at muddy shorelines, especially along the north-central parts of the eastern coastline in the tidal zones. These forests were the main source of wood and camel fodder in the past, but currently, they are semi-protected as a result of extensive camel grazing. Many studies have examined the ecophysiology of the plants in this area and the structural features that enable them to resist the high salinity levels of the seawater.

The mangrove forests have several important roles in the ecosystem, such as reducing erosion on the coastlines. Karimi et al. [62] have discussed the role of *A. marina* in stabilizing the coastline by trapping sediments with its extensive root system, which reduces erosion caused by waves and tidal action. Another role is the conservation of marine and terrestrial species, which include fish and crustaceans, as well as providing nesting sites for birds and feeding numerous organisms [63].

The mangrove forests also support the biodiversity of various plant and animal species by providing shelter, food, and mini-habitats for breeding for various organisms such as fish species [64]. They also improve water quality by acting as natural filters. This is accomplished by many methods, such as trapping of organic and inorganic pollutants and sediment from runoff and allowing them to settle to the bottom of the sea, as well as absorbing nutrients and removing contaminants from the seawater. These two methods help to make the marine environment safer and healthier [65,66].

The mangrove forests also function as carbon sinks, and many studies have shown that they are efficient in sequestering CO_2 from the atmosphere. This occurs through the storage of large amounts of carbon in biomass and the soil beneath the mangrove trees. Thus, mangroves could help to mitigate climate change [67]. Furthermore, they provide protection against storms, which helps coastal communities. The forests act as a natural barrier that protects inland areas from flooding and property damage during waves of storms, hurricanes, and other extreme weather events [68].

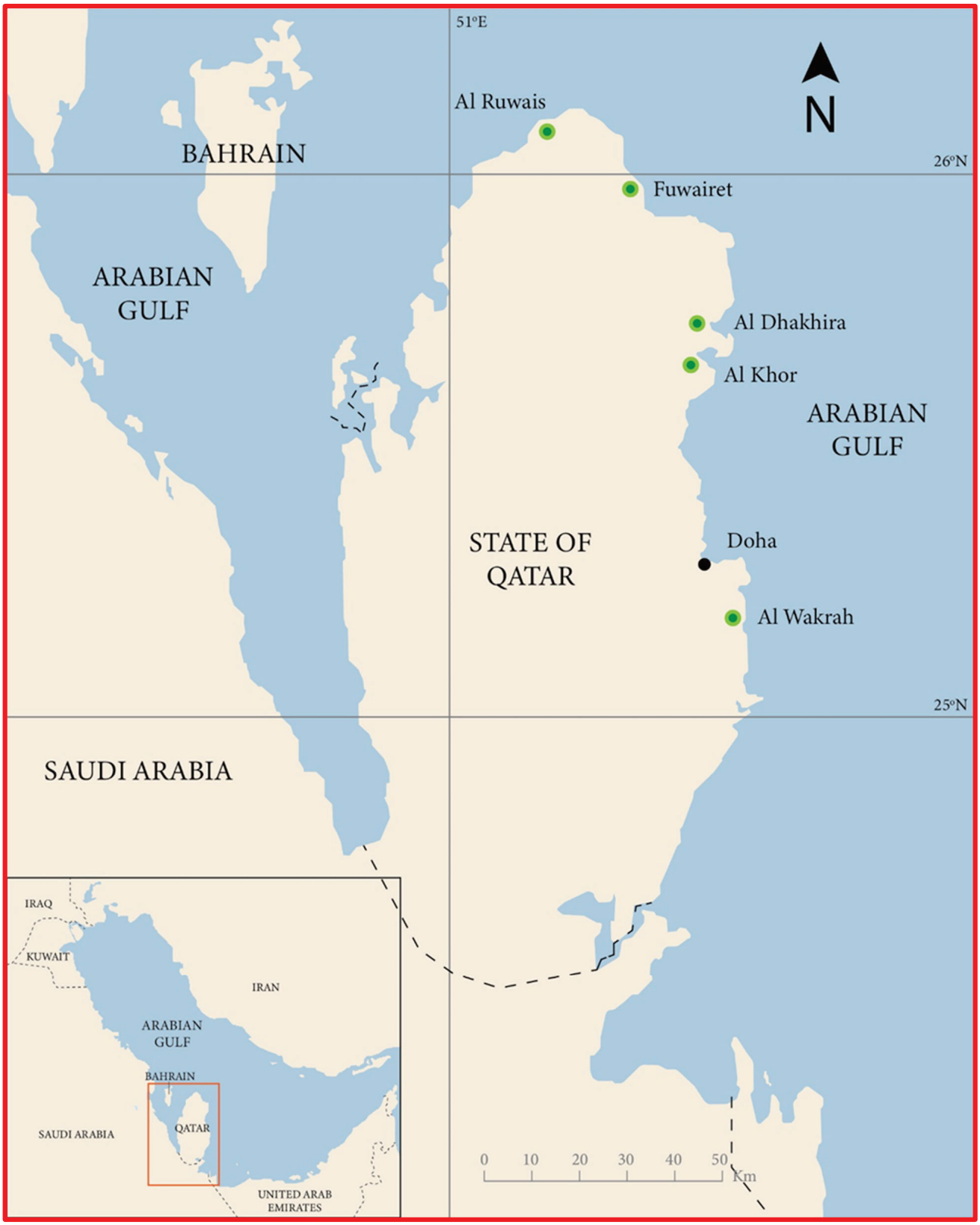

Figure 1. Map of Qatar showing the locations of mangrove forests on the eastern coastline.

Figure 2. *Avicennia marina* is the only species represented in mangroves in Qatar. A part of a mangrove forest showing trees and propagules.

Lastly, *A. marina* has economic value and can be used as a medicinal plant. It provides many advantages to the local communities, including fishing, tourism, and protection of shorelines, as discussed above. It has edible seeds for humans with high amounts of vitamins and carbohydrates, and its leaves are edible and preferred for cattle and camels. Some of its organic components, such as betulic acid, taraxerol, and taraxerone [69], as well as other sterol components, could make it beneficial as a medicinal plant for numerous health applications, including smallpox, aphrodisiacs, poultices, and accelerated suppuration of boils and abscesses [70,71].

4.1. Phytoremediation

In general, the ability of native plants to remediate polluted soils and waters is limited by different factors, including environmental and genetic factors. However, many reports have shown some success in absorption, translocation, sequestration, and degradation of petroleum hydrocarbons [72]. Numerous elements (including heavy metals such as As, Cd, Co, Cr, Cs, Cu, Fe, Hg, Mn, Ni, Pb, and Zn) have been reported to be remediated by Qatari native plants by different methods [10,21,73,74] (Table S1). However, the remediation of organic components has been a main concern of scientists and research centers, as very little has been accomplished to show the degradation of organic components from oil and gas industrial activities by Qatari native plants (Table S2). Some native flora of Qatar have proven efficient in remediating industrial wastewater produced during anthropogenic and industrial activities, such as *Phragmites australis*, *Typha domingensis*, *Sporobolus* spp., *Medicago* spp., and possibly others [10,25]. More data can be found in more supplementary articles which include tables (Tables S3 and S4).

Wild mangrove plants could be promising candidates for phytoremediation and phytomanagement due to high biomass production and their adaptation to seawater. Particularly, *A. marina* has proven efficient in phytoremediation. Many studies from around the world in the last 20 years has confirmed this, and various related plant species can remove and remediate heavy metals and organic petroleum hydrocarbons. These plants and their associated microorganisms can efficiently remove heavy metals and metabolize organic

petroleum hydrocarbons [75–77]. Early reports by Abdel-Bari et al. [78] found that *A. marina* from the eastern coast of Qatar (Ras Al-Matbakh) accumulated many heavy metals, such as Co, Cr, Cu, Fe, Ni, and Zn. Moreira et al. [75] found that *Avicennia schaueriana* is more efficient in the phytoremediation of petroleum hydrocarbons than microorganisms in benthal sediments. Such findings show that phytoremediation using mangrove plants is a promising strategy for coastlines impacted by wastewaters from the oil and gas industry.

In addition, the growth of microorganisms in the sediments might be stimulated by secretions produced by these plants, which facilitates degradation of organic components of petroleum hydrocarbons and leads to useful metabolic compounds [10,21,26]. Furthermore, interestingly, Moradi et al. [79] found that the activity of peroxidases such as ascorbate peroxidase and polyphenol oxidase increased in soil contaminated with organic components of oil, while superoxide dismutase decreased. These findings suggest that mangrove plants such as *A. marina* are promising candidates for phytoremediation of oil spills and residual oil pollution in coastal marine environments.

Modern technologies can be adopted and applied to improve the ability of these plants to degrade, metabolize, and accumulate petroleum hydrocarbons and heavy metals in plant tissues [80]. Moreover, modern biotechnology and genetic engineering could be used to develop active remediators to deal with various types of pollutants [21,26,60,81]. Worldwide records show that mangrove forests provide numerous supports to the ecosystem, and these reports cover many methods of phytoremediation where microorganisms work together with these plants [59,76,82]. These methods include (1) phytoextraction, (2) phytostabilization, (3) phytodegradation, (4) phytovolatilization, and (5) rhizofiltration [59,74,83,84].

To use such plants in phytoremediation processes, monitoring would be necessary to keep the ecosystem safe. The plant biomass can be recycled or used in industry to extract heavy metals [10,21]. The research performed thus far could be a source of information and experimental material for further research to increase the efficiency of these plants in remediating polluted soils and waters in the Arabian Gulf region.

Recent reports have discussed the related metabolic pathways [4,10,21] of native plants and crops that can absorb harmful petroleum hydrocarbons from contaminated soils and aquatic habitats [26]. Notably, numerous plants and their associated bacteria (including endophytic, phyllospheric, and rhizospheric bacteria) can metabolize petroleum hydrocarbons [11] and produce useful metabolites that might contribute to the metabolic pathways in plants [10]. Varjani [85] reviewed bioremediation for petroleum hydrocarbon pollutants and explanations of their metabolism in microorganisms. Some plants can absorb and transport petroleum hydrocarbons, including heavy metals, which can be sequestered in the root tissues or transported into the shoots and leaves, where they can be stored in vacuoles or volatilized into the atmosphere [11,59,86]. At least three heavy metals that are normally found in the industrial wastewater from gas activities (As, Hg, and Se) can be volatilized using native plants. These plants include swamp lily (*Crinum americanum*), water hyacinth (*Eichhornia crassipes*), hydrilla (*Hydrilla verticillata*, Royle), duckweed (*Lemna minor*, *Lemna obscura*), water lettuce (*Pistia stratiotes*), water moss (*Salvinia natans*), cattail (*Typha domingensis*), and possibly others [87–89].

Recent evidence has shown that aquatic plants in Qatar, such as *Phragmites australis*, *Typha domingensis*, and perhaps others, are efficient in remediating industrial wastewater from oil and gas activities [10]. Moreover, the growth of *P. australis* was improved by industrial wastewater, which can be explained by the activities of rhizospheric bacteria in providing some minerals and metabolites to the plant during the phytoremediation processes of petroleum hydrocarbons [21,26]. Autotrophs can utilize mineral nutrients and some metabolites, while some toxic compounds that result from partial degradation of organic compounds are sequestered in the vacuoles of living aquatic organisms such as algae, mangroves, and seagrasses [10,74].

4.2. Perspectives of Cultivation of Mangroves in Qatar

The peninsula of Qatar has a coastal length of about 563 km, and its coastline could be suitable for the cultivation of mangrove plants to achieve the benefits discussed thus far. This would involve a major governmental project that should consider all obstacles that might be faced and would require comprehensive scientific investigations to address all the challenges. Almahasheer [90] discussed the spatial coverage and distribution of mangroves, including extreme geographic and ecological factors in the Arabian Gulf region. They confirmed that mangroves in Qatar and other countries in the Arabian Gulf region have remained stable with a slight increase. Five steps that should be considered before conducting any real practical project have been suggested: (1) obtaining information, (2) recognizing problems, (3) setting plans, (4) finding solutions, and (5) maintaining sustainable monitoring [91].

Some studies from the last five years have indicated that compensatory planting of mangroves in new areas may be a successful long-term strategy for supporting benthic biodiversity. Furthermore, it could contribute to the mitigation of climate change by increasing long-term carbon storage [92]. Other recent studies on the benthic biodiversity in mangrove forests in Qatar showed that this plant could affect the biodiversity of some marine fauna and, possibly, all communities driven by environmental factors such as salinity and temperature [93]. Nevertheless, more studies are needed to determine the complete impact of mangrove forests on the biodiversity in these areas.

Abdel-Bari et al. [78] studied the ecophysiology of *A. marina* among other halophytes in Qatar. This plant accumulates the main ions found normally in the seawater, such as Na, Cl, Ca, and Mg. Using an exclusion mechanism, these ions are filtered by the root system to prevent the build-up of salts in the conducting system that leads to the green parts at the top of the plant. Notably, many ions are still transported to the leaves, where some of them accumulate, while many of them are excreted by salt glands [94] (Figure S2). This might attract camels and cattle to feed on the green leaves of the plant, which could endanger mangrove forests and possibly result in their disappearance. Therefore, this plant has developed major mechanisms to avoid high levels of salinity from seawater [74] (Figure S3).

Some chemical methods of soil and plants and modern techniques have been adopted for protection, management, and conservation of such the mangrove ecosystem in Qatar [95]. Mangroves have good nitrogen availability and high amounts of photosynthetic pigments. Remote sensing techniques have proven efficient in chlorophyll prediction and estimation. One major method of salt tolerance is osmoregulation, and some compatible osmolytes such as proline and glycinebetaine are accumulated in the cytoplasm of plant cells to balance the absorbed toxic ions that accumulate in the vacuoles [94,96].

5. Seagrasses

Seagrasses are flowering plants found in shallow coastal waters, where they are anchored to the seabed by roots that can tolerate saline seawater. Seagrasses are the only true marine plants that can live completely submerged under water, and the depth at which they are found is limited by water clarity, which determines the amount of light reaching the plant. Notably, seagrasses are a critical component of coastal components and provide various ecological and environmental benefits. One benefit is that they provide an essential habitat for various types of marine organisms, such as fish, invertebrates, and various species of algae [97].

Furthermore, seagrass improves water quality by trapping sediments and filtering out pollutants. Lee et al. [98] found that the seagrass *Zostera marina* is efficient in phyto-remediating heavy-metal-contaminated coastal sediments. They found that this plant accumulated substantial amounts of heavy metals, such as As, Cd, Co, Cu, Fe, Hg, Pb, and Zn. Many of these heavy metals are the main components of industrial waste water from gas activities.

Seagrass also protects the coastline and reduces coastal erosion by stabilizing sediments and attenuating wave energy [99], and it helps combat climate change by storing significant amounts of carbon in its biomass and sediments. Removing carbon dioxide from the atmosphere by photosynthesis helps to mitigate the negative impact of continuous increases in the carbon around the globe [100]. Seagrasses also support marine ecosystems by producing oxygen via photosynthesis [101]. Three main species of seagrass are found in the Arabian Gulf, which are monocots: *Halodule uninervis*, *Halophila ovalis*, and *Thalassia hemprichii*.

5.1. Halodule uninervis (Forssk.), Syn. Zostera uninervis Forssk

H. uninervis is an indigenous perennial seagrass with long rhizomes and linear leaves at the nodes. This widespread seagrass lives at shallow depths and forms dense meadows. This plant provides an important habitat and feed for marine organisms, and as such, its roles are being monitored in some Arab countries in the Arabian Gulf, such as the United Arab Emirates, Oman, and Qatar. Yasseen and Al-Thani reviewed the research on its role in the desalination of seawater [74].

Remediation of seawater includes the removal of Na^+, Cl^-, K^+, and some trace elements such as Cu, Fe, Ni, and Pb [102]. When such trace metals accumulate in the plants, they end up in the food chain and cause contamination of the ecosystem. Some organic compounds might be remediated by this plant as well [103–105]. Recent studies have shown that this plant might have an active role in removing carcinogenic polycyclic aromatic hydrocarbons, and dead leaves from this plant were used to adsorb petroleum hydrocarbons such as acenaphthylene, phenanthrene, and fluoranthene from seawater [106].

5.2. Halophila ovalis (R.Br.) Hook.f., Syn. Caulinia ovalis R. Br. (1810)

H. ovalis is a dioecious perennial seagrass that occurs at shallow depths with opposite ovate leaves. It has been extracted from waters in the areas of Ras Al Noof near Alkhore, Eastern Qatar. It is also commonly known as paddle weed, spoon grass, or dugong grass and belongs to the family Hydrocharitaceae. It is a small, herbaceous plant that occurs in sea beds and other saltwater environments. It is often found in meadows that dominate sand banks or other patches of the sea floor.

Early reports showed that this seagrass can be used as a bioindicator of pollution by various petrochemical compounds and heavy metals, such as Cu, Cd, Pb, and Zn, which is achieved by testing the chlorophyll fluorescence [107–109]. Ralph [110] used this seagrass to examine herbicide toxicity by adopting the same techniques. Runcie et al. [111] reviewed the toxic effects of petrochemicals on this seagrass, as well as morphological, structural, and physiological aspects. They discussed the resulting reduction in their resistance to other stress factors, reduction in growth rate, and toxic appearance on leaves and flowers that might lead to the death of the plant. Petrochemicals might break down the waxy cuticle, which leads to more penetration of toxic compounds and phytotoxicity. Furthermore, disturbances in the ultrastructure of cell organelles such as thylakoids of the chloroplasts can occur.

Thus, *H. ovalis* is not typically considered a viable candidate for the remediation of organic compounds and heavy metals from industrial wastewater from oil and gas activities, but is considered as a bioindicator. However, this plant might play limited biological and phytoremediation roles in seawater and sediments. This plant is sensitive to contamination with petroleum hydrocarbons, as high levels of pollutants could have a negative impact on it. The pollutants can damage the tissues and reduce the photosynthetic growth apparatus.

Furthermore, the plant thrives in clear, shallow marine water where light easily penetrates to boost autotroph growth. This plant lacks the physiological and structural capabilities to remediate pollutants and their degraded components by metabolizing or sequestering them in the vacuoles. Lastly, petroleum hydrocarbons could mainly be de-

graded by microorganisms, as the role of this seagrass in secreting substances to encourage and boost microorganism activities is limited [109].

5.3. Thalassia Hemprichii

T. hemprichii is also called Pacific turtlegrass. This widespread species is native to the shores of the Indian Ocean, Red Sea, Western Pacific Ocean, and the Arabian Gulf region. This plant has strap-like or curved sickle-shaped leaves that are 0.5–1 cm wide and 7–40 cm long (usually less than 25 cm). The tips are usually rounded and smooth. The leaves may appear speckled due to tannin cells that appear red, purple, or dark brown. The growth rate of this plant increases with the enrichment of CO_2, and it can tolerate lower light conditions caused by algal blooms.

Some studies have shown that this seagrass can accumulate high amounts of heavy metals such as Cd and Pb in the root system [112], while its ability to transport them to the shoot system is limited. This species adopts mechanisms similar to those described for *A. marina* [74]. While it is not a food source for humans or livestock, it has ecological roles as a source for marine herbivores such as crustaceans, fish, dugongs (marine mammals), and turtles [113].

The salts and other elements that are transported to the leaves and other parts of the plant are sequestered in the vacuoles, which is balanced by the accumulation of some compatible organic and inorganic solutes in the cytoplasm. Various research and review articles provide more details [9,114,115]. Phytoremediation of petroleum hydrocarbons using *T. hemprichii* has not been studied, but there are some indications that it might enhance microbial activities that stabilize and degrade these compounds. The degraded organic compounds might then be absorbed and metabolized inside the plant tissues [116].

6. Seaweeds

Seaweeds are multicellular and macroscopic algae autotrophs that grow in coastal areas in many water bodies such as oceans, seas, rivers, and lakes. Taxonomically, they are categorized into three groups (Divisions) based on their photosynthetic pigments: Chlorophyta (green algae), Rhodophyta (red algae), and Phaeophyta (brown algae). These algae are non-vascular photosynthetic organisms that lack true roots, stems, and leaves and absorb nutrients and water directly from the surrounding water. They have different shapes and sizes and play crucial ecological roles in marine ecosystems. These roles cover various functioning aspects in these environments, including climate change, health, and economy.

One of their roles is the production of significant amounts of organic components, such as sugars and oxygen. Thus, these organisms provide a significant source of food and energy. They also create habitats and shelter for a wide range of marine life, such as fish, invertebrates, and microorganisms. This role includes protection from predators and providing places to attach and grow for sessile organisms.

Many fish species also use seaweed beds as a safe environment for feeding and hiding, which increases their survival rate. Furthermore, seaweeds are good source of food and dietary components for various marine herbivores, such as urchins, sea slugs, and fish, and nutrient cycling is another role these seaweeds can play. They absorb and store nutrients from around seawater, but after their decay, the nutrients are released and support the ecosystem.

Seaweeds also absorb CO_2 and produce O_2 during photosynthesis, which helps to stabilize the ecosystem and mitigate the great negative effect of climate change around the globe. Moreover, they support marine life through the respiration process. Seaweeds help stabilize the shoreline by reducing the impact of waves and currents. Their holdfasts (root-like structures) anchor them to the substrate and act as a natural barrier against coastal erosion [117,118]. Seaweeds can also be used for various medical and industrial uses, including pharmaceutical, cosmetic, and food applications, as they contain bioactive compounds that are used for their medicinal and nutritional properties.

Biodiversity support is another role that seaweeds play by providing diverse microhabitats for a wide range of organisms. This role might increase species richness and ecological interactions within the marine ecosystem. Phytoremediation (or phycoremediation) plays a crucial role in the filtration of polluted water, which can help improve water quality in marine environments. Many macroalgae have proven efficient in removing organic and inorganic pollutants [59,119,120]. Furthermore, these macroalgae play an ecological role as primary producers in seawater and sustain several benthic animal communities that contribute to the food chain. They can also act as bioindicators of water quality for bioremediation [21,22,26,121,122].

6.1. Chemical Constituents and Uses

Chemical components of seaweeds have various uses and advantages. These constituents include proteins; amino acids; minerals including heavy metals; vitamins (water and lipid-soluble vitamins); lipids; dietary fibers; antioxidant compounds; and antibacterial, antifungal, and antiviral compounds. Notably, some components could be useful as food for animals and humans and as medicines or pharmaceuticals to treat many diseases.

All these components and their secondary metabolites, such as terpenoids, phenolic compounds, and compatible solutes, might be affected by environmental conditions and pollution levels in the Arabian Gulf. This is due to the continuous spills during transport, military exercises, and wars. It is not the objective of this article to discuss the roles of these components in seawater, which need further detailed follow-up to look into the impacts of these constituents on marine and human life in the Arabian Gulf. The potential for remediation of industrial wastewater by many seaweeds is discussed.

Rizk et al. prepared a list of seaweeds in the Arabian Gulf around the Qatari peninsula [123]. Tables 1–3 contain the species of seaweeds, their families, the main chemical constituents, and possible roles that they may play in the marine ecosystem. Their potential for remediation has been addressed in many studies. Further studies should examine their phycoremediation processes to avoid and reduce pollution in the Arabian Gulf region.

6.2. Phycoremediation

Phycoremediation is a promising method to utilize seaweeds such as green, brown, and red algae (macroalgae) to degrade or remove various pollutants from seawater. Macroalgae are efficient in these methods because their growth rate is significantly high, which leads to the production of substantial biomass, and they can absorb and accumulate many heavy metals, including those involved in oil and gas activities. They can also metabolize organic compounds produced during oil and gas extraction, processing, and transportation [124,125]. Seaweeds use at least four methods to remediate these pollutants: (a) biosorption, (b) bioaccumulation, (c) biodegradation, and (d) nutrient uptake [126,127].

Table 1. List of Chlorophyta (green algae) species and the possible constituents and roles.

Species	Family	Main Constituents	Possible Roles	References
Acetabularia caliculus	Polyphysaceae	Proteins (4.5%), lipids (4.2%), carbohydrates (33.4%,), and ash including minerals (57.3%), others (0.6%) as secondary metabolites such as phenolic compounds and terpenoids	Phycoremediation of: Cd, Cr, Cu, Hg, Ni, Pb, and Zn, organic components, and nutrients such as nitrogen and phosphorus, antioxidants	[123,128,129]
Avrainvillea amadelpha	Dichotomosiphonaceae	Rawsonol [a], isorawsonol-steroids, bromophenols, Sulfono-glycolipid	Antioxidants, anticancer, H_2O_2 scavenging activity, hemagglutination, antibacterial, heavy metal phycoremediation: (Cd, Cu, Pb) *	[123,130–132]

Table 1. *Cont.*

Species	Family	Main Constituents	Possible Roles	References
Boodlea composita	Boodleaceae	β-sitosterol, loliolide [b] and 13 [2] -hydroxy-(13 [2] -S)-phaeophytin-a, fatty acids, sterols, sulphated polysaccharide, agglutinins, glycinebetaine, prolinebetaine	Possible remediation role in polluted saline waters	[123,124,133–136]
Bryopsis implexa	Bryopsidaceae	Xylan, carotenoids, free amino and fatty acids, sterols, bryopsin, kahalalide F	Possible role in remediating polluted and saline waters, anticancer action	[119,123,130,137]
Caulerpa mexicana	Caulerpaceae	Siphonaxanthin [c], siphonein [d], various polysaccharides, fatty acids, amino acids	Degradation of petroleum hydrocarbons, possible removal of heavy metals, nutritional uses, medical uses: antiviral, antibacterial, etc.	[123,138–140]
Chaetomorpha spp., (5 species): *C. aerea*, *C. indica*, *C. linum*, *C. koeiei*, *C. patentarama*	Cladophoraceae	Sulphated polysaccharides; containing arabinose, and galactose, and other sugars such as glucose, xylose, and fucose, hemolytic saponin	Anticoagulant activities (antithrombin type), possibly toxic, remediation of IWW	[123,141–145]
Cladophora spp., (3 species): *C. koeie*, *C. patentirama*, *C. sericoides*	Cladophoraceae	Pigments such as β-carotene, xanthophyll, xanthophyll-epoxide, violaxanthin, and other related pigments, water-soluble sulphated polysaccharides, other related compounds, various types of amino acids	Phytoremediation of petroleum hydrocarbons; antibacterial and antiviral activities; antimitotic and cytotoxic activities; monitoring heavy metals such as Cd, Co, Cr, Cu, Fe, Hg, Mn, Ni, Pb, and Zn	[123,146–150]
Cladophoropsis sundanensis	Boodleaceae	Xanthophyll, loroxanthin siphonaxanthin	Little is known about role in phytoremediation; needs more investigation	[123,151,152]
Dictyosphaeria cavernosa	Siphonocladaceae	Alkylxanthate, bicyclic lipid, dictyosphaerin, some heavy metals	Possible phycoremediation of heavy metals, anti-mosquito larvae	[123,128,153–155]
Enteromorpha spp., (2 species): *E. kylinii*, *E. ramulosa*	Ulvaceae	Water-soluble polysaccharides, fatty acids and sterol, essential amino acids	Bioactivity such as hypocholesterolemic effect, antibacterial and diuretic activities, mutagenic activity, indicator of pollution	[123,156–159]
Rhizoclonium kochianum	Cladophoraceae	Scanty information, crystalline cellulose	Antibacterial, beta-blocker, 5-hydroxytryptamine blocker, folk medicine for burns, vermifuge, possible phycoremediation of heavy metals and organic compounds, nutritional value	[123,160]
Ulva purtusa	Ulvaceae	Polysaccharides, fatty acids, non-acidic glycolipid fractions, monogalactosyl, diglyceride, isofucosterol, amino acids, ascorbic acid (vitamin C), heavy metals such as Fe, Mn, Ti, Ni, Cu, Pb, and others	Bioindicator of seawater pollution, remediation of petroleum hydrocarbons and heavy metals	[123,158,161–164]

[a] Rawsonol and Isorawsonol: polybromophenols (a type of terpenoid, an inhibitor), [b] β-sitosterol, loliolide is one of several phytosterols of plant sterols, [c] carotenoid, [d] C19 acylated siphonaxanthin. * Definition of heavy metal: the definition of heavy metals can come from three criteria. These are the density, atomic weight, and the behavior of a metal beyond a certain limit [165,166].

Table 2. List of Phaeophyta (brown algae) species and the possible constituents and roles.

Species	Family	Main Constituents	Possible Roles	References
Colpomenia sinuosa	Scytosiphonaceae	Cytotoxic fractions with complex mixture of saturated and unsaturated fatty acids, carotenoid fucoxanthin, some amino acids	Possible role of heavy metal remediation, its presence is a sign of pollution	[123,167–169]
Cystophyllum muricatum	Ceratophyllaceae	Little information available, presence of some fatty acids	Possible remediation of heavy metals and organic components	[123,170]
Cystoseira spp., (2 species): *C. myrica*, *C. trinodis*	Sargassaceae	A sulphated polysaccharide containing some soluble sugars, fucoidan, glycinebetaine and related compounds, alginic acid, uronic acid, laminaran, mannitol, amino acids, palmitic acid, lipid components, diterpenoids, etc.	Remediation of heavy metals in seawater	[119,123,163,171–173]
Dictyota cervicornis	Dictyotaceae	Fucoidan, diterpenes, diterpenoids, sterols such as fucosterol, phloroglucinol as toxic compound	Cytotoxic effects, many deterred feedings by some sea animals such as fish and sea urchins, etc., possible phytoremediation of heavy metals and petroleum hydrocarbons	[123,174]
Ectocarpus mitchellae	Ectocarpaceae	Mannitol, ectocarpene, fucoidan, alginin, ectocarpene	Sexual pheromone, hemagglutinin activity, possible remediation of heavy metals and petroleum hydrocarbons	[123,158,175]
Giffordia mitchellae	Acinetosporaceae	Giffordene, stereoisomers	Hemagglutinin activity, no reports about remediation, needs to be tested for phycoremediation	[123]
Hormophysa cuneiformis	Sargassaceae	Carbohydrates (59%), proteins (9%), lipids (7%), and ash (25%); sterols; fatty acids; amino acids; some heavy metals are found such as Fe, Zn, Co, Pb, Cu, Mn, and Al	Bioindicators for heavy metal pollution, anticancer and possible antimicrobial potential	[119,123,176,177]
Padina australis	Dictyotaceae	Sulphated heteropolysaccharides; fucan contained monosaccharides; neutral sugars such as arabinose, fucose, galactose, glucose, mannose, rhamnose, and xylose; other sugar component complexes are found such as uronic acid and fucosterol; fatty and amino acids such as glutamic acid, arginine, and proline	Anticoagulation activity, human HL-60 leukemia cell-line, bioactive primary and secondary metabolites with antibacterial activity against Bacillus spp and Staphylococcus spp., monitoring heavy metals, high capacity of the polyphenols for the chelating of heavy metals, possible heavy metal phycoremediation	[123,178–181]
Sargassum spp., (2 species): *S. aquifolium*, *S. boveanum*	Sargassaceae	Polysaccharides, sargassan: many monosaccharides in this compound are found; amino acids are found in the peptide portion; high fucoidan content containing some complex polysaccharides; high percentage of alginate and mannitol; fatty acids of various types are found; glycerides and many other complex compounds, etc.	High nutritional values, trace elements are found such as Ag, Al, As, Au, Ba, Ce, Co, Cr, Sr, Cs, Fe, Mn, Sb, Sc, Te, V, U, and Zn; remediation of trace elements is very likely; biological activities; antitumor activity; interferon-activity; immunosuppressive effects; anticoagulant activity; hypo-cholesterolemic activity; other medical uses have been reported	[123,163,182–184]

Table 2. *Cont.*

Species	Family	Main Constituents	Possible Roles	References
Turbinaria conoides	Sargassaceae	Alginic acid, alginate, laminaran, fucan complex contains monosaccharides, D-mannitol, fucosterol, antibiotic sarganin, antifungal activity, turbinaric acid	Antibacterial and antifungal activities, cytotoxic activity, herbivorous activity, possible phycoremediation activity of some heavy metals such as thulium, role in biosynthesis of nanoparticles	[123,185–187]

Table 3. List of Rhodophyta (red algae) species and the possible constituents and roles.

Species	Family	Main Constituents	Possible Roles	References
Amphiroa fragilissima	Corallinaceae	Cholesterol, non-protein amino acids; low-molecular-weight carbohydrates; floridoside, mannoglyceric acid; bioactive compounds such as ellagic acid, gallic acid, and phenolic compounds; major polyamines are found; trace elements are found such as Fe, Zn, Co, Pb, Mn, Cu, Al, etc.	Possible role of remediation in polluted water; ellagic acid may help prevent cancer cells from growing; gallic acid contains antioxidant, anti-inflammatory, and antineoplastic properties; phenolic compounds may have more roles: antitumoral, anticoagulant, antiviral, and hypocholesterolemic	[123,188,189]
Centroceras calvulatum	Ceramiaceae	Rich in protein, non-protein amino acids, fatty acids, cholesterol, rich in vitamin C	Might be non-conventional food and feed, possible remediation role in polluted sea water	[123,190]
Ceramium luetzelbergii	Ceramiaceae	Agar, some complex compounds containing monosaccharides are found, carotenoids, cholesterols, bromoperoxidase containing vanadium (V), trimethylamine, nitrate, choline, crystalline sulfur, Hg is found in some species of Ceramium	Possible indicator of Hg, possible universal monitor for heavy metals, antibacterial activity, antimitotic activity, agglutinin activity, folk medicine used for chest diseases	[123,191–193]
Chondria armata	Rhodomelaceae	Polysaccharides composed of mannose and galactose; xylogalactan sulphate; chondriol: a halogenated acetylene; volatile acids: sarganin and chonalgin; amino acids with some new amino acids; chondriamides; hemmagglutinins; cyclic polysuphides; some trace elements are found such as: Fe, Zn, Co, Pb, Mn, Cu, and Al	Possible role in remediation of heavy metals, antibiotic action, cytotoxic activity, activity against animal erythrocytes; other medical activities were recorded such as antitumor, antimicrobial, and antiviral effects	[60,123,194]
Digenea simplex	Rhodomelaceae	Agar contains: galactose, glucose, xylose, etc., agarose, sulphate ester; pectin analysis showed the presence of galactose, fructose, and arabonic acid, floridoside, digenic acid (kainic acid)	Some constituents can be used in medicine, food, and cosmetic industries; digenic acid is effective in expelling ascaris, possibly remediates heavy metals and organic compounds	[123,195,196]

Table 3. *Cont.*

Species	Family	Main Constituents	Possible Roles	References
Hypnea spp., (2 species): *H. cervicornis*, *H. valentiae*	Cystocloniaceae	Sulphated galactans; carotenoids such as α-carotene, β-carotene, lutein, and possibly others; peptidic agglutanins; phycolloid-containing ƙ-carrageenan; various forms of sterols and fatty acids; contains some elements such as Ca, Mg, K, Al, Fe, Mn, Cr, Ni, Cd, and Co	Food and animal feed, some agglutanins have agglutinating activity towards a variety of biological cells, including tumors, against human blood groups A, B, and O and animal erythrocytes; sulphated polysaccharides might have a role in supporting bones and may be used as anti-inflammatory agents and for other medical uses; pharmacological constituents could play various roles such as muscle relaxant, hypothermic activity, and phytoremediation of heavy metals such as Cd	[120,123,187,197,198]
Jania spp. (2 species were recorded): *J. adhaerens*, *J. ungulata*	Corallinaceae	Various carotenoids such as β-carotene, zeaxanthin, fucoxanthin, 9˜-cis-fucoxanthin, fucoxanthinol, 9˜-cis-fucoxanthinol, and epimeric mutatoxanthins; other organic compounds might be found; some heavy metals might be found	Phytoremediation of heavy metals is possible; not much information is available for some species; ameliorative effect on the toxicity of heavy some heavy metals for some animals and possibly humans	[123,199,200]
Laurencia spp. (6 species were recorded): *L. elata*, *L. glandulifera*, *L. intermedia*, *L. paniculata*, *L. papillosa*, *L. perforata*	Rhodymeniaceae	Various types of polysaccharides, sesquiterpenoides, diterpenoids, triterpenoids, other compounds such as C_{15}-acetogensis, secondary metabolites such as sterols, fatty acids, amino acids, mineral elements: K, Na, Ca, Mg, Fe, Zn, Pb, Co, Cu, Mn, Al, possibly others: Cr, Ni, Cd, etc.	Various roles played by this macro-alga as food, medicine, numerous ecological roles *, refuge for marine organisms, hosts of various microorganisms and parasitic algae (such as *Janczewskia*); they are fed on by some grazers such as crabs, queen conch, and sea hares; possible roles in phycoremediation	[123,151,201]
Polysiphonia spp. (4 species were recorded): *P. brodiei*, *P. crassicolis*, *P. ferulacea*, *P. kampsaxii*	Rhodomelaceae	Sulphated galactans; polysaccharides belong to the agar class and agarose, other related residues such as mannitol and trehalose, etc., bromophenols, fatty acids, phospholipids, polar lipids, some structural components	Antibiotic (antibacterial and antifungal) and antioxidant activities; other roles such as antimitotic activity, increase survival of vorticellids; serum lipolytic activity; agglutinin; heavy metals are found such as As, Cd, Cr, Cu, Fe, Hg, Mn, Mo, Ni, Pb, Ti, V, and Zn; possible phycoremediation of petroleum hydrocarbons	[123,163,202,203]
Spyridia filamentosa	Callithamniaceae	Sterols such as cholesterol, fatty acids, and agglutinin are found in some species; main elements found are Al, Ca, Co, Cu, Fe, K, Mg, Mn, Na, Pb, and Zn	Antifungal activity of aqueous extracts, biosynthesis of silver nanoparticles, removing heavy metals from industrial wastewater	[123,204,205]
Wurdemannia miniatat	Solieriaceae	Little information is known about the chemical constituents (needs to be investigated)	No reported roles of this species	[123]

Tissues of some seaweeds accumulate heavy metals, particularly those found in the industrial wastewater of gas activities, such as As and Hg. Examples include *Acetabularia caliculus*, *Cladophora* spp. (green algae), *Sargassum* spp. (brown algae), and *Polysiphonia* spp. (red algae) (see Tables 1–3). Some other heavy metals found in industrial wastewater from oil and gas activities are found in many seaweeds as well, including Al, As, Ba, Cd, Co, Cr, Cu, Fe, Hg, Mn, Mo, Ni, Pb, V, and Zn [21,25,59,206].

Al-Thani and Yasseen [26] recently showed that heavy metals from industrial wastewater might accumulate in the tissue of marine animals or bind to the cell walls of algae, which could lead to negative impacts or disturbances in the food chain and human health. Therefore, monitoring the ecosystem in the Arabian Gulf could help to avoid or reduce the detrimental impacts of these trace elements on marine life. Some reported seaweeds in the Arabian Gulf have the ability to efficiently remediate heavy metals, including *Acetabularia caliculus*, *Avrainvillea amadelpha*, *Cladophora* spp., and *Ulva purtusa* (green algae); *Hormophysa cuneiformis* and *Sargassum* spp. (brown algae); and *Amphiroa fragilissima*, *Ceramium luetzelbergii*, *Chondria armata*, *Hypnea* spp., *Jania* spp., *Laurencia* spp., *Polysiphonia* spp., and *Spyridia filamentosa* (red algae). Organic components could be absorbed by seaweed biomass, biodegraded into smaller less toxic units, or metabolized [21,163,207].

Notably, microorganisms in seawater may be freely floating or are otherwise associated with or harbored by living marine organisms, including seaweeds. They might play significant roles in the degradation of organic compounds by converting them into smaller, less toxic units. Degradation of organic industrial wastewater can be achieved completely or partially (to less-toxic components) by microorganisms, particularly bacteria, that are sequestered in the vacuoles of seaweed tissues or involved in the metabolic pathways. Recent reports [21,22,26] have discussed the most common bacteria species found in the Arabian Gulf around the peninsula of Qatar that might play crucial roles in biodegradation and bio-stabilization of organic and inorganic components of industrial wastewater [163,208–210].

Seaweeds might also absorb extra essential elements such as nitrogen and phosphorus to avoid eutrophication in marine environments [211], which would lead to a loss of aquatic biodiversity, as well as a reduction in ecosystem services related to various important aspects of human life, such as fisheries, aquaculture, and recreation. Moreover, toxins released from some harmful algal blooms could have detrimental impacts on marine life and great negative consequences on human life.

Practical methods of phycoremediation using seaweeds include encouraging the cultivation of seaweeds that have proven efficient in removing toxic trace elements and metabolizing organic components of industrial wastewater (Tables 1–3). These seaweeds can be cultivated alongside fish and shellfish, which might help to improve the water quality and lead to healthier environments for aquaculture species. Construction of wetlands that involve seaweeds could improve the water quality by removing or stabilizing pollutants, and polluted seawater can be remediated under controlled conditions using seaweeds. They can be considered as bioreactors where contaminated water is treated and allow for the optimization of conditions for maximum pollutant removal [21,60,126,212].

Despite the success of practical methods of phycoremediation, some challenges and considerations should be considered. One of the most important issues is the monitoring the success of ecological restoration and maintaining a healthy environment [86]. Furthermore, the biomass of plants and seaweeds should be involved in various industrial and agro-biotechnological activities [213], such as manufacturing furniture, paper, domestic products, and food. They could also be used in composting, fertilizers, and transformation into less toxic forms and non-degradable complex molecules, as well as incineration for the chemical and electronics industries.

All the components need to be monitored and recycled safely to keep the toxic metals and any other dangerous components away from the food chain and to maintain the safety of ecosystems [21]. It is also important to spread awareness about the effects of environmental factors on remediation methods, such as temperature, salinity, light, and the presence of other pollutants [214]. Lastly, the introduction of edible plants and seaweeds to any remediation programs must be avoided to prevent any deterioration of the ecosystem, and monitoring in this regard should be involved in every step of the remediation [10].

7. Conclusions

The biological approach has emerged recently to solve pollution problems of industrial wastewater. It is an environmentally friendly solution for many issues facing the ecosystem and human life at various sectors of health, agriculture, and the economy. Recognizing the marine autotrophic organisms that have proven efficient in remediating polluted seawater is the first step in the right direction to speed up the process of removing or avoiding toxic components that result from oil and gas activities. Several plants, seaweeds, and microorganisms are promising candidates for remediation of the polluted seawater around the Arabian Gulf. Joint works are desperately needed to make the water of the Gulf suitable for marine life and humans. Such efforts are important in the context of increasing demands for energy components and with the great impacts of wars, conflicts, competition, and economic activities. Future research on sustainable ecological restoration in the Arabian Gulf should concentrate on the following aspects: (a) encouraging cultivation of autotropic living organisms reported in this article, (b) recognizing more autotrophs to boost the efforts for more active remediation of industrial wastewater, (c) establishing a continuous monitoring system of the seawater and the biomass of these marine organisms to set up a database and determine the possible threat of pollution at the ecosystem, (d) engaging the biomass of these living organisms with agro-biotechnology and recycling their components in various industrial activities, and (e) conducting modern bio-technological research like genetic engineering and tissue culture to develop transgenic marine autotrophs to boost the efforts of remediation methods.

Supplementary Materials: The following supporting information can be downloaded at: https://www.mdpi.com/article/10.3390/toxics12090625/s1, Figure S1: A cable network of breathing roots (pneumatophores) that support the growth of plants in this stressful habitat; Figure S2: Salt glands are the main features of *Avicennia marina* that play vital role in ion regulation and homeostasis [94]; Figure S3: SEM of the adaxial surface (upper side) of leaves of *Avicennia marina*, scattered salt crystals are found (with magnification of X1200); Table S1: Analysis of heavy metals in industrial and anthropogenic wastewater. These compounds were determined during a joint project between Qatar University and Exxonmobil company (2012–2014), and a project sponsored by ESC (QU); Table S2: Analysis of petroleum hydrocarbons in industrial wastewater (mean of four replicates ± standard deviation); Table S3: Concentration of selected pollutants with elevated levels in relation to coastal and marine pollution [130]; Table S4: Mean values of physical and chemical features and heavy metals in the studied locations of the Arabian Gulf shore sediments and water [215].

Funding: This research received no external funding.

Acknowledgments: We would like to thank the University of Qatar for their continuous encouragement and support of scientific research, as well as the Environmental Studies Centre (ESC) of Qatar University for allow us to use some of their publications to support this review. We also thank Nada Abbara for drawing the map of Qatar and preparing the graphical abstract. The authors acknowledge the editing service of the American Manuscript Editors, USA.

Conflicts of Interest: The authors declare no conflict of interest.

References

1. Ghazanfar, S.A.; Böer, B.; Al Khulaidi, A.W.; El-Keblawy, A.; Alateeqi, S. Plants of Sabkha Ecosystems of the Arabian Peninsula. In *Sabkha Ecosystems, Tasks for Vegetation Science*; Gul, B., Böer, B., Khan, M., Clüsener-Godt, M., Hameed, A., Eds.; Springer: Cham, Switzerland, 2019; Volume 49, pp. 55–80. [CrossRef]
2. Van Aken, B.; Correa, P.A.; Schnoor, J.L. Phytoremediation of polychlorinated biphenyls: New trends and promises. *Environ. Sci. Technol.* **2010**, *44*, 2767–2776. [CrossRef] [PubMed]
3. Kamath, R.; Rentz, J.A.; Schnoor, J.L.; Alvarez, P.J.J. Phytoremediation of hydrocarbon-contaminated soils: Principles and applications, Chapter 16. *Stud. Surf. Sci. Catal.* **2004**, *151*, 447–478. [CrossRef]
4. Wang, M.; Ding, M.; Yuan, Y. Bioengineering for the Microbial Degradation of Petroleum Hydrocarbon Contaminants. *Bioengineering* **2023**, *10*, 347. [CrossRef]
5. Alkorta, I.; Garbisu, C. Phytoremediation of organic contaminants in soils. *Bioresour. Technol.* **2001**, *79*, 273–276. [CrossRef]
6. Vidali, M. Bioremediation. An overview. *Pure Appl. Chem.* **2001**, *73*, 1163–1172. [CrossRef]

7. Van Beilen, J.B.; Funhoff, E.G.; van Loon, A.; Just, A.; Kaysser, L.; Bouza, M.; Holtackers, R.; Rothlisberger, M.; Li, Z.; Witholt, B. Cytochrome P450 alkane hydroxylases of the CYP153 family are common in alkane-degrading eubacteria lacking integral membrane alkane hydroxylases. *Appl. Environ. Microbiol.* **2006**, *72*, 59–65. [CrossRef] [PubMed]
8. Ben Chekroun, K.; Sanchez, E.; Baghour, M. The role of algae in bioremediation of organic pollutants. *Int. Res. J. Public Environ. Health* **2014**, *1*, 19–32.
9. Al-Thani, R.F.; Yasseen, B.T. Solutes in native plants in the Arabian Gulf region and the role of microorganisms: Future research. *J. Plant Ecol.* **2018**, *11*, 671–684. [CrossRef]
10. Al-Thani, R.F.; Yasseen, B.T. Phytoremediation of polluted soils and waters by native Qatari plants: Future perspectives. *Environ. Pollut.* **2020**, *259*, 113694. [CrossRef]
11. Gkorezis, P.; Daghio, M.; Franzetti, A.; Van Hamme, J.D.; Sillen, W.; Vangronsveld, J. The interaction between plants and bacteria in the remediation of petroleum hydrocarbons: An environmental perspective. *Front. Microbiol.* **2016**, *7*, 1836. [CrossRef] [PubMed]
12. Sun, X.; Kostka, J.E. Hydrocarbon-degrading microbial communities are site specific, and their activity is limited by synergies in temperature and nutrient availability in surface ocean waters. *Appl. Environ. Microbiol.* **2019**, *85*, e00443-19. [CrossRef] [PubMed]
13. Jin, Q.; Kirk, M.F. pH as a primary control in environmental microbiology: 1. Thermodynamic perspective. *Sec. Microbiol. Chem. Geomicrobiol.* **2018**, *6*, 21. [CrossRef]
14. Obahiagbon, K.O.; Amenaghawon, A.N.; Agbonghae, E.O. Effect of initial pH on the bioremediation of crude oil polluted water using a consortium of microbes. *Pac. J. Sci. Technol.* **2014**, *15*, 452–457.
15. Li, H.; Lai, R.; Jin, Y.; Fang, X.; Cui, K.; Sun, S.; Gong, Y.; Li, H.; Zhang, Z.; Zhang, G.; et al. Directional culture of petroleum hydrocarbon degrading bacteria for enhancing crude oil recovery. *J. Hazard. Mater.* **2020**, *390*, 122160. [CrossRef] [PubMed]
16. Cao, S.; Duan, M.; Zhang, X.; Yang, Z.; Zhuo, R. Bacterial community structure analysis of sludge from Taozi lake and isolation of an efficient 17β-Estradiol (E2) degrading strain *Sphingobacterium* sp. GEMB-CSS-01. *Chemosphere* **2024**, *355*, 141806. [CrossRef]
17. Abercron, S.-M.M.-V.; Marín, P.; Solsona-Ferraz, M.; Castañeda-Cataña, M.-A.; Marqués, S. Naphthalene biodegradation under oxygen-limiting conditions: Community dynamics and the relevance of biofilm-forming capacity. *Microb. Biotechnol.* **2017**, *10*, 1781–1796. [CrossRef]
18. Bian, H.; Li, C.; Zhu, J.; Xu, L.; Li, M.; Zheng, S.; He, N. Soil moisture affects the rapid response of microbes to labile organic C addition. *Front. Ecol. Evol.* **2022**, *10*, 857185. [CrossRef]
19. Al-Thani, R.F.; Yasseen, B.T. Halo-Thermophilic bacteria, and heterocyst cyanobacteria found adjacent to halophytes at Sabkhas–Qatar: Preliminary study and possible roles. *Afr. J. Microbiol. Res.* **2017**, *11*, 1346–1354.
20. Al-Thani, R.F.; Yasseen, B.T. Biological soil crusts and extremophiles adjacent to native plants at Sabkhas and Rawdahs, Qatar: The possible roles. *Front. Environ. Microbiol.* **2018**, *4*, 55–70. [CrossRef]
21. Al-Thani, R.F.; Yasseen, B.T. Perspectives of future water sources in Qatar by phytoremediation: Biodiversity at ponds and modern approach. *Int. J. Phytoremediat.* **2021**, *23*, 866–889. [CrossRef]
22. Al-Thani, R.F.; Yasseen, B.T. Microbial ecology of Qatar, the Arabian Gulf: Possible roles of microorganisms. *Front. Mar. Sci.* **2021**, *8*, 697269. [CrossRef]
23. Abou Khalil, C.; Prince, V.L.; Prince, R.C.; Greer, C.W.; Lee, K.; Zhang, B.; Michel, C.; Boufadel, M.C. Occurrence and biodegradation of hydrocarbons at high salinities. *Sci. Total Environ.* **2021**, *762*, 143165. [CrossRef] [PubMed]
24. Teamkao, P.; Thiravetyan, P. Bioremediation of MEG, DEG, and TEG: Potential of Burhead plant and soil microorganisms. *Int. J. Biotechnol. Bioeng.* **2012**, *6*, 947–950.
25. Al-Sulaiti, M.Y.; Al-Shaikh, I.M.; Yasseen, B.T.; Ashraf, S.; Hassan, H.M. Ability of Qatar's native plant species to phytoremediate industrial wastewater in an engineered wetland treatment system for beneficial water reuse. *Qatar Found. Annu. Res. Forum Proc.* **2013**, *2013*, EEO-010. [CrossRef]
26. Al-Thani, R.F.; Yasseen, B.T. Possible future risks of pollution consequent to the expansion of oil and gas operations in Qatar. *Environ. Pollut.* **2023**, *12*, 12–52. [CrossRef]
27. Hutchinson, S.L.; Schwab, A.P.; Banks, M.K. Biodegradation of Petroleum Hydrocarbons in the Rhizosphere, Chapter 11. In *Phytoremediation: Transformation and Control of Contaminants*; McCutcheon, S.C., Schnoor, J.L., Eds.; Wiley: New York, NY, USA, 2003; pp. 355–386. [CrossRef]
28. Eze, M.O.; Amuji, C.F. Elucidating the significant roles of root exudates in organic pollutant biotransformation within the rhizosphere. *Sci. Rep.* **2024**, *14*, 2359. [CrossRef]
29. Kvesitadze, E.; Sadunishvili, T.; Kvesitadze, G. Mechanisms of organic contaminants uptake and degradation in plants. *Int. J. Biomedic. Biolog. Engin.* **2009**, *3*, 361–371.
30. Moënne-Loccoz, Y.; Mavingui, P.; Combes, C.; Normand, P.; Steinberg, C. Microorganisms and Biotic Interactions, Chapter 11. In *Environmental Microbiology: Fundamentals and Applications: Microbial Ecology*; Bertrand, J.-C., Caumette, P., Lebaron, P., Matheron, R., Normand, P., Ngando, T.S., Eds.; Springer: Dordrecht, The Netherlands, 2015. [CrossRef]
31. Dhawi, F. The Role of plant growth-promoting microorganisms (PGPMs) and their feasibility in hydroponics and vertical farming. *Metabolites* **2023**, *13*, 247. [CrossRef]
32. Alves, A.R.A.; Yin, Q.; Oliveira, R.S.; Silva, E.F.; Novo, L.A.B. Plant growth-promoting bacteria in phytoremediation of metal-polluted soils: Current knowledge and future directions. *Sci. Total Environ.* **2022**, *838 Pt 4*, 15435. [CrossRef]

33. Kurzbaum, E.; Kirzhner, F.; Armon, R. A hydroponic system for growing gnotobiotic vs. sterile plants to study phytoremediation processes. *Int. J. Phytoremediat.* **2014**, *16*, 267–274. [CrossRef]
34. French, K.E. Engineering mycorrhizal symbioses to alter plant metabolism and improve crop health. *Front. Microbiol.* **2017**, *8*, 1403. [CrossRef] [PubMed]
35. Hestrin, R.; Hammer, E.C.; Mueller, C.W.; Lehmann, J. Synergies between mycorrhizal fungi and soil microbial communities increase plant nitrogen acquisition. *Commun. Biol.* **2019**, *2*, 233. [CrossRef]
36. Ratna, S.; Rastogi, S.; Kumar, R. Phytoremediation: A Synergistic Interaction Between Plants and Microbes for Removal of Unwanted Chemicals/Contaminants. In *Microbes and Signaling Biomolecules Against Plant Stress*; Springer: Singapore, 2020. [CrossRef]
37. Das, N.; Chandran, P. Microbial degradation of petroleum hydrocarbon contaminants: An overview. *Biotechnol. Res. Int.* **2011**, *2011*, 941810. [CrossRef]
38. Dave, S.; Das, J. Role of Microbial Enzymes for Biodegradation and Bioremediation of Environmental Pollutants: Challenges and Prospects. In *Bioremediation for Environmental Sustainability*; Elsevier: Amsterdam, The Netherlands, 2021. [CrossRef]
39. Zhuo, R.; Fan, F. A comprehensive insight into the application of white rot fungi and their lignocellulolytic enzymes in the removal of organic pollutants. *Sci. Total Environ.* **2021**, *778*, 146132. [CrossRef]
40. Kalia, A.; Sharma, S.; Semor, N.; Babele, P.K.; Sagar, S.; Bhatia, R.K.; Walia, A. Recent advancements in hydrocarbon bioremediation and future challenges: A review. *3 Biotech* **2022**, *12*, 135. [CrossRef]
41. Lin, S.; Wei, J.; Yang, B.; Zhang, M.; Zhuo, R. Bioremediation of organic pollutants by white rot fungal cytochrome P450: The role and mechanism of CYP450 in biodegradation. *Chemosphere* **2022**, *301*, 134776. [CrossRef]
42. Aziz, Z.S.; Jazza, S.H.; Dageem, H.N.; Banoon, S.R.; Balboul, B.A.; Abdelzaher, M.A. Bacterial biodegradation of oil-contaminated soil for pollutant abatement contributing to achieve sustainable development goals: A comprehensive review. *Results Eng.* **2024**, *22*, 102083. [CrossRef]
43. Kawasaki, A.; Okada, S.; Zhang, C.; Delhaize, E.; Mathesius, U.; Richardson, A.E.; Watt, M.; Gilliham, M.; Ryan, P.R. A sterile hydroponic system for characterizing root exudates from specific root types and whole-root systems of large crop plants. *Plant Methods* **2018**, *14*, 114. [CrossRef] [PubMed]
44. Gogoi, B.; Das, I.; Begum, S.; Dutta, G.; Kumar, R.; Borah, D. Microbes and Their Genes Involved in Bioremediation of Petroleum Hydrocarbon. In *Sustainable Materials: Bioremediation for Environmental Pollutants*; Bentham Books: Loosdrecht, The Netherlands, 2023. [CrossRef]
45. Pal, S.; Kundu, A.; Banerjee, T.D.; Mohapatra, B.; Roy, A.; Manna, R.; Sar, P.; Kazy, S.K. Genome analysis of crude oil degrading *Franconibacter pulveris* strain DJ34 revealed its genetic basis for hydrocarbon degradation and survival in oil contaminated environment. *Genomics* **2017**, *109*, 374–382. [CrossRef]
46. Al-Thani, R.F.; Abd-El-Haleem, D.; Al-Shammri, M. Isolation, biochemical and molecular characterization of 2-chlorophenol degrading Bacillus isolates. *Afr. J. Biotechnol.* **2007**, *6*, 2675–2681. [CrossRef]
47. Al-Thani, R.F.; Abd-El-Haleem, D.A.; Al-Shammri, M. Isolation and characterization of polyaromatic hydrocarbons-degrading bacteria from different Qatar soils. *Afr. J. Microbiol. Res.* **2009**, *3*, 761–766.
48. Fotedar, R. Identification of Bacteria from the Marine Environment Surrounding Qatar. In *Proceedings of the Qatar Foundation Annual Research Forum Proceedings*; Hamad bin Khalifa University Press (HBKU Press): Ar Rayyan, Qatar, 2013; p. EEP-074. [CrossRef]
49. Anand, A.; Zeyara, A.; Al-Malaki, A.; Al-Ghanim, M.M.; Hitha, P.K.; Taj-Aldeen, S.; Al-Marri, S.; Fotedar, R. Isolation and identification of potentially pathogenic vibrio species from Qatari coastal seawaters. In *Proceedings of the Qatar Foundation Annual Research Conference Proceedings*; Hamad bin Khalifa University Press (HBKU Press): Ar Rayyan, Qatar, 2016; p. EESP2323.
50. Ashfaq, M.Y.; Al-Ghouti, M.A.; Qiblawey, H.; Rodrigues, D.F.; Hu, Y.; Zouari, C. Isolation, identification, and biodiversity of antiscalant degrading seawater bacteria using MALDI-TOF-MS and multivariate analysis. *Sci. Total Environ.* **2019**, *656*, 910–920. [CrossRef] [PubMed]
51. Catania, V.; Cappello, S.; Di Giorgi, V.; Santisi, S.; Di Maria, R.; Mazzola, A.; Vizzini, S.; Quatrini, P. Microbial communities of polluted sub-surface marine sediments. *Mar. Pollut. Bull.* **2018**, *131*, 396–406. [CrossRef]
52. Hoshino, T.; Doi, H.; Uramoto, G.-I.; Wörmer, L.; Adhikari, R.R.; Xiao, N.; Morono, Y.; D'Hondt, S.; Hinrichs, K.-U.; Inagaki, F. Global diversity of microbial communities in marine sediment. *Proc. Natl. Acad. Sci. USA* **2020**, *117*, 27587–27597. [CrossRef]
53. Zhuang, J.; Zhang, R.; Zeng, Y.; Dai, T.; Ye, Z.; Gao, Q.; Yang, Y.; Guo, X.; Li, G.; Zhou, J. Petroleum pollution changes microbial diversity and network complexity of soil profile in an oil refinery. *Front. Microbiol. Terr. Microbiol.* **2023**, *14*, 1193189. [CrossRef]
54. Liu, Q.; Tang, J.; Bai, Z.; Hecker, M.; Giesy, J.P. Distribution of petroleum degrading genes and factor analysis of petroleum contaminated soil from the Dagang Oilfield. *Sci. Rep.* **2015**, *5*, 11068. [CrossRef]
55. Epstein, E.; Norlyn, J.D.; Rush, D.W.; Kingsbury, R.W.; Kelly, D.B.; Cummingham, G.A.; Wrona, A.F. Saline culture of crops: A genetic approach. *Science* **1980**, *210*, 399–404. [CrossRef] [PubMed]
56. Svoboda, K.K.H.; Reenstra, W.R. Approaches to studying cellular signaling: A primer for morphologists. *Anat. Rec.* **2002**, *269*, 123–139. [CrossRef]
57. Czako, M.; Feng, X.; He, Y.; Liang, D.; Marton, L. Genetic modification of wetland grasses for phytoremediation. *Z. Naturforsch. C. J. Biosci.* **2005**, *60*, 285–291. [CrossRef]

58. Hussain, M.S.; Fareed, S.; Ansari, S.; Rahman, M.A.; Ahmad, I.Z.; Saeed, M. Current approaches toward production of secondary plant metabolites. *J. Pharm. Bioallied Sci.* **2012**, *4*, 10–20. [CrossRef] [PubMed]
59. Yasseen, B.T. Phytoremediation of Industrial Wastewater from Oil and Gas Fields using Native Plants: The Research Perspectives in the State of Qatar. *Cent. Eur. J. Biol.* **2014**, *3*, 6–23.
60. Yan, A.; Wang, Y.; Tan, S.N.; Yusof, M.L.M.; Ghosh, S.; Chen, Z. Phytoremediation: A promising approach for revegetation of heavy metal-polluted land. *Front. Plant Sci.* **2020**, *11*, 359. [CrossRef] [PubMed]
61. Al-Khayat, J.A.; Balakrishnan, P. *Avicennia marina* around Qatar: Tree, seedling, and pneumatophore densities in natural and planted mangroves using remote sensing. *Int. J. Sci.* **2014**, *3*, 18–27.
62. Karimi, Z.; Abdi, E.; Deljouei, A.; Cislaghi, A.; Shirvany, A.; Schwarz, M.; Hales, T.C. Vegetation-induced soil stabilization in coastal area: An example from a natural mangrove forest. *CATENA* **2022**, *216*, 106410. [CrossRef]
63. Friis, G.; Killilea, M.E. Mangrove Ecosystems of the United Arab Emirates. In *A Natural History of the Emirates*; Burt, J.A., Ed.; Springer: Cham, Switzerland, 2024. [CrossRef]
64. Farshid, Z.; Balef, R.M.; Zendehboudi, T.; Dehghan, N.; Mohajer, F.; Kalbi, S.; Hashemi, A.; Afshar, A.; Bafghi, T.H.; Baneshi, H.; et al. Reforestation of grey mangroves (*Avicennia marina*) along the northern coasts of the Persian Gulf. *Wetl. Ecol. Manag.* **2023**, *31*, 115–128. [CrossRef]
65. Zouhaier, B.; Hussain, A.A.; Saleh, K. Traits allowing *Avicennia marina* propagules to overcome seawater salinity. *Flora* **2018**, *242*, 16–21. [CrossRef]
66. Akram, H.; Hussain, S.; Mazumdar, P.; Chua, K.O.; Butt, T.E.; Harikrishna, J.A. Mangrove Health: A review of functions, threats, and challenges associated with mangrove management practices. *Forests* **2023**, *14*, 1698. [CrossRef]
67. Chatting, M.; Al-Maslamani, I.; Walton, M.; Skov, M.W.; Kennedy, H.; Husrevooglu, Y.S.; Vay, L.L. Future mangrove carbon storage under climate change and deforestation. *Front. Mar. Sci.* **2022**, *9*, 781876. [CrossRef]
68. Asari, N.; Suratman, M.N.; Ayob, N.A.M.; Abul Hamid, N.H. Mangrove as a Natural Barrier to Environmental Risks and Coastal Protection. *Mangroves: Ecol. Biodivers. Manag.* **2021**, *13*, 305–322. [CrossRef]
69. Rizk, A.M. *The Phytochemistry of the Flora of Qatar*; Scientific and Applied Research Centre, University of Qatar, Kingprint: Richmond, UK, 1986.
70. Mossa, J.S.; Al-Yahya, M.A.; Al-Meshal, I.A. *Medicinal Plants in Saudi Arabia*; King Saud Univ. Libraries: Riyadh, Saudi Arabia, 1987.
71. Rizk, A.M.; El-Ghazaly, A. *Medicinal and Poisonous Plants of Qatar*; Scientific and Applied Research Centre, University of Qatar: Doha, Qatar, 1995.
72. Kafle, A.; Timilsina, A.; Gautam, A.; Adhikari, K.; Bhattarai, A.; Aryal, N. Phytoremediation: Mechanisms, plant selection and enhancement by natural and synthetic agents. *Environ. Adv.* **2022**, *8*, 100203. [CrossRef]
73. Usman, K.; Al-Ghouti, M.A.; Abu-Dieyeh, M.H. The assessment of cadmium, chromium, copper, and nickel tolerance and bioaccumulation by shrub plant *Tetraena qataranse*. *Sci. Rep.* **2019**, *9*, 5658. [CrossRef]
74. Yasseen, B.T.; Al-Thani, R.F. Endophytes and halophytes to remediate industrial wastewater and saline soils: Perspectives from Qatar. *Plants* **2022**, *11*, 1497. [CrossRef]
75. Moreira, I.T.A.; de Oliveira, O.M.C.; Triguis, J.A.; Queiroz, A.; Ferreira, S.L.C.; Martins, C.M.S.; Silva, A.C.M.; Falcão, B.A. Phytoremediation in mangrove sediments impacted by persistent total petroleum hydrocarbons (TPH's) using *Avicennia schaueriana*. *Mar. Pollut. Bull.* **2012**, *67*, 130–136. [CrossRef] [PubMed]
76. Ivorra, L.; Cardoso, P.G.; Chan, S.K.; Cruzeiro, C.; Tagulao, K.A. Can mangroves work as an effective phytoremediation tool for pesticide contamination? An interlinked analysis between surface water, sediments, and biota. *J. Clean. Prod.* **2021**, *295*, 126334. [CrossRef]
77. Meng, S.; Peng, T.; Pratush, A.; Huang, T.; Hu, Z. Interactions between heavy metals and bacteria in mangroves. *Mar. Pollut. Bull.* **2021**, *172*, 112846. [CrossRef] [PubMed]
78. Abdel Bari, E.M.; Yasseen, B.T.; Al-Thani, R.F. *Halophytes in the State of Qatar*; (Sponsored by Environmental Studies Centre); Qatar University: Doha, Qatar, 2007; ISBN 99921-52-98-2.
79. Moradi, B.; Maivan, H.Z.; Hashtroudi, M.S.; Sorahinobar, M.; Rohloff, J. Physiological responses and phytoremediation capability of *Avicennia marina* to oil contamination. *Acta Physiol. Plant.* **2021**, *43*, 1–12. [CrossRef]
80. Araji, S.; Theresa, A.; Grammer, T.A.; Gertzen, R.; Anderson, S.D.; Mikulic-Petkovsek, M.; Veberic, R.; Phu, M.L.; Solar, A.; Leslie, C.A.; et al. Novel roles for the polyphenol oxidase enzyme in secondary metabolism and the regulation of cell death in Walnut. *Plant Physiol.* **2014**, *164*, 1191–1203. [CrossRef] [PubMed]
81. De Mello-Farias, P.C.; Chaves, A.L.S.; Lencina, C.L. Transgenic Plants for Enhanced Phytoremediation-Physiological Studies, Chapter 16. In *Genetic Transformation*; Alvarez, M., Ed.; Intech Open: Rijeka, Croatia, 2011.
82. Mahadik, S.; Ghosh, S.; Banerjee, S. Mangroves as potential agents of phytoremediation: A review. *Res. J. Chem. Environ.* **2022**, *26*, 138–144. [CrossRef]
83. Jadia, C.D.; Fulekar, M.H. Phytoremediation of heavy metals: Recent technique. *Afr. J. Biotechnol.* **2009**, *8*, 921–928; ISSN 1684-5315. Available online: http://www.academicjournals.org/AJB (accessed on 19 April 2024).
84. Yuliasni, R.; Kurniawan, S.B.; Marlena, B.; Hidayat, M.R.; Kadier, A.; Ma, P.C.; Imron, M.F. Recent progress of phytoremediation-based technologies for industrial wastewater treatment. *J. Ecol. Eng.* **2023**, *24*, 208–220. [CrossRef]
85. Varjani, S.J. Microbial degradation of petroleum hydrocarbons. *Bioresour. Technol.* **2017**, *223*, 277–286. [CrossRef] [PubMed]

86. Reichenauer, T.G.; Germida, J.J. Phytoremediation of organic contaminants in soil and groundwater. *Chem. Sus. Chem.* **2008**, *1*, 708–817. [CrossRef] [PubMed]
87. Carvalho, K.M.; Martin, D.F. Removal of aqueous selenium by four aquatic plants. *J. Aquat. Plant Manag.* **2001**, *39*, 33–36.
88. Liu, S.; Wang, Y.; Yu, L.; Oakey, J. Volatilization of mercury, arsenic and selenium during underground coal gasification. *Fuel* **2006**, *85*, 1550–1558. [CrossRef]
89. Pang, Y.L.; Quek, Y.Y.; Lim, S.; Shuit, S.H. Review on phytoremediation potential of floating aquatic plants for heavy metals: A promising approach. *Sustainability* **2023**, *15*, 1290. [CrossRef]
90. Almahasheer, H. Spatial coverage of mangrove communities in the Arabian Gulf. *Environ. Monit. Assess.* **2018**, *190*, 85. [CrossRef]
91. Yasseen, B.T.; Al-Thani, R.F. Ecophysiology of Wild Plants and Conservation Perspectives in the State of Qatar, Chapter 3. In *Agricultural Chemistry*; Stoytcheva, M., Zlatev, R., Eds.; InTech: Rijeka, Croatia, 2013; pp. 37–70, ISBN 978-953-51-1026-2. [CrossRef]
92. Al-Khayat, J.A.; Abdulla, M.A.; Alatalo, J.M. Diversity of benthic macrofauna and physical parameters of sediments in natural mangroves and in afforested mangroves three decades after compensatory planting. *Aquat. Sci.* **2019**, *81*, 4. [CrossRef]
93. Al-Khayat, J.A.; Vethamony, P.; Nanajkar, M. Molluscan diversity influenced by mangrove habitat in the Khors of Qatar. *Wetlands* **2021**, *41*, 45. [CrossRef]
94. Yasseen, B.T.; Abu-Al-Basal, M.A. Ecophysiology of *Limonium axillare* and *Avicennia marina* from the Coastline of Arabian Gulf-Qatar. *J. Coast. Conserv.* **2008**, *12*, 35–42. [CrossRef]
95. Al-Naimi, N.; Al-Ghouti, M.A.; Balakrishnan, P. Investigating chlorophyll and nitrogen levels of mangroves at Al-Khor, Qatar: An integrated chemical analysis and remote sensing approach. *Environ. Monit. Assess.* **2016**, *188*, 268. [CrossRef]
96. Larcher, W. *Physiological Plant Ecology, Ecophysiology and Stress Physiology of Functional Groups*, 4th ed.; Springer: Berlin, Germany, 2003.
97. Jian, Z.; Huang, D.; Fang, Y.; Cui, L.; Zhao, C.; Liu, S.; Wu, Y.; Chen, Q.; Ranvilage, C.I.P.M.; He, J.; et al. Home for marine species: Seagrass leaves as vital spawning grounds and food source. *Front. Mar. Sci.* **2020**, *7*, 2020. [CrossRef]
98. Lee, G.; Suonan, Z.; Kim, S.H.; Hwang, D.-W.; Lee, K.-S. Heavy metal accumulation and phytoremediation potential by transplants of the seagrass *Zostera marina* in the polluted bay systems. *Mar. Pollut. Bull.* **2019**, *149*, 110509. [CrossRef] [PubMed]
99. James, R.K.; Lynch, A.; Herman, P.M.J.; van Katwijk, M.M.; van Tussenbroek, B.I.; Dijkstra, H.A.; van Westen, R.M.; der Boog, C.G.; Klees, R.; Slobbe, C.; et al. Tropical biogeomorphic seagrass landscapes for coastal protection: Persistence and wave attenuation during major storms events. *Ecosystems* **2021**, *24*, 301–318. [CrossRef]
100. Montero-Hidalgo, M.; Tuya, F.; Otero-Ferrer, F.; Haroun, R.; Santos-Martín, F. Mapping and assessing seagrass meadows changes and blue carbon under past, current, and future scenarios. *Sci. Total Environ.* **2023**, *872*, 162244. [CrossRef]
101. Ganguly, D.; Singh, G.; Ramachandran, P.; Selvam, A.P.; Banerjee, K.; Ramachandran, R. Seagrass metabolism and carbon dynamics in a tropical coastal embayment. *Ambio* **2017**, *46*, 667–679. [CrossRef]
102. Bu-Olayan, A.H.; Thomas, B.V. Accumulation, and translocation of trace metals in *Halodule uninervis*, in the Kuwait coast. *Biosci. Biotechnol. Res. Asia* **2010**, *7*, 25–32.
103. Durako, M.J.; Kenworthy, W.J.; Fatemy, S.M.R.; Valavi, H.; Thayer, G.W. Assessment of the toxicity of Kuwait crude oil on the photosynthesis and respiration of seagrasses of the northern Gulf. *Mar. Pollut. Bull.* **1993**, *27*, 223–227. [CrossRef]
104. Khalafallah, A.A.; Geneid, Y.A.; Shaetaey, S.A.; Shaaban, B. Responses of the seagrass *Halodule uninervis* (Forssk.) Aschers. to hypersaline conditions. *Egypt. J. Aquat. Res.* **2013**, *39*, 167–176. [CrossRef]
105. Al-Arbash, A.; Al-Bader, D.; Suleman, P. Structural and biochemical responses of the seagrass *Halodule uninervis* to changes in salinity in Kuwait Bay, Doha area. *Kuwait J. Sci.* **2016**, *43*, 131–142.
106. Akinpelu, A.A.; Nazal, M.K.; Abuzaid, N. Adsorptive removal of polycyclic aromatic hydrocarbons from contaminated water by biomass from dead leaves of *Halodule uninervis*: Kinetic and thermodynamic studies. *Biomass Convers. Biorefin.* **2023**, *13*, 8301–8313. [CrossRef]
107. Ralph, P.J.; Burchett, M.D. Impact of petrochemicals on the photosynthesis of *Halophila ovalis* using chlorophyll fluorescence. *Mar. Pollut. Bull.* **1998**, *36*, 429–436. [CrossRef]
108. Ralph, P.J.; Burchett, M.D. Photosynthetic response of *Halophila ovalis* to heavy metal stress. *Environ. Pollut.* **1998**, *103*, 91–101. [CrossRef]
109. Singh, S.; Lal, M.M.; Southgate, P.C.; Wairiu, M.; Singh, A. Trace metal content in sediment cores and seagrass biomass from a tropical southwest Pacific Island. *Mar. Pollut. Bull.* **2021**, *171*, 112745. [CrossRef] [PubMed]
110. Ralph, P.J. Herbicide toxicity of *Halophila ovalis* assessed by chlorophyll a fluorescence. *Aquat. Bot.* **2000**, *66*, 141–152. [CrossRef]
111. Runcie, J.; Macinnis-Ng, C.; Ralph, P. *The Toxic Effects of Petrochemicals on Seagrasses: Literature Review*; Report Prepared by Institute for Water and Environmental Resource Management and Department of Environmental Sciences University of Technology, Sydney; Australian Maritime Safety Authority: Canberra, Australia, 2005.
112. Tupan, C.I.; Uneputty, P.A. Concentration of heavy metals lead (Pb) and cadmium (Cd) in water, sediment, and seagrass *Thalassia hemprichii* in Ambon Island waters. *AACL Bioflux* **2017**, *10*, 1610–1617.
113. McKenzie, L.J.; Yoshida, R.L.; Aini, J.W.; Andréfouet, S.; Colin, P.L.; Cullen-Unsworth, L.C.; Hughes, A.T.; Payri, C.E.; Rota, M.; Shaw, C.; et al. Seagrass ecosystem contributions to people's quality of life in the Pacific Island Countries and Territories. *Mar. Pollut. Bull.* **2021**, *167*, 112307. [CrossRef]
114. Yasseen, B.T. *Physiology of Water Stress in Plants*; University of Mosul: Mosul, Iraq, 1992.

115. Yasseen, B.T.; Al-Thani, R.F.; Alhadi, F.A.; Abbas, R.A.A. Soluble sugars in plants under stress at the Arabian Gulf region: Possible roles of microorganisms. *J. Plant Biochem. Physiol.* **2018**, *6*, 224. [CrossRef]
116. Nazal, M.K.; Ditta, M.; Rao, G.D.; Abuzaid, N.S. Treatment of water contaminated with petroleum hydrocarbons using a biochar derived from seagrass biomass as low-cost adsorbent: Isotherm, kinetics, and reusability studies. *Sep. Sci. Technol.* **2022**, *57*, 1–16. [CrossRef]
117. Wilding, C.; Tillin, H.; Stewart, E.J.; Lubelski, A.; Burrows, M.; Smale, D. *Hand Harvesting of Seaweed: Evidence Review to Support Sustainable Management*; NRW Evidence Report Series Report No: 573; NRW: Bangor, Maine, 2021; 275p.
118. Hand Harvesting of Seaweed: Evidence Review to Support Sustainable Management. Available online: https://www.mba.ac.uk/wp-content/uploads/2022/05/Wilding_et_al_2021_NRW_Hand-harvesting-seaweed.pdf (accessed on 20 March 2024).
119. Al-Homaidan, A.A.; Al-Ghanayem, A.A.; Al-Qahtani, H.S.; Alabbad, A.; Alabdullatif, J.A.; Alwakeel, S.; Ameen, F. Effect of sampling time on the heavy metal concentrations of brown algae: A bioindicator study on the Arabian Gulf coast. *Chemosphere* **2021**, *263*, 127998. [CrossRef]
120. Ameen, F.; Al-Homaidan, A.A.; Al-Mahasheer, H.; Dawoud, T.; Al-Wakeel, S.; Al-Maarofi, S. Biomonitoring coastal pollution on the Arabian Gulf and the Gulf of Aden using macroalgae: A review. *Mar. Pollut. Bull.* **2022**, *175*, 113156. [CrossRef]
121. Lourenço-Lopes, C.; Garcia-Oliveira, P.; Carpena, M.; Fraga-Corral, M.; Jimenez-Lopez, C.; Pereira, A.G.; Prieto, M.A.; Simal-Gandara, J. Scientific approaches on extraction, purification and stability for the commercialization of fucoxanthin recovered from brown algae. *Foods* **2020**, *9*, 1113. [CrossRef]
122. Choudhary, P.; Subhash, G.V.; Khade, M.; Savant, S.; Musale, A.; Kumar, G.R.K.; Chelliah, M.S.; Dasgupta, S. Empowering blue economy: From underrated ecosystem to sustainable industry. *J. Environ. Mang.* **2021**, *291*, 112697. [CrossRef]
123. Rizk, A.M.; Al-Easa, H.S.; Kornprobst, J.M. *The Phytochemistry of the Macro and Blue-Green Algae of the Arabian Gulf*; Faculty of Science, The University of Qatar: Doha, Qatar, 1999; ISBN 999921-46-64-8.
124. Koul, B.; Sharma, K.; Shah, M.P. Phycoremediation: A sustainable alternative in wastewater treatment (WWT) regime. *Environ. Technol. Innov.* **2022**, *25*, 102040. [CrossRef]
125. Ogundele, O.D.; Adewumi, A.J.; Oyegoke, D.A. Phycoremediation: Algae as an effective agent for sustainable remediation and waste water treatment. *Environ. Earth Sci. Res. J.* **2023**, *10*, 7–17. [CrossRef]
126. Ankit, B.K.; Korstad, J. Phycoremediation: Use of algae to sequester heavy metals. *Hydrobiology* **2022**, *1*, 288–303. [CrossRef]
127. Kumar, A.; Ponmani, S.; Sharma, G.K.; Sangavi, P.; Chaturvedi, A.K.; Singh, A.; Malyan, S.K.; Kumar, A.; Khan, S.A.; Shabnam, A.A.; et al. Plummeting toxic contaminates from water through phycoremediation: Mechanism, influencing factors and outlook to enhance the capacity of living and non-living algae. *Environ. Res.* **2023**, *239*, 117381. [CrossRef]
128. Heiba, H.I.; Dorgham, M.M.; Al-Nagdy, S.A.; Rizk, A.M. Phytochemical studies on the marine algae of Qatar, Arabian Gulf. *Qatar Univ. Sci. Bull.* **1990**, *10*, 99–113.
129. Garcia, E.M.; Reyes Gil, R.E. Bioconcentration of Hg in *Acetabularia caliculus*: Evidence of a polypeptide in whole cells and anucleated cells. *Toxicol. Environ. Chem.* **1996**, *55*, 11–18. [CrossRef]
130. Freije, A.M. Heavy metal, trace element and petroleum hydrocarbon pollution in the Arabian Gulf: Review. *J. Assoc. Arab Univ. Basic Appl. Sci.* **2015**, *17*, 90–100. [CrossRef]
131. Henriques, B.; Rocha, L.S.; Lopes, C.B.; Figueira, P.; da Costa Duarte, A.; Garcia do Vale, C.A.; Pardal, M.A.; Pereira, E. A macroalgae-based biotechnology for water remediation: Simultaneous removal of Cd, Pb and Hg by living *Ulva lactuca*. *J. Environ. Manag.* **2017**, *191*, 275–289. [CrossRef]
132. Hawas, U.W.; Abou El-Kassem, L.T.; Al-Farawati, R.; Shaher, F.M. Halo-phenolic metabolites and their in vitro antioxidant and cytotoxic activities from the Red Sea alga *Avrainvillea amadelpha*. *Z. Naturforsch C. J. Biosci.* **2021**, *76*, 213–218. [CrossRef] [PubMed]
133. Prasada Rao, N.V.S.A.V.; Sastry, K.V.; Venkata, R.K. Studies on Indian seaweed polysaccharides, Part 1. Isolation and characterization of the sulphated polysaccharides of *Spongomorpha indica* and *Boodlea struveoides*. *Indian J. Pharm. Sci.* **1982**, *44*, 144–146.
134. Hori, H.; Miyazawa, K.; Ito, K. Isolation and characterization of polyconjugate-specific isoagglutinins from a marine green algae *Boodlea coacta* (Dickie) Murray et De Toni. *Bot. Mar.* **1986**, *29*, 323–328. [CrossRef]
135. Mshigeni, K.E.; Durgham, M.M. *Benthic Marine Algae of Qatar, A Preliminary Survey*; UNESCO Regional Office Report: Doha, Qatar, 1987.
136. Praveen, P.J.; Singh, K.; Naik, B.G.; Parameswaran, P.S. Phytochemical studies of marine green algae *Boodlea composita* from Ukha, west coast of India. *J. Indian Chem. Soc.* **2017**, *94*, 637–640.
137. Kim, H.; Kim, H.T.; Jung, S.H.; Han, J.W.; Jo, S.; Kim, I.G.; Kim, R.K.; Kahm, Y.J.; Choi, T.I.; Kim, C.H.; et al. A Novel anticancer peptide derived from *Bryopsis plumosa* regulates proliferation and invasion in non-small cell lung cancer cells. *Mar. Drugs* **2023**, *21*, 607. [CrossRef]
138. Rushdi, M.I.; Abdel-Rahman, I.A.M.; Attia, E.Z.; Abdelraheem, W.M.; Saber, H.; Madkour, H.A.; Amin, E.; Hassan, H.M.; Abdelmohsen, U.R. A review on the diversity, chemical and pharmacological potential of the green algae genus *Caulerpa*. *S. Afr. J. Bot.* **2020**, *132*, 226–241. [CrossRef]
139. Landi, S.; Santini, G.; Vitale, E.; Di Natale, G.; Maisto, G.; Arena, C.; Esposito, S. Photosynthetic, molecular, and ultrastructural characterization of toxic effects of zinc in *Caulerpa racemosa* indicate promising bioremediation potentiality. *Plants* **2022**, *11*, 2868. [CrossRef]

140. Caronni, S.; Quaglini, L.A.; Franzetti, A.; Gentili, R.; Montagnani, C.; Citterio, S. Does *Caulerpa prolifera* with its bacterial coating represent a promising association for seawater phytoremediation of diesel hydrocarbons? *Plants* **2023**, *12*, 2507. [CrossRef]
141. Bohnic, P.; Korbar-Samid, J.; Sedej, A. Saponins in the sea lettuces (Ulvaceae). *Farm. Vestn. (Ljubljana)* **1973**, *24*, 125–129.
142. Shun, M.; Kasuyuki, W. Gas chromatographic analysis of cell/wall polysaccharides in certain siphonocladalean and cladophoralean algae. *Rep. Usa Mar. Biol. Inst. Karachi Univ.* **1985**, *7*, 9–14.
143. Williams, J.O.; Ntorn, Q. Remediation of a crude oil polluted river in B-Dere in orgonila and rivers State using *Chaetomorpha* and *Nostoc* species. *IOSR J. Environ. Sci. Toxicol. Food Technol.* **2019**, *13*, 1–8. [CrossRef]
144. Aquilino, F.; Paradiso, A.; Trani, R.; Longo, C.; Pierri, C.; Corriero, G.; de Pinto, M.C. *Chaetomorpha linum* in the bioremediation of aquaculture wastewater: Optimization of nutrient removal efficiency at the laboratory scale. *Aquaculture* **2020**, *523*, 735133. [CrossRef]
145. Alsafran, M.; Saleem, M.H.; Al Jabri, H.; Rizwan, M.; Usman, K. Principles and Applicability of Integrated Remediation Strategies for Heavy Metal Removal/Recovery from Contaminated Environments. *J. Plant Growth Regul.* **2023**, *42*, 3419–3440. [CrossRef]
146. Chmielewská, E.; Medved, J. Bioaccumulation of heavy metals by green algae *Cladophora glomerata* in a refinery sewage lagoon. *Croat. Chem. Acta* **2001**, *74*, 135–145.
147. Lee, Y.-C.; Chang, S.-P. The biosorption of heavy metals from aqueous solution by *Spirogyra* and *Cladophora* filamentous macroalgae. *Bioresour. Technol.* **2011**, *102*, 5297–5304. [CrossRef]
148. Michalak, I.; Messyasz, B. Concise review of *Cladophora* spp.: Macroalgae of commercial interest. *J. Appl. Phycol.* **2021**, *33*, 133–166. [CrossRef]
149. Ross, M.E.; Stanley, M.S.; Day, J.G.; Semião, A.J.C. Removal of metals from aqueous solutions using dried *Cladophora parriaudii* of varying biochemical composition. *J. Environ. Manag.* **2021**, *290*, 112620. [CrossRef]
150. Khan, S.; Ullah, A.; Ayaz, T.; Aziz, A.; Aman, K.; Habib, M.; Yilmaz, S.; Farid, A.; Yasmin, H.; Ali, Q. Phycoremediation of industrial wastewater using *Vaucheria debaryana* and *Cladophora glomerata*. *Environ. Monit. Assess.* **2023**, *195*, 825. [CrossRef]
151. El-Beltagi, H.S.; Mohamed, A.A.; Mohamed, H.I.; Ramadan, K.M.A.; Barqawi, A.A.; Mansour, A.T. Phytochemical and potential properties of seaweeds and their recent applications: A review. *Mar. Drugs* **2022**, *20*, 342. [CrossRef]
152. Tarfeen, N.; Ul Nisa, K.; Hamid, B.; Bashir, Z.; Yatoo, A.M.; Ashraf Dar, M.; Mohiddin, F.A.; Amin, Z.; Ahmad, R.A.; Sayyed, R.Z. Microbial remediation: A promising tool for reclamation of contaminated sites with special emphasis on heavy metal and pesticide pollution: A review. *Processes* **2022**, *10*, 1358. [CrossRef]
153. Khalaf, F.I.; Gab-Alla, A.A.-F.; Ahmed, A.I. Ecological study of the impact of oil pollution on the fringing reef of Ras Shukeir, Gulf of Suez, Red Sea, Egypt. *Egypt. J. Biol.* **2002**, *4*, 119–126.
154. Al-Shwafi, N.A.; Rushdi, A.I. Heavy metal concentrations in marine green, brown, and red seaweeds from coastal waters of Yemen, the Gulf of Aden. *Environ. Earth Sci.* **2008**, *55*, 653–660. [CrossRef]
155. Mearns, A.J.; Reish, D.J.; Oshida, P.S.; Morrison, A.M.; Rempel-Hester, M.A.; Arthur, C.; Rutherford, N.; Pryor, R. Effects of pollution on marine organisms. *Water Environ. Res.* **2016**, *88*, 1693–1807. Available online: https://www.jstor.org/stable/26662431 (accessed on 24 April 2024). [CrossRef] [PubMed]
156. Jacques, N.R.; McMartin, D.W. Evaluation of algal phytoremediation of light extractable petroleum hydrocarbons in subarctic climates. *Remediat. J.* **2009**, *20*, 119–132. [CrossRef]
157. Ben Chekroun, K.; Baghour, M. The role of algae in phytoremediation of heavy metals: A review. *J. Mater. Environ. Sci.* **2013**, *4*, 873–880.
158. Baghour, M. Effect of seaweeds in phyto-remediation, Chapter Book. In *Biotechnological Applications of Seaweeds*; Nova Publishers Sciences: Hauppauge, NY, USA, 2017; pp. 47–83, ISBN 978-1-53610-968-9.
159. Agarwal, S.; Albeshr, M.F.; Mahboobb, S.; Atique, U.; Pramanick, P.; Mitra, A. Bioaccumulation factor (BAF) of heavy metals in green seaweed to assess the phytoremediation potential. *J. King Saud Univ.-Sci.* **2022**, *34*, 102078. [CrossRef]
160. Danouche, M.; El Ghachtouli, N.; El Arroussi, H. Phycoremediation mechanisms of heavy metals using living green microalgae: Physicochemical and molecular approaches for enhancing selectivity and removal capacity. *Heliyon* **2021**, *7*, e07609. [CrossRef]
161. Krupina, M.V. Use of *Cystoseira* and *Ulva* macrophytes for monitoring marine pollution by heavy metals. *Deposited Doc. VINITI* **1981**, *5484-81*, 33–34.
162. Areco, M.M.; Salomone, V.N.; Afonso, M.S. *Ulva lactuca*: A bioindicator for anthropogenic contamination and its environmental remediation capacity. *Mar. Environ. Res.* **2021**, *171*, 105468. [CrossRef] [PubMed]
163. Akl, F.M.A.; Ahmed, S.I.; El-Sheekh, M.M.; Mofida, E.M.; Makhlof, M.E.M. Bioremediation of *n*-alkanes, polycyclic aromatic hydrocarbons, and heavy metals from wastewater using seaweeds. *Environ. Sci. Pollut. Res.* **2023**, *30*, 104814–104832. [CrossRef]
164. El-Mahrouk, M.E.; Dewir, Y.H.; Hafez, Y.M.; El-Banna, A.; Moghanm, F.S.; El-Ramady, H.; Mahmood, Q.; Elbehiry, F.; Brevik, E.C. Assessment of bioaccumulation of heavy metals and their ecological risk in sea lettuce (*Ulva* spp.) along the coast Alexandria, Egypt: Implications for sustainable management. *Sustainability* **2023**, *15*, 4404. [CrossRef]
165. Chen, L.; Zhang, X.; Zhang, M.; Zhu, Y.; Zhuo, R. Removal of heavy-metal pollutants by white rot fungi: Mechanisms, achievements, and perspectives. *J. Clean. Prod.* **2022**, *354*, 131681. [CrossRef]
166. Deng, S.; Zhang, X.; Zhu, Y.; Zhuo, R. Recent advances in phyto-combined remediation of heavy metal pollution in soil. *Biotechnol. Adv.* **2024**, *72*, 108337. [CrossRef]
167. Dadolahi-Sohrab, A.; Nikvarz, A.; Nabavi, S.M.B.; Safahieh, A.; Mohseni, M.K. Environmental monitoring of heavy metals in seaweed and associated sediment from the Strait of Hormuz, I.R. Iran. *World J. Fish Mar. Sci.* **2011**, *3*, 576–589.

168. El Asri, O.; Ramdani, M.; Latrach, L.; Haloui, B.; Ramdani, M.; Afilal, M.E. Comparison of energy recovery after anaerobic digestion of three Marchica lagoon algae (*Caulerpa prolifera*, *Colpomenia sinuosa*, *Gracilaria bursa-pastoris*). *Sustain. Mater. Technol.* **2017**, *11*, 47–52. [CrossRef]
169. Alprol, A.E.; Mansour, A.T.; Abdelwahab, A.M.; Ashour, M. Advances in green synthesis of metal oxide nanoparticles by marine algae for wastewater treatment by adsorption and photocatalysis techniques. *Catalysts* **2023**, *13*, 888. [CrossRef]
170. Blanco-Vieites, M.; Suárez-Montes, D.; Delgado, F.; Álvarez-Gil, M.; Hernández Battez, A.; Rodríguez, E. Removal of heavy metals and hydrocarbons by microalgae from wastewater in the steel industry. *Algal Res.* **2022**, *64*, 102700. [CrossRef]
171. Kravtsova, A.; Milchakova, N.; Frontasyeva, M. Elemental accumulation in the black sea brown algae *Cystoseira* studied by neutron activation analysis. *Ecol. Chem. Eng. S* **2014**, *21*, 9–23. [CrossRef]
172. Koshlaf, E.; Ball, A.S. Soil bioremediation approaches for petroleum hydrocarbon polluted environments. *AIMS Microbiol.* **2017**, *3*, 25–49. [CrossRef]
173. Gupta, G.S.; Yadav, G.; Tiwari, S. Bioremediation of heavy metals: A new approach to sustainable agriculture. Restoration of wetland ecosystem. In *Restoration of Wetland Ecosystem: A Trajectory towards a Sustainable Environment*; Springer: Berlin/Heidelberg, Germany, 2020. [CrossRef]
174. Abdullahi, U.; Khandaker, M.M.; Alias, N.; Shaari, E.M.; Alam, M.A.; Badaluddin, N.A.; Mohd, K.S. Sea weed effects on plant growth and environmental remediation: A review. *J. Phytol.* **2021**, *13*, 6903. [CrossRef]
175. Rahhou, A.; Layachi, M.; Akodad, M.; El-Ouamari, N.; Aknaf, A.; Skalli, A.; Oudra, B.; Kolar, M.; Imperl, J.; Petrova, P.; et al. Analysis and health risk assessment of heavy metals in four common seaweeds of Marchica lagoon (a restored lagoon, Moroccan Mediterranean). *Arabian J. Chem.* **2023**, *16*, 105281. [CrossRef]
176. Ahmed, H.; Heneidak, S.; El Shoubaky, G.A.; Rasmey, A.-H.M. In vitro comparative antimicrobial potential of bioactive crude and fatty acids extracted from abundant marine macroalgae, Egypt. *Front. Sci. Res. Technol.* **2023**, *7*, 11–20. [CrossRef]
177. Osman, N.A.H.K.; Abd-Elazeem, O.M.; Al-Eisa, R.A.; El-Shenawy, N.S. Anticancer and antimicrobial evaluation of extract from brown algae *Hormophysa cuneiformis*. *J. Appl. Biomed.* **2023**, *21*, 121–136. [CrossRef]
178. Engdahl, S.; Mamboya, F.; Mtolera, M.; Semesi, A.K.; Björk, M. The brown macroalga *Padina boergesenii* as an indicator of heavy metal contamination in the Zanzibar channel. *Ambio* **1998**, *27*, 694–700.
179. Mantiri, D.M.H.; Kepel, R.C.; Manoppo, H.; Paulus, J.J.H.; Nasprianto, D.S.P. Metals in seawater, sediment and *Padina australis* (Hauck, 1887) algae in the waters of North Sulawesi. *AACL Bioflux* **2019**, *12*, 840–851. Available online: http://www.bioflux.com.ro/aacl (accessed on 23 May 2024).
180. Foday, E.H., Jr.; Bo, B.; Xu, X. Removal of toxic heavy metals from contaminated aqueous solutions using seaweeds: A review. *Sustainability* **2021**, *13*, 12311. [CrossRef]
181. Samar, J.; Butt, G.Y.; Shah, A.A.; Shah, A.N.; Ali, S.; Jan, B.L.; Abdelsalam, N.R.; Hussaan, M. Phycochemical and biological activities from different extracts of *Padina antillarum* (Kützing) Piccone. *Front. Plant Sci.* **2022**, *13*, 929368. [CrossRef] [PubMed]
182. Vijayaraghavan, K.; Teo, T.T.; Balasubramanian, R.; Joshi, U.M. Application of *Sargassum* biomass to remove heavy metal ions from synthetic multi-metal solutions and urban storm water runoff. *J. Hazard. Mater.* **2009**, *164*, 1019–1023. [CrossRef]
183. Kumar, M.; Aparna Seth, A.; Singh, A.K.; Rajput, M.S.; Mohd Sikandar, M. Remediation strategies for heavy metals contaminated ecosystem: A review. *Environ. Sustain. Ind.* **2021**, *12*, 100155. [CrossRef]
184. Fernández, L.A.G.; Frometa, A.E.N.; Alvarez, C.C.; Ramirez, R.F.; Flores, P.E.D.; Ramos, V.C.; Polo, M.S.; Martin, F.C.; Castillo, N.A.M. Valorization of *Sargassum* Biomass as Potential Material for the Remediation of Heavy-Metals-Contaminated Waters. *Int. J. Environ. Res. Public Health* **2023**, *20*, 2559. [CrossRef]
185. Rangabhashiyam, S.; Vijayaraghavan, K. Biosorption of Tm (III) by free and polysulfone-immobilized *Turbinaria conoides* biomass. *J. Ind. Eng. Chem.* **2019**, *80*, 318–324. [CrossRef]
186. Mukherjee, A.; Sarkar, D.; Sasmal, S. A review of green synthesis of metal nanoparticles using algae. *Front. Microbiol.* **2021**, *12*, 693899. [CrossRef]
187. Elhady, S.S.; Habib, E.S.; Abdelhameed, R.F.A.; Goda, M.S.; Hazem, R.M.; Mehanna, E.T.; Helal, M.A.; Hosny, K.M.; Diri, R.M.; Hassanean, H.A.; et al. Anticancer effects of new Ceramides isolated from the Red Sea, red algae *Hypnea musciformis* in a model of ehrlich ascites carcinoma: LC-HRMS analysis profile and molecular modeling. *Mar. Drugs* **2022**, *20*, 63. [CrossRef] [PubMed]
188. Gupta, P.K.; Ranjan, S.; Gupta, S.K. Phycoremediation of petroleum hydrocarbon-polluted sites: Application, challenges, and Future prospects. In *Application of Microalgae in Wastewater Treatment*; Springer: Berlin/Heidelberg, Germany, 2019. [CrossRef]
189. Jimenez-Lopez, C.; Pereira, A.G.; Lourenço-Lopes, C.; Garcia-Oliveira, P.; Cassani, L.; Fraga-Corral, M.; Prieto, M.A.; Simal-Gandara, J. Main bioactive phenolic compounds in marine algae and their mechanisms of action supporting potential health benefits. *Food Chem.* **2021**, *341*, 128262. [CrossRef] [PubMed]
190. Murphy, C. An Investigation into the Bioaccumulation of Chromium by Macroalgae. Ph.D. Thesis, Waterford Institute of Technology, Waterford, Ireland, 2016.
191. Augier, H.; Gilles, G.; Ramonda, G. The benthic red alga *Ceramium ciliatum* var. robustum (J.Ag.) G. Mazoyer is a remarkable biological indicator of littoral mercury pollution (Translated from French). *C. R. Acad. Hebd. Seances Acad. Sci. D* **1977**, *284*, 445–447.
192. Gaur, N.; Flora, G.; Yadav, M.; Tiwari, A. A review with recent advancements on bioremediation-based abolition of heavy metals. *Environ. Sci. Process Impacts* **2014**, *16*, 180–193. [CrossRef]

193. Jitar, O.; Teodosiu, C.; Oros, A.; Plavan, G.; Nicoara, M. Bioaccumulation of heavy metals in marine organisms from the Romanian sector of the Black Sea. *New Biotechnol.* **2015**, *32*, 369–378. [CrossRef]
194. Stout, E.P.; Kubanek, J. Marine macroalgal natural products. In *Reference Module: Chemistry, Molecular Sciences and Chemical Engineering Comprehensive Natural Products II Chemistry and Biology*; Elsevier: Amsterdam, The Netherlands, 2010; Volume 2, pp. 41–65.
195. Amasha, R.H.; Aly, M.M. Removal of dangerous heavy metal and some pathogens by dried green algae collected from Jeddah coast. *Pharmacophore* **2019**, *10*, 3–13.
196. El-Malek, F.; Rofeal, M.; Zabed, H.M.; Nizami, A.-S.; Rehan, M.; Qi, X. Microorganism-mediated algal biomass processing for clean products manufacturing: Status, challenges, and outlook. *Fuel* **2022**, *311*, 122612. [CrossRef]
197. Rathinam, A.; Maharshi, B.; Janardhanan, S.K.; Jonnalagadda, R.R.; Nair, B.U. Biosorption of cadmium metal ion from simulated wastewaters using *Hypnea valentiae* biomass: A kinetic and thermodynamic study. *Bioresour. Technol.* **2010**, *101*, 1466–1470. [CrossRef]
198. Fawzy, M.A. Phycoremediation and adsorption isotherms of cadmium and copper ions by *Merismopedia tenuissima* and their effect on growth and metabolism. *Environ. Toxicol. Pharmacol.* **2016**, *46*, 116–121. [CrossRef]
199. Qari, R.; Siddiqui, S.A. A comparative study of heavy metal concentrations in red seaweeds from different coastal areas of Karachi, Arabian Sea. *Indian J. Mar. Sci.* **2010**, *39*, 27–42.
200. Hamdy, S.M.; Shaban, A.M.; Abdel Aziz, Y.S.; Mahmoud, A.M.; Moemen, L.A.; Ibrahim, W.M.; Gad, N.S. Ameliorative role of *Jania rubens* alga against toxicity of heavy metal polluted water in male rats. *Sci. Technol. Public Policy* **2018**, *2*, 38–46. [CrossRef]
201. Nonomura, A.M. Development of *Janczewskia morimotoi* (Ceramiales) on its host *Laurencia nipponica* (Ceramiales, Rhdophyceae). *J. Phycol.* **1979**, *15*, 154–162. [CrossRef]
202. Kim, S.-K.; Vo, T.-S.; Ngo, D.-H. Potential application of marine algae as antiviral agents in medicinal food. *Adv. Food Nutr. Res.* **2011**, *64*, 245–254. [PubMed]
203. Baweja, P.; Kumar, S.; Sahoo, D.; Levine, I. Biology of seaweeds, Chapter 3. In *Seaweed in Health and Disease Prevention*; Fleurence, J., Levine, I.A., Eds.; Academic Press: Cambridge, UK, 2016; pp. 41–106. [CrossRef]
204. Kowanga, K.; Mauti, G.O.; Mauti, E.M. Biosorption for lead (II) ions from aqueous solutions by the biomass of *Spyridia filamentosa* algal species found in Indian Ocean. *J. Sci. Innov. Res.* **2015**, *4*, 218–220. [CrossRef]
205. Valarmathi, N.; Ameen, F.; Almansob, A.; Kumar, P.; Arunprakash, S.; Govarthanan, M. Utilization of marine seaweed *Spyridia filamentosa* for silver nanoparticles synthesis and its clinical applications. *Mater. Lett.* **2020**, *263*, 127244. [CrossRef]
206. Osuji, L.C.; Onojake, C.M. Trace heavy metals associated with crude oil: A case study of Ebocha-8 oil-spill-polluted site in Niger Delta, Nigeria. *Chem. Biodivers.* **2004**, *1*, 1708–1715. [CrossRef]
207. Baghour, M. Algal degradation of organic pollutants. In *Handbook of Eco-Materials*; Martínez, L., Kharissova, O., Kharisov, B., Eds.; Springer: Cham, Switzerland, 2019. [CrossRef]
208. Juhmani, A.-S.; Vezzi, A.; Wahsha, M.; Buosi, A.; De Pascale, F.; Schiavon, R.; Sfriso, A. Diversity and dynamics of seaweed associated microbial communities inhabiting the lagoon of Venice. *Microorganisms* **2020**, *8*, 1657. [CrossRef] [PubMed]
209. Menaa, F.; Wijesinghe, P.A.U.I.; Thiripuranathar, G.; Uzair, B.; Iqbal, H.; Khan, B.A.; Menaa, B. Ecological and industrial implications of dynamic seaweed-associated microbiota interactions. *Mar. Drugs* **2020**, *18*, 641. [CrossRef] [PubMed]
210. Ren, C.-G.; Liu, Z.-Y.; Wang, X.-L.; Qin, S. The seaweed holobiont: From microecology to biotechnological applications. *Microb. Biotechnol.* **2022**, *15*, 738–754. [CrossRef] [PubMed]
211. Fei, X. Solving the coastal eutrophication problem by large scale seaweed cultivation. *Hydrobiologia* **2004**, *512*, 145–151. [CrossRef]
212. Mocek-Płóciniak, A.; Mencel, J.; Zakrzewski, W.; Roszkowski, S. Phytoremediation as an effective remedy for removing trace elements from ecosystems. *Plants* **2023**, *12*, 1653. [CrossRef]
213. Laurens, L.M.L.; Lane, M.; Nelson, R.S. Sustainable seaweed biotechnology solutions for carbon capture, composition, and deconstruction. *Trends Biotechnol.* **2020**, *38*, 1232–1244. [CrossRef]
214. Butt, M.A.; Voronkov, G.S.; Grakhova, E.P.; Kutluyarov, R.V.; Kazanskiy, N.L.; Khonina, S.N. Environmental monitoring: A comprehensive review on optical waveguide and fiber-based sensors. *Biosensors* **2022**, *12*, 1038. [CrossRef] [PubMed]
215. Amin, S.A.; Almahasheer, H. Pollution indices of heavy metals in the Western Arabian Gulf coastal area. *Egypt. J. Aquat. Res.* **2022**, *48*, 21–27. [CrossRef]

toxics

MDPI

Review

Research on the Application and Mechanisms of Electroactive Microorganisms in Toxicants Monitoring: A Review

Fei Xing [1,2], Liang Duan [1,2,*], Haiya Zhang [1,2], Hengliang Zhang [1] and Shilong Li [1]

[1] State Key Laboratory of Environmental Criteria and Risk Assessment, Chinese Research Academy of Environmental Sciences, Beijing 100012, China; feixgy@126.com (F.X.); flying850612@126.com (H.Z.); 201831470030@mail.bnu.edu.cn (H.Z.); slone_li@126.com (S.L.)

[2] State Environmental Protection Key Laboratory of Estuarine and Coastal Environment, Chinese Research Academy of Environmental Sciences, Beijing 100012, China

* Correspondence: duanliang@craes.org.cn; Tel./Fax: +86-010-84915322

Abstract: A biological treatment is the core process for removing organic pollutants from industrial wastewater. However, industrial wastewater often contains large amounts of toxic and harmful pollutants, which can inhibit the activity of microorganisms in a treatment system, precipitate the deterioration of effluent quality, and threaten water ecological security from time to time. In most of the existing anaerobic biological treatment processes, toxic effects on microorganisms are determined according to the amounts of end-products of the biochemical reactions, and the evaluation results are relatively lacking. When microorganisms contact toxic substances, changes in biological metabolic activity precede the accumulation of reaction products. As sensitive units, electroactive microorganisms can generate electrical signals, a change in which can directly reflect the toxicity level. The applications of electroactive microorganisms for the toxicity monitoring of wastewater are very promising. Further attention needs to be paid to considering the appropriate evaluation index, the influence of the environment on test results, mechanisms, and other aspects. Therefore, we reviewed the literature regarding the above aspects in order to provide a research foundation for the practical application of electroactive microorganisms in toxicant monitoring.

Keywords: microbial fuel cell (MFC); electroactive microorganisms; toxic monitoring; influence factor; mechanisms

1. Introduction

Microbial fuel cells (MFCs) are reactors that use electroactive microorganisms to generate electricity [1]. In addition to being used in energy production [2–4] and wastewater treatments [5–8], electroactive microorganisms are often used as a sensitive unit for detecting water quality [9–11]. Electroactive microorganisms can reflect the magnitude of a toxic effect through changes in an output electrical signal, so they can be applied to the water quality monitoring [12] of domestic sewage [13,14], petrochemical wastewater [15], rivers, and groundwater [11,16], and they can even be used to monitor the damage inflicted by acid rain on crops [17].

The research and applications in the toxic monitoring of wastewater are very promising. Biological treatment is the core process in removing organic pollutants in industrial wastewater [18]. However, industrial wastewater often contains numerous toxic and harmful pollutants, which inhibit the activity of microorganisms in the treatment system [19], precipitating the deterioration of effluent water quality and threatening water ecological safety.

Toxicants in wastewater will affect microorganisms in biological treatment systems. According to the type of sewage-focused biological treatment process used, biological treatment can be divided into aerobic biological treatments and anaerobic biological treatments, as shown in Figure 1. The toxicity measurement approaches [20] of aerobic biological

processes are relatively mature, and commonly used methods include the activated sludge oxygen consumption rate inhibition test [21], the nitrification rate inhibition test [21], etc. For many high-concentration refractory organic wastewaters, before aerobic biological treatment, anaerobic pretreatment can reduce the concentration of organic matter and improve biodegradability, so the anaerobic biological treatment unit bears the brunt of the impact. Therefore, the evaluation and control of the toxicity of wastewater via anaerobic processes deserve great attention. However, the current domestic and foreign toxicity measurement methods are still limited to the direct determination of the final products of biochemical reactions, and these methods mainly include assessing anaerobic methane production via monitoring the methane content [18], evaluating hydrolytic acidification by monitoring the content of volatile fatty acids [18], and so on. It is well known that, in the process of contact between microorganisms and toxic substances, changes in biological metabolic activity precede the accumulation of reaction products. Therefore, the method of expressing biological metabolic activity with light and electrical signals, thereby indicating the toxicity of wastewater, offers the advantages of fast detection speed and strong sensitivity and is a promising method for assessing the toxicity of wastewater.

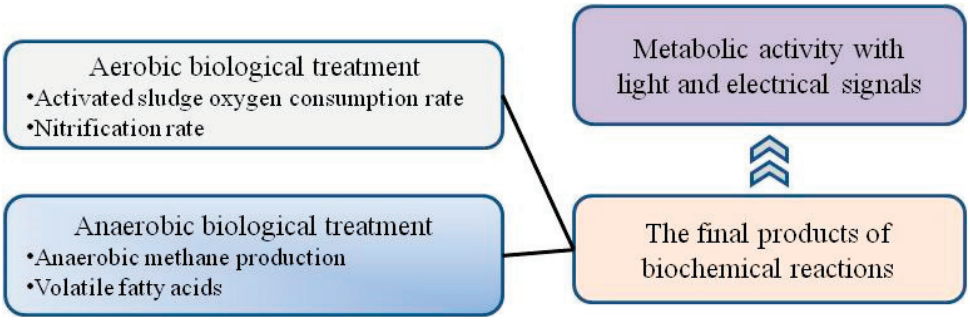

Figure 1. Characteristics of toxicity assessment methods.

2. Principle and Application of Electroactive Microorganism in Toxicants Monitoring

2.1. The Principle of MFCs

Using microorganisms to efficiently convert chemical energy into electrical energy is the working principle of MFC [22]. A schematic diagram of the structure of an MFC [1] is shown in Figure 2. The electroactive microorganisms at the anode degrade organic matter through biological oxidation reactions and produce electrons, which are transferred to the outside of the cell, and protons are released into the solution at the same time. The electrons are transferred to a cathode via an electrode, an external wire, and load, and the protons that pass through the proton exchange membrane enter the cathode chamber [22]. The electrons, the protons, and the final electron acceptor complete the reduction reaction at the cathode [3].

Electroactive microorganisms can indicate the inhibition of toxicants because these microorganisms are very sensitive to environmental changes. When the influent contains toxicants, the activity of microorganisms is inhibited [23], and the voltage or current generated immediately decrease [24]. Changes can reflect the concentration and the toxicity of the toxic substances.

Electroactive microorganisms mainly originate from soil, river bottom mud [6], deep sea rock mud, and activated sludge from sewage treatment plants [25]. Taxonomic statistics of electroactive microorganisms isolated from different systems have revealed that these microorganisms are mainly distributed in the phyla Proteobacteria, Firmicutes, Acidobacteria, Bacteroidetes, etc. [1,26]. Proteobacteria is an important category of electrically active microorganisms, among which the *Shewanella* spp. and the *Geobacter* spp. are representative model bacteria.

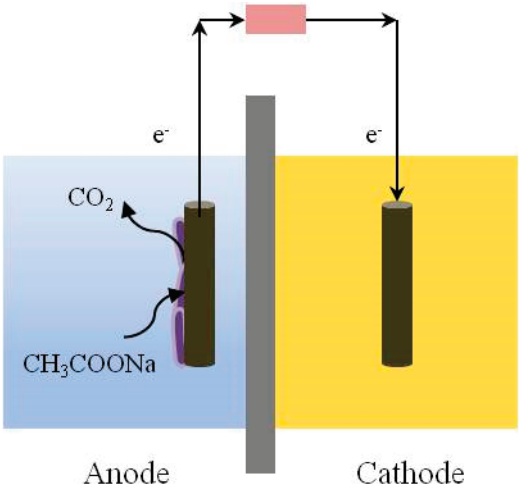

Figure 2. A schematic diagram of the structure of an MFC.

2.2. Configuration of MFCs

The configurations of MFCs are mainly dual-chambered and single-chambered. The cathode can be a biological or chemical cathode; in the latter, potassium ferricyanide is often used. The use of a chemical such as Fe (III) can improve the energy output of an MFC, but it also involves chemical losses in the cathode. The classic reactor format of an MFC for inhibitory responses is shown in Figure 2. A reactor with a small volume usually has a lower internal resistance and a higher sensitivity. For example, the micro-MFCs fabricated by Di Lorenzo using 3D-printing technology can rapidly detect cadmium in water at 1–25 μg/L [27]. The cathode-shared MFCs sensor array proposed by Jiang was applied to monitoring toxic substances in reclaimed water [28]. Zhao demonstrated the feasibility of using both bioanodes and biocathodes for suppression detection with continuous flow membrane-less MFCs [7]. Qi combined luminescent bacteria with electroactive microorganisms, allowing the simultaneous detection of electrical and optical signals [29].

The cathode of a single-chamber MFC is often an air cathode [6], but the proton exchange membrane has difficulty in completely isolating the air, and oxygen can therefore infiltrate into the anode, snatching electrons and reducing the sensitivity of the anode. With the increase in operating time, the side of the proton exchange membrane in contact with the air is prone to the formation of a biofilm [25] or salting out [30], increasing resistance. Air cathodes have been modified [31] by means such as the use of nano silver particles [32], quaternary ammonium salt [33], or enrofloxacin [34] to reduce the effects of this phenomenon. The half-wavelength alternating current is applied to counteract fouling and purify air cathodes [31]. Ionic liquids' proton-exchange membranes have recently received widespread attention [8]. They have unique physicochemical properties (in a liquid state at room temperature), containing organic cations [35] presenting excellent conductivity and thermal stability [36,37], and they can also reduce the size of cathode biofilms.

2.3. Electrode Material Modification

Many scholars are committed to the development of new electrode materials by adding active agents or modifying materials to improve the biocompatibility of the electrode. In doing so, more electroactive microorganisms can be enriched on the electrode surface, and the conductivity between the biofilm and the electrode can be improved. The transfer efficiency of MFCs can be improved [38].

The superhydrophilic semiconductor polydopamine is an efficient anode modification material that can shorten the startup time of MFCs and increase power density. The experimental results show that, after adding the polydopamine, the startup time of MFCs is shortened from 88 h to 76 h, the maximum power density is increased from 613 ± 9 to 803 ± 6 mW/m^2, and the power generation efficiency is increased by 29%. In addi-

tion, polydopamine can affect the anode microbial community structure, increasing the proportion of Proteobacteria and Firmicutes [39].

Zhang developed a novel graphene and manganese anode carbon felt coating using graphene and manganese oxide. This binder-free anode material has excellent electrical conductivity and a large surface area, resulting in a 154% increase in maximum power density, with a final value of 2065 mW/m^2 [38].

2.4. Application of Electroactive Microorganisms in Toxicants Monitoring

Kim and colleagues used MFCs for toxic substances detection in 1999. After decades of development, they are now suitable for testing various wastewaters and can enable the toxicity measurement of various substances such as organics, antibiotics, and heavy metals [40]. The common forms of MFC used for toxicity monitoring include single-chamber and double-chamber designs, and the electrical signals monitored include voltage, current, and power. Table 1 shows the application of the electroactive microorganisms reported in a toxicity assessment.

Table 1. Application of electroactive microorganisms in the evaluation of toxicants.

Toxicants		Reactor	Signal	Detection Concentration (mg/L)	References
Organics	Formaldehyde	double-chamber	current	0.1% *v/v*	[41]
	Acetic Acid	double-chamber	voltage	15	[42]
	p-Nitrophenol	single-chamber	current	50	[43]
	Azide	single-chamber	current	0.02	[44]
	2,4-Dichlorophenol	double-chamber	voltage	0.7	[45]
	Pyridine	double-chamber	voltage	0.1	[45]
Antibiotics	Levofloxacin	single-chamber	current	0.0001	[46]
	Imipenem	double-chamber	voltage	1.25	[47]
	Tobramycin	single-chamber	current	0.1	[48]
	Neomycin Sulphate	single-chamber	voltage	20	[49]
Heavy metals	Cu(II)	double-chamber	current	2	[28]
	Cd(II)	double-chamber	current	0.001	[27]
	Cr(VI)	single-chamber	voltage	1	[50]
	Fe(III)	single-chamber	power	2.8	[51]

3. Common Indicators for the Toxicity Assessment of Electroactive Microorganisms

The inhibition degree of electroactive microorganisms can be compared by response time or inhibition. Response time consists of the time when a current begins to significantly drop [40,52]. The magnitude of the response level can be calculated using current (I) [27], voltage (U) [28,53], and charge [24]. The difference between current and voltage changes can be directly indicated by ΔI and ΔU [52,54,55], and the corresponding calculations are shown in Equations (1) and (2), respectively.

$$\Delta I = (I_{nor} - I_{tox}) \quad (1)$$

$$\Delta U = (U_{nor} - U_{tox}) \quad (2)$$

Among them, I_{nor} and U_{nor} are stable electrical signals (mA or mV) under normal conditions; I_{tox} and U_{tox} are the signals (mA or mV) after adding toxic substances; and ΔI and ΔU are the changes in current and voltage (mA or mV) with toxic substances.

Among the above indicators, the voltage inhibition rate is currently the most commonly used indicator in research for indicating inhibition [28,40,56]. The calculation method is as follows (Equation (3)):

$$IR_U\ (\%) = 100 \times (U_{nor} - U_{tox})/U_{nor} \quad (3)$$

Among the terms of the equation above, IR_U is the voltage inhibition rate (%); U_{nor} is the maximum voltage (mV) before adding toxic substances; and U_{tox} is the voltage (mV) after adding toxic substances.

There are two ways to calculate the voltage inhibition rate. If the inhibition rate is calculated according to the maximum voltage in one power generation cycle, the results can be obtained after two cycles with and without toxic samples. Therefore, this method takes a long time: for 2~4 mg/L Cu^{2+}, the calculation period of the voltage inhibition rate is 50–60 h [53].

Another method consists of calculating the inhibition rate according to the voltage values before and after the addition of toxic samples in one power generation cycle. This method takes a relatively short time. For example, it takes 4 h for a voltage inhibition rate of 5 mg/L of Cu^{2+} to reach 30% [56]. But, as the measurement time is prolonged, the voltage may continue to decrease, so the inhibition rate calculated at different times is different (as shown in Figure 3a). The choice of reaction endpoint varies in studies, ranging from 10 min [27] to several hours [24], making it difficult to compare the levels of toxicity with different studies.

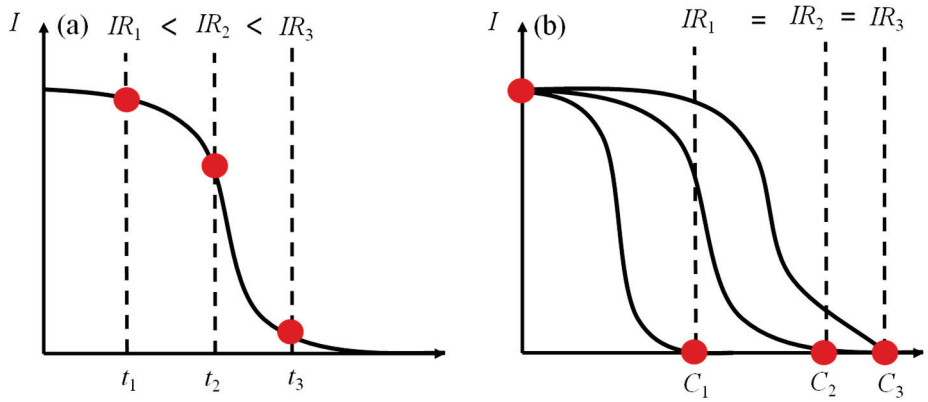

Figure 3. Voltage inhibition rate under different conditions: (**a**) inhibition rate of the same concentration at different times; and (**b**) inhibition rate at different concentrations and times.

In addition, the electrical signal curve usually changes with different concentrations of a sample, as shown in Figure 3b. The electrical signal immediately decreases with the addition of a higher-concentration toxic sample, and it decreases after a significant hysteresis period at a lower concentration. But, the final stable voltage is almost the same as that at a high concentration.

4. Factors Affecting the Toxicity Assessment of Electroactive Microorganisms

The factors influencing the toxicity assessment of electroactive microorganisms are the pH, the temperature, the flow rate, the incubation time, the acetate concentration, and the sodium chloride concentration. Among these, temperature, pH, acetate concentration, and ionic salinity are the characteristics of water quality related to a sample. These factors affect the activity and electrochemical performance of anode biofilms. Electroactive microorganisms are especially sensitive to acids, which affect microbial activity [28]. Temperature is associated with the bacterial metabolism. Chouler found that, when the temperature was changed in the range of 15–35 °C, the output current of MFCs changed by only 8% [57]. Studies have suggested that neutral pH conditions at room temperature are more suitable for the growth of microorganisms [58,59]. Acetate concentration and sodium chloride concentration will affect the components content of extracellular polymers in microorganisms and indirectly affect the performance of the bioanode [60]. The flow rate and the incubation time are influencing factors related to operating conditions, and the flow rate affects biofilm formation. Different thicknesses of the biofilms formed on the electrode surface over different incubation times directly affect the response time. It has been found that, when the concentration of sodium acetate is 1 g/L and the corresponding

biofilm is cultured for about 7 days, the monitoring sensitivity of toxic substances is higher. Other monitoring conditions need to be scrutinized to improve the monitoring accuracy of sensors.

4.1. Flow Rate

Studies have shown that the flow rate affects the power generation and sensitivity of electroactive microorganisms. Di Lorenzo found that reducing the flow rate led to better power generation efficiencies [61]. Shen found that reducing the flow rate could accelerate the response to Cu^{2+}, and intermittent nitrogen perturbation could increase the contact speed of toxic substances with microorganisms and accelerate the response to toxic substances [56].

Chen found that higher flow rates favored matrix diffusion into biofilms but increased biofilm density, causing the rate of matrix diffusion within the biofilm to decrease [62]. Under a high flow rate, a biofilm is dense with a high shear rate, and toxic substances do not easily diffuse into the biofilm, a circumstance which is not conducive to the system's response to said toxic substances [56,62]. A high flow rate causes an irreversible loss of biofilm, so a reasonable shear rate has an important impact on the attachment of electroactive microorganisms [63]. The effects of flux on biofilm properties such as biofilm density and porosity have been reported. It is necessary to carry out research on the responses of different flow rates and explore reasonable flow rates suitable for responses.

4.2. Culture Time

One of the advantages of MFCs is that they can operate for a long time and generate energy continuously [64], but long-term operation leads to the formation of thick biofilms [56]. A thick biofilm reduces the performance of an anode. The electron transfer of biofilms depends on the conductivity of the substrate, and the thicker the biofilm, the lower the conductivity [65]. As the thickness of the biofilm increases, the resistance to biomass production and mass transfer increases [56]. After long-term operation, a thick biofilm reduces the electron transfer efficiency and increases charge transfer resistance [66–68]. The material exchange rate can be accelerated by scraping the biofilm to improve the performance of the anode [69]. Studies have shown that long-term culturing will reduce anode performance and is unfavorable in terms of responses to toxic substances. It is necessary to study responses to culture time in order to improve the sensitivity of the responses of MFCs by enhancing anode redox capacity and microbial community structure.

4.3. Substrate Concentration

The available substrates for electroactive microorganisms are acetate, ethanol, glucose, etc. Substrate oxidation involves many electrochemical and biochemical reactions, and the generated current can indicate the oxidation rate of the substrate [40]. Different substrates of MFCs have different electricity production capacities and byproducts. When the substrate is glucose, glucose is hydrolyzed to form acetone and then hydrolyzed to lactic acid and acetic acid. There are three main stages in generating electrons [70]. Compared with low-molecular-weight substrates, glucose is less efficient in electricity production [71], and electroactive microorganisms are more likely to utilize low-molecular-weight substrates (such as acetate) as electron sources [71,72] and respond faster.

Ledezma studied the effect of substrate concentration on the electricity production of MFCs and found that, when the acetate concentration was greater than 100 mM, the current was no longer enhanced, and the substrate reached a saturated concentration, which was in line with the growth in microbial-saturated substrates' kinetics [73]. Chouler added 0.1–200 mM of potassium acetate, and the response to potassium acetate conformed to the Mono equation [57]. For marine microbial fuel cells cultured with mixed bacteria, current density is close to a constant value when the acetate concentration is greater than 0.50 mM [74].

Earlier studies showed that the current in response to substrate concentration corresponds to a first-order equation: that is, a finite substrate concentration corresponds to a low current density [75]. Acetate concentration is one of the key factors affecting microbial community composition and extracellular polymer composition [76]. There have been many reports on the effect of acetate concentration on electricity production but few on the response to toxic substances. In most studies, the acetate concentration was 1 g/L [77]. Therefore, it is necessary to carry out research on the responses to toxic substances measured for different acetate concentrations in order to obtain relatively accurate response results.

4.4. Sodium Chloride Concentration

NaCl concentration affects the activity of anode microorganisms and the electrochemical performance of MFC biosensors [57]. The pH of a solution and that of an electrode are often controlled using a buffer solution [78]. A phosphate-buffered solution is often used for MFCs because its pKa is close to neutral, and its biocompatibility is better [79,80]. The concentration of sodium chloride affects extracellular electron transfer and, thus, the power density of MFCs. Studies have shown that power density and output voltage reach a maximum when the concentration of sodium chloride is 1% (*w*/*v*) [81]. Although increasing the concentration of NaCl can increase the conductivity of the solution, it does not improve the electrical performance [82,83]. When the sodium chloride concentration is 0.1 M, the power density of the *Geobacter* spp. largely fluctuates [84]. Applying more than 0.1 M NaCl changes the bacterial species' presence in anode biofilms and, ultimately, reduces electricity generation [85]. The effect of sodium chloride concentration on electricity production in MFCs has been reported, but there are few reports on the corresponding response, and the effects on biological activity and redox capacity are even less reported. Therefore, it is necessary to carry out research on different sodium chloride concentrations to ensure reliability.

5. Reasons for Indicating the Toxicity of Electroactive Microorganisms

5.1. Electron Transfer of Electroactive Microorganisms

Electroactive microorganisms are mostly Gram-negative bacilli, which can oxidize electron donors in the cytoplasm, generate electrons, H^+, etc., and transfer electrons to electron acceptors through the outer membrane of cells. The generation and transmission of electrons are mainly realized through respiration in the cell and via the nanowires of cytochrome *c* and mediators outside the cell. Respiration occurs in the cell membrane (including the outer membrane, inner membrane, and periplasm). The proteins required for the transfer of electrons are usually five intermediate proteins: reduced coenzyme I, dehydrogenase, ubiquinone, coenzyme Q, and cytochrome [86].

For some specific bacterial strains, such as the *Shewanella* spp. and the *Geobacter* spp. direct electron transfer is considered an efficient electron transfer pathway. Research on the conduction mechanism of nanowires or cytochrome *c* in direct electron transfer can be realized by technical means such as gene chips and gene knockouts. Islam reported that nanowires did not show high electrical conductivity [67]. Through genomics studies, it was found that the electron transfer process of *Shewanella oneidensis* MR-1 involves six cytochromes *c*. The CymA of the inner membrane transfers electrons to Fcc3 and STC in the periplasm and then to the complex protein on the outer membrane. The electron transport process of the outer membrane involves MtrA, MtrB, and MtrC [11,87]. In one study, when the gene related to CymA was knocked out, the rate of metabolism using extracellular solid and dissolved electron acceptors was inhibited [88].

The electron transfer process of *Geobacter sulfurreducens* PCA (Figure 4) is more complicated than that of *Shewanella oneidensis* MR-1. Through genomics studies, it was found that lmcH and CbcL in the inner membrane transfer electrons to PpcA in the periplasm; these electrons are then transferred to the four complex proteins on the outer membrane, respectively. The electron transport process of these four outer membrane complex proteins

involves 2643, 2644, and 2642; OmaB, OmbB, and OmcB; OmaC, OmbC, and OmcC; and 2725, 2726, and 2742 [11,87].

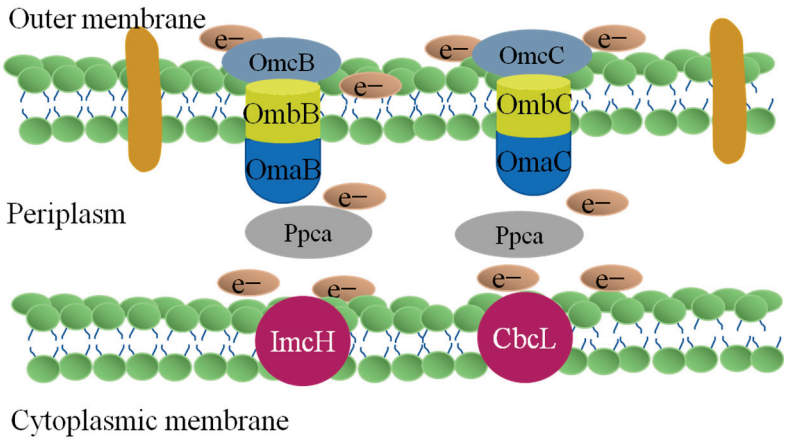

Figure 4. Electron transfer pathways of *Geobacter sulfurreducens* PCA.

Electron mediators are redox-active substances that can be used as electron carriers for periodic cyclic electron transfer between extracellular electron acceptors/donors and microbial cells. The indirect extracellular electron transfer mediated by electron mediators enables substances to undergo redox reactions without entering the intracellular membrane and periplasmic space. Electronic mediators include cellular secretions and agents added via exogenous dosing. Among these, the mediators secreted by cells include riboflavin [68], pyocyanin [89], phenols, proteins, and quinines, as well as the exogenous addition of phenazine and neutral red and so on.

5.2. Electron Transfer and Metabolism Change between Electroactive Microorganisms

According to the electron transfer mechanism of electroactive microorganisms, the electroactive microorganisms in the anode chamber of MFCs not only use themselves as electron donors and electrode materials as electron acceptors but also complete the transfer and transformation of electrons through other forms. Electroactive microorganisms can cooperate with other microorganisms in a heterotrophic metabolic pattern. Interspecific electron transfer is another syntrophic metabolic mechanism different from intraspecific electron transfer. Microorganisms transfer the electrons generated via the metabolism to other microorganisms through their own nanowires or cytochromes *c* and conductive substances. One study found that *Arcobacter* [90] and *Desulfovibrio* [91] can transfer electrons to each other.

The syntrophic metabolizing microorganisms that transfer energy through interspecific electron transfer channels are Gram-positive bacilli such as *Clostridium pasteurianum*, *Geobacter sulfurreducens*, and anaerobic photosynthetic bacteria. In the system in which *Geobacter sulfurreducens* coexists with other flora, *Geobacter sulfurreducens* oxidizes acetate, and electron transfer is realized by cytochrome *c* and nanowires (Equation (4)) [70,92]. In addition, *Klebsiella*, *Aeromonas*, and *Tolumonas* can carry out direct interspecies electron transfer by oxidizing electrons from glucose through cytochrome *c* to the anode complex (Equation (5)). Therefore, electron transport in a wide variety of mixed bacteria is the result of the coexistence of multiple electron transport modes [70].

$$\text{Acetate} + 2H_2O \overset{\text{cytochromes/pili}}{\rightarrow} 2CO_2 + 8H^+ + 8e^- \quad (4)$$

$$NADH \overset{\text{cytochromes}}{\rightarrow} NAD^+ + H^+ + 2e^- \quad (5)$$

Life activities are inseparable from energy metabolism, which directly affects microbial respiration, in turn affecting metabolic flux and redox balance [93]. Organic molecules undergo glycolysis to produce acetyl-CoA and then participate in the tricarboxylic acid cycle. Microbial redox reactions and energy production are inseparable from NAD(H) [94], as NAD(H) is an important carrier for extracellular electron transfer [94,95]. During substrate metabolism, dehydrogenase is an important enzyme involved in redox reactions [96] and can also transfer electrons between metabolic intermediates [97]. Studies have shown that extracellular acetic acid enters the cell and is then converted into acetyl-CoA. After isotope labeling, the enzyme generates ethanol through NADPH. Through metabolomic analysis, it was found that microbial respiration in this context was enhanced, the ratio of ATP/ADP was higher, and the ratios of NAD^+/NADH and $NADP^+$/NADPH were lower [93]. Toxic substances not only inhibit the energy synthesis of microorganisms but also inhibit the enzymes that the microorganisms need to synthesize during respiration [53], blocking the transfer of electrons and causing a voltage drop.

5.3. Mechanism of Electroactive Microorganisms to Resist Adverse Environment

i. Changes in the intracellular antioxidant enzymes of electroactive microorganisms

In recent years, scholars have found that membrane damage caused by oxidative stress is the main bactericidal mechanism behind the toxicity of toxic substances to microorganisms [98]. Microbial cell membranes are prone to change after being attacked by pollutants [99], and heavy-metal stress causes microorganisms to produce superoxide radicals or hydrogen peroxide, which damage proteins, lipids, and nucleic acids [100]. Microorganisms secrete various antioxidant enzymes such as superoxide dismutase [101], catalase [101], and glutathione peroxidase to carry out oxidative stress detoxification, thereby protecting cells from oxidative stress damage [102]. Lipids are the main targets of oxidative stress damage. Free radicals directly react with polyunsaturated fatty acids on cell membranes, causing lipid peroxidation, resulting in decreases in cell membrane fluidity, changes in cell membrane properties, and the destruction of cell membrane proteins [103]. The protein aggregation of cell membrane and the loss of activity forms ion channels. Then, the integrity of the cell membrane is destroyed, and the membrane's permeability is changed [103], finally leading to the disintegration and death of the bacteria. At present, there are relatively few studies on the inhibitory mechanisms of electroactive microorganisms. Therefore, by examining the single-electron transfer pathway related to respiration on the cell membrane and the changes in the related enzymes, it is possible to explore the effects of toxic substance inhibition mechanisms.

ii. Changes in electroactive microbial extracellular polymers

Electroactive microorganisms first contact toxic substances via the extracellular polymer (extracellular polymeric substances, EPSs) on the outermost layer of bacteria. The main components of the extracellular polymer include exopolysaccharide, protein, nucleic acid, and other substances [104]. Regarding the cause of toxicity, it is inseparable from microbial cell membrane adsorption [99]. EPSs are key structures in bacterial cells [105] and have important physiological effects on bacteria [106,107]. The content of EPSs affects the sensitivity of electroactive microorganisms [11,76].

6. Toxicity Evaluation Methods of Anaerobic Biological Treatments

For industrial wastewaters with a high organic concentration and a high toxicity [108], hydrolytic acidification is used as the first biological treatment process to improve biodegradability. Therefore, it is necessary to pay attention to the inhibition of hydrolytic acidification and acid production. In addition, due to its short monitoring time, high sensitivity, and automation, the acute toxicity test for luminescent bacteria is often used in various biological toxicity or inhibition tests.

6.1. The Toxicity Assay of Anaerobic Methane Production

The anaerobic toxicity assay (ATA) [18] based on methane production is a toxicity evaluation method for evaluating the effect of substrates on methanogenesis. Similar to the CO_2 emission test, the ATA (Figure 5a) measures methane production in batches and uses the ratio of methane production relative to the control to assess substrate toxicity. The ATA method based on methane production is widely used and well developed. In tests conducted in different laboratories, the inhibition rate of 32 mg/L-510 of mg/L 3,5-DCP for microorganisms in an anaerobic treatment system was 50%, as per the evaluation standard [109]. Most ATA experiments are carried out under anaerobic conditions at mesophilic temperatures (about 35 °C). The commonly used calculation method in the ATA consists in determining the specific methane production rate of toxic substances in a sample. The calculation formula is as follows:

$$I_{ATA} = 100\% \times (1 - R_t/R_0) \quad (6)$$

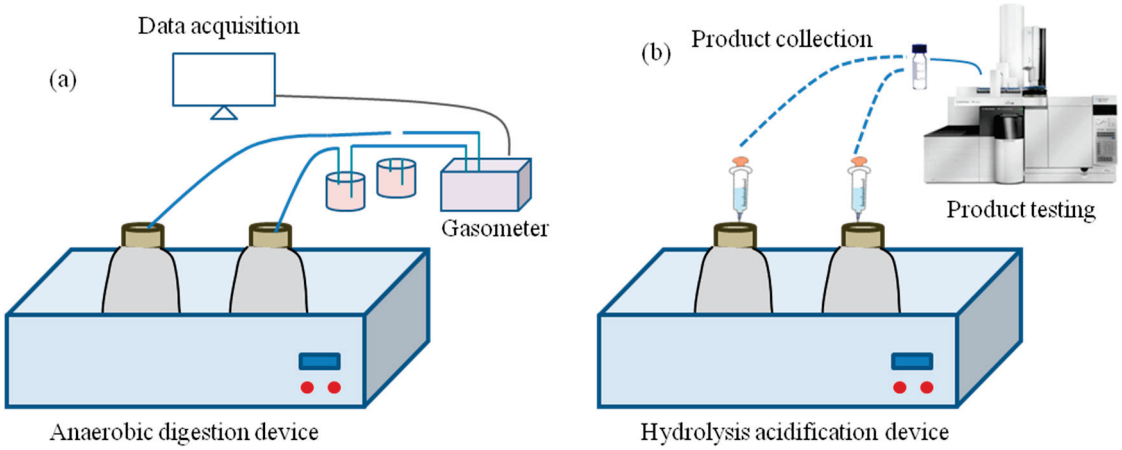

Figure 5. Toxicity evaluation methods: (**a**) the toxicity assay of methane production; and (**b**) the volatile fatty acids assay.

Among the terms of the equation above, I_{ATA} is the inhibition rate of methane production (%); R_t is the methane production rate of the tested wastewater group (mL/h); and R_0 is the methane production rate of the blank control group (mL/h).

6.2. The Inhibition of Acid Production by Hydrolysis and Acidification

Volatile fatty acids (VFA) are metabolic intermediates that exist in biological reaction systems and can reflect the acid production capacity of fermentation systems [18]. In an anaerobic reactor, the accumulation of VFA (Figure 5b) can reflect the inactive state of hydrolytic acidifying bacteria [19]. Higher VFA concentrations have an inhibitory effect on methanogens. The toxicity of toxic substances can be investigated by comparing the changes in the production rate of VFA before and after adding toxic substances. The formula for calculating the inhibition rate of volatile fatty acid production is as follows:

$$I_{VFA} = 100\% \times (1 - R_t/R_0) \quad (7)$$

Among the terms of the equation, I_{VFA} is the acid production inhibition rate (%); R_t is the production rate of total volatile fatty acids (mg/(L·h)); and R_0 is the production rate of total volatile fatty acids in the control group (mg/(L·h))

6.3. Evaluation of Relative Luminescence Inhibition

The toxicity evaluation of luminescent bacteria involves the use of photoelectric detection technology, which is applied in the evaluation of pollutants and environmental

monitoring. At present, this method has been applied to assess the quality of industrial wastewater and the toxicity of marine sediments and in the toxicity evaluation and environmental monitoring of some toxic organic pollutants and heavy metals.

There are generally three types of expressions for acquiring toxicity evaluation results using luminescent bacteria: the relative luminescence rate, the relative inhibition rate, and EC_{50}. EC_{50} is the concentration of a substance at which the relative light inhibition rate reaches 50% or more. The precision standard [110] stipulates that the relative deviation of the three repeated determination results of a sample should not be greater than 15%.

The toxicity toward luminescent bacteria is expressed by the relative photo inhibition rate, and the calculation formula is as follows:

$$I = 100\% \times (1 - R_t/R_0) \tag{8}$$

Among the terms of the equation, I is the photoacid production rate inhibition rate (%); R_t is the light intensity of the sample (cd); and R_0 is the light intensity of the control group (cd).

6.4. The Toxicity Assay of Electroactive Microorganisms

Traditional toxicity measurement methods can be used to monitor the types and concentrations of toxic substances in water, but the pre-treatment process is cumbersome, and the monitoring results are often lacking. Compared with traditional analytical methods, electroactive microorganisms do not require complex pre-treatment, are inexpensive, and can be used to effectively monitor toxic and harmful substances, revealing promising application prospects.

When the voltage is maintained at 620 ± 20 mV and kept stable for three cycles, it can be used for toxicity testing. The calculations for the inhibition rate, a toxicity evaluation indicator, include the entire toxic process [45]. The average current inhibition rate refers to the average current, taking into account the stable current of MFCs after adding toxic substances and comparing it with the normal current without toxic substances added.

The average current and its inhibition rate are calculated as follows:

$$\overline{I} = \left(\int_{t_1}^{t_2} I\mathrm{d}t\right)/(t_2 - t_1) \tag{9}$$

$$I_I\ (\%) = 100\ \times\ (I_{nor} - \overline{I})/I_{nor} \tag{10}$$

Among the terms of the equation above, t_1 is the time it takes for the current to decrease more than 5% of the normal value; t_2 is the time required to stabilize again with a fluctuation of no more than 5%; $\overline{I}$ is the average current of the toxic test; and I_{nor} is the normal value before adding toxic substances.

Among all the microorganisms that act as sensing elements, electroactive bacteria and luminescent bacteria are the two most important, because, without any additional chemical mediators, they can generate detectable fluorescence and current as warning signals [11]. Luminescent bacteria have been used in toxicity assays, and TOXcontrol® has developed an online bioluminescence assay system. However, it has been found that, as an indirect measure, luminescent bacteria may be too sensitive and often trigger false positive signals in wastewater assessments [18].

By investigating the toxicity evaluation method, an evaluation method consisting of electrical signals that can output toxicity levels online and in a timely fashion was developed. Electroactive microorganisms have been introduced into wastewater toxicity evaluation as a supplementary method to enrich toxicity evaluation methods and provide technical support for ensuring stable operations in wastewater biological treatment.

7. Conclusions and Perspectives

When using indicators to evaluate toxicity levels, the instantaneous values of electrical signals can easily lead to biased results. Before the voltage becomes stable, the inhibition rates at different times inevitably increase over time. Therefore, the selection of evaluation indicators requires consideration of the overall evaluation results. The environment has a significant impact on toxicant monitoring, especially in terms of cultivation time, substrate flow rate, sodium chloride concentration, and acetate concentration, which affect the characteristics and community composition of microorganisms. Therefore, these aspects greatly affect the power generation performance and sensitivity of electroactive microorganisms. In order to apply electroactive microorganisms in wastewater toxicity assessment, it is necessary to clarify the influencing factors and optimal operating conditions. The contributions of electroactive microorganisms in electron generation and transfer are different, and the competitive or complementary effects with respect to toxic substances are not yet clear. It is necessary to reveal their mechanisms with regard to toxic substances based on the characteristics of electron conduction, growth metabolism, and self-defense behavior.

Author Contributions: Writing—original draft, F.X.; Writing—review & editing, Funding acquisition, L.D.; Writing—review & editing, H.Z. (Haiya Zhang); Resources, Supervision, H.Z. (Hengliang Zhang); Formal analysis, S.L. All authors have read and agreed to the published version of the manuscript.

Funding: This research was funded by [Liang Duan] grant number (2022YSKY-14); [Fei Xing] grant number (2023YSKY-08).

Data Availability Statement: No new data were created or analyzed in this study. Data sharing is not applicable to this article.

Conflicts of Interest: The authors declare no conflicts of interest.

References

1. Logan, B.E.; Rozendal, R.; Schröder, U.; Keller, J.; Freguia, S. Microbial fuel cells: Methodology and technology. *Environ. Sci. Technol.* **2006**, *40*, 5181–5192. [CrossRef]
2. Asensio, Y.; Fernandez-Marchante, C.M.; Lobato, J.; Canizares, P.; Rodrigo, M.A. Influence of the fuel and dosage on the performance of double-compartment microbial fuel cells. *Water Res.* **2016**, *99*, 16–23. [CrossRef] [PubMed]
3. Moqsud, M.A.; Omine, K.; Yasufuku, N.; Hyodo, M.; Nakata, Y. Microbial fuel cell (MFC) for bioelectricity generation from organic wastes. *Waste Manag.* **2013**, *33*, 2465–2469. [CrossRef] [PubMed]
4. Yang, Q.; Wang, X.; Feng, Y.; Lee, H.; Liu, J.; Shi, X.; Qu, Y.; Ren, N. Electricity generation using eight amino acids by air–cathode microbial fuel cells. *Fuel* **2012**, *102*, 478–482. [CrossRef]
5. Li, T.; Zhou, L.; Qian, Y.; Wan, L.; Du, Q.; Li, N.; Wang, X. Gravity settling of planktonic bacteria to anodes enhances current production of microbial fuel cells. *Appl. Energy* **2017**, *198*, 261–266. [CrossRef]
6. Liao, C.; Wu, J.; Zhou, L.; Li, T.; An, J.; Huang, Z.; Li, N.; Wang, X. Repeated transfer enriches highly active electrotrophic microbial consortia on biocathodes in microbial fuel cells. *Biosens. Bioelectron.* **2018**, *121*, 118–124. [CrossRef]
7. Zhao, T.; Xie, B.; Yi, Y.; Liu, H. Sequential flowing membrane-less microbial fuel cell using bioanode and biocathode as sensing elements for toxicity monitoring. *Bioresour. Technol.* **2019**, *276*, 276–280. [CrossRef] [PubMed]
8. Hernández-Fernández, A.; Iniesta-López, E.; Garrido, Y.; Ieropoulos, I.A.; Hernández-Fernández, F.J. Microbial fuel cell using a novel Ionic-liquid-type membrane-cathode assembly with heterotrophic anodic denitrification for slurry treatment. *Sustainability* **2023**, *15*, 14817. [CrossRef]
9. Hassan, S.H.; Van Ginkel, S.W.; Hussein, M.A.; Abskharon, R.; Oh, S.E. Toxicity assessment using different bioassays and microbial biosensors. *Environ. Int.* **2016**, *92–93*, 106–118. [CrossRef]
10. Kaur, A.; Kim, J.R.; Michie, I.; Dinsdale, R.M.; Guwy, A.J.; Premier, G.C. Microbial fuel cell type biosensor for specific volatile fatty acids using acclimated bacterial communities. *Biosens. Bioelectron.* **2013**, *47*, 50–55. [CrossRef]
11. Qi, X.; Wang, S.; Li, T.; Wang, X.; Jiang, Y.; Zhou, Y.; Zhou, X.; Huang, X.; Liang, P. An electroactive biofilm-based biosensor for water safety: Pollutants detection and early-warning. *Biosens. Bioelectron.* **2021**, *173*, 112822. [CrossRef] [PubMed]
12. Liu, W.; Yang, G.; Jia, H.; Wang, J. A novel UASB-MFC dual sensors system for wastewater treatment: On-line sensor recovery and electrode cleaning in the long-term operation. *Chemosphere* **2020**, *246*, 125751. [CrossRef]
13. Corbella, C.; Hartl, M.; Fernandez-gatell, M.; Puigagut, J. MFC-based biosensor for domestic wastewater COD assessment in constructed wetlands. *Sci. Total Environ.* **2019**, *660*, 218–226. [CrossRef] [PubMed]
14. Feng, Y.; Kayode, O.; Harper, W.F. Using microbial fuel cell output metrics and nonlinear modeling techniques for smart biosensing. *Sci. Total Environ.* **2013**, *449*, 223–228. [CrossRef] [PubMed]

15. Prévoteau, A.; Clauwaert, P.; Kerckhof, F.M.; Rabaey, K. Oxygen-reducing microbial cathodes monitoring toxic shocks in tap water. *Biosens. Bioelectron.* **2019**, *132*, 115–121. [CrossRef]
16. Velasquez-Orta, S.B.; Werner, D.; Varia, J.C.; Mgana, S. Microbial fuel cells for inexpensive continuous in-situ monitoring of groundwater quality. *Water Res.* **2017**, *117*, 9–17. [CrossRef]
17. Li, T.; Wang, X.; Zhou, Q.; Liao, C.; Zhou, L.; Wan, L.; An, J.; Du, Q.; Li, N.; Ren, Z.J. Swift acid rain sensing by synergistic rhizospheric bioelectrochemical responses. *ACS Sens.* **2018**, *3*, 1424–1430. [CrossRef]
18. Xiao, Y.; De Araujo, C.; Sze, C.C.; Stuckey, D.C. Toxicity measurement in biological wastewater treatment processes: A review. *J. Hazard. Mater.* **2015**, *286*, 15–29. [CrossRef]
19. Song, G.; Yu, Y.; Liu, T.; Xi, H.; Zhou, Y. Performance of microaeration hydrolytic acidification process in the pretreatment of 2-butenal manufacture wastewater. *J. Hazard. Mater.* **2019**, *369*, 465–473. [CrossRef]
20. Zhang, Z.; Yang, Y.; Xi, H.; Yu, Y.; Song, Y.; Wu, C. Evaluation methods of inhibition to microorganisms in biotreatment processes: A review. *Water Cycle* **2023**, *4*, 70–78. [CrossRef]
21. Yuan, Y.; Yu, Y.; Xi, H.; Zhou, Y.; He, X. Comparison of four test methods for toxicity evaluation of typical toxicants in petrochemical wastewater on activated sludge. *Sci. Total Environ.* **2019**, *685*, 273–279. [CrossRef]
22. ReneÄ, A.; Rozendal, H.U.M.H.; Ceesj, N.B. Effects of membrane cation transport on pH and microbial fuel cell performance. *Environ. Sci. Technol.* **2006**, *40*, 5206–5211.
23. Yilmazel, Y.D.; Zhu, X.; Kim, K.Y.; Holmes, D.E.; Logan, B.E. Electrical current generation in microbial electrolysis cells by Ghyperthermophilic archaea *Ferroglobus placidus* and *Geoglobus ahangari*. *Bioelectrochemistry* **2018**, *119*, 142–149. [CrossRef] [PubMed]
24. Kim, M.; Sik Hyun, M.; Gadd, G.M.; Joo Kim, H. A novel biomonitoring system using microbial fuel cells. *J. Environ. Monit.* **2007**, *9*, 1323. [CrossRef]
25. Yuan, Y.; Zhou, S.; Tang, J. In situ investigation of cathode and local biofilm microenvironments reveals important roles of OH^- and oxygen transport in microbial fuel cells. *Environ. Sci. Technol.* **2013**, *47*, 4911–4917. [CrossRef] [PubMed]
26. Yates, M.D.; Kiely, P.D.; Call, D.F.; Rismani-Yazdi, H.; Bibby, K.; Peccia, J.; Regan, J.M.; Logan, B.E. Convergent development of anodic bacterial communities in microbial fuel cells. *ISME J.* **2012**, *6*, 2002–2013. [CrossRef]
27. Di Lorenzo, M.; Thomson, A.R.; Schneider, K.; Cameron, P.J.; Ieropoulos, I. A small-scale air-cathode microbial fuel cell for on-line monitoring of water quality. *Biosens. Bioelectron.* **2014**, *62*, 182–188. [CrossRef] [PubMed]
28. Jiang, Y.; Liang, P.; Liu, P.; Yan, X.; Bian, Y.; Huang, X. A cathode-shared microbial fuel cell sensor array for water alert system. *Int. J. Hydrogen Energy* **2017**, *42*, 4342–4348. [CrossRef]
29. Qi, X.; Liu, P.; Liang, P.; Hao, W.; Li, M.; Huang, X. Dual-signal-biosensor based on luminescent bacteria biofilm for real-time online alert of Cu(II) shock. *Biosens. Bioelectron.* **2019**, *142*, 111500. [CrossRef] [PubMed]
30. An, J.; Li, N.; Wan, L.; Zhou, L.; Du, Q.; Li, T.; Wang, X. Electric field induced salt precipitation into activated carbon air-cathode causes power decay in microbial fuel cells. *Water Res.* **2017**, *123*, 369–377. [CrossRef]
31. Zhou, L.; Liao, C.; Li, T.; An, J.; Du, Q.; Wan, L.; Li, N.; Pan, X.; Wang, X. Regeneration of activated carbon air-cathodes by half-wave rectified alternating fields in microbial fuel cells. *Appl. Energy* **2018**, *219*, 199–206. [CrossRef]
32. An, J.; Jeon, H.; Lee, J.; Chang, I.S. Bifunctional silver nanoparticle cathode in microbial fuel cells for microbial growth inhibition with comparable oxygen reduction reaction activity. *Environ. Sci. Technol.* **2011**, *45*, 5441–5446. [CrossRef]
33. Li, N.; Liu, Y.; An, J.; Feng, C.; Wang, X. Bifunctional quaternary ammonium compounds to inhibit biofilm growth and enhance performance for activated carbon air-cathode in microbial fuel cells. *J. Power Sources* **2014**, *272*, 895–899. [CrossRef]
34. Liu, W.; Cheng, S.; Sun, D.; Huang, H.; Chen, J.; Cen, K. Inhibition of microbial growth on air cathodes of single chamber microbial fuel cells by incorporating enrofloxacin into the catalyst layer. *Biosens. Bioelectron.* **2015**, *72*, 44–50. [CrossRef]
35. Ortiz-Martínez, V.M.; Ortiz, A.; Fernández-Stefanuto, V.; Tojo, E.; Colpaert, M.; Améduri, B.; Ortiz, I. Fuel cell electrolyte membranes based on copolymers of protic ionic liquid [HSO_3-BVIm][TfO] with MMA and hPFSVE. *Polymer* **2021**, *179*, 121583. [CrossRef]
36. Gancarz, P.; Zorębski, E.; Dzida, M. Influence of experimental conditions on the electrochemical window, case study on bis(trifluoromethylsulfonyl)imide-based ionic liquids. *Electrochem. Commun.* **2021**, *130*, 107107. [CrossRef]
37. Tiago, G.A.O.; Matias, I.A.S.; Ribeiro, A.P.C.; Martins, L.M.D.R.S. Application of ionic liquids in electrochemistry-recent advances. *Molecules* **2020**, *25*, 5812. [CrossRef] [PubMed]
38. Zhang, C.; Liang, P.; Yang, X.; Jiang, Y.; Bian, Y.; Chen, C.; Zhang, X.; Huang, X. Binder-free graphene and manganese oxide coated carbon felt anode for high-performance microbial fuel cell. *Biosens. Bioelectron.* **2016**, *81*, 32–38. [CrossRef] [PubMed]
39. Du, Q.; An, J.; Li, J.; Zhou, L.; Li, N.; Wang, X. Polydopamine as a new modification material to accelerate startup and promote anode performance in microbial fuel cells. *J. Power Sources* **2017**, *343*, 477–482. [CrossRef]
40. Jiang, Y.; Yang, X.; Liang, P.; Liu, P.; Huang, X. Microbial fuel cell sensors for water quality early warning systems: Fundamentals, signal resolution, optimization and future challenges. *Renew. Sustain. Energy Rev.* **2018**, *81*, 292–305. [CrossRef]
41. Chouler, J.; Cruz-Izquierdo, Á.; Rengaraj, S.; Scott, J.L.; Di Lorenzo, M. A screen-printed paper microbial fuel cell biosensor for detection of toxic compounds in water. *Biosens. Bioelectron.* **2018**, *102*, 49–56. [CrossRef] [PubMed]
42. Park, Y.; Cho, H.; Yu, J.; Min, B.; Kim, H.S.; Kim, B.G.; Lee, T. Response of microbial community structure to pre-acclimation strategies in microbial fuel cells for domestic wastewater treatment. *Bioresour. Technol.* **2018**, *233*, 176–183. [CrossRef] [PubMed]

43. Santoro, C.; Mohidin, A.F.; Grasso, L.L.; Seviour, T.; Palanisamy, K.; Hinks, J.; Lauro, F.M.; Marsili, E. Sub-toxic concentrations of volatile organic compounds inhibit extracellular respiration of *Escherichia coli* cells grown in anodic bioelectrochemical systems. *Bioelectrochemistry* **2016**, *112*, 173–177. [CrossRef] [PubMed]
44. Ahn, Y.; Schröder, U. Microfabricated, continuous-flow, microbial three-electrode cell for potential toxicity detection. *BioChip J.* **2014**, *9*, 27–34. [CrossRef]
45. Xing, F.; Xi, H.; Yu, Y.; Zhou, Y. A sensitive, wide-ranging comprehensive toxicity indicator based on microbial fuel cell. *Sci. Total Environ.* **2020**, *703*, 134667. [CrossRef]
46. Zeng, L.; Li, X.; Shi, Y.; Qi, Y.; Huang, D.; Tadé, M.; Wang, S.; Liu, S. $FePO_4$ based single chamber air-cathode microbial fuel cell for online monitoring levofloxacin. *Biosens. Bioelectron.* **2017**, *91*, 367–373. [CrossRef]
47. Schneider, G.; Czeller, M.; Rostas, V.; Kovacs, T. Microbial fuel cell-based diagnostic platform to reveal antibacterial effect of beta-lactam antibiotics. *Enzym. Microb. Technol.* **2015**, *73–74*, 59–64. [CrossRef]
48. Wu, W.; Xu, S.; Wang, L.; Liu, H. Impact of tobramycin on the performance of microbial fuel cell. *Microb. Cell Factories* **2014**, *13*, 7. [CrossRef]
49. Catal, T.; Yavaser, S.; Enisoglu-Atalay, V.; Bermek, H.; Ozilhan, S. Monitoring of neomycin sulfate antibiotic in microbial fuel cells. *Bioresour. Technol.* **2018**, *268*, 116–120. [CrossRef]
50. Liu, B.; Lei, Y.; Li, B. A batch-mode cube microbial fuel cell based "shock" biosensor for wastewater quality monitoring. *Biosens. Bioelectron.* **2014**, *62*, 308–314. [CrossRef]
51. Li, F.; Zheng, Z.; Yang, B.; Zhang, X.; Li, Z.; Lei, L. A laminar-flow based microfluidic microbial three-electrode cell for biosensing. *Electrochim. Acta* **2016**, *199*, 45–50. [CrossRef]
52. Di Lorenzo, M.; Curtis, T.P.; Head, I.M.; Scott, K. A single-chamber microbial fuel cell as a biosensor for wastewaters. *Water Res.* **2009**, *43*, 3145–3154. [CrossRef] [PubMed]
53. Yu, D.; Bai, L.; Zhai, J.; Wang, Y.; Dong, S. Toxicity detection in water containing heavy metal ions with a self-powered microbial fuel cell-based biosensor. *Talanta* **2017**, *168*, 210–216. [CrossRef]
54. Jiang, Y.; Liang, P.; Zhang, C.; Bian, Y.; Yang, X.; Huang, X.; Girguis, P.R. Enhancing the response of microbial fuel cell based toxicity sensors to Cu(II) with the applying of flow-through electrodes and controlled anode potentials. *Bioresour. Technol.* **2015**, *190*, 367–372. [CrossRef]
55. Stein, N.E.; Keesman, K.J.; Hamelers, H.V.M.; van Straten, G. Kinetic models for detection of toxicity in a microbial fuel cell based biosensor. *Biosens. Bioelectron.* **2011**, *26*, 3115–3120. [CrossRef] [PubMed]
56. Shen, Y.; Wang, M.; Chang, I.S.; Ng, H.Y. Effect of shear rate on the response of microbial fuel cell toxicity sensor to Cu(II). *Bioresour. Technol.* **2013**, *136*, 707–710. [CrossRef]
57. Chouler, J.; Di Lorenzo, M. Pesticide detection by a miniature microbial fuel cell under controlled operational disturbances. *Water Sci. Technol.* **2019**, *79*, 2231–2241. [CrossRef] [PubMed]
58. Li, X.M.; Cheng, K.Y.; Wong, J.W. Bioelectricity production from food waste leachate using microbial fuel cells: Effect of NaCl and pH. *Bioresour. Technol.* **2013**, *149*, 452–458. [CrossRef]
59. Oh, S.E.; Logan, B.E. Hydrogen and electricity production from a food processing wastewater using fermentation and microbial fuel cell technologies. *Water Res.* **2005**, *39*, 4673–4682. [CrossRef]
60. Xing, F.; Xi, H.; Yu, Y.; Zhou, Y. Anode biofilm influence on the toxic response of microbial fuel cells under different operating conditions. *Sci. Total Environ.* **2021**, *775*, 145048. [CrossRef]
61. Di Lorenzo, M.; Scott, K.; Curtis, T.P.; Head, I.M. Effect of increasing anode surface area on the performance of a single chamber microbial fuel cell. *Chem. Eng. J.* **2010**, *156*, 40–48. [CrossRef]
62. Chen, Y.M.; Wang, C.T.; Yang, Y.C. Effect of wall boundary layer thickness on power performance of a recirculation microbial fuel cell. *Energies* **2018**, *11*, 1003. [CrossRef]
63. Ren, H.; Lee, H.S.; Chae, J. Miniaturizing microbial fuel cells for potential portable power sources: Promises and challenges. *Microfluid. Nanofluidics* **2012**, *13*, 353–381. [CrossRef]
64. Tommasi, T.; Lombardelli, G. Energy sustainability of microbial fuel cell (MFC): A case study. *J. Power Sources* **2017**, *356*, 438–447. [CrossRef]
65. Vilas Boas, J.; Oliveira, V.B.; Marcon, L.R.C.; Simoes, M.; Pinto, A. Optimization of a single chamber microbial fuel cell using *Lactobacillus pentosus*: Influence of design and operating parameters. *Sci. Total Environ.* **2019**, *648*, 263–270. [CrossRef] [PubMed]
66. Bond, D.R.; Strycharz-Glaven, S.M.; Tender, L.M.; Torres, C.I. On electron transport through *Geobacter* biofilms. *ChemSusChem* **2012**, *5*, 1099–1105. [CrossRef]
67. Islam, M.A.; Woon, C.W.; Ethiraj, B.; Cheng, C.K.; Yousuf, A.; Khan, M.M.R. Ultrasound driven biofilm removal for stable power generation in microbial fuel cell. *Energy Fuels* **2016**, *31*, 968–976. [CrossRef]
68. Marsili, E.; Rollefson, J.B.; Baron, D.B.; Hozalski, R.M.; Bond, D.R. Microbial biofilm voltammetry: Direct electrochemical characterization of catalytic electrode-attached biofilms. *Appl. Environ. Microbiol.* **2008**, *74*, 7329–7337. [CrossRef]
69. Qi, X.; Liu, P.; Liang, P.; Hao, W.; Li, M.; Li, Q.; Zhou, Y.; Huang, X. Biofilm's morphology design for high sensitivity of bioelectrochemical sensor: An experimental and modeling study. *Sci. Total Environ.* **2020**, *729*, 138908. [CrossRef]
70. Zhang, Y.; Jiang, J.; Zhao, Q.; Wang, K.; Yu, H. Analysis of functional genomes from metagenomes: Revealing the accelerated electron transfer in microbial fuel cell with rhamnolipid addition. *Bioelectrochemistry* **2018**, *119*, 59–67. [CrossRef]

71. Kim, K.Y.; Chae, K.J.; Choi, M.J.; Ajayi, F.F.; Jang, A.; Kim, C.W.; Kim, I.S. Enhanced coulombic efficiency in glucose-fed microbial fuel cells by reducing metabolite electron losses using dual-anode electrodes. *Bioresour. Technol.* **2011**, *102*, 4144–4149. [CrossRef] [PubMed]
72. Hwang, J.H.; Kim, K.Y.; Resurreccion, E.P.; Lee, W.H. Surfactant addition to enhance bioavailability of bilge water in single chamber microbial fuel cells (MFCs). *J. Hazard. Mater.* **2019**, *368*, 732–738. [CrossRef] [PubMed]
73. Ledezma, P.; Greenman, J.; Ieropoulos, I. Maximising electricity production by controlling the biofilm specific growth rate in microbial fuel cells. *Bioresour. Technol.* **2012**, *118*, 615–618. [CrossRef]
74. Quek, S.B.; Cheng, L.; Cord-Ruwisch, R. Microbial fuel cell biosensor for rapid assessment of assimilable organic carbon under marine conditions. *Water Res.* **2015**, *77*, 64–71. [CrossRef]
75. Jadhav, G.S.; Ghangrekar, M.M. Performance of microbial fuel cell subjected to variation in pH, temperature, external load and substrate concentration. *Bioresour. Technol.* **2009**, *100*, 717–723. [CrossRef]
76. Li, T.; Zhou, Q.; Zhou, L.; Yan, Y.; Liao, C.; Wan, L.; An, J.; Li, N.; Wang, X. Acetate limitation selects *Geobacter* from mixed inoculum and reduces polysaccharide in electroactive biofilm. *Water Res.* **2020**, *177*, 115776. [CrossRef]
77. Li, T.; Wang, X.; Zhou, L.; An, J.; Li, J.; Li, N.; Sun, H.; Zhou, Q. Bioelectrochemical sensor using living biofilm to in situ evaluate flocculant toxicity. *ACS Sens.* **2016**, *1*, 1374–1379. [CrossRef]
78. Rossi, R.; Pant, D.; Logan, B.E. Chronoamperometry and linear sweep voltammetry reveals the adverse impact of high carbonate buffer concentrations on anode performance in microbial fuel cells. *J. Power Sources* **2020**, *476*, 228715. [CrossRef]
79. Popat, S.C.; Ki, D.; Young, M.N.; Rittmann, B.E.; Torres, C.I. Buffer pKa and transport govern the concentration overpotential in electrochemical oxygen reduction at neutral pH. *ChemElectroChem* **2014**, *1*, 1909–1915. [CrossRef]
80. Ye, Y.; Zhu, X.; Logan, B.E. Effect of buffer charge on performance of air-cathodes used in microbial fuel cells. *Electrochim. Acta* **2016**, *194*, 441–447. [CrossRef]
81. Adelaja, O.; Keshavarz, T.; Kyazze, G. The effect of salinity, redox mediators and temperature on anaerobic biodegradation of petroleum hydrocarbons in microbial fuel cells. *J. Hazard. Mater.* **2015**, *283*, 211–217. [CrossRef]
82. Lefebvre, O.; Tan, Z.; Kharkwal, S.; Ng, H.Y. Effect of increasing anodic NaCl concentration on microbial fuel cell performance. *Bioresour. Technol.* **2012**, *112*, 336–340. [CrossRef]
83. Md Khudzari, J.; Tartakovsky, B.; Raghavan, G.S.V. Effect of C/N ratio and salinity on power generation in compost microbial fuel cells. *Waste Manag.* **2016**, *48*, 135–142. [CrossRef] [PubMed]
84. Miyahara, M.; Kouzuma, A.; Watanabe, K. Sodium chloride concentration determines exoelectrogens in anode biofilms occurring from mangrove-grown brackish sediment. *Bioresour. Technol.* **2016**, *218*, 674–679. [CrossRef] [PubMed]
85. Miyahara, M.; Kouzuma, A.; Watanabe, K. Effects of NaCl concentration on anode microbes in microbial fuel cells. *AMB Express* **2015**, *5*, 123. [CrossRef] [PubMed]
86. Kumar, R.; Singh, L.; Wahid, Z.A.; Din, M.F.M. Exoelectrogens in microbial fuel cells toward bioelectricity generation: A review. *Int. J. Energy Res.* **2015**, *39*, 1048–1067. [CrossRef]
87. Shi, L.; Dong, H.; Reguera, G.; Beyenal, H.; Lu, A.; Liu, J.; Yu, H.Q.; Fredrickson, J.K. Extracellular electron transfer mechanisms between microorganisms and minerals. *Nat. Rev. Microbiol.* **2016**, *14*, 651–662. [CrossRef] [PubMed]
88. Carsten Schwalb, S.K.C.; Graeme, A.R. The tetraheme cytochrome CymA is required for anaerobic respiration with dimethyl sulfoxide and nitrite in *Shewanella* oneidensis. *Biochemistry* **2003**, *42*, 9491–9497. [CrossRef] [PubMed]
89. Korneel Rabaey, P.C.; Peter, A.; Willy, V. Tubular microbial fuel cells for efficient electricity generation. *Environ. Sci. Technol.* **2005**, *39*, 8077–8082. [CrossRef] [PubMed]
90. Pereira-Medrano, A.G.; Knighton, M.; Fowler, G.J.; Ler, Z.Y.; Pham, T.K.; Ow, S.Y.; Free, A.; Ward, B.; Wright, P.C. Quantitative proteomic analysis of the exoelectrogenic bacterium *Arcobacter butzleri* ED-1 reveals increased abundance of a flagellin protein under anaerobic growth on an insoluble electrode. *J. Proteom.* **2013**, *78*, 197–210. [CrossRef]
91. Bao, Y.; Guo, C.; Lu, G.; Yi, X.; Wang, H.; Dang, Z. Role of microbial activity in Fe(III) hydroxysulfate mineral transformations in an acid mine drainage-impacted site from the Dabaoshan Mine. *Sci. Total Environ.* **2018**, *616–617*, 647–657. [CrossRef]
92. Bond, D.R.; Lovley, D.R. Electricity production by *Geobacter sulfurreducens* attached to electrodes. *Appl. Environ. Microbiol.* **2003**, *69*, 1548–1555. [CrossRef]
93. Song, J.; Sasaki, D.; Sasaki, K.; Kato, S.; Kondo, A.; Hashimoto, K.; Nakanishi, S. Comprehensive metabolomic analyses of anode-respiring *Geobacter sulfurreducens* cells: The impact of anode-respiration activity on intracellular metabolite levels. *Process Biochem.* **2016**, *51*, 34–38. [CrossRef]
94. Yong, X.Y.; Feng, J.; Chen, Y.L.; Shi, D.Y.; Xu, Y.S.; Zhou, J.; Wang, S.Y.; Xu, L.; Yong, Y.C.; Sun, Y.M.; et al. Enhancement of bioelectricity generation by cofactor manipulation in microbial fuel cell. *Biosens. Bioelectron.* **2014**, *56*, 19–25. [CrossRef]
95. Berríos-Rivera, S. The Effect of NAPRTase overexpression on the total levels of NAD^+, the NADH/NAD^+ Ratio, and the distribution of metabolites in *Escherichia coli*. *Metab. Eng.* **2002**, *4*, 238–247. [CrossRef] [PubMed]
96. Kiran Kumar, A.; Venkateswar Reddy, M.; Chandrasekhar, K.; Srikanth, S.; Venkata Mohan, S. Endocrine disruptive estrogens role in electron transfer: Bio-electrochemical remediation with microbial mediated electrogenesis. *Bioresour. Technol.* **2012**, *104*, 547–556. [CrossRef] [PubMed]
97. Nikhil, G.N.; Venkata Subhash, G.; Yeruva, D.K.; Venkata Mohan, S. Synergistic yield of dual energy forms through biocatalyzed electrofermentation of waste: Stoichiometric analysis of electron and carbon distribution. *Energy* **2015**, *88*, 281–291. [CrossRef]

98. Miran, W.; Nawaz, M.; Jang, J.; Lee, D.S. Chlorinated phenol treatment and in situ hydrogen peroxide production in a sulfate-reducing bacteria enriched bioelectrochemical system. *Water Res.* **2017**, *117*, 198–206. [CrossRef]
99. Cheng, Z.; Zhang, X.; Kennes, C.; Chen, J.; Chen, D.; Ye, J.; Zhang, S.; Dionysiou, D.D. Differences of cell surface characteristics between the bacterium *Pseudomonas veronii* and fungus *Ophiostoma stenoceras* and their different adsorption properties to hydrophobic organic compounds. *Sci. Total Environ.* **2019**, *650 Pt 2*, 2095–2106. [CrossRef] [PubMed]
100. Rahman, S.; Kim, K.H.; Saha, S.K.; Swaraz, A.M.; Paul, D.K. Review of remediation techniques for arsenic (As) contamination: A novel approach utilizing bio-organisms. *J. Environ. Manag.* **2014**, *134*, 175–185. [CrossRef]
101. Shi, Z. Methylome and metabolome analyses reveal adaptive mechanisms in *Geobacter sulfurreducens* grown on different terminal electron acceptors. *J. Proteome Res.* **2019**, *18*, 1494–1502. [CrossRef]
102. Khare, T.; Esteve-Núñez, A.; Nevin, K.P.; Zhu, W.; Yates, J.R.; Lovley, D.; Giometti, C.S. Differential protein expression in the metal-reducing bacterium *Geobacter sulfurreducens* strain PCA grown with fumarate or ferric citrate. *Proteomics* **2006**, *6*, 632–640. [CrossRef]
103. Liu, Q.; Kong, W.; Hu, S.; Kang, Y.; Zhang, Y.; Ng, T.B. Effects of Oudemansiella radicata polysaccharide on postharvest quality of oyster mushroom (pleurotus ostreatus) and its antifungal activity against penicillium digitatum. *Postharvest Biol. Technol.* **2020**, *166*, 111207. [CrossRef]
104. Kostakioti, M.; Hadjifrangiskou, M.; Hultgren, S.J. Bacterial biofilms: Development, dispersal, and therapeutic strategies in the dawn of the postantibiotic era. *Cold Spring Harb. Perspect. Med.* **2013**, *3*, a010306. [CrossRef] [PubMed]
105. Branda, S.S.; Vik, S.; Friedman, L.; Kolter, R. Biofilms: The matrix revisited. *Trends Microbiol.* **2005**, *13*, 20–26. [CrossRef] [PubMed]
106. Billings, N.; Millan, M.; Caldara, M.; Rusconi, R.; Tarasova, Y.; Stocker, R.; Ribbeck, K. The extracellular matrix component Psl provides fast-acting antibiotic defense in *Pseudomonas aeruginosa* biofilms. *PLoS Pathog* **2013**, *9*, e1003526. [CrossRef] [PubMed]
107. Boles, B.R.; Horswill, A.R. Staphylococcal biofilm disassembly. *Trends Microbiol.* **2011**, *19*, 449–455. [CrossRef] [PubMed]
108. Wu, C.; Li, Y.; Zhou, Y.; Li, Z.; Zhang, S.; Liu, H. Upgrading the Chinese biggest petrochemical wastewater treatment plant: Technologies research and full scale application. *Sci. Total Environ.* **2018**, *633*, 189–197. [CrossRef] [PubMed]
109. *ISO 13641*; Water Quality Determination of Inhibition of Gas Production of Anaerobic Bacteria. International Organization for Standardization: Geneva, Switzerland, 2003.
110. *GB/T15441*; Water Quality Determination of the Acute Toxicity-Luminescent Bacteria Test. China Zhijian Publishing House: Beijing, China, 1995.

MDPI AG
Grosspeteranlage 5
4052 Basel
Switzerland
Tel.: +41 61 683 77 34

Toxics Editorial Office
E-mail: toxics@mdpi.com
www.mdpi.com/journal/toxics

Academic Open
Access Publishing

mdpi.com

ISBN 978-3-7258-6355-6